METALLOPROTEIN ELECTRON TRANSFER. CYTOCHROME aa_3 REDUCTION KINETICS AND THEORETICAL FORMULATION OF DISTANCE DEPENDENCE

Thesis by

Robert Allen Scott

In Partial Fulfilment of the Requirements

for the Degree of

Doctor of Philosophy

California Institute of Technology

Pasadena, California

1980

(Submitted August 6, 1979)

ACKNOWLEDGMENTS

Recognition is due many people for help, collaboration, and companionship during my stay at Caltech. Harry deserves acknowledgment for establishment of an atmosphere conducive to independent research and for introducing me to responsibilities (*e.g.*, proposal writing) which should serve me well in my academic future. Scot Wherland receives thanks for helping me develop my interest in computers and statistics. Grant Mauk gets special recognition for teaching me how to spread my organizational abilities over at least three filing cabinets and for those evenings in "Margueritaville." Thanks also to Marcia Mauk for her tolerance of "Saturday Night Live," her intolerance of "Monty Python," and her *Dieffenbachia*. Yo gets an acknowledgment for her undying optimism and propitious selection of research projects. Steve Schichman is recognized for teaching me how to do control experimenmts. Thanks to Penny for nickel- and dime-ing me to death, to Bob Kanne for being such an accomplished volleyball organizer, and to DT, KT, and MT for keeping me from dozing off on those late evenings (of work) at home. Noboru Oyama receives special recognition as a superb athlete on the rinks (er, links). Special thanks also go to other group members: Diane (and Phil) Cummins, Pam Peerce, Dave ("Doo") Dooley, Vern Taniguchi, Vanessa Lum, Bill Trogler, and John Dawson.

Sincere sympathy (and thanks) should be expressed for the shop people upon whose back I resided for much of my time here:

Erich Segal, one of the best glassblowers around (and Sig), Bill Schuelke, and his cohorts in the instrument shop who did all the machining responsible for the figures in the Experimental Section of Chapter 1.

Recognition should also be given to people who have helped me on my way: Professor Helmut Beinert and Dr. Robert Shaw of the Enzyme Institute, Professor Graham Palmer of Rice, "Uncle Gil" Haight (for suggesting Caltech in the first place), Keith Hodgson and group of Stanford (for some wonderful nights at SSRL), and Steve Cramer of Exxon ("Mr. EXAFS" who taught me the true meaning of "living").

Thanks should be expressed to my parents who have always encouraged independence and creativity, and expecially to my wife, Pom, who makes it all worthwhile.

ABSTRACT

The kinetics of anaerobic reduction of beef heart mitochondrial cytochrome *c* oxidase (cytochrome aa_3) by hexammine ruthenium(II) (RuA_6^{2+}) were measured. At wavelengths in the Soret and at 605 nm the kinetics are biphasic, neither phase exhibiting (pseudo-)first order behavior. A complete nonlinear optimization analysis showed that the slow phase obeyed strict second order kinetics, the fast phase being apparently more complex. Kinetic difference spectra observed for the RuA_6^{2+} reduction of native and cyanide-treated enzyme clearly demonstrate that the fast phase is due to reduction of cytochrome a^{3+} while the slow phase is due to reduction of a_3^{3+}. The slow phase is independent of RuA_6^{2+} concentration with a second order rate constant of (1.04±.06) x 10^5 M^{-1}-s^{-1} (25°C) and activation parameters $\Delta H^{\ddagger}$ =16.6±0.6 kcal-mol^{-1}, $\Delta S^{\ddagger}$= +20.2± 2.0 cal-deg^{-1}-mol^{-1} (pH=6.0 (cacodylate), μ=0.10 *M*) for native aa_3. The oxidized-cyanide derivative gave a second order rate constant of (1.99±.06) x 10^4 M^{-1}-s^{-1} (pH=6.0 (cacodylate), μ= 0.10 *M*, 25°C). Analysis of the fast phase as a second order decay gave temperature-independent second order rate constants which are linearly dependent on RuA_6^{2+} concentration. The third order rate constant from this fit is (1.68±.02) x 10^{11} M^{-2}-s^{-1} (pH=6.0 (cacodylate), μ=0.10 *M*, 25°C). The second order slow phase is interpreted as involving *inter*molecular electron transfer between half-reduced (cytochrome *a* reduced) species in reduction of cytochrome a_3.

A detailed description of the nonlinear least squares optimization techniques used for analysis of the cytochrome aa_3 kinetics is given along with a general description of a complete kinetics analysis computer routine package. Emphasis is placed on correct error analysis and weighting procedures.

In addition, a theoretical description of the dependence of the rate of metalloprotein electron transfer on the distance over which the transfer must occur is presented. The exponential dependence of rate on distance derived in several theoretical formulations of electron tunneling in biological systems is assumed and several known cases of metalloprotein electron transfer with small molecule reagents are examined to determine the distance of transfer. The results are compared with known structural data and discussed in terms of the accessibility of protein metal sites to external reagents.

TABLE OF CONTENTS

ACKNOWLEDGMENTS ii
ABSTRACT iv
TABLE OF CONTENTS vi
CHAPTER I. Cytochrome aa_3 1
INTRODUCTION 2
CURRENT KNOWLEDGE 4
Structure 4
Active Sites 15
Electronic Absorption Spectra 16
Liganded Derivatives 23
Redox Potentials 39
Magnetic Properties 57
Catalytic Activity 73
Cytochrome *c* Oxidation 74
Dioxygen Reduction 80
EXPERIMENTAL 85
Materials 85
Equipment 87
Methods 101
Cytochrome aa_3 101
Hexammineruthenium(II) Reagent 109
Kinetics 110
Kinetics Analysis 114
RESULTS 115
DISCUSSION 130
CONCLUSION 137
REFERENCES AND NOTES 138

CHAPTER II. Analytical Techniques 157
INTRODUCTION 158
PART I. BASIC TECHNIQUES 159
Notation 160
Mean and Standard Deviation 161

Weighting 163
Propagation of Errors 165
Least Squares 169
Chi Square 176
PART II. APPLICATIONS 179
Propagation of Errors - Specific Formulae 179
Double Reciprocal Plot (Routine DRFIT) 181
Eyring Plot (Routine EYRFIT) 183
Van't Hoff Plot (Routine VHFIT) 184
First Order Kinetics Analysis with Absorbance Data (Routine FORABS) . . 185
Guggenheim Analysis with Absorbance Data (Routine GUGABS) . . 187
Swinbourne Analysis with Absorbance Data (Routine SWNABS) . . 189
Second Order Kinetics Analysis with Absorbance Data (Routine SORABS) . . 190
PART III. NONLINEAR LEAST SQUARES 192
General Theory 193
Applications - KINPRO 195
First Order 196
Second Order 200
Pseudo-First Order Reversible 202
Second Order (Two Reactants) 210
Summary 213
REFERENCES AND NOTES 214

CHAPTER III. The Importance of Distance in Electron Transfer . . . 218
INTRODUCTION 219
THEORY 221
S & M APPROACH 239
Methods 240
RESULTS AND DISCUSSION 249
REFERENCES AND NOTES 255

PROPOSITIONS 261
I. Copper EXAFS of Non-Blue Copper Proteins - Amine Oxidases . . 262
II. Selenium Protein EXAFS 275

III. Difference EXAFS. Studies on Copper Dimers as Models for Copper Proteins . . 284

IV. A Model for the (a_3-Cu_u) Site of Cytochrome aa_3 298

V. Sepharose-Viologen, An Immobilized Reductant 304

CHAPTER I

Cytochrome aa_3

INTRODUCTION

The terminal reaction of the mitochondrial electron transport chain (*i.e.*, the actual reduction of dioxygen to water) is accomplished by cytochrome aa_3 (cytochrome *c* oxidase or ferrocytochrome $c:O_2$ oxidoreductase, EC 1.9.3.1). Cytochrome aa_3 is a multi-subunit complex containing four active sites: two hemes and two coppers. In the intact enzyme, both the coppers and the hemes are spectrally distinct. Thus, cytochrome aa_3 has four different metal centers. The enzyme is capable of accepting four reducing equivalents from its physiological reductant, cytochrome *c* and transferring them to O_2, forming H_2O. The formation of the thermodynamically unstable superoxide anion (O_2^-) may be circumvented by an initial two electron reduction to $O_2^=$ (peroxide).[1] The free energy gained in this redox reaction is stored by conversion of two equivalents of adenosine diphosphate (ADP) to adenosine triphosphate (ATP). The extreme importance of these reactions in physiological respiration has resulted in large expenditures of time and effort by many groups toward elucidation of the structure and mechanisms involved in this enzyme.

One of the more interesting questions to be answered is how the electrons are transferred within the enzyme during the catalytic cycle. The availability of a broad spectrum of inorganic redox reagents useful for probing the active sites of electron transfer metalloproteins

(*e.g.*, ref. 2) has made it possible to choose the redox reagent which should yield the most information about the electron transfer kinetics of cytochrome aa_3. The original goal of the work described herein was to find a reagent which would reduce cytochrome a^{3+} specifically so that the intramolecular ($a \rightarrow a_3$) step could be observed. Because of its size and charge, $Ru(NH_3)_6^{2+}$ was chosen for this study. The extremely complex kinetics observed for the reduction of aa_3 by $Ru(NH_3)_6^{2+}$ provide some information about the characteristics of the cytochrome aa_3 electron transfer processes. However, to fully understand the importance of such studies, a discussion of the current state of knowledge of cytochrome aa_3 is desirable.

CURRENT KNOWLEDGE

The eukaryotic cytochromes aa_3 are rather large membranous protein complexes of molecular weight ~250,000 (~120,000 per heme or per copper). The enzyme is ubiquitous but the majority of the studies to date have been performed on the enzyme from *Neurospora crassa*, *Saccharomyces cerevisiae* (bakers' yeast), or mammalian mitochondria (usually from beef heart, rat liver, or pigeon breast). By far the most work has been done on beef heart mitochondrial cytochrome aa_3. The membrane bound enzyme seems to reside (*in vivo*) on (or in) the inner mitochondrial membrane and appears to be transmembranous.[3] This type of orientation has been suggested to be favorable for vectorial transfer of electrons and perhaps protons and may have some significance for the energy coupling properties of the enzyme.

Structure

The subunit structure of beef heart aa_3 is not settled after several years of intensive investigation in several laboratories. A major obstacle is the varying electrophoretic behavior of the subunits under different conditions. Depending on the techniques used, beef heart aa_3 contains six,[3-9] seven,[10-19] eight,[20-22] nine,[23] or ten[24] subunits. These subunits are of two distinct types. The heavier subunits are lipophilic with a low content of polar residues[6,7,10,21] and appear to be of intramitochondrial biosynthetic origin[9,25] whereas the lighter subunits are more polar (hydrophilic) and are apparently

synthesized at the cytoplasmic ribosomes. This clear distinction of subunit structure has led Green to propose that cytochrome aa_3 is actually made up of two different complexes: an electron transfer complex (ETC) and an ion transfer complex (ITC) which he has claimed to have separated.[26] Prior to this work, Mahler, *et. al.*, reported the isolation of a cytochrome aa_3 fragment which had been stripped of the heaviest subunits but which apparently still maintained all of the active sites.[6,7] Thus, it appears that the disparity in subunit structural characteristics may also be reflected in their functional roles.

The anomalous behavior of subunit migration under various electrophoretic conditions mentioned above has been discussed recently in terms of the coelectrophoresis of different pairs of subunits under different conditions.[11,20,24] Recently, Capaldi and coworkers have separated ten distinct bands, but have shown that three of these bands are probably impurities.[27] They claim that the operational complex contains only seven subunits and using their nomenclature, it is possible to map the electrophoretic behavior of the subunits of beef heart aa_3 as reported in all of the work to date on this enzyme (see Table 1-1). In Table 1-1, the numbers represent the reported molecular weights of the individual subunits (in kdaltons) and the Roman numerals in parentheses reflect the subunit nomenclature used by those authors. The relationships of the several subunit nomenclature systems used to date can thus be easily deduced from a cursory glance at Table 1-1. Although, there are still minor ambiguities and the coelectrophoretic

Table 1-1. Subunits of Cytochrome aa_3 - Nomenclature, Molecular Weights, and Orientation.

Subunits										Method[a]	Reference
I[b]	II	III	IV	(a)	V	(b)	(c)	VI	VII		27
	M,C[c]	M,C	M		M				M		
	(II)										15
	cyt										
35.4[d](I)	24.1(II)	21(III)	16.8(IV)		12.4(V)			8.2(VI)	4.4(VII)	SM	10,12
35.3(I)	25.2(II)	21(III)	16.2(IV)		12.1(V)			6.7(VI)	3.4(VII)	SM	11
42(I)	27(II)	22(III)	15(Va,b)		13(VIa,c)			11(VIb)	5(VII)	SM	24
36.7(I)	24.3(II)	20.4(III)	17.3(IV)		12.3(V)			8.7(VI)	5.1(VII)	SM	18
	C		M		C,M				C,M		
44.6(I)	22.7(II)	23.5(III)	16.9(IV)		9.4(V)			7.6(VI)	4.3(VII)	SM	264
35.4(I)	24.1(II)	21(III)	16.8(IV)		12.4(V)			8.2(VI)	4.4(VII)	SM	17
			M								
39.0	27.0	21.5	15.0		12.5	10.0		9.0	6.5	SM	22
37.0(I)	26.0(II)	21.0(III)	18.0(IV)		15.5(V)	13.5(VI)		10.0(VII)	4.5(VIII)	SM	20
43.0	25.0		16.0	13.0	11.0			9.0		WO	24
38.0(I)	19.0(II)		25.0(III)	13.8(IV)	6(V)			8.6(VI)	4.3(VII)	WO	11
40.0(I)	21.0(II)		14.8(III)	13.5(IV)	11.6(V)			9.5(VI)	7.6(VII)	WO	14,34,35
a,Cu?	Cu				a						
	22.0									WO	33
	Cu										
40(I)	22.5(II)		15(III)	11.2(IV)	9.8(V)			7.3(VI)		WO	3,5
	C		M		C						
39.0(I)	21.5(II)		15.5(III)	11.5(IV)	9.5(V)			7.5(VI)		WO	8
	C		M		cyt,C						

Table 1-1. (Cont.)

Subunits									Method	Reference
40.0(I)	22.5(II)		15.0(III)	11.2(IV)	9.8(V)		7.3(VI)		WO	4
47.5(I)	20.4(II)		14.5(III)	14.5(IV)	13(V)		11(VI)		WO	6,7
42.0(I)	24.0(II)		18.0(III)	17.5(IV)	13(V,VI)		15.5(VII)	14.5(VIII)	WO	20
35.3(I)	(II)		(III)	(IV)	12.1(V)		(VI)	3.4(VII)	WO	13
a	Cu?		*a*,Cu?		Cu			Cu		
36.0(I)	28.0(II)	19.0(III)	14.0(IV)		12.5(V)	11.0(VI)	10.0(VII)	6.0(VIII)	F	21
33.0(I)	21.3(II)	19.0(III)	14.0(IV)		12.5(V)		8.5(VI)	4.9(VII)	F	11
34.0(I)	23.7(II)	19.4(III)	14.2(IV)		12.4(V)		8.2(VI)	4.4(VII)	F	16
	cyt									
45.0(I)	29.0(II)		20.0(III)	17.0(IV)	13.0(V)		10.5(VI)			9
					11.0		9.0			265
					cyt					

[a]SDS electrophoretic method used (SM, Swank-Munkres; WO, Weber-Osborn; F, Fairbanks)

[b]Roman numerals indicate the subunit nomenclature used

[c]The notation is: M-accessible to the matrix (M) side of the membrane; C-accessible to the cytoplasm (C) side of the membrane; Cu-copper containing subunit; *a*-heme *a* containing subunit; cyt-cytochrome *c* binding subunit

[d]The numbers refer to molecular weight of subunit in kdaltons

behavior of all the bands (under different conditions) is by no means exactly determined (especially in the case of the low molecular weight subunits), the general relationships in Table 1-1 are of use in helping to define the ultrastructure and active site locations in the beef heart aa_3 complex.

Several elegant labelling and cross-linking techniques have been developed recently for determination of subunit nearest-neighbor relationships, cyt c-aa_3 binding sites, and aa_3-mitochondrial membrane alignments. Also, mild denaturation and covalent heme-binding techniques have been used in attempts to localize the active sites of aa_3 within the various subunits of the complex. An overview of the progress made in the past few years may (with the help of Table 1-1) shed light on some of the details of the aa_3 protein structure.

First, it should be noted that, for most of the cases shown in Table 1-1, the relative amounts of each subunit detected are approximately equal (in the Weber-Osborn system, however, subunits II and III coelectrophorese[27]). Thus, summing the molecular weights of the subunits usually gives a minimum ("monomeric") molecular weight of ~120-140 kdaltons.[6,7,12,21,27] However, there is some question as to the active site content of such a "monomer" (*i.e.*, whether it contains one copper and one heme, or two coppers and two hemes). Love, *et. al.*, had earlier described the formation of monomers (with molecular weights of ca. 100,000) at high pH which had slightly different spectral characteristics than the dimer (at neutral pH).[28-30] They suggested that the monomer contained one of each type of active site (one heme and one copper) and that the hemes were identical

in this case. However, in a recent study, Capaldi and coworkers[27] remeasured the molecular weight of the enzyme in nonionic detergents and in bile salts. They found that the enzyme probably exists as a dimer (eight active sites) in nonionic detergents, but is dissociated into monomers in bile salts. This may explain some of the functional differences observed in these two types of media.[31]

The identity of the subunits that contain the active sites of the enzyme has eluded experimenters to date due to the rather easy dissociation of the active sites upon SDS denaturation (prior to subunit separation by electrophoresis). Recently, however, milder denaturation conditions have been used in an attempt to keep the active sites attached to their subunits. By this method, Mason and coworkers[13] have detected copper and heme associated with several subunits (see Table 1-1). The problem with such a determination is the possibility of scrambling of the active sites during denaturation and electrophoresis. This may account for their finding of partial occupancy of active sites on many of the subunits.

Since the original isolation of a potential copper-binding subunit from aa_3 by MacLennan and Tzagoloff[32] the subunit of 22,000 molecular weight has been suggested as a copper-binding subunit by several laboratories.[13,14,33] It is notable that this subunit contains several cysteines and a partial sequence displays potential copper-binding sites.[33] Other work has supported the assertion that the subunits of 12,000 and ~40,000 molecular weights are the heme subunits of aa_3[13,14,34,35]

and recently the amino acid sequence of the 12,000 dalton subunit has been determined.[36] (All of these results are also displayed in Table 1-1.)

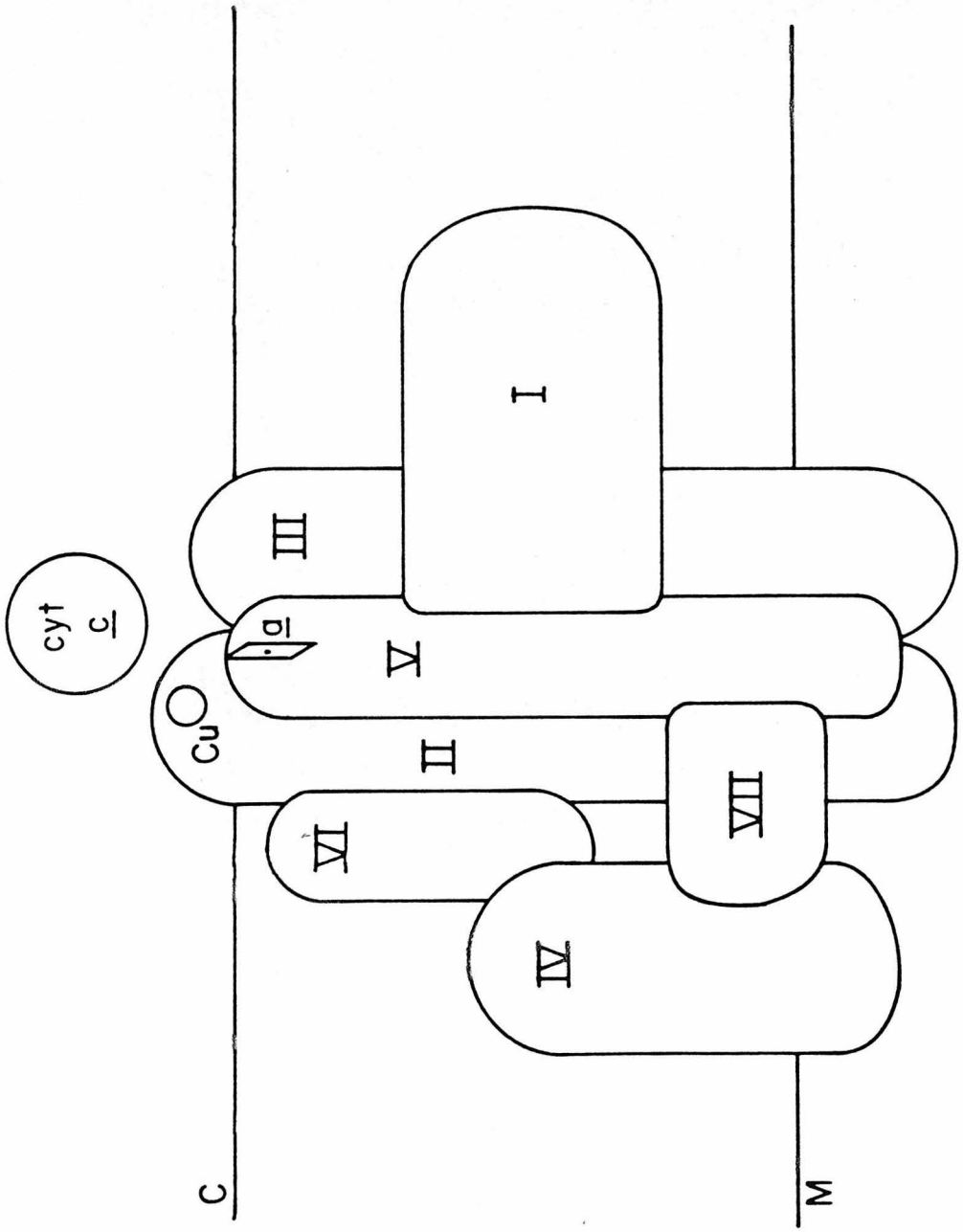
Of importance in the determination of the subunit location of the hemes in cytochrome aa_3 is the identity of the subunit(s) which binds cytochrome *c*. Since it is established that cytochrome *c* binds electrostatically to aa_3 in the region of heme *a*, this information may provide a valuable clue as to the overall architecture of the aa_3 complex. Various cross-linking techniques have been used to bind cytochrome *c* covalently to the intact aa_3 complex, after which the complex was dissociated and the subunits separated by electrophoresis.[8,15,16,19,37] As can be seen from Table 1-1, the results of such experiments are strongly dependent on the nature of the bifunctional cross-linking agent and other experimental parameters. These cross-linking techniques have also been used to determine nearest-neighbor relationships between the subunits of aa_3. Two studies by Briggs and Capaldi[12,15] have identified the following adjacent pairs of subunits: I-V, II-V, III-V, V-VII, II-VI, IV-VI, IV-VII.

The configuration of the beef heart aa_3 complex in the membrane has been examined by the use of various membrane-impermeable radioactive labelling agents as well as cytochrome aa_3 antibodies (and antibodies to individual subunits).[5,8,17,18] By making use of the inverted nature of the inner mitochondrial membrane in submitochondrial particles, these studies have been able to label specific subunits which are exposed to either (or both) the M (matrix) side and/or the C (cytoplasm) side of the inner membrane. Studies of label-binding to isolated aa_3 are then

used to rule out the possibility of a subunit being exposed but not binding the label. Similar techniques have been used by Racker and coworkers[3,38] to demonstrate that cytochrome *a* is accessible to the same side of the membrane as cytochrome *c* (*i.e.*, the C side) and that cytochrome a_3 is accessible to the same side of the membrane as coupling factor 1 (ATPase). These results are also summarized in Table 1-1 (using Racker's notation of membrane-sidedness - M and C).

All the above results (as summarized in Table 1-1) were utilized to create a partial description of the disposition of the cytochrome aa_3 complex in the mitochondrial membrane. This is presented in Fig. 1-1 (*cf.*, ref. 39). This picture is obviously not unique in all aspects, but it seems that several tentative conclusions can be drawn from the available data: (1) A subunit with a molecular weight around 12,000 daltons (V) appears to be a central "core" of the aa_3 complex, being "nearest neighbor" to many of the other subunits;[5] (2) This subunit also appears to contain a heme prosthetic group and is accessible to the M and C sides[18,27] of the membrane. (A recent study using transglutaminase to label isolated cytochrome aa_3 found that this subunit was labelled first.[22]); (3) A subunit with a molecular weight around 22,000 daltons (II) probably is a copper-binding subunit; (4) Subunit II is accessible to the C side (and probably also the M side) of the membrane; (5) The cytochrome *c* crosslinking studies (except for one[19]) show that these subunits may both bind cytochrome *c*. Thus, the 12,000 dalton subunit (V) could be the domain of the cytochrome *c* oxidase complex referred to as cytochrome *a*. The copper of subunit II may then

Fig. 1-1. Schematic representation of proposed orientation of cytochrome aa_3 subunits across the inner mitochondrial membrane. See text for details.


cyt c
Cu
a
I
III
IV
II
VII
VI
IIA
IV
C
M

be Cu_d (the "detectable" copper site associated with heme *a*); (6) Subunit I (the heaviest at ~40 kdaltons) is probably buried within the membrane, inaccessible from either side.[5,8,18,27,39] However, subunit I has also been implicated as a heme binding subunit,[13,34,35] which does not seem to agree with the accessibility of a_3 to the M side of the membrane[3] (however, there is some evidence for a_3 being buried in some type of "pocket"[40-42]); (7) There is some evidence that the smaller subunits IV and VII may be exposed to the M side of the membrane,[5,8,17,27] but Seiter and coworkers have implicated these very subunits in the binding of cytochrome *c*.[19] (There is one report of subunit VII being available to the C-side of the membrane.[18]); (8) Subunit III appears to be accessible to both sides of the membrane;[27] (9) Subunit VI may[3,5,8] or may not[27] be accessible to the C-side of the membrane.

Recently, Chance and coworkers have suggested a much more detailed model for the arrangement of cytochrome aa_3 subunits across the membrane.[43,44] This model places all of the active sites near the C-side of the membrane and accounts for the accessibility of a_3 from the M-side by postulating an "O_2-channel", extending through the membrane to the a_3 site (which is placed in subunit V where heme *a* was placed in Fig. 1-1). There is some circumstantial evidence for the existence of such a "gas channel". CO binding studies have shown that CO may have one or more intermediate binding states[40-42] and when bound, the CO infrared band is very narrow, indicating a restricted environment, not accessible to the solvent medium.[45,46] The existence of such intermediate states may also explain some of the initial O_2-intermediates observed

in low temperature studies (*e.g.*, ref 47). The above model[43] places heme *a* in the same subunit as the Cu and assumes that this is also the cytochrome *c*-binding subunit. A gated proton channel is also incorporated into the model to explain the energy coupling (or respiratory control) properties of cytochrome aa_3. At present, it is probably not possible to decide on the best representation of the detailed structure of the cytochrome *c* oxidase complex. It will be of interest to re-examine such models in the light of future structural work.

It should be emphasized that, until higher resolution electrophoretic procedures (such as two-dimensional gels) become more widely used, any tentative conclusions about the arrangement of the cytochrome aa_3 complex in the mitochondrial membrane will remain mostly speculative. Perhaps future studies on Mahler's four-subunit enzyme[6,7] or on the "electron transfer complex" of Green and coworkers[26] will help shed light on this interesting problem.

Active Sites

The existence of four active sites in cytochrome aa_3 (as well as in other O_2-reducing enzymes, such as laccase) is intriguing since the complete reduction of O_2 to $2H_2O$ requires four electrons. The ability of cytochrome aa_3 to accept four electrons per molecule has been known for some time.[48] However, the fully oxidized (resting) enzyme does not exhibit the expected characteristics of two ferric hemes and two oxidized coppers. Also, varying amounts of the four active sites become detectable at intermediate oxidation states of the enzyme. The answers

to these questions will probably yield the clues necessary to reveal the detailed electron transfer mechanism(s) involved in this enzyme.

Electronic Absorption Spectrum. One of the main problems encountered in attempting to investigate specific active sites in cytochrome aa_3 is the difficulty in assigning spectral features to individual metal centers. The resting (fully oxidized) enzyme has a Soret maximum at ~420 nm and a weak absorption in the α-region (at ~600 nm). Upon reduction, the Soret increases in intensity and moves to λ_{max} ~444 nm and the α-band increases several-fold in intensity with a shift of the band maximum to ~605 nm. A weak band in the near-infrared region (~830 nm) can be seen in the resting enzyme, but disappears upon reduction. The majority of work with this band has attributed it to copper absorption (apparently, only Cu_d). However, this band may also contain a contribution from heme.[49,50] Recently, a band at ~655 nm (which becomes more apparent in reflectance spectra[51,52]) has been suggested to be associated with cytochrome a_3.[51,53,54] Even more recently, a temperature-induced band (at low temperatures) occurring at ~666 nm (and unassociated with the 655 nm band) was observed in the presence of CO or O_2 and suggested to be associated with the "binding" of gas in a "pocket" near the heme of cytochrome a_3.[42] Further studies will be required to establish the exact nature of this spectroscopic feature.

Evidence from many areas (*e.g.*, spectra of half-reduced liganded forms, biphasic kinetics, etc.) indicates that both the Soret and α transitions have contributions from both cytochrome a and cytochrome a_3.

The accurate separation of spectral features corresponding to the individual cytochromes is made even more difficult (if not impossible) by the existence of interactions between the hemes such that the properties of one heme are dependent upon the oxidation state or ligation state of the other heme. The spectral contributions to the two major electronic absorption bands and the exact nature and extent of the heme-heme interactions form the basis for the major differences between the various postulated hypotheses on cytochrome aa_3. Since comparison of these various hypotheses (and predictions derived from them) can be a determinant in selection of the important experimental work to be done, a brief discussion of their major points seems in order.

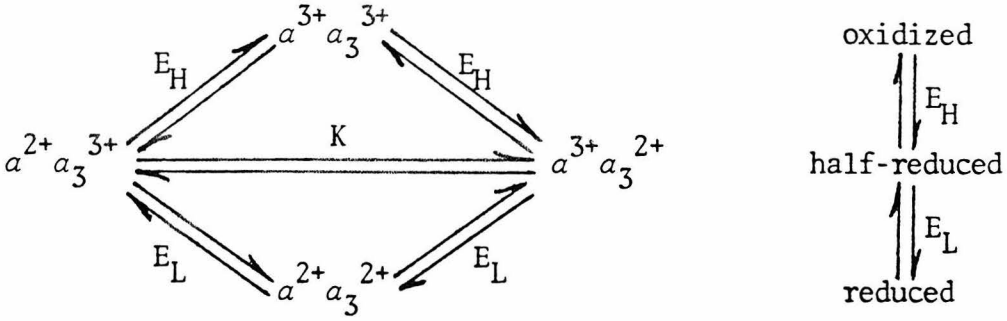
As pointed out by Wilson and coworkers,[55] there are basically two points of view about the nature of cytochromes a and a_3 from which the hypotheses stem: (1) cytochromes a and a_3 are chemically distinct entities with different properties; and (2) cytochromes a and a_3 are chemically indistinguishable but strongly interacting (by heme-heme interactions as discussed above). The classical hypothesis takes the first point of view and was originated by Keilin and Hartree in their elegant early work on cytochrome c oxidase.[56] They pointed out the existence of two separate a-type cytochromes, and assigned the label a_3 to the cytochrome which combined with ligands (such as CO, cyanide, O_2, etc.). The classical hypothesis holds that a and a_3 are chemically, spectroscopically, and perhaps structurally distinct, Keilin and Hartree asserting that the reduced α-band at 605 nm was due mainly to cytochrome a with little or no contribution from a_3. The classical hypothesis found

widespread acceptance[53,57] since the difference spectrum of a^{2+}-a^{3+} (obtained upon ligand binding to a_3, "locking" a_3 into one oxidation state) appeared very similar to the total ($a^{2+}a_3{}^{2+}$-$a^{3+}a_3{}^{3+}$) difference spectrum. This finding suggests that $a_3{}^{2+}$ contributes very little to the reduced α-band, but suffers from the criticism that the binding of a ligand to a_3 may have changed the properties of a due to heme-heme interactions. Specifically, a heme-heme interaction affecting the spectral properties of the hemes is required for this criticism to be valid.

The 50/50 hypothesis[53] was developed by Wilson and coworkers[58] as an explanation of their potentiometric titration results. Upon potentiometric reduction of native cytochrome aa_3, they observed two (potentiometrically) separable components which contributed approximately equally (50/50) to the absorption changes at both 605 nm and 445 nm. Thus, the 50/50 hypothesis assumes that a and a_3 (in their "free" forms) contribute equally to the α-band and that ligation of a_3 causes (through heme-heme interaction) the spectrum of a to change such that it contributes relatively more to the α-band. This extinction coefficient change of cytochrome a must be ~70%[58] (at 605 nm) to account for the observed differences. As pointed out by Wikström, *et. al.*,[53] the binding of different ligands required different amounts of proposed extinction coefficient changes and even led to the proposal that azide was unique in binding to cytochrome a, not a_3.[58-61] These discrepancies caused Wikström, *et. al.*[53] to suggest that the data could be better interpreted in terms of a model in which heme-heme interactions affect only the

redox potentials of the sites and not the spectral characteristics. This suggestion was originally made by Nicholls and coworkers[62] and led to the development of the so-called neo-classical hypothesis.[53]

The neo-classical hypothesis still assumes (as in the classical hypothesis) that a and a_3 are chemically and spectrally distinct. However, in this hypothesis, the two cytochromes have very similar reduction potentials in the native enzyme. Heme-heme interactions are involved in lowering the reduction potential of one heme upon reduction of the other (a sort of negative cooperativity - the reduction of one site makes the other site harder to reduce). Thus, the first heme reduction establishes a mixture of the two (distinguishable) half-reduced states: $a^{2+}a_3{}^{3+}$ and $a^{3+}a_3{}^{2+}$. Then, the total absorbance change (at any particular wavelength) is dependent on the ratio of the two half-reduced species formed. For example, the potentiometric titration results of Wilson, *et. al.*,[58] can be explained if equal amounts of the two half-reduced species are present. The reduction of native cytochrome aa_3 under the neo-classical hypothesis would occur by the following scheme:



(The two half-reduced forms may be[53,62] but are not required to be[62-63] in equilibrium. In the latter case, K just refers to the relative amounts of the two formed.) The differences observed when a_3 binds a ligand can be handled in the neo-classical hypothesis by postulation of potential shifts (due to heme-heme interactions) resulting in different values of K (or different relative amounts of the two half-reduced species being formed).[53]

The second major point of view mentioned above (*i.e.*, that the hemes are indistinguishable in the native enzyme) seems to be a result of the finding by van Gelder and coworkers that (in the absence of cytochrome *c*) the two hemes reduce with the same potential under reductive titrations.[64-66] Thus, the separation of the heme potentials (*i.e.*, the only difference between the hemes) is triggered by the presence of some cytochrome *c*. They also find (in concord with the 50/50 hypothesis) that the hemes contribute about equally to the absorbance in the Soret and at the α-band (in the absence or presence of cytochrome *c*).[65,66]

The major difference between the two types of hypotheses is the relative contributions to the α-band of cytochromes *a* and a_3 (in the native enzyme). Perhaps an examination of the published attempts to separate the *a* and a_3 spectral contributions can shed some light on this problem. Most early attempts at measuring separate difference spectra for *a* or a_3 involved the use of a ligated form of the enzyme to achieve a stable half-reduced (mixed valence) state. Thus, Vanneste has used appropriate difference spectra of cyanide-inhibited derivatives

to give "a^{2+}-a^{3+}" and "a_3^{2+}-a_3^{3+}" difference spectra.[67] These show that cytochrome a is characterized by an oxidized Soret peak at ~425 nm, a reduced Soret peak at ~444 nm, and a reduced α peak at ~603 nm, while cytochrome a_3 has an oxidized Soret peak at ~412 nm, a reduced Soret peak at ~444 nm, and a reduced α peak at ~604 nm. In these spectra, a^{2+} contributes ~80% to the reduced α peak. The mixed valence-sulfide derivative ($a^{2+}a_3^{3+}\cdot H_2S$) exhibits an α-band with an intensity nearly identical to the α-band in the reduced enzyme ($a^{2+}a_3^{2+}$)[68] indicating that the α-band can be fully accounted for by a^{2+}. The formate mixed-valence state (actually a steady state[69]), may be an even better form to use for these comparisons since the formate-bound form of a_3 is still high spin (unlike the cyanide form).[70] The "a_3^{2+}-a_3^{3+}" spectrum (obtained as the $a^{2+}a_3^{2+}$-$a^{2+}a_3^{3+}\cdot$HCOOH difference) indicates that a_3 has an oxidized Soret peak at ~412 nm, a reduced Soret peak at ~445 nm and a very weak reduced α peak at ~607 nm.[70]

Perhaps a more reliable means of determining individual cytochrome difference spectra is by examination of kinetic difference spectra in cases where the kinetics are clearly biphasic. The reduction of aa_3 by Cr^{2+} [71] was biphasic and the kinetic difference spectra were interpreted as exhibiting initial (fast) reduction of cytochrome a, followed by a slower reduction of cytochrome a_3. The cytochrome a spectrum showed a Soret band at ~425 nm (oxidized), ~443 nm (reduced) and a reduced α band at ~605 nm. Cytochrome a_3 had a Soret band at ~417 nm (oxidized), ~441 nm (reduced) and a reduced α band at ~585 nm. The intensity of the reduced α band of a^{2+} was about four times the intensity of the a_3^{2+} α band. An examination of the $Fe(CN)_6^{4-}$ inhibition of the activity of

cytochrome aa_3[72] indicated that in the $Fe(CN)_6^{4-}$-treated form, cytochrome a was reduced and cytochrome a_3 was oxidized. The appropriate difference spectra (involving this mixed-valence state) showed that a had a Soret band at ~425 nm (oxidized), ~444 nm (reduced) and a reduced α peak at ~601 nm (contributing ~80% of the total absorbance change). Cytochrome a_3 had a Soret at ~415 nm (oxidized), ~443 nm (reduced) and a reduced α peak at a wavelength somewhat greater than 601 nm (with a ~20% contribution to the total absorbance change). Perhaps the most complete study involved the trapping of the half-reduced (with dithionite) native enzyme at low temperatures.[73] Since the dithionite reduction was biphasic, the reaction could be stopped after one heme was reduced (but while the other heme was mostly oxidized). Low temperature difference spectra then indicated that cytochrome a had a Soret with the oxidized maximum at ~426 and a split reduced maximum (at 442 and 447 nm). The reduced α band was at ~601 nm. Cytochrome a_3 had a Soret at ~412 nm (oxidized), ~444 nm (reduced) and a reduced α band at ~604 nm. The a_3^{2+} α band was considerably less intense than the a^{2+} α band and the experimental method caused this spectrum to be contaminated with ~10% a^{2+}.[73] Thus, most of the reduced α band could be attributed to cytochrome a.

The simplest conclusion to be drawn from the above studies is that cytochrome a has a Soret band at ~425 nm (oxidized), ~444 nm (reduced) (split to 447, 442 nm at low temperatures) and a reduced α band at ~604 nm which accounts for $\geq$80% of the reduced minus oxidized absorbance difference at this wavelength. Cytochrome a_3 has a Soret

band at ~415 nm (oxidized), ~444 nm (reduced) and a much less intense reduced α band at a less well-determined position (585-605 nm). It seems reasonable then to prefer hypotheses that ascribe most of the absorbance change at 605 nm to a^{2+}. It is suggested that the majority (if not all) of the experimental observations can be predicted by a version of the neo-classical hypothesis that treats cytochromes a and a_3 as chemically, spectroscopically, and kinetically distinct, but thermodynamically similar.

Liganded Derivatives. Although no major spectral changes due to heme-heme interactions need be postulated, small shifts in the absorption bands have been seen upon addition of ligands to cytochrome a_3.[74-76] Similar spectral shifts can be seen upon energization of intact mitochondria (by addition of ATP) and these differences probably represent conformational changes linked to heme spin state changes (*e.g.*, see refs. 53, 77-79). Because of the importance of the various liganded derivatives of cytochrome aa_3 for aiding elucidation of the active site characteristics, a brief overview of the important derivatives is deemed appropriate.

Carbon Monoxide. The binding of CO to the reduced form of cytochrome aa_3 (and its inhibition of the activity) was first reported by Keilin and Hartree in their elegant initial studies of the cytochromes in the respiratory chain.[56] The binding site has since been shown to be a heme[80] and, although initial infrared work was interpreted as evidence for the binding of one CO per heme,[81] this has been redone and it is now clear that the stoichiometry is one CO per two hemes.[46,80,82-84] By definition,[56] this binding site is assigned as the heme iron of cytochrome a_3.

CO preferentially binds to the reduced cytochrome (a_3^{2+}) as shown by oxidative titrations of the reduced aa_3-CO complex, in which it is difficult to reoxidize the a_3^{2+}-CO moiety [63,85] and by reductive titrations in the presence of CO, in which the a_3^{2+}-CO moiety is completely formed before a^{3+} or Cu_d^{2+} begin reducing.[86,87] This can be explained by a shift of the redox potential of a_3 (upon CO binding) to higher potential[63] by as much as 100 mV.[85,88-90] It has also been shown that the CO derivative titrates as an n=2 species[88,89,91] and that binding of CO requires the acceptance of two electrons by the enzyme.[92] Thus, a_3 and one other electron acceptor must be reduced before CO will bind to the enzyme. After addition of two electrons per enzyme molecule (aa_3) in the presence of CO, a^{3+} and Cu_d^{2+} can be shown to be still oxidized[87,92,93] so that Cu_u must be the second electron acceptor which must be reduced in this CO derivative (which has been called the mixed valence-CO derivative). The possibility that CO bridges heme a_3 and Cu_u is not consistent with the frequency of the C=O stretch in the infrared.[45]

Binding of CO to reduced cytochrome aa_3 causes a shift in the α band to the blue from 605 nm to 590 nm.[56,94,95] The Soret band shifts from 448 nm to 452 nm.[56] There is also a band at ~605 nm[74,95] which is not present in the mixed valence-CO derivative[95,96] and thus can probably be assigned to a^{2+}.[53] Thus, the 590 nm peak is due to a_3^{2+}-CO.[53] These assignments are not firm since there is obviously some heme-heme interaction occurring, the exact nature of which is open to debate (see below). Recently, a new CO-induced cytochrome aa_3

derivative (made by mixing CO with oxidized aa_3 for a few minutes) has been reported[97] having absorption bands at 606, 565 and 435 nm and which only slowly decays to the normal mixed valence-CO derivative. The characteristics of this derivative have not yet been fully examined.

CO is a fairly high affinity ligand for a_3, being able to displace azide but not cyanide[98] (see below). The dissociation constant has been measured as 4.6×10^{-7} *M* in mitochondria[82] and 3.5×10^{-7} *M* for reduced isolated aa_3.[99,100] These compare well with the measured $K_i = 3.2 \times 10^{-7}$ *M* (for strictly competitive inhibition[88] of the O_2 reaction).[101] The "on" and "off" rate constants have been measured as 7.0×10^4 M^{-1} s^{-1} and 2.5×10^{-2} s^{-1} in isolated cytochrome aa_3.[100] The "off" rate constant for photodissociation has been measured as $\sim 3 \times 10^{-3}$ s^{-1}.[102] The binding of CO to the mixed valence enzyme was earlier reported to be kinetically different from the binding to the reduced form[96] but more recent results have shown that the binding is independent of the oxidation state of cytochrome *a*.[94] In mitochondria, the binding of CO is accelerated by addition of ATP (energization)[103] thus suggesting a link between a conformational change at cytochrome a_3 and the energization state of the mitochondria (possibly related to energy coupling or respiratory control - see below). A similar effect on the O_2 reactions of cytochrome aa_3 due to energization of the mitochondrial membrane has been noticed.[104]

In both the fully reduced aa_3-CO complex and the mixed valence-CO complex, both hemes are low spin (at room temperature)[105,106] and since unliganded a_3^{2+} is known to be high spin (see below), CO must

induce a high to low spin state conversion upon binding to a_3. The a_3^{2+}-CO moiety is thus diamagnetic and does not contribute to the electron paramagnetic resonance (epr) spectrum. However, addition of CO to a partially oxidized (with oxidants other than O_2) aa_3 sample causes an immediate change (<5 milliseconds) of the rhombic high spin heme signal (attributed to a_3^{3+} - see below) to a new high spin heme signal with greater rhombicity which decays (to the normal non epr-active state) only after a much longer time.[107] This type of epr signal is also observed upon photodissociation of CO at low temperatures[60,98,108-110] and may indicate an intermediate state of ligand capture (before binding). Such intermediate states have been suggested to be the cause of the non-Arrhenius temperature dependence of CO-binding kinetics[40] and may be attributable to the existence of a hindered site for heme a_3 in some type of protein "channel" as mentioned in the previous section. The very narrow infrared band of a_3^{2+}-CO has been interpreted as meaning that the binding site is inaccessible to the solvent medium.[46] A recent study of CO photodissociation and recombination kinetics at low temperatures has been interpreted as evidence for the existence of an intermediate in the rebinding step[111] but this result has been challenged by Chance, *et. al.*,[102] as being due to the neglect of photodissociation by the monitoring beam.

The photodissociation of CO by light (mentioned above) was first exploited by Chance and coworkers[112] as a means of generating unliganded a_3^{2+} in the presence of O_2 to study the O_2 reactions of cytochrome aa_3.[96,113] They have since generated a large body of experimental

data on oxygen intermediates of cytochrome aa_3 which have been invaluable in helping elucidate the mechanisms involved in this enzyme (*e.g.*, see refs. 43, 47, 114, 115). One interesting aspect of the CO photodissociation phenomenon is that the reaction appears to be irreversible below ~100 K[106] whereas most other heme protein-CO complexes are reversible to much lower temperatures.[116] This unique feature of the a_3^{2+}-CO complex may be related to the unique binding features mentioned above (*e.g.*, the narrow infrared band).

Cyanide. As one of the classical respiratory poisons shown to operate on cytochrome a_3,[56] cyanide has been extensively exploited as a ligand and inhibitor of cytochrome aa_3. It has been shown to bind to cytochrome aa_3 (in oxidized, reduced, or intermediate oxidation states in mitochondria or isolated samples) in a ratio of one molecule of cyanide per two hemes.[117-120] The pH dependence of inhibition of oxygen reduction has suggested that the actual bound species is the protonated HCN[74] and this will be assumed as the active species from here one. Cyanide titrations show that 50% of the heme of cytochrome aa_3 is reactive toward O_2[121] and thus, HCN is assumed to bind to cytochrome a_3 (as originally denoted by Keilin and Hartree[56]).

The binding of HCN to oxidized cytochrome aa_3 is two orders of magnitude slower than binding to the reduced enzyme,[117,118,122] (as exhibited by the "on" rate constants[100,122]) but the dissociation constants ($K_d^{red} \approx 5 \times 10^{-4}$ *M*, $K_d^{ox} \approx 1 \times 10^{-6}$ *M*)[100,119,122] show that the oxidized a_3^{3+}·HCN complex is over two orders of magnitude stronger than the reduced a_3^{2+}·HCN complex. This oxidation state-dependent binding should be reflected in

an increase of over 100 mV in the redox potential of a_3-HCN over free a_3 (this has yet to be studied in detail) and thus an increased stability of a_3^{3+}·HCN to reduction. The latter effect has been observed[123,124] and a "half-reduced" cyanide derivative exists[125] with the redox state $a^{2+}Cu_d^{+}Cu_u^{+}a_3^{3+}$·HCN[123] or $a^{2+}Cu_d^{+}Cu_u^{2+}a_3^{3+}$·HCN.[124] The kinetics of HCN binding to reduced cytochrome aa_3 are clearly bimolecular,[117,118,122] but binding of HCN to the oxidized enzyme has been reported to be [CN^-]-independent[122] (although this is not universally observed[120,126]). A [CN^-]-independent binding suggests a rate-limiting conformational change prior to binding. In this regard it is interesting to note that HCN displacement of azide from the oxidized azide complex proceeds faster than HCN binding to unliganded oxidized aa_3[117,118] suggesting that azide may have "prepared" the enzyme for ligation.

The binding of HCN to reduced cytochrome aa_3 can be detected by a shift of the Soret band from 448 to 452 nm[56] whereas the oxidized aa_3-cyanide derivative has bands at 598, 545 and ~428 nm.[95,125] The kinetics of reduction of the oxidized aa_3-cyanide derivative show an intermediate species with bands at 415, 445, and 605 nm which eventually decays to the normal "half-reduced" species with a Soret band at 430-435 nm and α-band at 605 nm (and nothing at 415 nm).[125] (This intermediate may be a result of heme-heme interactions - see below.) Both the a_3^{2+}·HCN and a_3^{3+}·HCN moieties contain low spin hemes as observed by magnetic circular dichroism (mcd),[63,105] by epr (a_3^{3+}-HCN exhibits a signal at g~3.6).[52,107,127,128] and by magnetic susceptibility.[63,129-131] In particular, recent temperature-dependent magnetic

susceptibility measurements[63,130,131] have shown that the reduced aa_3-cyanide derivative is completely diamagnetic and that the oxidized aa_3-cyanide derivative consists of contributions from magnetically isolated cytochrome a^{3+} (low spin, S = 1/2) and Cu_d^{2+} (S = 1/2), and an antiferromagnetically coupled (a_3^{3+}(low spin)-Cu_u^{2+}) HCN site (*i.e.*, S' = 0 ground state with -J~40 cm^{-1}).

As mentioned above, HCN is a strong ligand for a_3^{3+}. In addition to being able to displace azide,[117,118] HCN cannot be displaced by CO[98] (nor any of the weaker ligands, such as fluoride, etc.). Sulfide can displace very little[132] if any[74] HCN, but HCN cannot displace sulfide either.[74] Thus, HCN and sulfide are the strongest ligands yet observed for a_3^{3+}. It should be noted that HCN, azide, sulfide, and bisulfite have all been shown to compete for the same binding site.[132,133]

The cyanide inhibition of cytochrome *c* oxidase activity can be observed at much lower cyanide concentrations than required for binding to either the reduced or oxidized enzyme[121] and this is exhibited by inhibition constants (K_i) which are lower than the K_d's quoted above (*e.g.*, $K_i = 2 \times 10^{-7}$ *M* for noncompetitive inhibition of O_2 reduction,[101] K_i' (based on HCN as inhibiting species) $\approx 7 \times 10^{-8}$ *M*[74]). In other studies, cyanide-inhibited turnover was found to be biphasic[134] and also noncompetitive toward ferrocytochrome *c* (cytochrome c^{2+}) oxidation.[117,118] All of these results suggest that HCN can bind to intermediate oxidation states of cytochrome aa_3 (*e.g.*, under turnover conditions) more readily than to reduced or oxidized forms.[121,134,135] HCN has been shown to bind more readily to various (poorly defined) "oxygenated" species as

well.[135,136] Kinetic studies of cytochrome c^{2+} reduction of the oxidized aa_3-cyanide derivative have shown that reduction of a^{3+} and Cu_d^{2+} are unaffected by cyanide, whereas further reduction (of a_3^{3+}-HCN) is much slower than for free a_3^{3+} [117,118] or not observed at all.[137] This suggests that cytochrome a_3^{3+} is more readily bound to HCN when cytochrome a is reduced than when it is oxidized.[125] This is yet another demonstration of heme-heme interaction in cytochrome aa_3.

The affinity of cyanide for "oxygenated" or "activated" intermediates is also exhibited in some recent epr studies by Beinert and coworkers.[52,107] In these studies, cyanide was shown to react immediately (within 10 msec) with the species responsible for intermediate rhombic high spin heme (g~6) epr signals (attributed to high spin a_3^{3+}) generated by partial oxidation of reduced aa_3 (with oxidants other than O_2). The familiar g~3.6 low-spin a_3^{3+}·HCN signal was formed immediately[52,107] indicating rapid binding of cyanide to this intermediate "activated" form of a_3^{3+}.

Azide. As in the case of cyanide, azide was originally classified as a respiratory inhibitor specific for cytochrome a_3 by Keilin and Hartree.[56] Although a more weakly binding ligand than cyanide, these two inhibitors have many properties in common. Circular dichroism (cd) has been used to demonstrate that azide- and cyanide-binding are conformationally similar, yet very different from CO-binding.[138] Azide competes for the same binding site as cyanide, sulfide, and CO[98,132,133] and is displaced by all of these ligands.[98,118,132,139] Thus, despite earlier suggestions that azide might bind cytochrome a^{2+},[58-61,73,139] it appears that, like cyanide, azide has an affinity

for a_3^{3+} with stoichiometry of one azide per enzyme molecule.[120,140] HN_3 has also been suggested to be the bound species[140,141] as with cyanide. Addition of azide to respiring mitochondria results in spectral shifts which have been interpreted as electron redistribution to make a more reduced and a_3 more oxidized.[139,142] This suggests a greater affinity of HN_3 for a_3^{3+} than for a_3^{2+} (in analogy with the cyanide derivatives). It has since been demonstrated (by epr) that the a_3^{3+}-HN_3 moiety is rather difficult to reduce.[143] The oxidized aa_3-HN_3 derivative has a Soret peak at 421 nm (shifted from 424 nm)[95,125,140] and an α peak at ~600 nm (blue-shifted).[74,95,144] However, these spectral shifts appear to be somewhat dependent on the azide concentration.[144] Reduction of the oxidized aa_3-HN_3 derivative (apparently to a partly-reduced state) causes minor blue shifts in the a^{2+} α-band[125,139,142] to ~602 nm[74] as well as small shifts in the a_3^{3+}-HN_3 Soret.[125,144] These spectral shifts are not nearly as well-defined as in the cyanide derivatives.

The a_3^{3+}-HN_3 moiety is characterized by a new heme signal in the epr at g~2.9, 2.2, 1.67[86,143,145] (as well as a minor component at g~2.75[86]). Thus, a_3 is a ferric low spin heme in this derivative. As in the case of cyanide, azide prevents the formation of the intermediate high spin heme signals at g~6 during reductive titrations.[143,145] However, the abolishment by azide of the rhombic high spin heme signals (at g~6) observed upon partial oxidation of reduced aa_3 (by oxidants other than O_2) is much slower than the analogous cyanide reaction.[52,107] Only after several hundred milliseconds, does an azide-induced low spin

heme signal (at g~2.77, 2.2, 1.76) replace the intermediate high spin heme signals , and this initial signal then decays to the "normal" a_3^{3+}-HN_3 signal (g~2.9, 2.2, 1.67) at an even slower rate.[52,107] This apparent biphasic binding may be analogous to the azide-binding mechanism exhibited by resting aa_3. The binding kinetics consist of an initial fast bimolecular, pH-dependent reaction, followed by a slower pH-independent, $[N_3^-]$-independent phase:[141,146]

$$\text{oxid. } aa_3 + \text{az} \underset{k_{off}}{\overset{k_{on}}{\rightleftharpoons}} a_3^{3+} - \text{az} \underset{k_{-2}}{\overset{k_2}{\rightleftharpoons}} (a^{3+} - \text{az})^*$$

$$K_d = k_{off}/k_{on}$$

in which $(a_3^{3+} - \text{az})^*$ is considered to be related to $a_3^{3+} - \text{az}$ by some form of conformational equilibrium (k_{-2} is assumed small). At pH's around 7, the constants have been measured as follows: basing the calculations on total azide gives K_i (or K_d) $\approx$ (2-3) x 10^{-5} M,[100,101,140,141] k_{on} = 4.6 x 10^3 M^{-1} s^{-1},[100,140,141] k_{off} = 0.3-0.4 s^{-1},[100,140,141] $k_2 \approx 0.02$ s^{-1};[141,146] basing the calculations on HN_3 as the bound species, $K_i' \approx 10^{-7}$ M,[74] $k_{on} \approx 2 \times 10^6$ M^{-1} s^{-1}.[100,140,141] The existence of the k_2 step has been interpreted as evidence of a hindered binding site.[141,146] Azide has also been shown to be an uncompetitive inhibitor of O_2 reduction.[101]

Sulfide. Sodium sulfide (Na_2S) was one of the respiratory inhibitors shown by Keilin and Hartree[56] to react much like cyanide with

aerobic heart muscle preparations. Like cyanide it is a slow-binding inhibitor, but it is specific for oxidized cytochrome a_3 (a_3^{3+}).[73] Sulfide (or hydrogen sulfide) has been shown to compete for the same binding site as azide and cyanide[74,132] and binds with approximately the same affinity as cyanide[68] since cyanide cannot displace sulfide[74] and sulfide can displace cyanide only slightly[132] if at all.[74] However, sulfide will completely displace azide.[132]

The binding of sulfide to a_3^{3+} causes a spectral shift of approximately 1 nm (to the blue) of the a^{2+} α-band.[68,74,125,144] This mixed valence-sulfide derivative ($a^{2+}a_3^{3+}$-sulfide), however, differs from other liganded derivatives in exhibiting an intensified Soret at 445 nm.[74] This was originally suggested to be due to some S → Fe LMCT character, but has since been demonstrated to be due to the overlap of the a^{2+} and a_3^{3+}-sulfide Soret bands.[144] The blue shift of the a^{2+} α-band is similar to the shift seen in the cyanide derivative and suggests that a_3^{3+} undergoes a high spin to low spin transition upon sulfide binding.[144] Sulfide binding is accompanied by the appearance of a new low-spin heme epr signal (g = 2.54, 2.23, 1.87)[132] which is assignable to the a_3^{3+}-sulfide moiety. Some decrease in the normal (a^{3+}) low spin heme signal at g~3 and in the copper signal at g~2 is observed indicating that sulfide has the capability of acting as a reductant.[132,147] Other changes in the g2 signal observed by Seiter and coworkers[147] were interpreted as a new copper signal attributable to Cu_u^{2+}. However, Beinert and coworkers were unable to reproduce this observation.[107] As with cyanide and azide, sulfide is reactive

toward species (probably a_3^{3+}) responsible for the intermediate rhombic high spin heme signals observed after partial reoxidation of reduced cytochrome aa_3 (with oxidants other than O_2). Addition of sulfide immediately causes these signals to disappear with the formation of a new low spin heme signal at g = 2.77, 2.23, 1.71 which reverts to the normal a_3^{3+}-sulfide signal mentioned above.[107]

Other than this, sulfide has been shown not to prefer intermediate oxidation states of aa_3 (like cyanide) since sulfide binding is dependent on the oxidation state of cytochrome a_3 only.[74] The dissociation constant for a_3^{3+}-sulfide has been reported to have an upper limit of 10^{-7} *M*[74] and the "on" and "off" rate constants have limits of: $k_{on} \geq 10^4\ M^{-1}\ s^{-1}$, $k_{off} < 10^{-3}\ s^{-1}$.[68] Sulfide-inhibited cytochrome c^{2+} oxidation can be described by: $k_{on} = 1.5 \times 10^4\ M^{-1}\ s^{-1}$, $k_{off} = 6 \times 10^{-4}\ s^{-1}$, K_i (based on total sulfide) $\approx 2.4 \times 10^{-7}\ M$, K_i' (based on H_2S as active species) $\approx 2 \times 10^{-8}\ M$.[74] Sulfide is a noncompetitive inhibitor of O_2 reduction with $K_i = 2 \times 10^{-7}\ M$.[101]

Fluoride. Fluoride is a very weak inhibitor of cytochrome aa_3[56,120] and exhibits a rather complicated inhibition pattern.[148] For these reasons, the interactions of fluoride with cytochrome aa_3 have not been studied to the extent of some of the stronger binding ligands. Thus, the binding site for fluoride has not been determined and it has been suggested that two fluorides bind per cytochrome aa_3.[120] The binding of fluoride is accompanied by small spectral shifts (the oxidized Soret shifts from 423 nm to 421 nm and the reduced α-band shifts from 597 nm to 598 nm[95,148]) and also affects the intermediate high spin

heme epr signals seen during reductive titrations, apparently making the species responsible for these g6 signals harder to reduce.[145]

Fluoride is a mixed-type inhibitor[148] with an inhibition constant $K_i \approx 10^{-2}$ *M*.[74,148] The species responsible for the inhibition is not known, but if HF is the active species, K_i' (based on HF) = 2.0×10^{-6} *M* which is in the same range as other stronger ligands (*e.g.*, azide, cyanide, sulfide). Thus, perhaps the explanation for the weak inhibition by fluoride is the low concentration of HF at neutral pH. The binding kinetics are triphasic with the first phase first order in [total fluoride] ($k_{on} = 4\ M^{-1}\ s^{-1}$, $k_{off} = 2.9 \times 10^{-2}\ s^{-1}$), the second phase independent of [total fluoride] ($k = 2.4 \times 10^{-2}\ s^{-1}$), and a third phase being very slow ($t_{1/2}$ ~ 10 minutes).[148]

Nitric Oxide (and Hydroxylamine, Nitrite). Keilin and Hartree observed inhibition of their aerobic heart muscle preparation by hydroxylamine.[56] Several studies were performed on this inhibition[120,133,149] before it was shown that the reaction of hydroxylamine (NH_2OH) with oxidized cytochrome aa_3 yields the NO complex of reduced cytochrome a_3 (a_3^{2+}-NO).[150] The same species can be generated by addition of nitrite (NO_2^-) or nitric oxide (NO) gas[152] to reduced cytochrome aa_3. This a_3^{2+}-NO complex is paramagnetic[61,150] (NO itself has one unpaired electron) and exhibits a fairly isotropic epr signal near g2 ($g_x = 2.09$, $g_y = 2.00$, $g_z = 2.006$[150,152]). This signal can be doubly integrated and shown to correspond to 50% of the hemes of cytochrome aa_3.[61] Using $Fe(CN)_6^{3-}$ to poise mitochondria (+NO) at ~400 mV, Wilson and coworkers were able to observe epr signals due to a^{3+} (low spin heme,

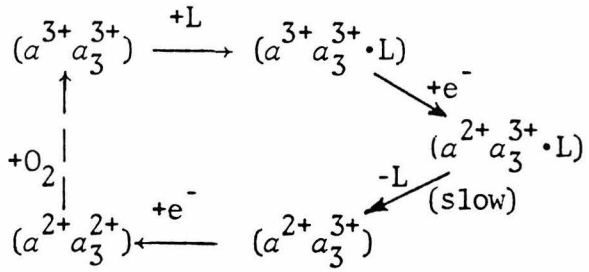
g~3) and Cu_d^{2+} (g~2) in addition to shifts in the a_3^{3+}-NO signal.[61] Thus, under these circumstances, three of the four metal sites of cytochrome aa_3 are epr-detectable. The shifts in the a_3^{2+}-NO signal were suggested to be due to heme-heme interactions (due to oxidation of cytochrome *a*).[61]

NO is similar to CO in binding preferentially to a_3^{2+}. Measurements of the circular dichroism spectra show that CO- and NO-binding are conformationally similar (but very different from the effects of cyanide or azide).[138] The a_3^{2+}-NO epr signal is unique (among cytochrome aa_3 derivatives) in exhibiting well-resolved superhyperfine splitting from two inequivalent nitrogens.[61,150,152] Comparison of the superhyperfine structure in the ^{14}NO and ^{15}NO derivatives[152] shows that the larger hyperfine coupling constant is due to the NO ligand (A_N (^{14}NO) = 20.3[152] or 21.1 G;[150] A_N(^{15}NO) = 28.2 G[152]) while the smaller splitting is independent of the NO isotope used and is probably due to the fifth ligand of the a_3^{2+} heme[153] (A_N' = 6.7 - 6.8 G[150,152]). The most likely candidate for this fifth ligand is histidine.[150,152] A recent study with anisotropic oriented multilayers of reduced cytochrome aa_3-NO has suggested that the NO is bound to the heme Fe at an Fe-N-O angle of ~135°.[154]

Formate. Inhibition of cytochrome *c* oxidase activity was first demonstrated by Nicholls[75] and exhibits $K_i \approx 2 \times 10^{-2}$ *M*[75,101] (uncompetitive with respect to O_2 reduction). The pH dependence of this inhibition indicates, however, that HCOOH is the species responsible for binding[70,75] and recalculation of the inhibition

constants based on HCOOH gives: $K_i' = 2 \times 10^{-6}$ *M*, $k'_{on} = 8 \times 10^{3}$ M^{-1}-s^{-1}, $k'_{off} = 1.6 \times 10^{-2}$ s^{-1}.[75] The site of HCOOH binding is unavailable in reduced cytochrome aa_3[75] and is apparently identical to the azide binding site[75] so that HCOOH binds to a_3^{3+} specifically. Mcd results show that the heme of the a_3^{3+}-HCOOH moiety is high spin[69] and, in this respect, formate differs from the "strong field" ligands cyanide, azide, sulfide, CO, and NO. Binding of HCOOH to oxidized aa_3 causes a blue shift in the Soret band[70,75,144] and this shift also occurs in partly reduced derivatives.[70]

Recently, it has been shown that aerobic reduction of the oxidized formate derivative ($a^{3+}a_3^{3+}$-HCOOH) by ascorbate/N,N,N',N'-tetramethyl-p-phenylenediamine (TMPD) results in incomplete reduction (as opposed to dithionite reduction) leading to a "mixed valence" formate derivative.[69] The epr spectrum of this derivative indicates that both cytochrome *a* and Cu_d are reduced (a^{3+} is low spin with g3 signal in the oxidized formate complex). However, closer examination[69] revealed that the "mixed valence" formate derivative is actually a steady state species which becomes fully reduced (with concomitant loss of formate assumed) upon exhaustion of O_2 (in excess reductant). The steady-state cycle was suggested[69] to be due to rate-limiting formate dissociation (L ≡ HCOOH):



Summary. In addition to the small effects that ligation of cytochrome a_3 has on the α and Soret absorption bands, addition of ATP to (*i.e.*, energization of) intact mitochondria has been found to induce similar shifts in the cytochrome aa_3 spectrum.[76,78] This effect has been mimicked in the isolated enzyme by the use of Ca^{2+} ions.[155] These spectral shifts have been discussed in terms of conformational changes and spin state changes involved in the "activation" of the enzyme for catalytic functioning or perhaps in the energy coupling (or respiratory control) mechanism.[53,79,125,144] It is becoming apparent that the resting (fully oxidized) cytochrome aa_3 is not a catalytically active form since it is not a good electron acceptor.[53,54,156,157] Some kind of activation is necessary to transform resting aa_3 into a well-functioning electron transport enzyme. This "activated" form is probably closely related to the "oxygenated",[136,158,159] "pulsed",[157] or other intermediates which show an enhanced degree of catalytic activity. This type of activation (conformational change?) may be initiated *in vivo* by energization of the mitochondrial membrane with the formation of the "resting" conformation being an exhibition of respiratory control.[77,104] As in the liganded forms, these "activated" forms (and the enzyme in the steady-state) show spectral shifts which may indicate the importance of the above-mentioned conformational changes.[144] Some intermediates which may have similar relevance have recently been observed by epr and will be discussed later.

Redox Potentials. Elucidation of the kinetic mechanism of electron transfer through cytochrome aa_3 will undoubtedly require an understanding of the thermodynamics of the redox reactions involved. Thus, knowledge of the reduction potentials of native cytochrome aa_3 as well as the various liganded derivatives is of considerable importance. Although much effort has been expended toward this goal, the thermodynamic nature of the redox processes involved is far from being settled. In fact, many of the differences in the various hypothetical descriptions (discussed above) proposed for this enzyme stem directly from differences in results (and interpretations) of redox potential studies. This appears to be the one area of research on cytochrome aa_3 that has substantial room for improvement, both with respect to the techniques used and interpretive theoretical work. A summary of the results of studies performed to date on the thermodynamic features of the redox properties of cytochrome aa_3 follows.

Most of the work in this area has been performed by only a few groups, each using slightly different techniques for measurement of the reduction potentials of the various active sites in cytochrome aa_3. Each method also requires a means of being able to calculate the relative amounts of reduced and oxidized forms of the various active sites. Usually, the absorption spectrum is monitored and changes in absorbance (at different wavelengths) are interpreted as conversion of the site(s) from one oxidation state to the other. Similarly, other observables which reflect differences in oxidation states have been used, including cd and epr. Studies involving the use of magnetic

susceptibility titrations have been suggested[160] but no such studies have yet appeared in published form. Another important technique is the use of mcd to monitor oxidation and spin states during redox titrations. Use of this technique has recently been reported.[63,87]

The classical method of redox potential measurements involves the use of various redox titrants to establish a series of intermediate oxidation states which can then be monitored by an appropriate technique (*e.g.*, electronic absorption spectroscopy). This technique has been modified by Hartzell (in his early work with Kuwana) (*e.g.*, see refs. 48, 161, 162) to include electrochemical generation of the titrant, the amount of titrant "added" being proportional to the amount of charge introduced. In this method, absorption versus charge (A/Q) plots are used to observe the redox behavior of the various sites. Hartzell has recently begun using a computer to generate simulated titrations (at various wavelength components) to fit actual titration data (*e.g.*, see refs. 85, 90). Wilson has perfected the method of potentiometric titration which involves the use of a series of mediators and a potentiostat to "poise" the sample at a particular (known) redox potential allowing the enzyme to equilibrate (through the mediators) with the potential of the electrode (*e.g.*, see refs. 163-165). Thus, the electronic absorption spectrum (or other appropriate observable) can be monitored as a function of potential with the potential for half-conversion (*i.e.*, half-reduction or half-oxidation) of a particular site being equivalent to the redox potential of that site. This technique has been used extensively for measurements on intact mitochondria or SMP.

It should be apparent throughout this discussion that the major obstacle to interpretation of the data (obtained by any of the above procedures) is the inability to assign specific spectral features to individual active sites (especially in comparisons between native and liganded derivatives of the enzyme). Closely related to this problem is the fact that conversion of one site between oxidation states can directly (or indirectly) affect the spectral behavior of another site. As an example of this, it has been pointed out[53] that the observation of two reduction components in a titration curve measured at 605 nm does not necessarily imply that the sites to which these components are assigned have to both absorb at 605 nm. This type of behavior could be a direct result of site-site (or specifically heme-heme) interaction. The major differences between the hypotheses mentioned above stem from the interpretation of exactly how the site-site interactions are manifested. The 50/50 hypothesis postulates the existence of spectral interactions in which oxidation (or ligation) changes in one site induce major spectral (*i.e.*, extinction coefficient) changes in the other site.[53,58,166] In contrast, the neo-classical hypothesis attributes all of the interaction to potential differences (*i.e.*, oxidation state changes in one site cause the reduction potential of the other site to change).[53,62] The latter hypothesis allows the spectra to be interpreted without major changes in extinction coefficients, but still allows for small shifts in peaks as discussed above. A recent reanalysis of a portion of the important titration data to a model allowing different types of pairwise site-site interactions found that both the epr and

optical absorption data could be fit using a scheme involving only potential interaction (with no need for spectral interaction)[160] (*cf.*, refs. 63, 87).

Native Enzyme. Since the question of assignment of the various active sites to individual spectral components (or to individual reduction potentials) is still not satisfactorily solved, the discussion of specific results will not attempt to address these assignments. Instead, the potentials observed will be labelled (for the most part) as to whether they are from heme or copper and what range they are in. Specifically, there are potentials for four possible sites: a_H (high potential heme), a_L (low potential heme), Cu_H (high potential copper), and Cu_L (low potential copper) (this is the nomenclature of Hartzell and coworkers[85,90]). Historically, cytochrome a_3 has been assigned as the high potential heme (a_H), and the copper associated with it (Cu_u) as the high potential copper. Although, there is some evidence to support this assignment, it is by no means a unique interpretation of the results[160] and the possibility exists that such an assignment is an artificial one since the neo-classical hypothesis[53,62] postulates that half-reduction produces an equilibrium mixture of reduced a and reduced a_3.

The results of reduction potential measurements on native cytochrome aa_3 (as well as several other derivatives and forms of the enzyme) are tabulated in Table 1-2. Although Table 1-2 shows that much work has been performed in this area, the inability to observe directly some of the active sites (in various derivatives and by various

Table 1-2. Redox Potentials of Active Sites of Cytochrome aa_3.

Derivative	$a_H(a_3)$[a] E_m(mV)	n	$a_L(a)$ E_m(mV)	n	$Cu_H(Cu_u)$[a] E_m(mV)	n	$Cu_L(Cu_d)$ E_m(mV)	n	Observable[b]	Conditions/Additions pH	Method[c]	Enzyme Form[d]	Reference(Year)[e]
native	380		210						A	7.0	ICT	M,SMP	174(1978)
native	350		215				250		E(g6,g3,g2)		RT,OT	I	63,87(1978)
native	385		210		340				A		PT	M	55(1978)
native	340		210		350		225		A	7.0	OT	I	90(1977)
native	340		220		340		240		A	7.0	RT,OT	I	85(1977)
native	(380)[f]		(190)						E(g6)	7.0	PT	SMP	61(1976)
native	360		205						A		PT	I	60(1974)
native	340±15		209±15		340±15		209±15		A	7.0	ICT	I	169(1974)
native	280	1.0	280	1.0			280	1.6	A	7.0	RT	I	65(1973)
native	350±10	1	215±10	1	350±10	1	215±10	1	A	7.0	ICT	I	161(1973)
native	280	1	280	1					A	7.0	RT	I	66(1972)
native	(380)		(230)				250	1.0	E(g6,g3,g2)	7.0	PT	M,SMP	59(1972)
native	285	0.5	285	0.5			225	1.0	A	7.0	PT	I	168(1971)
native	375	1.0	225	1.0			225	1.0	A	7.0	PT	PP	168(1971)
native							274-284		A	7.0	RT	I	167(1969)
native	380				340				A	7.2	PT	M	91(1975)
native							245		A	7.2	PT	M.SMP,I	172(1975)
native	285		285						CD	7.2	PT		64(1974)
native			210±10						A	7.2	PT	M	170(1974)
native	(380)		(220)						A	(reinterpretation of results below)			53,166(1974,76)
native	385		210						A	7.2	PT	PHM	165,171,173(1973)
native	380		220						A	7.2	PT	PHM	58(1972)
native							225	1.0	E(g2)	7.2	PT	I	168(1971)
native	365	1	205	1					A	7.2	PT	BHM	164(1970)
native	390	1	205	1					A	7.2	PT	RLM	164(1970)

Table 1-2. (Cont.)

Derivative	$a_H(a_3)$ E_m(mV) n	$a_L(a)$ E_m(mV) n	$Cu_H(Cu_u)$ E_m(mV) n	$Cu_L(Cu_d)$ E_m(mV) n	Observable	Conditions/Additions pH	Method	Enzyme Form	Reference(Year)
native	395	190			A	6.8	PT	RLM	163(1970)
native	350		340		A	7.8	PT	M	91(1975)
native			340±10		(indirect)	7.8	PT	M,SMP,I	172(1975)
native	315±10 1				A	7.8	PT	PHM,I	88(1974)
native	320		340		A	8.2	PT	M	91(1975)
native	300	175			E(g6)	8.5	PT	SMP	61(1976)
+ CO		255			A	7.2 sat. [CO]	PT	M	55(1978)
+ CO		240	360	215	A	7.0 sat. [CO]	OT	I	90(1977)
+ CO		260	340	240	A	7.0 sat. [CO]	RT,OT	I	85(1977)
+ CO	450				A	7.0 [CO]=600 μM	PT	SMP,I	89(1977)
+ CO		250±10 1	340±10 1	190±20 1	A	7.0 sat. [CO]	ICT	I	182(1976)
+ CO		255±15			A	7.2 sat. [CO]	PT	M	170(1974)
+ CO	355±10 (n=1.5-1.8)				A	7.8 [CO]=3 μM	PT	PHM,I	88(1974)
+ CO	385±10 2.0				A	7.8 [CO]=30 μM	PT	PHM,I	88(1974)
+ CO	410±10 2.0				A	7.8 [CO]=300 μM	PT	PHM,I	88(1974)
+ CO		(260)			A	(reinterpretation of results below)	M		166(1974)
+ CO		255			A	7.2 sat. [CO]	PT	PHM	165,173(1973)
+ CO		260			A	7.2 +ATP (+FCCP), sat.[CO]	PT	PHM	181(1972)
+ HCN		270			A	xs [HCN]	PT	M	55(1978)
+ HCN		270±15			A	7.2 xs [HCN]	PT	M	170(1974)
+ HCN		275			A	7.2 xs [HCN]	PT	PHM	165(1973)
+ HCN		265 0.5			A	6.8 xs [HCN]	PT	RLM	163(1970)

Table 1-2. (Cont.)

Derivative	$a_H(a_3)$ E_m(mV) n	$a_L(a)$ E_m(mV) n	$Cu_H(Cu_u)$ E_m(mV) n	$Cu_L(Cu_d)$ E_m(mV) n	Observable	pH	Conditions/Additions	Method	Enzyme Form	Reference(Year)
+ HN_3		290			A		xs [HN_3]	PT	M	55(1978)
+ HN_3		290±15			A	7.2	xs [HN_3]	PT	M	170(1974)
+ HN_3		290			A	7.2	xs [HN_3]	PT	PHM	165(1973)
+ H_2S		220			A		xs [H_2S]	PT	M	55(1978)
+ H_2S		220±15			A	7.2	xs [H_2S]	PT	M	170(1974)
+ H_2S		230			A	7.2	xs [H_2S]	PT	PHM	165(1973)
+ NO		260			A		xs [NO]	PT	M	55(1978)
+ ATP		270			A		xs ATP	PT	M	55(1978)
+ ATP	(265)	(150)			A		(reinterpretation of results below)		M	53(1976)
+ ATP	160		340		A	7.2	xs ATP	PT	M	91(1975)
+ ATP	130		340		A	7.8	xs ATP	PT	M	91(1975)
+ ATP	100		340		A	8.2	xs ATP	PT	M	91(1975)
+ ATP	(270)	(160)			A	7.2	xs ATP (reinterpretation)		M	166(1974)
+ ATP	155	265			A	~ 7	xs ATP	PT	M	171(1973)
+ ATP	155	260			A	7.2	xs ATP	PT	PHM	173(1973)
+ ATP		265			A	7.2	xs ATP	PT	PHM	165(1973)
+ ATP	150 1	265 1			A	7.2	6 mM ATP	PT	PHM	181(1972)
+ ATP	300	190			A	6.8	xs ATP	PT	RLM	163(1970)
+ ATP,+ CO		215			A		xs ATP, sat. [CO]	PT	M	55(1978)
+ ATP,+ CO		(220)			A		(reinterpretation of results below)		M	166(1974)
+ ATP,+ CO		220			A	7.2	xs ATP, sat. [CO]	PT	PHM	173(1973)
+ ATP,+ CO		220			A	7.2	6 mM ATP, sat. [CO]	PT	PHM	181(1972)

Table 1-2. (Cont.)

Derivative	$a_H(a_3)$ E_m(mV) n	$a_L(a)$ E_m(mV) n	$Cu_H(Cu_u)$ E_m(mV) n	$Cu_L(Cu_d)$ E_m(mV) n	Observable	Conditions/Additions pH		Method	Enzyme Form	Reference(Year)
+ cyt *c*	360	230	365-370	230-240	A	7.0	aa_3-*c* complex	OT	I	90(1977)
+ cyt *c*	340-360	205-220	340	240	A	7.0		OT	I	186(1977)
+ cyt *c*	360	205			A			PT	I	60(1974)
+ cyt *c*	350	225			CD	7.2	$\lesssim$ stoichiom. cyt *c*	PT		64(1974)
+ cyt *c*	370 1.0	230 1.0		280 1.0	A	7.0	"	RT	I	65(1973)
+ cyt *c*	350	210			A	7.0		ICT(RT)	I	162(1973)
+ cyt *c*	350	225			A	7.0		ICT(OT)	I	162(1973)
+ cyt *c*	335-360 (n=1.2)	200-250 (n=1.0)			A	7.0		RT	I	66(1972)
+cyt *c*,+CO		240	360	215	A	7.0		OT	I	90(1977)

[a]The heme a_H is usually (although not always) identified with heme a_3; Cu_H is usually identified with Cu_u.

[b]Quantity monitored during titration (A-absorbance; E-epr; CD-circular dichroism).

[c]Titration method employed (PT-potentiometric titration; OT-oxidative titration; RT-reductive titration; ICT-indirect coulometric titration).

[d](M-intact mitochondria (source unspecified); BHM-beef heart mitochondria; PHM-pigeon heart mitochondria; RLM-rat liver mitochondria; SMP-submitochondrial particles; I-isolated enzyme; PP-partially purified enzyme).

[e]Within each group (one derivative at one set of conditions), the entries are listed in reverse chronological order based on year of publication.

[f]Potential in parentheses indicates that the assignment was unsure or not given or this is a reinterpretation of data from a different reference (always denoted as such).

techniques) have resulted in a large number of incomplete studies. This has contributed to the inability to achieve a consistent picture of the redox thermodynamics of this enzyme. Each section of Table 1-2 represents a different derivative, or different conditions and each will be discussed separately starting with the native enzyme.

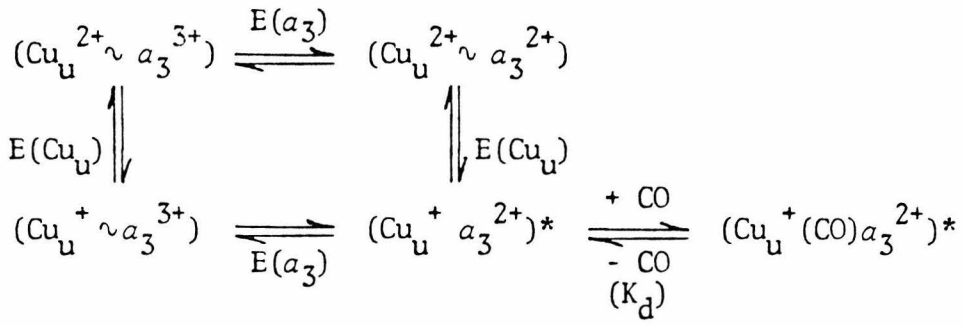
Early potentiometric titration work on the native enzyme in intact mitochondria indicated the presence of two titratable heme groups (seen in absorption spectra) with different potentials.[164] These were originally assigned to cytochrome a_3 (high potential, ~380 mV versus normal hydrogen electrode (NHE)) and cytochrome a (low potential, ~205 mV versus NHE). These two potentials will be the basis for the a_H and a_L nomenclature to be used from here on. The detectable copper (Cu_L) (at 830 nm) in isolated aa_3 was found by reductive titrations to have an intermediate potential of ~280 mV.[167] The potentiometric titration technique was later used to estimate the copper (Cu_L) potential as ~225 mV in isolated aa_3 (by examination of either the 830 nm band or the g2 epr signal).[168] This same study found that upon isolation of aa_3, the hemes became indistinguishable with a potential of 285 mV (and an n value of 0.5) although the Cu_L potential (of ~225 mV) was the same in intact mitochondria and in isolated aa_3.[168] This apparent anomaly has also been observed by van Gelder and coworkers, who claim that in isolated cytochrome aa_3, the hemes titrate with a single potential (~280 mV), while the addition of a catalytic amount of cytochrome c causes the hemes to separate (with potentials a_H ~370 mV and a_L ~230 mV).[64-66] Although these authors (at least until

1974) have found this phenomenon consistently, no other verification has been published. The potentiometric titration studies on isolated aa_3 were redone and found to be in error (a_H = 360 mV, a_L = 205 mV independent of presence of cytochrome c)[60] and many more recent studies on isolated aa_3 have indicated the presence of two distinct heme reduction potentials (a_H ~340-385 mV, a_L ~205-220 mV).[85,90,161,169] The low spin heme epr signal at g~3 is a manifestation of cytochrome a^{3+} and has been found to exhibit a reductive titration curve indicative of two separate potentials (380 mV and 230 mV, in intact mitochondria or SMP).[59] This signal thus mimics the pattern of reduction seen at 605 nm and, in fact, shows that the titrations at 605 nm can be explained on the basis of the neo-classical hypothesis (only a absorbs at 605 nm). During reductive titration, a high spin heme signal (or signals) at g~6 (which are not present to any extent in either the reduced or resting state spectra) appear, then disappear. The potentiometric titration method indicates their appearance with a half-reduction potential of 190-230 mV in mitochondria or SMP.[59,61] Although these g6 signals were assigned to a^{3+},[59] this assignment is not settled (see below) and the pattern of appearance and disappearance of these signals has been used to support the neo-classical view of the active sites.[53] The redox potential of the invisible (or undetectable) copper (Cu_u) is not easily determined but can be estimated by assuming it has an indirect effect on absorption measurements (by merely accepting reducing equivalents). Measurements at neutral (or near neutral) pH (6.8-7.2) thus appear to be in rather good agreement (except for the

work of van Gelder in the absence of cytochrome c[64-66]as to the values of the four measurable potentials exhibited by native cytochrome aa_3 (in isolated form, in mitochondria, or in SMP): a_H≈340-395 mV; a_L≈190-220 mV; Cu_H≈340-350 mV; Cu_L ≈ 210-250 mV.[55,58-61,63,85,87,90,91,161,163-165,169-174]

The pH-dependence of the reduction potentials of cytochrome aa_3 is of importance since the catalytic reduction of O_2 to $2H_2O$ requires four protons. Also, cytochrome aa_3 has been suggested to be a proton pump (*e.g.*, see refs. 175-178) and this may have its origin in the catalytic requirement for protons. Wilson first suggested that the high-potential heme (a_3) had a pH-dependent redox potential and that this dependence could be explained by a titratable group with pK_a~7.0.[58] Subsequent potentiometric titration studies (mainly in mitochondria and SMP) have shown that the reduction potential of a_H changes by -60 mV/pH unit (pH 7.2-8.2)[88,91,172] suggesting the participation of one proton in the reduction of this heme. The Cu_H potential was found to be pH-independent.[91,172] Van Gelder and coworkers have recently done a similar study on isolated cytochrome aa_3 (in the presence of cytochrome c) and found that at pH 7.0, oxidation of both hemes results in the release of one proton.[179] They also found the copper potentials to be pH-independent. pH-dependent changes in epr signals have also been interpreted as pH-dependent electron redistributions which predict that the potential of some epr-undetectable component (perhaps a_3 or a_H) increases upon lowering the pH.[86,180] Thus, it appears that at least one proton is directly involved in the redox reaction of the heme of cytochrome a_3 (or a_H).

Carbon Monoxide. CO is known to bind nearly specifically to the reduced heme of cytochrome a_3 (a_3^{2+}).[63,85-87] This specificity can be described as a large increase in the potential of cytochrome a_3 upon addition of CO. With a saturating amount of CO (*e.g.*, under a pure CO atmosphere), this increase in potential is enough to cause auto-reduction of a_3^{3+} to a_3^{2+}-CO (the mixed-valence derivative) in the presence of some endogenous electron donor.[63,87,92,96] At lower concentrations of CO, Wilson and coworkers[88,89] have been able to perform reductive potentiometric titrations and measure the half-potential for formation of the a_3^{2+}-CO moiety (observed at 590 nm). This potential (ascribed to a_3^{2+}-CO or a_H in the presence of CO was found to be dependent on [CO], increasing 30 mV per decade of [CO].[88] The measurements were carried out at a higher pH (7.8) in order to take advantage of the lowering of the a_H potential (into a measurable range) upon an increase in pH (see above). The potential of a_H was an n=1 process in the absence of CO, but changed rapidly upon addition of small amounts of CO to an n=2 process (as suggested by the 30 mV/decade increase).[88] The conclusion drawn from this study was that CO would only bind to a_3^{2+} only if a_3 and the undetectable copper Cu_u were both reduced. The remaining titratable heme (a_L) exhibits a potential (slightly increased from its value in the native enzyme) of ~240-260 mV in the presence of saturating [CO].[55,165,170,173,181] A scheme has been developed to account for the necessity of reduction of both a_3 and Cu_u before CO-binding. This scheme incorporates a major structural rearrangement upon reduction of both a_3 and Cu_u, allowing CO to bind (and bridge the two metal sites):



where, $E(a_3) \approx 385$ mV, $E(Cu_u) \approx 340$ mV, $K_d = 0.6$ μM (* represents the structural rearrangement).

The above result (of an n=2 CO-binding site) is very different from the results of oxidative titrations performed by Hartzell and coworkers.[85,90,182] These workers always find three titratable redox components (each with n=1.0) in oxidative titrations of isolated aa_3 in the presence of saturating [CO] ($a_L \approx 240$-260 mV, $Cu_H \approx 340$-360 mV, $Cu_L \approx 190$-240 mV), thus indicating that the high-potential copper component *can* be oxidized in the presence of CO. (These potentials are in agreement with the 45 mV difference between a_L and Cu_L observed by Palmer and coworkers in the presence of CO.[63,87]) They found it impossible to oxidize the a_H component with the titrants used and placed a lower limit of 465 mV on this site (presumably, a_3^{2+}-CO). In the presence of 600 μM CO at pH 7.0, the potential of this site has been measured as ~450 mV.[89] The reason for the discrepancy in the above results has yet to be discovered.

Other Ligands. Very little work has been performed toward the determination of the reduction potentials of liganded derivatives of

cytochrome a_3 with ligands other than carbon monoxide. All the work quoted in Table 1-2 was performed by Wilson and coworkers. They have measured the a_L potentials of derivatives with various ligands bound to a_3 (a_H).[55,163,165,170] In general, the binding of ligands to a_3 causes an increase in the potential measured for a_L but no other trends are apparent from the published data. This is an area of research on cytochrome aa_3 which is in need of much more work.

ATP (Energization) Effects. The importance of cytochrome aa_3 goes beyond its electron transport capabilities. The effect of ATP on the spectrum of cytochrome aa_3 *in vivo* (*i.e.*, in the mitochondrial membrane) has resulted in the acceptance of the importance of this enzyme in energy conservation processes as well. The first demonstration by Wilson and coworkers of an effect of ATP on the reduction potentials of cytochrome aa_3 (in intact mitochondria)[163] served to support the involvement of cytochrome aa_3 in energy coupling (and/or perhaps respiratory control). In this original report, the potentials were attributed to the hemes such that each heme experienced a decrease of ~50 mV upon addition of ATP (*i.e.*, $a_H \approx 300$ mV, $a_L \approx 190$ mV). However, subsequently Wilson and coworkers have reassigned the potentials such that $a_H(a_3)$ undergoes a decrease of ~200 mV ($a_H \approx 150$ mV) in the presence of ATP, while $a_L(a)$ undergoes an increase of ~40 mV ($a_L \approx 265$ mV) in the presence of ATP.[91,165,171,173,181] It has been shown that the "a_H" potential has a pH-dependence similar to the pH-dependence of a_H in the native enzyme.[91] Wikström[53,166] has suggested that Wilson's results are best interpreted (in the neo-

classical hypothesis[62]) as an ATP-induced shift in redox potentials such that a_3 becomes a better reductant (lower reduction potential), shifting the equilibrium toward $a_3^{2+}a^{3+}$ in the half-reduced state. This hypothesis can explain the shift in relative absorbance changes for the two components observed at 605 nm as well, whereas Wilson had postulated an ATP-linked extinction coefficient change as well. It is interesting to note here as well that Wikström's analysis[53] can also account for all the ligand-induced potential and spectral differences, making this a very attractive description of the thermodynamic interactions between the sites of cytochrome aa_3.

The effect of ATP in the presence of saturating [CO] was also examined by Wilson and coworkers.[55,173,181] The remaining titratable heme in the presence of both ATP and CO has a potential of ~220 mV, which represents a decrease of ~40 mV in the a_L potential upon the addition of CO. In the absence of ATP, however, the addition of CO was seen to cause an increase in the a_L potential of ~40-50 mV[55,165,173,181] which seems inconsistent with the interpretation of the results in the presence of ATP. If the above assignments (in the presence of ATP and absence of CO) are switched (to $a_H \approx 265$ mV, $a_L \approx 150$ mV), then the effect of CO (in the presence of ATP) appears more reasonable (increase in a_L of ~70 mV).

The potential of Cu_H has been determined (roughly) by studies of CO-complex formation in the presence of ATP and has been shown to exhibit a potential of ~340 mV, independent of pH and ATP.[91]

More detailed studies of the effect of ATP on the redox potentials of cytochrome aa_3 have shown that the potentials are actually dependent on the phosphate potential, ΔG_p ($\equiv$ [ATP]/[ADP][P_i]) and that the a_H potential decreases ~40 mV per unit of phosphate potential.[171] This effect (as well as the spectral shifts induced by ATP) were suggested to be due to a change in the fifth ligand of the heme of cytochrome a_3 (a_H) induced by ATP (according to the following scheme - (a_3^*) indicates the modified a_3 site[171]):

$$\begin{array}{ccc} a^{2+}(a_3^*)^{2+} + ADP + P_i & \overset{K_r}{\rightleftharpoons} & a^{2+}a_3^{2+} + ATP \\ E_L^* \uparrow\downarrow \quad \uparrow\downarrow E_H^* & & E_L \uparrow\downarrow \quad \uparrow\downarrow E_H \\ a^{3+}(a_3^*)^{3+} + ADP + P_i & \overset{K_o}{\rightleftharpoons} & a^{3+}a_3^{3+} + ATP \end{array}$$

where, $K_r = .06\ M^{-1}$, $K_o = 10^3\ M^{-1}$, $E_L = 210$ mV, $E_H = 385$ mV, $E_L^* = 265$ mV, $E_H^* = 155$ mV. This type of ATP-induced ligand change must be considered completely speculative for now.

It should be mentioned that Wilson's observation of ATP-induced potential changes has been challenged as an artifact due to the use of mediators which do not couple directly with cytochrome aa_3 but through other cytochrome components which may then be coupled to cytochrome aa_3 through ATP-dependent processes.[183] However, it seems that the ATP effects have been seen with a number of different mediators and the chances are probably good that the effects can be deemed "real".

Cytochrome c. As was mentioned previously, van Gelder and coworkers have consistently found that, in the absence of cytochrome *c*, both hemes of cytochrome aa_3 titrate together at a potential of ~280-285 mV.[64-66] They also found that with even a less than stoichiometric amount of cytochrome *c*, the heme potentials become separable and distinct. Thus, they postulated two conformational states of aa_3, the conversion between them being catalytically triggered by cytochrome *c*.[65] This catalytic effect of cytochrome *c* thus rules out complex formation as being responsible (alone) for the potential differences. It is well known that cytochrome *c* forms an electrostatic complex with cytochrome aa_3 at low ionic strength[184] and this is reflected in the ionic strength dependence of the cytochrome c^{2+}-cytochrome aa_3 reaction.[185]

In an early coulometric titration study, hysteresis was seen in the oxidation/reduction titration of heme a_L and it was suggested that the presence of cytochrome *c* may have been responsible for this anomaly.[162] However, more recent work in the presence of cytochrome *c* does not exhibit this phenomenon.[90,186] A potentiometric titration study by Wilson on isolated cytochrome aa_3 gave separable heme potentials irrespective of the presence of cytochrome *c*.[60] Recent oxidative titrations on aa_3 as a 1:1 complex with cytochrome *c*, as a 1:2 complex with cytochrome *c*, or in 1:1 mixtures with cytochrome *c* (at high ionic strength to avoid complexation) have shown that in all cases, the potentials are separable and only slightly dependent on complexation by cytochrome *c*. All of the above potentials are tabulated in

Table 1-2 along with potentials measured for the other active sites in the presence of cytochrome *c*. Since all the potentiometric work with intact mitochondria or SMP was most likely performed in the presence of cytochrome *c*, not many exhaustive studies of the potentials of cytochrome aa_3 in the *complete* absence of cytochrome *c* have been performed. Thus, it is difficult to assess the significance of van Gelder's finding that aa_3 behaves very differently in the absence of cytochrome *c*.

The preceding discussion of the available data on the reduction potentials of the active sites in cytochrome aa_3 points out the need for more extensive studies in this area. Of particular importance will be studies of titrations examined by several different techniques (such as optical spectroscopy, epr, mcd, and perhaps magnetic susceptibility (*e.g.*, see refs. 63, 87)). Also, it does not seem unreasonable to propose the use of a combination of electrochemical techniques to aid in the elucidation of these important thermodynamic characteristics. This method would be a "potentiocoulometric" method in which a sample (with appropriate mediators present in known concentrations) would be poised at various potentials (stepped in the reductive or oxidative direction) with monitoring by an appropriate spectroscopic technique and by coulometry. In this technique, the enzyme would be equilibrated to a known potential, a known amount of "titrant" (charge) would have been added, and the relative amount of the oxidation states of the species of interest would be measurable. A combination of spectroscopic techniques (as described above) could be used to aid in the determination of the oxidation states of the various species.

Better analytical methods will also be of use in the future to simulate titration curves monitored by any number of techniques. Such methods have now been developed[85,90,160] which solve the series of Nernst equations based on a set of potentials and contributions of each species to the appropriate monitored parameter. The analytical method described by Lanne and Vänngård[160] also allows any permutation of pairwise interactions based on the oxidation states of the various species.

With the accumulation of more data on redox titrations monitored by several different techniques, the use of more sophisticated analytical techniques will eventually lead to a consistent interpretation of the thermodynamic characteristics of the active sites of cytochrome aa_3. Since the site-site interactions which are manifested in these thermodynamic characteristics are probably responsible for many of the peculiarities of this enzyme, it will be very important and interesting to sort out these characteristics.

Magnetic Properties. It was recognized long ago that a solution to the problems posed by cytochrome aa_3 would require techniques more selective (or perhaps more sensitive) than the classical technique of electronic absorption spectroscopy. Thus, introduction of the use of electron paramagnetic resonance (epr) spectroscopy for examination of the active sites of cytochrome aa_3 was expected to yield the information necessary for a complete understanding of the active sites and their functions. Unfortunately, although epr spectroscopy did help in elucidating the role of copper in cytochrome aa_3,[187-189]

it was not the panacea hoped for[52] since some of the active sites are still undetectable even in the fully oxidized resting state. Recently, other techniques sensitive to the magnetic characteristics of the active sites have become more useful in the study of cytochrome aa_3. These include magnetic circular dichroism (mcd) spectroscopy and magnetic susceptibility measurements. The ability to use these techniques over wide temperature ranges has been extremely helpful in sorting out the oxidation and spin states of the active sites in this enzyme to the point where most of the stable enzyme derivatives have been completely electronically characterized. The emphasis has now shifted to the kinetically-important forms of the active sites and there is finally real hope that soon the actual detailed electron transfer mechanism(s) employed by this crucially important enzyme will begin to be revealed.

In the resting (fully oxidized) state, cytochrome aa_3 exhibits an epr spectrum which does not reflect properties of all of the active sites. The fact that only one of the hemes and ~50% of the copper were detectable by epr was observed ten years ago and was suggested to indicate that the epr-undetectable components were magnetically interacting.[143] The copper signal at g~2 (actually g = 2.185, 1.99, 2.03[190]) is unlike a normal Cu(II) (*e.g.*, Cu^{2+}(aq)) signal. Other than the rather low g values (even for Cu(II)), there is no observable copper hyperfine and it has been suggested that the signal looks more like a free radical (sulfur?) signal than Cu(II).[191,192] A recent reexamination of the g2 signal at X-, S-, and Q-band has

suggested that perhaps as much as ~100% of the copper is actually accounted for by this signal.[193] In light of the discussion to follow, this result is rather difficult to reconcile. An ENDOR study of the g2 signal indicates the presence of superhyperfine interaction with at least two protons and one nitrogen with a coupling large enough (~6 G) to be a "ligand" of the S = 1/2 center giving rise to the g2 signal.[194] Although no copper hyperfine has yet been detected by the ENDOR method, the existence of a nitrogen "ligand" suggests that the S = 1/2 center is more likely copper than a sulfur radical.[194] Most preparations contain ≳10% inactive copper along with the intrinsic copper.[190,195] The copper hyperfine coupling constants for the intrinsic copper were estimated to be anisotropic and rather small (*e.g.*, $A_z \approx .003$ cm^{-1}), this being explained by a nearly tetrahedral ligand environment with a rhombic distortion.[190]

The resting state epr spectrum also contains a signal at g ~ 3.0 which can be attributed to a low-spin ferric heme (g = 3.0, 2.2, 1.5) and assigned to a^{3+}.[52,92,196,197] The exact g values of this low spin signal are apparently pH-dependent although some of this small dependence may be accounted for by the presence of chloride ion.[180] Inevitably,the epr spectrum of the resting enzyme contains a small signal at g ~ 6 (due to a small amount of high-spin ferric heme) but this signal represents only a few percent (at most) of the total heme in the enzyme.[109] Also, a small amount of contaminating high-spin ferric iron is usually present and responsible for the signal at g ~ 4.3.[128] All of these epr signals and their assignments are

summarized in Table 1-3 (along with mcd and magnetic susceptibility results on this and all other derivatives).

The other two active sites (a_3 and Cu_u) are epr-undetectable, but have been suggested to be magnetically interacting.[143] Mcd results (see Table 1-3) indicate that the most likely assignment of the spin state of (presumably) oxidized a_3^{3+} is hign spin (in the resting enzyme)[198,199] even though earlier results suggested that a_3^{3+} might have existed in a spin equilibrium.[105] Early magnetic susceptibility results indicated that a_3^{3+} might be in spin equilibrium[200] or completely high spin[201] but recent room temperature[129] and variable temperature[130,131] susceptibility measurements have indicated (rather conclusively) that the high spin heme of cytochrome a_3^{3+} is antiferromagnetically coupled to Cu_u^{2+} to give a ground state (S = 2) with an exchange parameter, $-J \gtrsim 200\ cm^{-1}$.[130,131] The presence (and nature) of a bridging ligand between the two centers is still a matter for speculation. Palmer and coworkers suggest the presence of imidazolate as a bridge[130,202] in analogy to the case in superoxide dismutases (*e.g.*, see ref. 203). This suggestion has some support in the finding of nitrogen as the fifth ligand to a_3^{2+} in the reduced +NO derivative.[150,152] Other possibilities exist, including the use of the intersite space for binding of O_2 in preparation for its reduction to water.[204-206] Thus, it seems fairly well-established (but, see ref. 193) that the resting state enzyme contains one magnetically-isolated oxidized copper (Cu_d^{2+}), one magnetically-isolated low-spin oxidized heme (a^{3+}), and an antiferromagnetically coupled

Table 1-3. Magnetic Properties of Active Sites of Cytochrome aa_3.

Derivative	Abbrev.	Site	S epr[a]	S mcd[a]	S ms[a]	g	Comments	References
Resting (fully oxid.)	FO	a_3-Cu_u			2[b]		$-J \gtrsim 200$ cm^{-1}	129,130,131
		a_3		5/2				198,199
		a	1/2			3.0,2.2,1.5		52,92,193,196,197
						3.00,?,1.49	pH=6.4	180
						3.03,?,1.45	pH=7.4,8.4	180
		a		1/2				198,199
		a			1/2			129,130,131
		Cu_d	1/2			2.18,1.99,2.03		194
						2.185,1.99,2.03		190
		Cu_d			1/2			129,130,131
		[Cu(II)]	1/2			2.222,2.045	"inactive" copper	190
		[Fe(III)]	5/2			4.3	contaminant	128
		"Cu_u"	1/2			?	report of 100% Cu detectable	193
Fully reduced	FR	a_3		2				198,199
		a_3			2			129,130,131
		a		0				198,199
		a			0			129,130,131
		Cu_u			0			129,130,131
		Cu_d			0			129,130,131
FO + HCN	OCN	a_3		1/2				105,199
		a_3-Cu_u			0,1[c]		$-J \simeq 40$ cm^{-1}	130,131
		a		1/2				105,199
		a			1/2			130,131
		Cu_d			1/2			130,131

Table 1-3. (Cont.)

Derivative	Abbrev.	Site	S			g	Comments	References
			epr	mcd	ms			
FO + HF	OF	a_3		5/2				105,199
		a		1/2				105,199
FO + HCOOH	OFor	a_3		5/2				198
		a		1/2				198
FR + CO	RCO	a_3		0				105,198
		a		0				105,198
FR + HCN	RCN	a_3		0				105,199
		a_3			0			129,130,131
		a		0				105,199
		a			0			129,130,131
		Cu_u			0			129,130,131
		Cu_d			0			129,130,131
FR + NO	RNO	a_3-NO	1/2			2.091,2.006,2.0		150,152,154,188
FO + cyt c^{2+} (partly reduced)	PR(c)	a_3	5/2			6.41,5.37,~2	rhombic (pH ~ 7)	52,92,143,180,207
						~6	axial (low pH or in lipid)	52,180,207
		a	5/2				(alternative assignment)	63,(51,197)
		a_3	1/2			2.6,2.16,1.86	minor (more at high pH)	52,92,180,196,197
		a_3-Tris?	1/2			3.36,3.27	(assignment tentative)	196
FO + dithionite (partly reduced)	PR(d)	a_3	5/2			~6	axial predominant	51,197 (but, see 87)
PR(c) + CO	PCO'	a_3?	5/2			6.56,5.21,~2	rhombic (transient)	52,108,109
FO + CO (autoreduced)	PCO	a_3-CO		0			stable mixed-valence state	106
		a		1/2			"	106

Table 1-3. (Cont.)

Derivative	Abbrev.	Site	S epr	S mcd	S ms	g	Comments	References
PR + HCN	PCN	a_3-HCN	1/2			3.58		52,107,127
		a_3-HCN	1/2			3.63		128,132
(OCN+dithionite) (trapped)		a_3-HCN		1/2				199
		a		0				199
PR + HN_3	PN3	a_3-HN_3	1/2			2.9,2.2,1.67		52,100,107,132,209
						2.75	(minor component)	86
PR + H_2S	PSH	a_3-H_2S	1/2			2.54,2.23,1.87		52,100,107,132
		"Cu_u"	1/2			~2.19,2.05		147 (but, see 107)
OFor + ascorbate (trapped)	PFor	a_3-HCOOH		5/2				69,199
		a		0				69,199
PCO' + hν	P-CO'	a_3?	5/2			6.58,5.25,~2	transient	98,107
						6.60,5.37,~2		108
PCO + hν	P-CO	a_3		2				106
		a		1/2				106
FR + $Fe(CN)_6^{3-}$ (or porphyrexide)	AR	a_3	5/2			6.35,5.44,~2	rhombic (transient)	52,107,208
						~6	axial, low pH (transient)	52,107
		a_3?	1/2			2.6,2.2,1.8	(minor component)	107
AR + CO	ACO	a_3?	5/2			6.54,5.25,~2	rhombic (transient)	52,107
AR + HCN	ACN	a_3-HCN	1/2			3.58	(within 6 msec)	52,107
		?	5/2			~6	(some axial left)	52,107
AR + HN_3	AN3	a_3-HN_3?	1/2			2.77,2.2,1.76	(initial product)	52,107
		a_3-HN_3	1/2			2.9,2.2,1.67	(final product)	52,107

Table 1-3. (Cont.)

Derivative	Abbrev.	Site	S epr	S mcd	S ms	g	Comments	References
AR + H_2S	ASH	a_3-H_2S?	1/2			2.77,2.23,1.71	(initial product)	52,107
		a_3-H_2S	1/2			2.54,2.23,1.87	(final product)	52,107
FR + O_2	RO2	"a_3-O_2"?	?			~5,1.78,1.69	transient ($t_{1/2}$ ≃ 100 sec,16°C)	128,197

[a]The S values as determined by epr (electron paramagnetic resonance), mcd (magnetic circular dichroism), and ms (magnetic susceptibility).

[b]This is actually the ground state of an antiferromagnetically coupled S=1/2, S'=5/2 system, the excited state having S=3.

[c]The S value of the two levels of an antiferromagnetically coupled S=1/2, S'=1/2 system.

(S = 2) binuclear site consisting of an oxidized copper (Cu_u^{2+}) and a high-spin oxidized heme (a_3^{3+}) with an exchange parameter, $-J \gtrsim 200$ cm^{-1}. (The proximity of the "magnetically-isolated" sites is unknown, but it has been suggested that one explanation for the anisotropic linewidths derived from simulations of the g2 (Cu_d) signal may be a dipolar interaction with a low-spin Fe^{3+} (heme) at a distance of ~7 Å.[190])

Table 1-2 also shows results of magnetic studies on many other derivatives of cytochrome aa_3. The fully reduced enzyme exhibits no significant epr signals[52,143] indicating no odd-spin species. However, magnetic susceptibility studies show that the fully reduced enzyme is still paramagnetic (although significantly less so than the resting enzyme).[129-131] The paramagnetism can be fully accounted for by the presence of one high-spin heme iron and the mcd results are consistent with the existence of a_3^{2+} in the high spin (S = 2) ferrous state in the reduced enzyme.[198,199] Thus, cytochrome a is low spin in both the oxidized and reduced forms and cytochrome a_3 is high spin in both of these forms.

Addition of cyanide to the fully oxidized enzyme results in no new epr signals. Binding of HCN to a_3^{3+} causes the heme to undergo a transition from high to low spin. The low spin nature of a_3^{3+}·HCN is confirmed by mcd in which two low spin ferric hemes are found.[105,199] Recent magnetic susceptibility results indicate the existence of a weak antiferromagnetic coupling between low spin a_3^{3+}·HCN (S = 1/2) and Cu_u^{2+} (S = 1/2) to give a ground state with S = 0.[130,131] The exchange parameter for this case was measured as $-J \approx 40$ cm^{-1},[130,131] so that at ambient temperatures, both S = 0 and S = 1 levels would

be populated. The cyanide-bound reduced enzyme again does not exhibit an epr spectrum and magnetic susceptibility measurements indicate that it is completely diamagnetic.[130,131] Thus, both a^{2+} and a_3^{2+}·HCN are low spin ferrous hemes which is consistent with the mcd results.[105,199]

The reduced +CO derivative has no epr spectrum (as expected) and mcd results confirm that both hemes are low spin ferrous hemes[105,198] (as in the reduced +HCN derivative). The mixed valence-CO derivative (prepared by autoreduction of the oxidized enzyme under a CO atmosphere[96]) exhibits a room temperature mcd spectrum consistent with the formulation a^{3+} a_3^{2+}·CO (with both hemes being low spin).[106] Attempts to record the low temperature spectrum of this derivative resulted in the observation that below 100 K, the CO was irreversibly photolyzed (by the monitoring light) and a_3^{2+} had reverted to the high spin state.[106] Pertinent to this observation is the fact that photodissociation of CO from the mixed valence-CO complex (in the presence of $Fe(CN)_6^{3-}$) results in the formation of high spin heme epr signals at g ~ 6.6, ~5.3, ~2 which can be assigned to high spin a_3^{3+}.[98,107,108]

The binding of formate (HCOOH) to the oxidized enzyme results in an mcd which can be interpreted assuming that a_3^{3+} remains in the high spin state upon formate-binding.[198] The mixed valence formate derivative (which has been shown to be a steady state intermediate[69]) gives an mcd consistent with a_3^{3+}-HCOOH being high spin (as in the oxidized form) and a being a low spin ferrous heme.[69,199] As yet, no epr or magnetic susceptibility studies have been published on the

formate derivatives. Fluoride binding to the oxidized enzyme also does not disturb the high spin nature of cytochrome a_3^{3+}.[105,199]

Sulfide binding to oxidized aa_3 results in the appearance of a low spin heme signal with g ~ 2.54, 2.23, 1.87 which can be assigned to $a_3^{3+}\cdot H_2S$.[52,100,107,132] Upon addition of sulfide to oxidized aa_3, some reduction of the enzyme occurs as well (as monitored by decreases in the g2 (Cu_d) and g3 (a^{3+}) signals)[147] and changes observed in the g2 signal have been interpreted as "appearance" of the undetectable copper component (Cu_u).[147] However, this observation was not confirmed in a separate study.[107]

The binding of nitric oxide (NO) to the reduced enzyme gives rise to an epr signal with g ~ 2.091, 2.006, 2.0 which can be assigned to the paramagnetic (S = 1/2) species $a_3^{2+}\cdot NO$.[150,152,154,188] This signal shows clearly separated (super)hyperfine due to two nitrogen nuclei and studies with ^{15}NO[152] have confirmed the following values for the hyperfine coupling constants:[150,152] $A(^{14}NO)$ = 20.3 - 21.1 G, $A(^{15}NO)$ = 28.2 G, A(N') = 6.7 - 6.8 G. The splitting due to N' (the other axial ligand to a_3^{2+}) has been suggested to indicate the presence of a histidine imidazole nitrogen as the fifth ligand to a_3^{2+}.[150,152]

The assignments given above for the epr signals observed in the oxidized forms were aided by studies of the behavior of these signals during reductive titrations of the oxidized enzyme. It was discovered early that the epr spectrum gave rise to a wide variety of new signals upon partial reduction.[145] After partial reduction with cytochrome c^{2+} or other reductants) of the native (unliganded) aa_3,

the epr exhibits a new characteristic high spin heme epr signal at g ~ 6 and a separate low spin heme epr signal at g ~ 2.6.[145] Closer examination indicated that the g ~ 6 signal was actually made up of at least two separate signals, one approximately axially symmetric and the other rhombic (at g = 6.41, 5.37, ~2).[52,86,180,207] The new low spin heme signal is at g = 2.6, 2.16, 1.86.[52,92,180,196,197] In many preparations, other low spin heme epr signals appear at g = 3.27 and g = 3.36, but these have been attributed to the presence of Tris buffer (perhaps binding to a_3^{3+}).[196] Recently, the pH-dependence of g6 and g2.6 intermediate signals has been studied.[180] The results show that the high spin heme signals at g ~ 6 convert almost completely to the nearly axial signal at low pH (6.4), but a considerable rhombic signal is seen at higher pH. At higher pH, the low spin heme (g = 2.6) signal becomes more pronounced. This suggests some pH-induced conformational change (and spin state change). It was also found that cytochrome aa_3 in lipid vesicles exhibited a similar pH transition but shifted to higher pH.[180] The shape of the g6 signals is also dependent on the reductant used, reduction with dithionite giving a predominantly axial g6 signal.[51,197]

Integration of the g6 signals indicates that they correspond maximally to ~25 - 30% of the total heme present in the enzyme[86] and the disappearance of these signals upon ligand binding (see below) led van Gelder and Beinert to originally propose that the g6 signals were from the high spin heme of cytochrome a_3^{3+}.[143] However, further reductive titrations showed that disappearance of the low

spin heme signal (at g ~ 3) and appearance of the g6 signal corresponded rather closely, leading to the reassignment of the g6 signals to a high spin form of a^{3+} which exists in the presence of reduced undetectable components (*i.e.*, a_3^{2+}, Cu_u^{+}).[51,86,197] At the same time, reservations about this assignment were expressed[197] since, upon reoxidation of the reduced enzyme with $Fe(CN)_6^{3-}$, large amounts of the g6 signals were generated such that the sum of the g3 and g6 signals represented ~70% of the total heme. Palmer and coworkers have performed reductive titrations monitored by electronic absorption, mcd, and epr spectroscopies in which they claim that the g6 behavior closely parallels the mcd (measuring a^{2+}) and epr (measuring a^{3+} at g3) behavior, concluding that the g6 signals are best assigned to cytochrome a^{3+}.[63,87] Recent work by Beinert and coworkers on anaerobically reoxidized samples exhibiting large amounts of intermediate high spin heme signals have led these authors to reassign the g6 signals to a_3^{3+} (since as much as 80% of the heme becomes detectable in the epr).[52,107,128,208] It should be mentioned that all the above assignments refer only to the main (at pH ~7) intermediate rhombic high spin heme signals, with the assignment of the smaller ($\lesssim$10% of heme) axial signals remaining unclear (*e.g.*, see ref. 208).

During reductive titrations, the g3 low spin heme signal begins to disappear immediately, but the g2 "copper" signal does not begin to decrease until after approximately one equivalent (per aa_3) is added.[63,86,87,143] Thus, a^{3+} is reduced before Cu_d^{2+}. The g6 intermediate signals (along with the minor g2.6 signals) increase

until maximal at approximately two equivalents (per aa_3), then decrease and disappear after the g3 signals.[63,86,87,143]

As mentioned above, the presence of ligands affects the presence of the intermediate high spin heme (g6) signals. If reductive titrations are carried out in the presence of the strong field ligands cyanide, azide, or sulfide, the g6 signals are not formed at all. Instead new low spin heme signals form, the positions of which depend on the ligand. With cyanide,a low spin heme signal occurs at g ~ 3.6 in partially reduced aa_3.[52,107,127,128,132] Reductive titrations in the presence of azide exhibit a low spin heme signal at g = 2.9, 2.2, 1.67[100,132,209] (with a minor signal at g ~ 2.75[86]) appearing (in much the same manner as the g6 signals in unliganded aa_3) but not disappearing.[52,107] Addition of sulfide to the oxidized enzyme results in some reduction and the appearance of a low spin heme signal at g = 2.54, 2.23, 1.87 (as mentioned above).[52,100,107,132] It is assumed that, in analogy with azide and cyanide, the sulfide derivative of oxidized aa_3 would not exhibit any new epr signals (consistent with the observation[63,130] that cyanide does not disrupt the a_3^{3+}-Cu_u^{2+} coupling). Reductive titrations in the presence of CO, cause the reducing equivalents to shift more toward the epr-undetectable components as shown by the disappearance of the g3 and g2 signals at relatively higher levels of reduction.[86] The addition of CO to half-reduced aa_3 shows an increase in the g3 and g2 signal intensities as well.[92] These observations are consistent with the observed increase in reduction potential of a_3 in the presence of CO as discussed previously.

The effects described above for the case of reductive titrations are also observed (at least qualitatively) during kinetic reduction of cytochrome aa_3. Thus, reduction of oxidized cytochrome aa_3 by cytochrome c^{2+} (for example) frozen after a short period of time demonstrates the presence of very similar intermediate high spin (g ~ 6) signals and similar behavior of the other epr-detectable components.[197]

Generation of intermediate high spin heme signals (at g ~ 6) also occurs upon reoxidation of fully reduced (with cytochrome c^{2+}) cytochrome aa_3 by chemical oxidants such as ferricyanide or porphyrexide (but not by O_2).[52,107,208] The rhombic (g = 6.35, 5.44) portion of this signal achieves maximal intensity between 0.1 - 2 seconds after addition of oxidant and can then correspond to as much as 35 - 40% of the total heme in the enzyme.[208] Since this signal is observable in the presence of a fully-developed g3 signal, it must be due to a_3^{3+} and since its response to CO and pH mimics that of the intermediate high spin heme signal seen during partial reduction,[52,107] this intermediate rhombic high spin heme signal is also assignable to a_3^{3+}. (CO addition to either species causes an immediate shift in the rhombic splitting of the g6 signal to g ≈ 6.55, 5.23, ~2, followed by a slow disappearance of the g6 signals.[52,107-109]) The reactivity of this g6 signal generated upon anaerobic reoxidation (called the AR species by Beinert and coworkers[52]) suggests that it is an "activated" state of the enzyme with a_3^{3+} reacting rapidly with ligands (including O_2) and being reduced quickly by addition of cytochrome c^{2+}.[107]

The low spin signals generated by addition of the ligands cyanide, azide, and sulfide to the AR intermediate are summarized in Table 1-3. In general, the ligands react rapidly to generate an intermediate low spin signal (initial product) which is slowly converted to a second low spin signal (final product) with g values very similar to the normal ligand-induced low spin heme signals in the partially reduced enzyme discussed above.[52,107] The initial reactions of ligands with the AR species usually occur on the time scale of milliseconds, but the azide reactions are somewhat slower.[52,107]

This "activated" form of cytochrome aa_3 cannot be equated with any of the other O_2-activated forms (*e.g.*, the "oxygenated"[158] or "pulsed"[157] forms) since it is not formed in the presence of O_2. However, Beinert and coworkers have recently discovered a completely different transient signal upon O_2 reoxidation of reduced aa_3 (g = 1.78, 1.69, ~5) which may indeed be representative of an O_2-"activated" form of the enzyme.[128] This signal has been tentatively related to a_3^{3+} (probably under interaction with another site) and is closely associated with the 655 nm band which has been suggested to arise from a_3 or the a_3^{3+}-Cu_u^{2+} dimer.[54,202] It is interesting to note that at no time has any new signal or increase in intensity of the g2 signal been found that could be attributed to the undetectable copper. To the knowledge of this author, only three preliminary reports exist of epr signals attributed to the undetectable copper.[147,193,210] None of these reports can be claimed to show conclusively the existence of an epr signal due to this

copper. Assuming that the high spin heme intermediates discussed above are representative of cytochrome a_3^{3+} (with concomitant breaking of the antiferromagnetic coupling to Cu_u^{2+}), the failure to observe Cu_u^{2+} in the epr is one of the more intriguing current questions concerning the active site characteristics of aa_3.

Catalytic Activity

A direct examination of the reactions which are involved in the catalytic cycle is of course a necessity in the elucidation of the mechanisms employed by cytochrome aa_3. As is usually the case, however, the very efficiency which makes the enzymatic reactions interesting also precludes their observation by conventional (*i.e.*, slow) techniques. Thus, until recently, study was necessarily limited to the relatively stable derivatives of the enzyme. It is not surprising then that the "oxygenated" form of cytochrome aa_3 was one of the first "intermediates" of the catalytic cycle to be discovered, although now it appears that it is not a true catalytic intermediate and the only reason for its observation was its stability (as the end product of a series of intermediates which may actually be involved in the catalytic cycle[211]). With the development of new, faster techniques (*e.g.*, rapid quench epr, relaxation techniques, flash photolysis) and the increased use of low temperatures to separate the steps of the catalytic cycle, it has become possible to examine more closely the important individual reactions. This has allowed identification of a series of new "activated" forms and intermediates

of the cytochrome *c* oxidase reactions (as illustrated by the epr discussion above) and holds promise for unraveling the sequence of steps involved in the terminal reactions of respiration. The other technical difficulties involved in performing studies of this type cannot be overlooked. Inherent in the fact that cytochrome aa_3 reduces O_2 "for a living" is the necessity for strict exclusion of O_2 in control experiments. The ingenuity exhibited in attempts to meet the requirement of strict anaerobicity and faster reaction techniques has contributed as much to biochemistry in general as the results of these studies themselves.

The mechanistic question of how to use four separate reducing equivalents (from four ferrocytochrome *c* molecules) in the four-electron reduction of O_2 to $2H_2O$ without going through the thermodynamically unfavorable one-electron reduction of O_2 to superoxide ion[1,95] is one of the most interesting puzzles of biochemistry. It is probably no coincidence that cytochrome aa_3 has evolved as an enzyme with four active sites and an O_2-interaction site involving an antiferromagnetically coupled binuclear moiety (*cf.*, the active site make-up of laccase[212]). Cytochrome aa_3 somehow gathers reducing equivalents individually from cytochrome c^{2+} and transfers them to bound O_2 either in two-electron steps or in such a way that superoxide is stabilized (perhaps as a complex) in comparison to its free state.

Cytochrome *c* Oxidation. In the intact mitochondrial respiratory chain, cytochrome *c* acts as an electron shuttle bridging the gap between cytochrome bc_1 (cytochrome *c* reductase complex) and cytochrome

aa_3 (cytochrome *c* oxidase). The rate at which O_2 can be turned over during respiration requires that cytochrome *c* have an efficient means for performing its electron transfer task. Studies with isolated cytochrome aa_3 have shown that cytochrome *c* will form a complex with cytochrome aa_3[213,214] and this complex formation inhibits the reduction of ferricytochrome *c* (c^{3+}) by ascorbate.[214] Based on this inhibition, measurements show that perhaps 60 - 80% of the cytochrome *c* in intact mitochondria is bound.[214] Thus, this binding may be catalytically important. Analysis of the cytochrome *c* oxidase activity of aa_3 (by observing the aerobic oxidation of ferrocytochrome *c* (c^{2+}) in terms of Michaelis-Menton kinetics gives a K_m which is virtually identical to the K_d observed in direct binding studies.[213,215] Although further studies have indicated that there are actually two separate binding sites (and two K_m's observed in the kinetics (K_{m1} = 5×10^{-8} *M*, $K_{m2} \approx 1 \times 10^{-6}$ *M*[215])), the high-affinity site appears to be the one involved in the catalytic cycle since it is the one affected by addition of ATP to SMP.[215] The high affinity binding is extremely dependent on ionic strength, being stronger at low ionic strength.[213,214] This ionic strength dependence is also reflected in the cytochrome *c* oxidase activity[216-218] indicating that the binding of cytochrome *c* to cytochrome aa_3 is electrostatic in nature and that this binding leads to electron transfer. These observations have prompted a series of studies designed to map out the site on cytochrome *c* which is involved in the binding to cytochrome aa_3. Early studies showed that modification of cytochrome *c* lysine residues with neutralization of

the positive charge of the ε-amino groups effectively inhibited cytochrome *c* oxidase activity,[216,219] whereas guanidination of the lysines (the positive charge is retained upon guanidination) had little effect on the activity.[219] This implicates the involvement of the positively charged ε-amino groups of lysines in the electrostatic binding. This suggests that binding must occur to a negatively charged patch on aa_3 and pulse radiolytic studies show that hydrated electrons (e^-_{aq}) react with cytochrome c^{3+} with a rate constant of $4 \times 10^{10}\ M^{-1}\ s^{-1}$, but will only slowly reduce aa_3 in the absence of cytochrome *c*.[220] Further evidence for the anionic nature of the binding site on aa_3 comes from the fact that basic (*i.e.*, positively-charged at neutral pH) proteins and polypeptides (*e.g.*, protamine, salmine, poly-L-lysine) are potent inhibitors of the cytochrome *c* oxidase reaction[216,218,219] whereas the polypeptide made from lysine and glutamic acid is not inhibitory.[219] The involvement of the heme group in the electron transfer activity of cytochrome *c* with cytochrome aa_3 is shown in studies of cytochromes *c* with the heme modified either at the propionate side chain[221] or by substitution of Co for Fe[222] in which the cytochrome *c* oxidase activity was inhibited by use of these derivatives.

More recent studies involving the use of specific lysine modifications of cytochrome *c*[223-225] and antibodies prepared toward different regions of cytochrome *c*[226] have led to a fairly clear picture of the binding site employed in the reaction with cytochrome aa_3. This binding site involves various lysine residues near the "heme crevice" of cytochrome *c* and is approximately centered at the positive end of the average

dipole of cytochrome *c*.[227] This binding site is found to be slightly different from but overlapping with the site utilized in the reaction with cytochrome bc_1.[227] Thus, assuming that this binding is also involved in the catalytic cycle, the shuttle of electrons between bc_1 and aa_3 by cytochrome *c* must involve some diffusion (or rotation) of the cytochrome *c* molecule. It has recently been demonstrated that anionic lipids enhance cytochrome *c* oxidase activity and also shift the pH-dependence of this activity, an effect which is reversed at high ionic strength.[217] This was suggested to reflect the situation in intact mitochondria with cytochrome aa_3 residing in an anionic patch of the membrane, thus indicating that the cytochrome *c* electrostatic interactions may be more extensive *in vivo* (including some interaction with the membrane as well).[217]

The electrostatic nature of the cytochrome *c* binding reaction makes it reasonable to expect that c^{3+} might bind as well as, if not better than c^{2+}. In fact, the pseudo-first order character of the cytochrome *c* oxidase spectrophotometric assay (of aerobic cytochrome *c* oxidation)[228] has been suggested to be due to product inhibition[218] (*i.e.*, binding of c^{3+} preventing c^{2+} from reacting). Early measurements of c^{3+} binding indicated that the binding strength was independent of oxidation state[218,229] and this was assumed in analyzing turnover data in the most extensive study of the cytochrome *c*/cytochrome aa_3 aerobic reaction.[228] However, measurement of the potential of cytochrome *c* bound to aa_3[90] and direct binding measurements by an aqueous two-phase partitioning method[230] indicate that c^{3+} binds to aa_3 more strongly

than c^{2+} (by a factor of ~3 - 4). This may just be a result of the extra positive charge on the heme iron.

Studies on the anaerobic reduction of cytochrome aa_3 by ferrocytochrome c exhibit complicated (biphasic) kinetics with the initial step involving (at least) the reduction of cytochrome a.[50,137,156,231,232] The stoichiometry of this "burst" phase of cytochrome c^{2+} oxidation is not as well determined, varying between 1 (only cytochrome a reduced)[50,156] and 2 (both cytochrome a and Cu_d reduced).[137,220,232] The differences in measured stoichiometries may be due to the differences in cytochrome c^{2+} concentrations used. Greenwood and coworkers have shown that an initial reduction of cytochrome a is dependent on $[c^{2+}]$, while a second reduction of Cu_d is independent of $[c^{2+}]$.[232] Thus, the initial one-equivalent reduction of heme a will become well separated from the Cu_d reduction step at high $[c^{2+}]$. The bimolecular rate constant for the "burst" phase (*i.e.*, reduction of a^{3+}) is ~10^7 M^{-1} s^{-1}.[50,220] Assignment of this initial phase to the reduction of cytochrome a is supported by the observation that the rate is unaffected by azide[156] or cyanide[231] and is identical in the oxidized (resting) or mixed valence-CO forms.[233]

After the initial reductions of a^{3+} and Cu_d^{2+}, slower absorption changes occur which are interpreted as reduction of cytochrome a_3^{3+} (and probably Cu_u^{2+}) by intramolecular electron transfer.[50,231,232] This interpretation is supported by the fact that this slow phase is inhibited by cyanide[231] and is not observed at all in cytochorme c^{2+} reduction of the mixed valence-CO derivative.[233] The presence of

O_2 appears to accelerate this slower reaction,[50] and this intramolecular step is faster in the cytochrome c^{2+} reduction of "oxygenated" aa_3[234] and with the "pulsed" enzyme (cytochrome c^{2+}-reduced aa_3 reacted with a pulse of O_2)[157] Thus, it appears that the presence of O_2 or of "activated" forms of aa_3 causes some type of conformational change, which increases the rate of the intramolecular electron transfer step between cytochrome a^{2+} and $a_3{}^{3+}$. This suggests again that the resting enzyme is not a part of the catalytic cycle and must be reduced before it can function as an efficient electron transfer catalyst. In the presence of excess O_2 and cytochrome c^{2+}, catalytic turnover results in reoxidation of $Cu_d{}^{+}$ (monitored at 830 nm) which parallels the oxidation of cytochrome c^{2+}.[137,232] Thus, $Cu_d{}^{2+}$ formation is apparently the rate limiting step in turnover. The reoxidation of cytochrome a^{2+} during turnover was much slower. This can be interpreted in terms of the intramolecular $a \rightarrow a_3$ electron transfer being dependent on reduction of $Cu_d{}^{2+}$.[137,232,235] Thus, under turnover conditions, electrons are transferred initially to cytochrome a and from a to Cu_d. Once both a and Cu_d become reduced, intramolecular electron transfer occurs (of one or two electrons) to a_3 (and/or Cu_u). This allows a to immediately accept another electron from c^{2+} (this transfer is not rate limiting) and the process starts over. Under this proposed mechanism, a would appear to remain reduced but Cu_d would seem to be somewhat oxidized, depending on the total number of reducing equivalents (from cytochrome c^{2+}) flowing through the system.

Dioxygen Reduction. The other side of the catalytic reactions of cytochrome aa_3 (the O_2 reductase activity) is not as well-studied as the cytochrome *c* oxidase side. Early work by Gibson and Greenwood showed a fast phase of O_2 diffusion into aa_3 with $k \approx 10^8\ M^{-1}\ s^{-1}$, followed by oxidation of a_3^{2+} ($k \approx 3 \times 10^4\ s^{-1}$), oxidation of Cu_d^+ ($k \approx 7 \times 10^3\ s^{-1}$ at 830 nm), and oxidation of a^{2+} ($k \approx 7 \times 10^2\ s^{-1}$).[49,126,236] Much of this work was performed by the flow flash technique which consists of mixing O_2 with the reduced cytochrome aa_3-CO complex and initiating the reaction by flash photodissociating the CO before the O_2 can displace it.[236] The assignment of the initial O_2 reactions to cytochrome a_3 is supported by the observation of an identical rate during O_2 oxidation of the mixed valence-CO derivative (after photodissociation of CO).[96]

Turnover in the presence of cytochrome c^{2+} and O_2 can be monitored by polarographic measurements of O_2 remaining in solution as it is consumed by cytochrome aa_3. Although comparison of this assay method with the spectrophotometric assay mentioned above shows major differences in the activities measured,[237] studies of $[O_2]$-dependence and inhibitor effects on the polarographic assay results (*i.e.*, relative comparisons) should still be valid. $[O_2]$-dependence studies indicate that, in the ascorbate/cytochrome *c*/cytochrome aa_3/O_2 turnover system, the kinetics could be adequately fit with Minnaert's Mechanism IV[238] (with the assumption of equal binding constants for oxidized and reduced cytochrome *c*) giving an "on" rate constant (for O_2) of $\sim 10^8\ M^{-1}\ s^{-1}$ and a $K_m(O_2) = 9.5 \times 10^{-7}\ M$ (at [cytochrome c^{2+}] $\rightarrow \infty$).[239] This

mechanistic model was used to fit spectrophotometric assay results as well (with modification to two cytochrome *c*-binding sites).[228]

Inhibition of the O_2 reductase reaction has been examined with several aa_3 inhibitors with the following results:[101] CO is a strictly competitive inhibitor of O_2, suggesting that CO and O_2 both bind to reduced cytochrome a_3; azide and formate are uncompetitive inhibitors (explained by binding to oxidized cytochrome a_3 only); cyanide and sulfide are noncompetitive and are suggested to bind to an unspecified intermediate form of the enzyme and oxidized a_3 with equal affinity. Thus, cytochrome a_3^{2+} is the only reasonable choice as (at least part of) the O_2-binding site.

One of the most interesting aspects of O_2 reduction by cytochrome aa_3 is the proposed existence of several intermediates directly or indirectly involving O_2. Thus, O_2-reoxidation of dithionite-reduced aa_3 results in formation of the "oxygenated" form of the enzyme before conversion to the resting state.[158] This has been shown to actually involve three different intermediate species, the conversion of the first two of these to the third being strongly activated by the presence of cytochrome c^{2+}.[211] These species are rather long-lived and may not be genuine catalytic intermediates. If cytochrome aa_3 is reduced with an excess of cytochrome c^{2+} and reoxidized with a pulse of O_2, the "pulsed" enzyme formed appears to behave like a true catalytic intermediate.[157,240] Also (as discussed in the epr section) cytochrome aa_3 at various intermediate stages of reduction exhibits transient epr signals which appear to be "active" toward cytochrome c^{2+}, O_2 and ligands.[52,107,128,208]

By far the most extensive study undertaken toward examination of actual intermediates of the O_2 reoxidation of aa_3 (at low temperatures) is that initiated by Britton Chance and coworkers.[43,44,47,104,114,115,241-246] The technique used in these studies involves addition of O_2 to the reduced aa_3-CO derivative (at low enough temperatures to avoid O_2 displacement of CO), followed by freezing of the reaction mixtures at low temperatures ($\gtrsim$150 K), flash photodissociation of the CO and monitoring of the O_2 reoxidation of the "freed" aa_3 by dual-wavelength spectroscopy. This technique has resulted in the observation of several intermediates which are stabilized at different temperatures. Based on spectroscopic evidence, Chance and coworkers have suggested that the sequence of O_2 reoxidation of fully reduced cytochrome aa_3 is as follows:[43,114]

$$\begin{matrix} Cu_d^{+}\ a^{2+} \\ Cu_u^{+}\ a_3^{2+}\cdot CO \end{matrix} \xrightarrow[+O_2]{h\nu} \begin{matrix} Cu_d^{+}\ a^{2+} \\ Cu_u^{+}\ a_3^{2+}\cdot O_2 \end{matrix} \longrightarrow \begin{bmatrix} Cu_d^{+}\ a^{2+} \\ Cu_u^{+}\ a_3^{3+}\cdot O_2^{-} \end{bmatrix} \longrightarrow \begin{matrix} Cu_d^{+}\ a^{2+} \\ Cu_u^{2+}\ a_3^{3+}\cdot O_2^{=} \end{matrix} \longrightarrow \begin{matrix} \text{oxid.} \\ aa_3 \end{matrix}$$

$$A_1 \qquad B_1 \qquad B_2$$

(where B_1 is a transient and not directly observed). Thus, the initial formation of compound A_1 involves only binding of O_2 (no electron transfer). The existence of the oxidized state of a_3^{3+} in compound B (B_1 and B_2) is supported by observations that show the reappearance of the 655 nm band after compound A_1 formation.[54] At room temperature, the conversion of B_2 into oxidized aa_3 probably involves intramolecular

electron transfer from Cu_d and a to Cu_u and a_3, followed by further electron transfer to $O_2^{=}$. However, in the presence of cytochrome c^{2+} at low temperatures, Chance and coworkers have provided evidence which supports the direct reduction of a_3^{3+} and Cu_u^{2+} by cytochrome c^{2+} and have suggested a tunneling mechanism for this process.[44,244] The reaction of O_2 with the CO-photodissociated mixed valence state behaves similarly to the scheme given above (with Cu_d and a oxidized), but no 655 nm absorption is seen,[54] so that a_3 may remain in the reduced state:[43,114,115]

$$\begin{matrix} Cu_d^{2+}\ a^{3+} \\ Cu_u^{+}\ a_3^{2+}\cdot CO \end{matrix} \xrightarrow[+O_2]{h\nu} \underset{A_2}{\begin{matrix} Cu_d^{2+}\ a^{3+} \\ Cu_u^{+}\ a_3^{2+} \end{matrix}}\cdot O_2 \longrightarrow \underset{C_1}{\begin{pmatrix} Cu_d^{2+}\ a^{3+} \\ Cu_u^{+}\ a_3^{3+}\cdot O_2^{-} \end{pmatrix}} \longrightarrow \underset{C_2}{\begin{matrix} Cu_d^{2+}\ a^{3+} \\ Cu_u^{2+}\ a_3^{2+}\cdot O_2^{-} \end{matrix}}$$

Recently, Clore and E. M. Chance have performed experiments essentially identical to those of B. Chance and coworkers with a more elaborate analysis utilizing nonlinear optimization techniques.[247-249] They observed similar intermediates during O_2 reoxidation of fully reduced aa_3 but their assignments differ considerably. The scheme suggested by Clore and Chance suggests further electron transfer and involvement of Cu_d and a:[247-249]

$$\begin{matrix} Cu_d^{+}\ a^{2+} \\ Cu_u^{+}\ a_3^{2+}\cdot CO \end{matrix} \xrightarrow[+O_2]{h\nu} \underset{I(A_1)}{\begin{matrix} Cu_d^{+}\ a^{2+} \\ Cu_u^{+}\ a_3^{3+}\cdot O_2^{-} \end{matrix}} \longrightarrow \underset{II}{\begin{matrix} Cu_d^{+}\ a^{3+} \\ Cu_u^{2+}\ a_3^{2+}\cdot O_2^{=} \end{matrix}} \longrightarrow \underset{III(B)}{\begin{matrix} Cu_d^{2+}\ a^{3+} \\ Cu_u^{2+}\ a_3^{2+}\cdot O_2^{3-} \end{matrix}} \longrightarrow \text{oxid. } aa_3$$

The basis of these workers' assignment of a_3 being reduced in intermediate III is what they claim to be the failure to see any 655 nm absorption, but this claim appears to be incorrect. Denis[54] clearly states that the 655 nm band *is* observed after compound A formation in O_2 reoxidation of fully reduced cytochrome aa_3.

The detailed assignments of redox states to the various active sites in the O_2-intermediates discussed above is clearly not yet settled. However, the very fact that techniques have been developed to make observation of such a complicated series of rapid reactions possible suggests that application of other spectroscopic techniques in examination of these intermediates will soon shed light on the actual mechanisms involved.

EXPERIMENTAL

Materials

Cacodylic acid (dimethyl arsinic acid) was purchased from Matheson-Coleman-Bell and was recrystallized before use by the published method.[250] 3-(N-morpholino)propane sulfonic acid (MOPS) was purchased from Sigma and used without further purification. Cholic acid was purchased from Sigma and purification prior to use was *required*. The following procedure was used:[251] approximately 200 g. cholic acid was *slowly* added with overhead stirring to $\lesssim$2 l of boiling 95% ethanol (undenatured). After all the cholic acid had dissolved, approximately 15 g. of activated charcoal (Norit A from Bio-Rad was used) was added and stirring was continued until the suspension had boiled down to a volume of approximately 1200 ml. While still hot, the activated charcoal was removed by filtration on a Buchner funnel and the charcoal was washed once with approximately 100 ml of hot 95% ethanol to redissolve any precipitated cholic acid. The filtrate was then boiled down to approximately 750 ml and $\gtrsim$2 l. of H_2O was added. After cooling to ~4° C, the precipitate was collected on a Buchner funnel and the entire charcoal process was repeated at least once more. After the final purification cycle, the cholic acid was dried to constant weight *in vacuo* and dissolved in water with a stoichiometric amount of KOH (or NaOH) to give potassium (or sodium) cholate of the desired concentration. It was sometimes necessary to centrifuge this final solution to remove fine charcoal particles left from the purification steps.

The hexammine ruthenium(III) trichloride ($Ru(NH_3)_6Cl_3$) was from Matthey-Bishop (purchased through Alfa) and was recrystallized before use by the method of Taube.[252] Methylviologen (MV, 1,1'-dimethyl-4,4'-bipyridinium dichloride) was purchased from Aldrich as the hydrate and used without further purification. The cation radical of methyl viologen ($MV^{+\cdot}$) was generated electrochemically by constant potential electrolysis of a 1 m*M* solution at ~ -700 mV SCE. Proflavine monohydrochloride was purchased from Polysciences, Inc. and used without further purification. Proflavine was used as the photoacceptor of a $MV^{+\cdot}$-generating system which was used to scrub O_2 from Ar gas. The method used is a modification of the method suggested by Sweetser[253] and utilizes ethylenediaminetetraacetic acid (EDTA) as the electron donor. The scrubbing solution contains 50 μ*M* proflavine, 0.5 m*M* MV, 50 m*M* EDTA and is made up in sodium phosphate buffer (μ = 0.1, pH = 7.0). Unless under an anaerobic atmosphere, this solution was stored in the dark to prevent ambient turnover of EDTA.

The nonionic detergent, Tween-20 (polyoxyethylene sorbitan monolaurate), was used as the solubilizing agent for cytochrome aa_3 for all the studies reported herein. Tween-20 was purchased from Sigma and was cleaned by the following procedure:[251] a short, large diameter column of neutral alumina (Bio-Rad AG-7) equilibrated in pH 7 buffer was poured and a 50% aqueous solution of Tween-20 was eluted through it under pressure. The eluate was diluted to 20% Tween-20 and stored at ~4° C until needed. Just before use, the 20% Tween-20 was passed through a Millipore filter. The nonionic surfactant, Triton X-100,

was purchased from Rohm and Haas Co. and was allowed to settle before using the top (less viscous) portion.

Horse heart cytochrome *c* was Sigma Type VI and was used without further purification. For the cytochrome *c* oxidase activity assays, cytochrome *c* was reduced with a ten-fold excess of $Fe(EDTA)^{2-}$, then dialyzed anaerobically to remove the excess reductant. Glucose oxidase was purchased from Sigma as a solution containing 1385 units/ml and was used without further treatment.

All other chemicals were obtained commercially and used without further purification. Distilled water was passed through a Barnstead Nanopure water purification system before use. The conductivity was routinely as high as 18 megohm-cm.

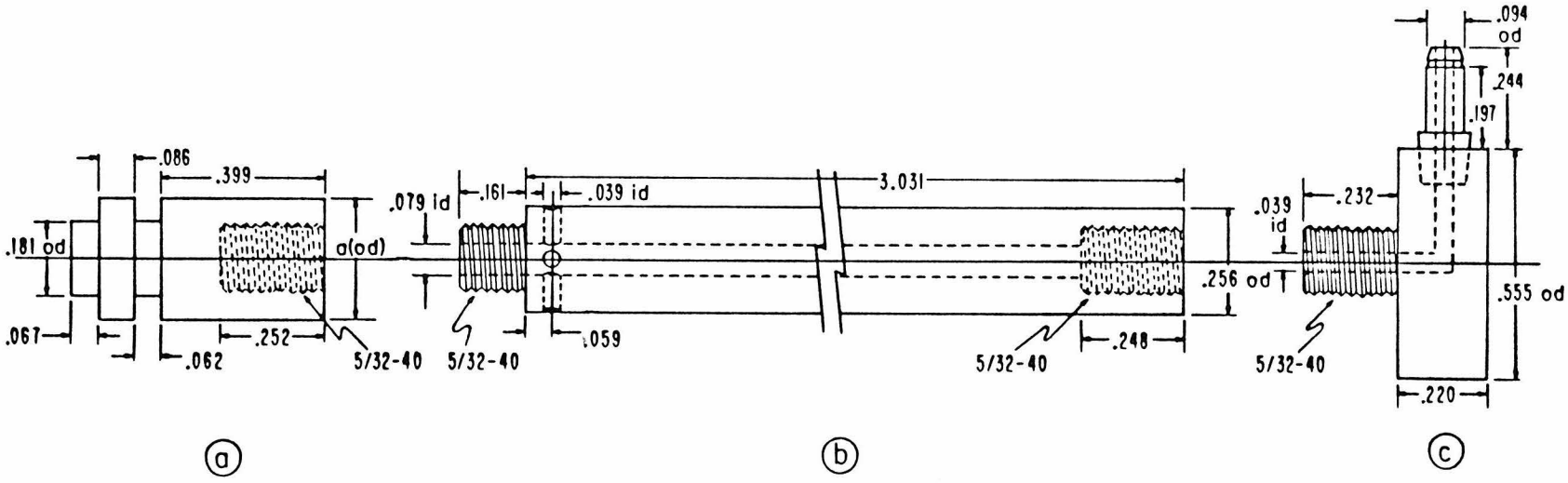
Equipment

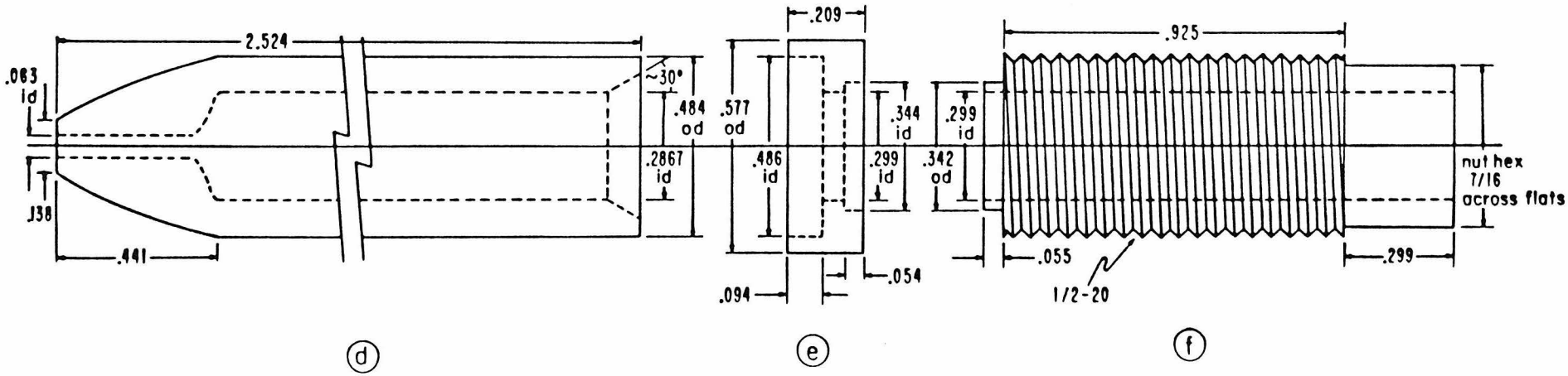
Kinetics data was collected on a Durrum D-110 stopped flow spectrophotometer modified for anaerobic work as described below. The data were simultaneously displayed on a Tektronix 564B storage oscilloscope and temporarily stored in an analog input buffer (with built-in ADC). Each set of data was subsequently sent under software control to a PDP-10 timesharing computer system and written on disk for later analysis. The stop syringe and pneumatic ram of the D-110 were set such that the data acquisition was triggered approximately ten milliseconds before the actual stoppage of flow, so that an accurate measure (within ~2 msec) could be made of zero time.

Several parts of the Durrum flow system were modified so that the instrument could be used for anaerobic kinetics studies. The

syringes and syringe plungers were modified as shown in Fig. 1-2. The original thin-walled glass syringe was sealed to the Durrum Kel-F mixing block through a tapered teflon cone with a central hole for solution flow. In an attempt to minimize the number of potentially leaky connections, the syringe barrel was converted to a one-piece glass design using thick-walled precision bore Pyrex tubing (.2867" id) purchased from Wilmad Glass Company. This tubing was modified by fusing thick-walled Pyrex capillary tubing to one end while a 1.5 mm diameter tungsten rod was inserted through the tip to keep the hole open, then grinding down the outer surface to a convex taper (see Fig. 1-2). The ground glass outer surface was then fire-polished so that a good seal with the Kel-F block was obtained. The original plunger tip design was maintained (Teflon with an O-ring seal) but different diameter tips were made for different temperature ranges (see legend of Fig. 1-2) to take into account the differing thermal expansion coefficients of Teflon and glass. Also, the plunger shaft and head were drilled to allow flushing of the space behind the plunger tips with pure, dry nitrogen. This minimizes the chance of O_2 leaking into the solutions stored in the syringes through the plunger tip seal. Once the syringes have been flushed several times with MV^+ (see below) to remove any residual O_2 adsorbed to the Teflon, the syringes will maintain MV^+ reduced indefinitely provided a sufficient N_2 purge is maintained behind the plunger tips. The Teflon gasket between the glass syringe barrel and the stainless threaded nut as well as the nut are very similar to the original design except that

Fig. 1-2. Modified Durrum syringes. (a) Teflon plunger tip of various outer diameters: a = .287 (~20-35° C); a = .288 (~15-25° C); a = .289 (~5-15° C). The groove accepts a Viton O-ring (9/32 od x 5/32 id) which extends slightly beyond the tip od. (b) Stainless steel plunger shaft drilled concentrically with four smaller ports at right angles just above plunger tip (for N_2 flush). (c) Stainless steel plunger head with small tubing connection for N_2 inlet. (d) Precision-bored thick-walled glass syringe barrel (tubing from Wilmad) with fused tapered tip and internally flared back end. (e) Teflon gasket for stainless to glass seal. (f) Stainless steel threaded nut. All dimensions are in inches. (See text for more details.)


.086
.399
.181 od
a(od)
.067
.062
.252
5/32-40
.079 id
.161
.039 id
5/32-40
.059
3.031
.256 od
5/32-40
.248
.039 id
.232
.094 od
.244
.197
.555 od
5/32-40
.220
ⓐ
ⓑ
ⓒ


2.524
.063 id
~30°
.484 od
.2867 id
.138
.441
.209
.577 od
.486 id
.344 id
.299 id
.094
.054
.925
.299 id
.342 od
.055
1/2-20
.299
nut hex 7/16 across flats
ⓓ
ⓔ
ⓕ

the knurled end of the stainless nut has been changed to a hex. The use of thick-walled glass tubing allows more pressure to be put on the syringe barrel to improve the seals.

The original Teflon reservoir adapters which ended in female luers for use with reservoir syringes have been replaced with Kel-F pieces as shown in Fig. 1-3. The Kel-F reservoir adapters are hand-tightened against the Kel-F mixing block by the use of aluminum threaded nuts which are similar to the original design except for the necessity of being constructed in two halves (fastened together with allen bolts). The top end of the Kel-F piece is designed to be fastened directly to glass reservoir flasks through O-ring joints which permit a much tighter seal than the original luer joints. The reservoir flasks are discussed a little later.

The Durrum valve stems and handles (all one-piece stainless steel rod originally) were replaced with two-piece valve stem assemblies as shown in Fig. 1-4. The valve stems were made hollow with an extra cross hole just above the Teflon valve tip (the original tips and roll pin fasteners were used with the new stems as well). The top of the valve stems were designed to accept tubing for purging the space directly above the valve tips with pure, dry N_2. The original threaded nuts, spacers, and spring washers were used to tighten down the valves and the N_2 purge bubbled up through the thermostatted bath water around the threads of these nuts. The valves were made in two pieces to allow the installation of the water bath cover (see below) prior to attaching the valve handles. Once the handles are in place

Fig. 1-3. Modified Durrum reservoir adapters. (a) Side and top views of aluminum threaded nut (two pieces each, held together by a pair of allen bolts); (b) Kel-F reservoir connector with tapered end for connection to Durrum Kel-F block and a top end which can be connected to a 12/5 glass O-ring joint on the reservoir flasks. All measurements in inches. (See text for more details.)

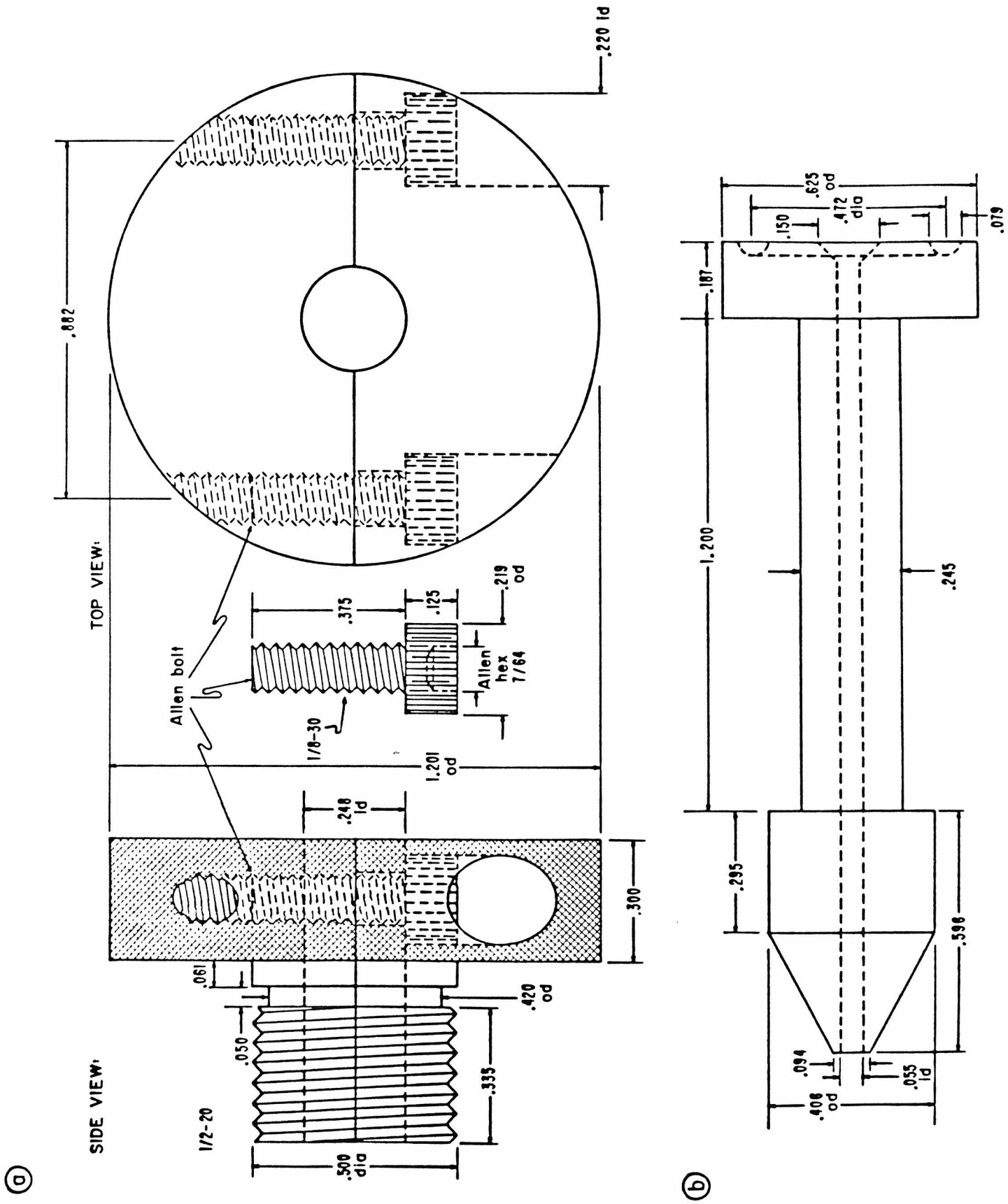
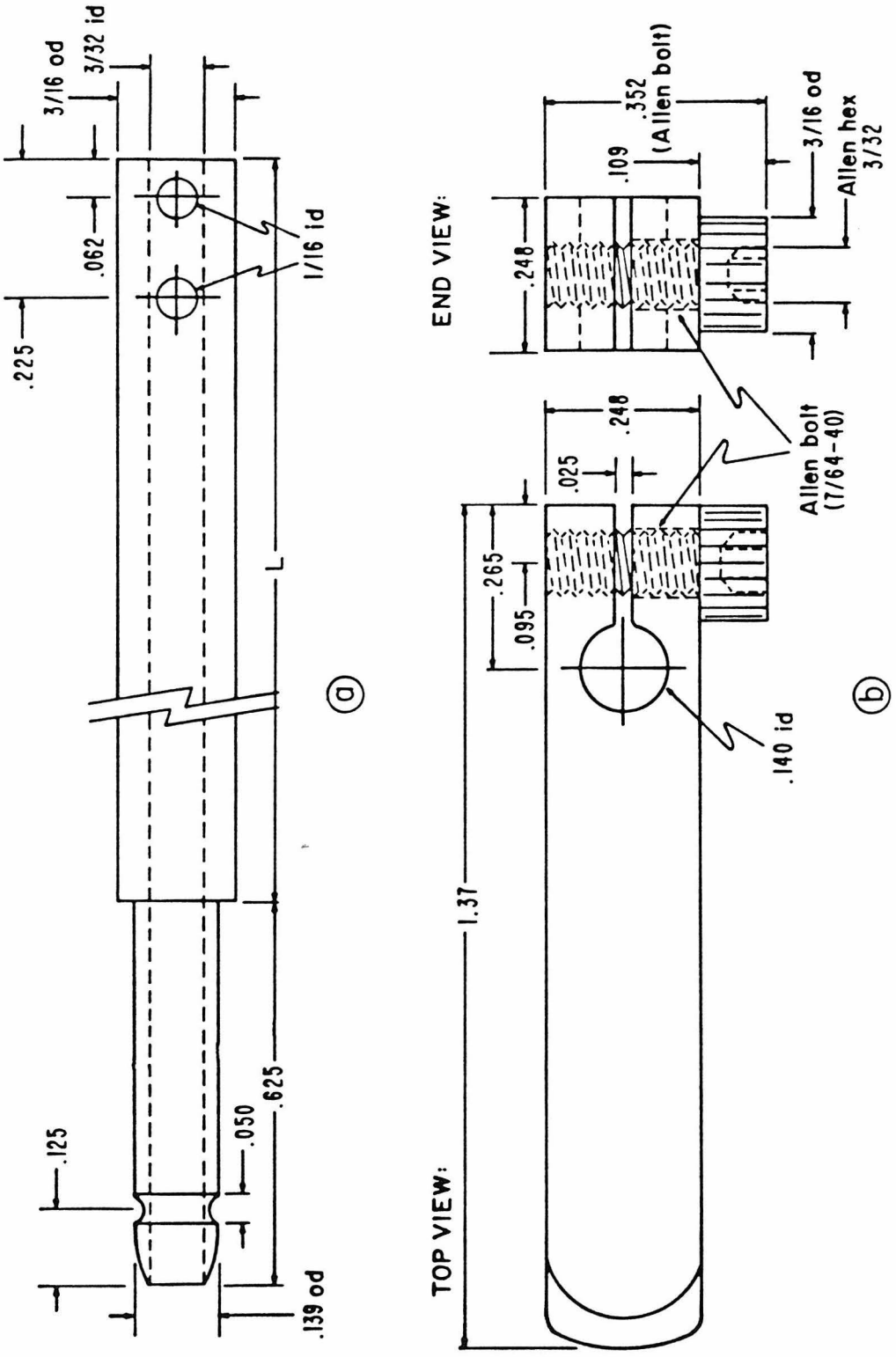

(a)
TOP VIEW:
.882
.220 id
Allen bolt
.375
.125
.219 od
Allen hex 7/64
1/8-30
1.201 od
.248 id
.300
SIDE VIEW:
.061
.420 od
.050
.335
1/2-20
.500 dia
(b)
.625 od
.472 dia
.150
.079
.187
1.200
.245
.295
.598
.094
.055 id
.408 od

Fig. 1-4. Modified Durrum valve stems and handles. (a) Stainless steel valve stems - hollowed to permit N_2 purge. Length L depends on valve number: #1, L = 4.06; #2, L = 4.76; #3, L = 4.65; #4, L = 5.35; #5, L = 1.97. (b) Stainless steel valve handle with allen bolt to tighten it onto stem. Each stem is scored so that handle can be properly aligned with the holes at the bottom of the stem which dictate the direction of the Teflon valve head (not shown). All dimensions in inches. (See text for more details.)

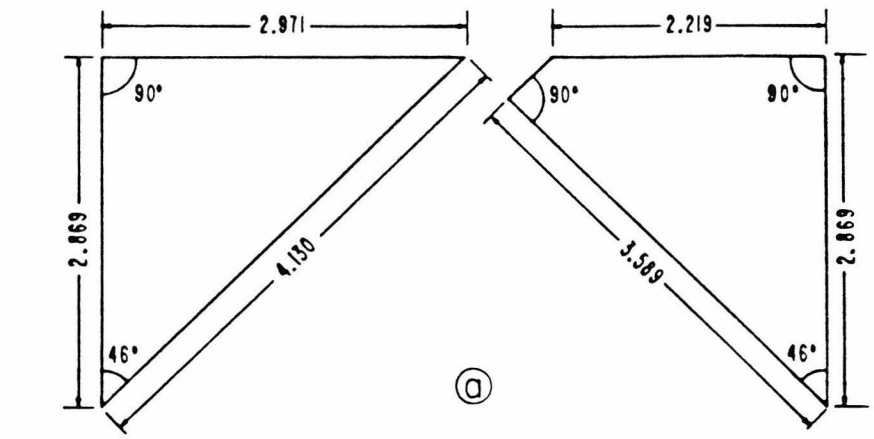

3/16 od
3/32 id
.062
1/16 id
.225
L
.125
.050
.625
.139 od
ⓐ
END VIEW:
.352
(Allen bolt)
.109
3/16 od
Allen hex
3/32
.248
Allen bolt
(7/64-40)
.248
.025
.265
.095
1.37
.140 id
TOP VIEW:
ⓑ

and properly aligned (as described in the legend of Fig. 1-4), the N_2 inlet tubes are attached to the exposed tops of the valve stems. The N_2 purge is maintained throughout the remainder of the run.

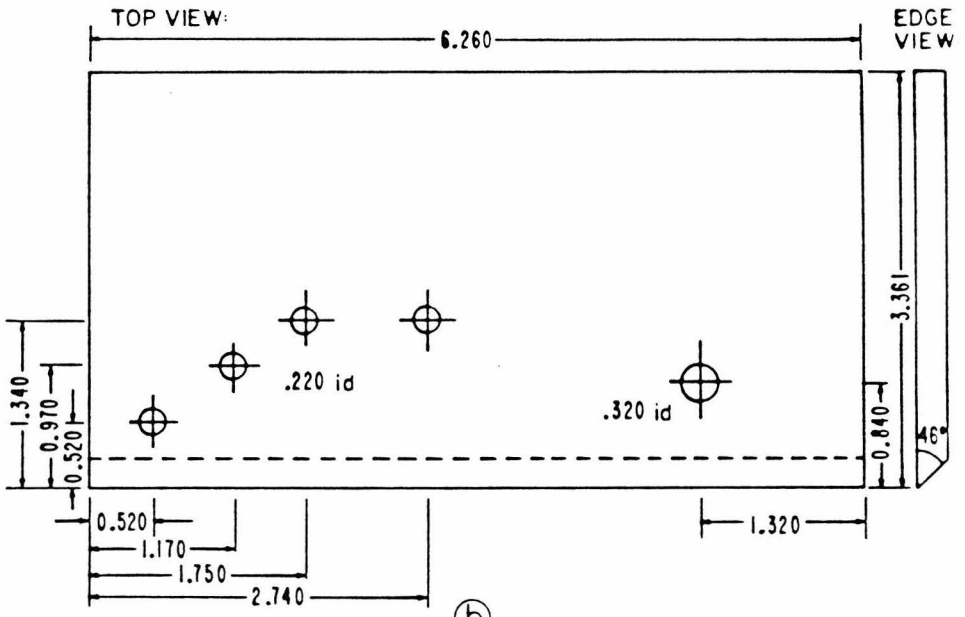
The water bath cover was made of lucite (see Fig. 1-5) and was originally designed to be sealed against the bath well enough to provide a fairly inert atmosphere above the bath water (and mixing block). Although it proved extremely difficult to achieve such a seal, the cover provided other advantages (*e.g.*, better stability of bath temperature) which made its use desirable. The bath water itself was continuouslybubbled with pure, dry N_2 from the valve purge and through a Hamilton male luer-to-male luer connector epoxied into the .320 id hole in the bath cover front (see Fig. 1-5(b)). The other four holes in the front piece are for the valve stems and the oblique hole in the back has an O-ring epoxied into it to hold a thermometer.

Two different reservoir flasks were designed for use with the inorganic reagent solution or the enzyme solution, respectively. The "enzyme flask" is depicted in Fig. 1-6. The flask is designed with a vacuum cup 3-way stopcock and a Teflon valve adapter (see Fig. 1-6(b)) for use on a vacuum line. The stirred protein solution is degassed on the vacuum line with the flask in an orientation "inverted" from that shown in Fig. 1-6, then sealed off with the Teflon valve and reinverted and installed on the Durrum (attached to the Kel-F reservoir adapters shown in Fig. 1-3). The third stopcock arm is used for flushing the stopcock and lower arm with anaerobic buffer and gas as described later.

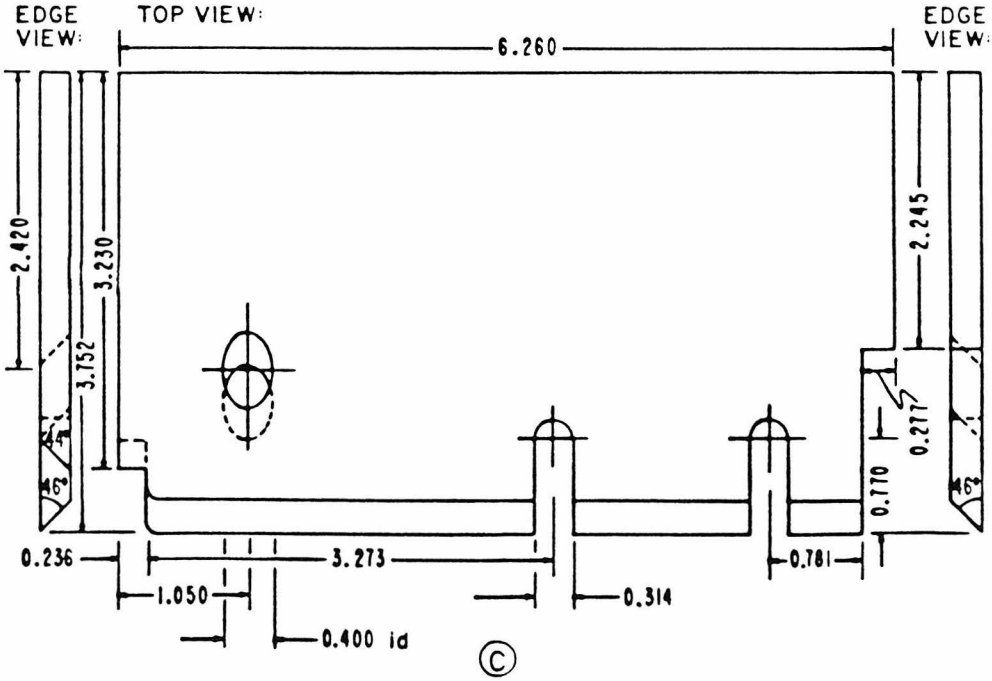
Fig. 1-5. Durrum lucite water bath cover. (a) End pieces. (b) Front piece with four holes for valve stems and larger hole for Hamilton connector (see text). (c) Back piece with cutouts for reservoir adapter stems and slanted thermometer hole. The pieces were "glued" together by the use of acetone on the edges. The construction is as follows: top edge of left end piece to left edge of back piece; top edge of right end piece to right edge of back piece; top edge of front piece to top edge of back piece; right edge of front piece to left edge of left end piece; left edge of front piece to right edge of right end piece. All dimensions in inches. (See text for more details.)


2.971
2.219
90°
90°
90°
2.869
2.869
4.130
3.589
46°
46°

ⓐ

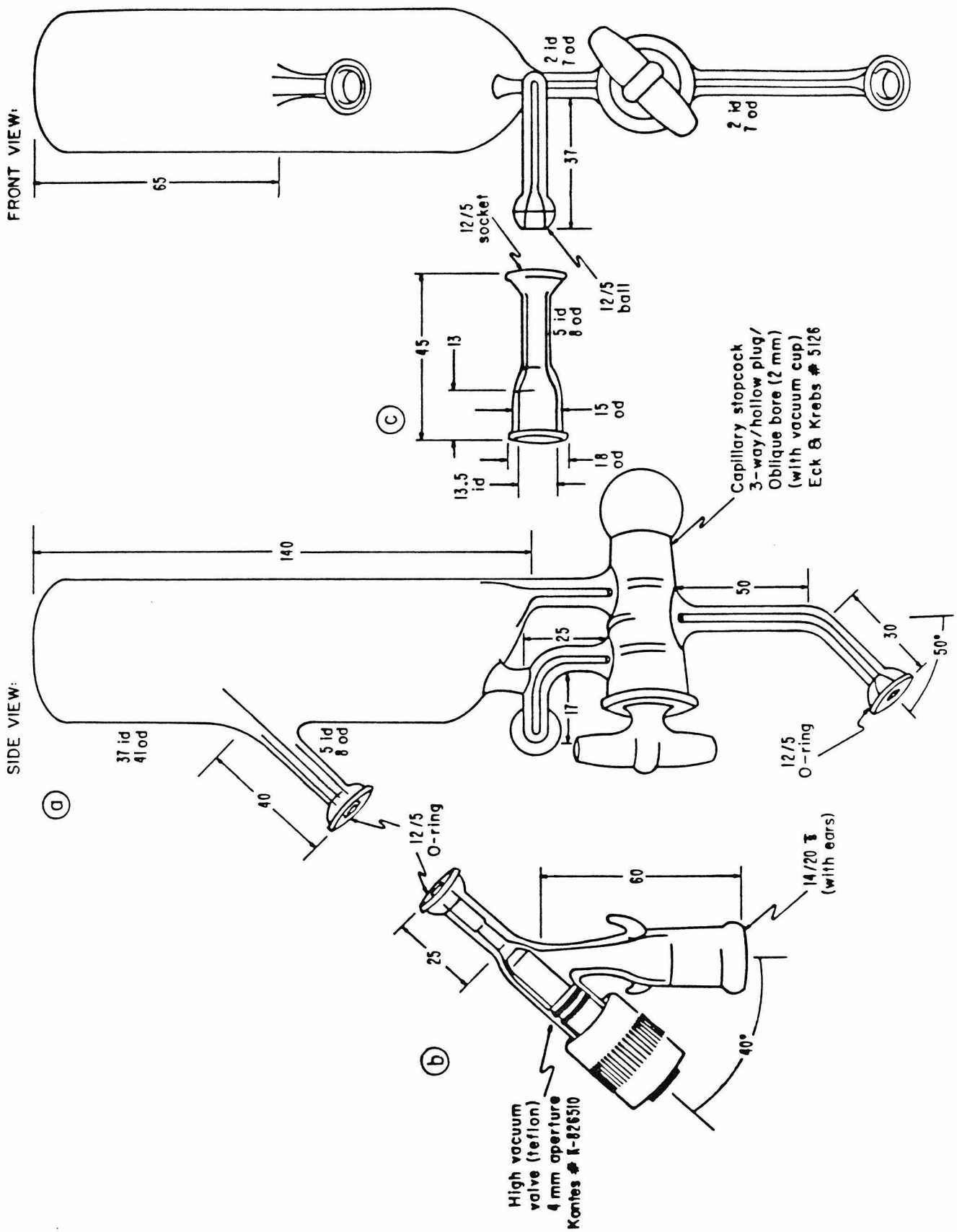

TOP VIEW:
6.260
EDGE VIEW
.220 id
.320 id
3.361
1.340
0.970
0.520
0.840
46°
0.520
1.170
1.750
2.740
1.320

ⓑ


EDGE VIEW:
TOP VIEW:
6.260
EDGE VIEW:
2.420
3.230
3.752
2.245
0.277
0.770
0.236
3.273
0.781
1.050
0.314
0.400 id

ⓒ

Fig. 1-6. Durrum "enzyme flask" reservoir. (a) Main body of flask made out of pyrex. (b) Adapter valve to vacuum line. (c) Adapter to serum stopper neck for preflush. All dimensions in mm. (See text for more details.)


FRONT VIEW:
SIDE VIEW:
65
140
40
37 id
41 od
5 id
8 od
12/5 O-ring
60
25
14/20 T (with ears)
40°
High vacuum valve (Teflon) 4 mm aperture Kontes # K-826510
Capillary stopcock 3-way/hollow plug/ Oblique bore (2 mm) (with vacuum cup) Eck & Krebs # 5126
50
25
17
30
50°
12/5 O-ring
2 id
7 od
37
12/5 socket
12/5 ball
45
13
5 id
8 od
15 od
18 od
13.5 id
a
b
c

The "reagent flask" is shown in Fig. 1-7. The reagent is degassed by bubbling with Ar so that only a solid plug high vacuum stopcock is required. Since several (usually, 5 or 6) reagent flasks are used at once, the design was intentionally kept simple and inexpensive with only a hose connection for the gas inlet and a neck for a serum stopper with a needle for the gas exit. Again the flask is attached to the Kel-F reservoir adapter on the Durrum by an O-ring seal and has an adapter (Fig. 1-7(b)) for preflushing (see Methods Section).

The $Ru(NH_3)_6^{2+}$ used for the present study was generated electrochemically by constant potential electrolysis. The two-compartment cell designed for this electrolysis is illustrated in Fig. 1-8. The cell was designed to hold ~100 ml in the working electrode compartment and ~5-10 ml in the counter electrode compartment. Both the counter and working electrodes were platinum and were held in place by serum stoppers. The reference electrode was saturated calomel and was fitted into the angled standard taper neck through a Teflon bushing lined with a silicon O-ring. The three-way capillary stopcock allowed bubbling through the solution before and flowing above the solution during the electrolysis.

Methods

Cytochrome aa_3. The enzyme was isolated from beef heart mitochondrial paste (A3 from the laboratory of D. E. Green) by the method of Hartzell and Beinert.[109] A detailed, well-commented description of the purification

Fig. 1-7. Durrum "reagent flask" reservoir. (a) Main body of flask made out of pyrex. (b) Adapter to serum stopper neck for preflush. All dimensions in mm. (See text for more details.)

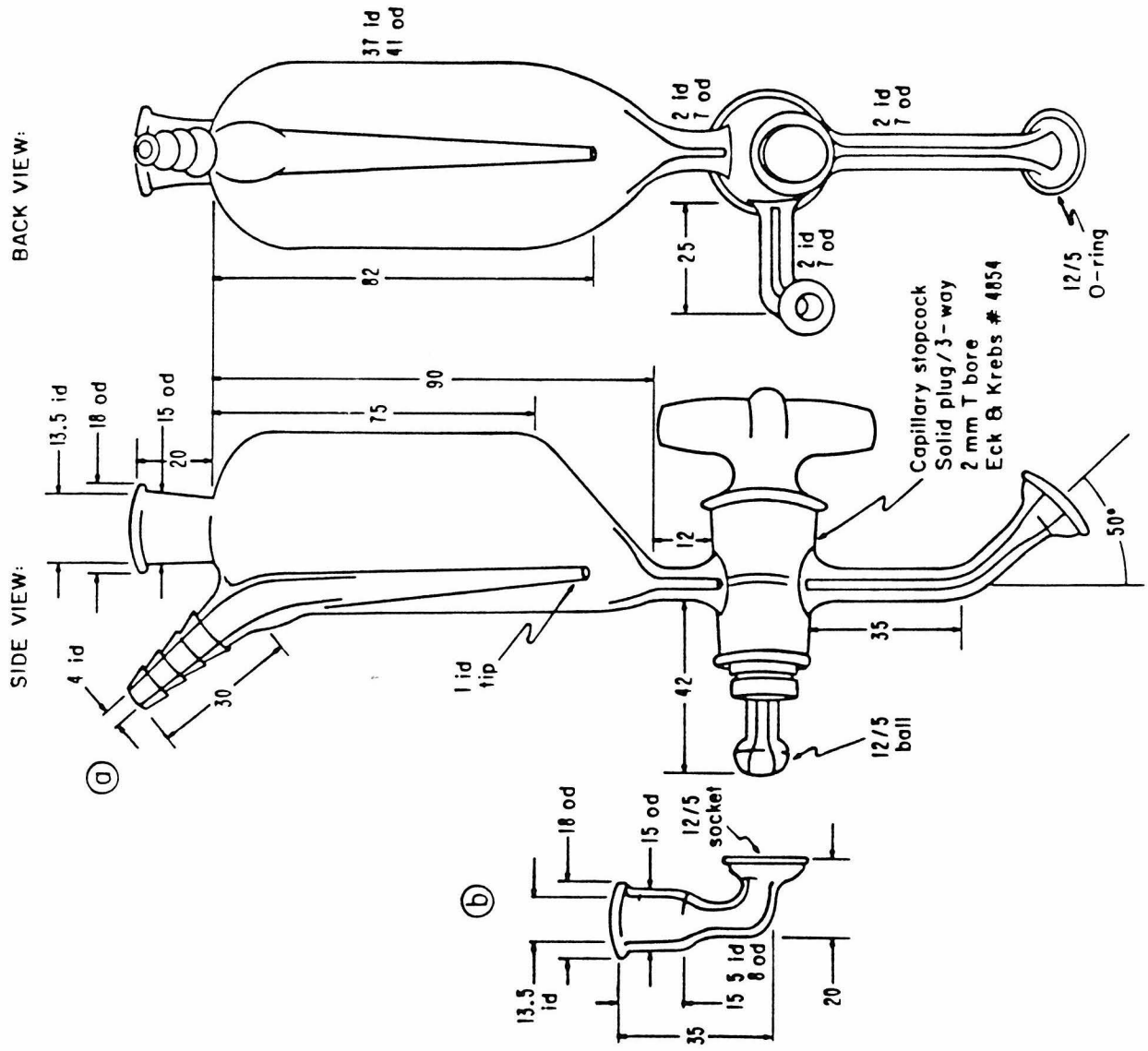
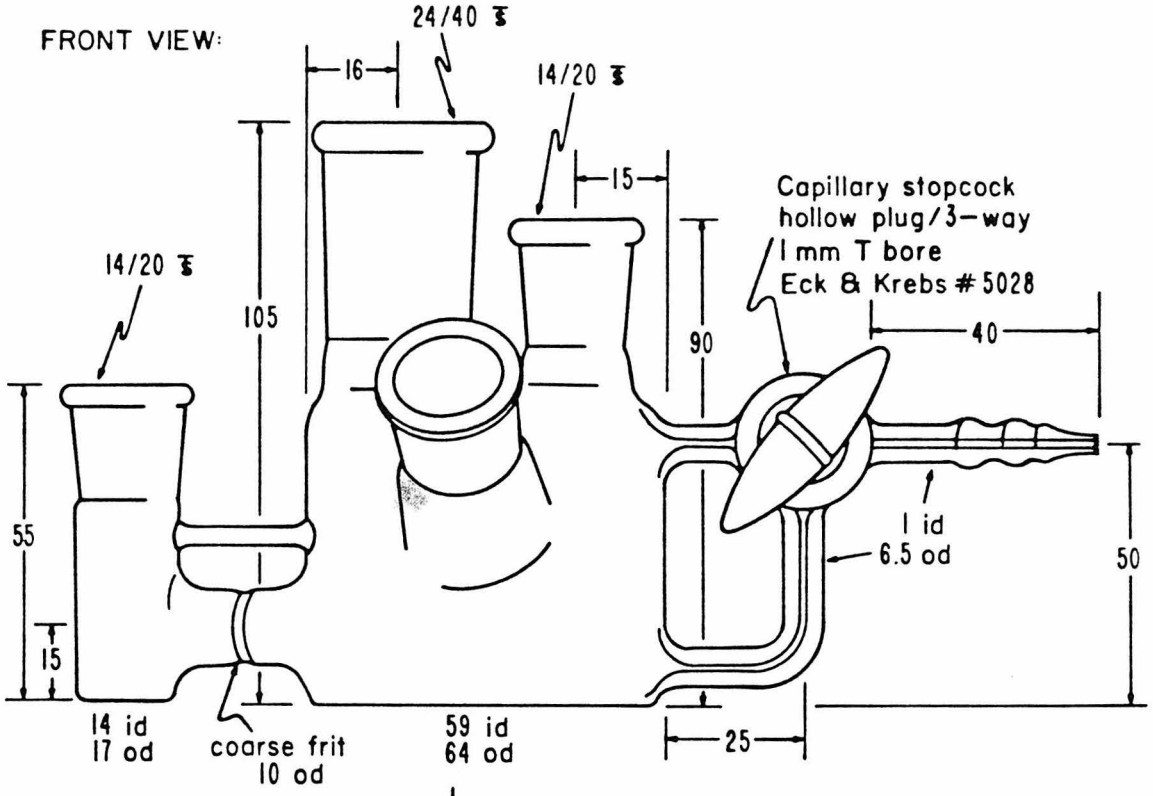
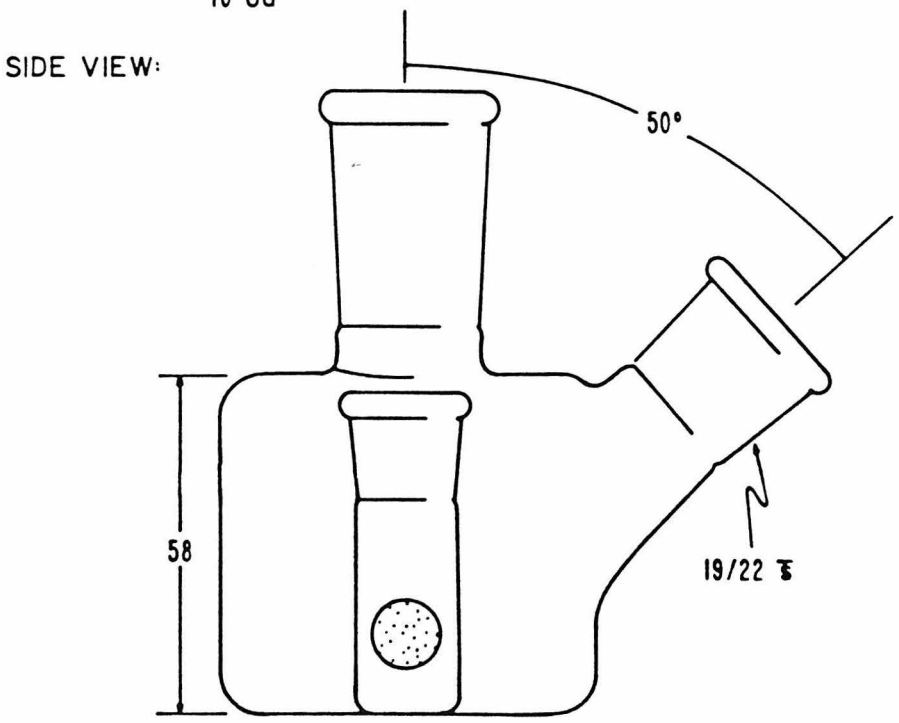

BACK VIEW:
SIDE VIEW:
37 id
41 od
2 id
7 od
2 id
7 od
2 id
7 od
82
25
90
75
13.5 id
18 od
15 od
20
30
4 id
1 id
tip
12
42
35
50°
Capillary stopcock
Solid plug/3-way
2 mm T bore
Eck & Krebs # 4854
12/5
O-ring
12/5
ball
a
b
18 od
15 od
12/5
socket
13.5
id
15 5 id
8 od
35
20

Fig. 1-8. Two-compartment electrochemical cell for $Ru(NH_3)_6^{3+}$ reduction. All dimensions in mm. (See text for more details.)


FRONT VIEW:
24/40 ♁
16
14/20 ♁
15
Capillary stopcock
hollow plug/3-way
1 mm T bore
Eck & Krebs # 5028
14/20 ♁
105
90
40
55
1 id
6.5 od
50
15
14 id
17 od
coarse frit
10 od
59 id
64 od
25


SIDE VIEW:
50°
58
19/22 ♁

procedure is available elsewhere[254] but briefly it consisted of extraction of cytochrome *b*, c_1, and *c* into a Triton X-114 suspension (the "red-green split") followed by ethanol and liquid nitrogen treatments designed to break up the association between the protein and the membrane. Then the protein was solubilized in cholate and was further purified by performing an ammonium sulfate fractionation. The final ammonium sulfate step results in a tight pellet of extremely concentrated (>1 m*M*) cytochrome aa_3 which is soluble in H_2O (without detergents) at high concentrations. The protein was thus stored as a highly concentrated solution in purified H_2O, frozen in liquid nitrogen. It is stable in this condition for an indefinite period. To avoid repetitive thawing of the enzyme, the concentrated solution was aliquotted by freezing individual drops in liquid nitrogen and storing it as such. The uniformity of the drops was sufficient to allow a certain number of drops to be thawed for each kinetics run resulting in a fairly predictable enzyme concentration. Since the enzyme as stored is still associated with cholate, it was necessary to perform a detergent-exchange (to Tween-20) before use. The concentrated enzyme was treated with a few drops of concentrated (20% w/v) Tween-20 and loaded onto a small (~0.5 x 20 cm) G-25 column which was equilibrated with the buffer to be used for kinetics (with 0.1% Tween-20). The enzyme was then slowly eluted as a fairly tight band with the same buffer and was then diluted to the desired concentration. Since all the work described herein was performed at pH = 6.0, it was found to be extremely important to obtain complete exchange of Tween-20 for

cholate, since any residual cholate has a tendency to make the solution turbid. (Cholate has a pK of ~6.4[179] and the acid form is relatively insoluble in water.)

For some types of experiments (*e.g.*, magnetic susceptibility or EXAFS), it is necessary to be able to obtain a highly concentrated enzyme solution in the absence of cholate (or excess ammonium sulfate). A concentration technique for the preparation of such samples was developed by Palmer and coworkers[130] and consists of adding concentrated Tween-20 to concentrated aa_3, diluting with appropriate buffer, then ultracentrifuging at ≳100,000 g for ~12 hours. This procedure results in a relatively tight pellet of concentrated aa_3 which can be recycled through the same procedure as many times as necessary.

Protein concentrations were determined by the Lowry method[255] and enzyme preparations routinely exhibited heme/protein ratios of ≳12 nmoles heme/mg protein. The cytochrome *c* oxidase activity of the enzyme was measured spectrophotometrically using a slight modification of a standard method.[256] The assay was performed in MOPS buffer at pH 7.0, μ = 0.1 *M*. The ferrocytochrome *c* was generated by $Fe(EDTA)^{2-}$ as described above and was diluted to an initial concentration of ~15 μM. The assay was performed at 25° C in a total volume of 2 ml. The molecular activity (MA) in units of μM ferrocytochrome *c* oxidized-(μM cytochrome aa_3)$^{-1}$-sec^{-1} is then given by (*e.g.*, see refs. 117, 257):

$$MA \equiv k_{obs}[\text{cyt } c^{2+}]_0/[\text{cyt } aa_3]$$

where k_{obs} is the first order rate constant measured for the decay of A_{550}, [cyt c^{2+}]$_0$ is the initial concentration of ferrocytochrome *c*, and [cyt aa_3] is the concentration of the enzyme. Values of the molecular activity for the Hartzell and Beinert preparations used for the present studies were usually ~100 sec^{-1} and were unchanged after more than a day at room temperature.

Although the anaerobic modifications to the Durrum helped significantly in reducing the level of O_2 in the system, it was not possible to consistently achieve an O_2 concentration low enough for examination of "anaerobic" kinetics with cytochrome aa_3. Thus, short periods of steady state behavior were observed in some cases when the anaerobicity was not optimal. For this reason, the final traces of O_2 were scavenged from the reactant solutions with the glucose/glucose oxidase system.[258,259] Glucose was added to all buffers to a final concentration of 50 mM and glucose oxidase was added to a final concentration of ~0.1-0.2 units/ml *after* the solutions were degassed. Since the amount of O_2 scavenged by the glucose oxidase under these conditions should be minimal, it was considered unnecessary to add catalase to clean up the small amount of H_2O_2 formed.

The protein solution was degassed by several pump/flush cycles (with Ar) with continuous stirring while on ice. The evacuation was carefully controlled to avoid excessive foaming of the protein-detergent solution during degassing. After the first pumping cycle, glucose oxidase was added to the enzyme solution and the degassing procedure was then completed.

The cyanide derivative of oxidized cytochrome aa_3 was prepared by incubating the enzyme in a 500-fold excess of NaCN. Since cyanide reacts only very slowly with oxidized cytochrome aa_3,[117,118,122] the sample was allowed to incubate overnight at room temperature at a high concentration of enzyme. The complete formation of the cyanide derivative was checked spectrophotometrically before performing kinetics with this derivative.

Hexammineruthenium(II) Reagent. $Ru(NH_3)_6^{2+}$ stock solutions were prepared by electrochemical reduction of the Ru(III) complex at a Pt electrode. Constant potential coulometry was performed at a potential of -300 mV SCE (~100 mV below the $E^{\circ\prime}$ of the Ru(II, III) couple, 50 mV NHE). The stock solution usually consisted of 0.5 m*M* $Ru(NH_3)_6^{2+}$ in the appropriate buffer (see below) in the absence of Tween-20. (Tween-20 was added to the buffers used for dilution of the Ru(II) stock solution since the presence of this detergent in the stock solution caused fouling of the electrode.) Electrolysis was carried out until the charge passed had stopped accumulating (~3-4 hours under well-stirred conditions with a Pt gauze working electrode and a coiled Pt wire counter electrode), but the stock Ru(II) solution was maintained at -300 mV SCE throughout the kinetics run to minimize any reoxidation. Since $Ru(NH_3)_6^{2+}$ is susceptible to aquation, the $Ru(NH_3)_6Cl_3$ was dissolved in buffer immediately prior to electrochemistry and the Ru(II) complex was used for kinetics as soon as possible after reduction. In no instance was the $Ru(NH_3)_6^{2+}$ solution

older than ~12 hours when used for kinetics. The Ru(II) complex also seems to be less stable (presumably toward aquation) at pH 7 than at pH 6 and since the pH optimum of cytochrome *c* oxidase activity is also $\lesssim$6, all kinetics were performed at pH 6.

Once the $Ru(NH_3)_6^{2+}$ stock solution was prepared, various concentrations were obtained by diluting aliquots of the stock solution into the appropriate buffer which had already been degassed by Ar bubbling. All transfers were performed in a Hamilton gastight syringe with a gas flush modification which was kept under Ar flow at all times.

Kinetics. The reduction of cytochrome aa_3 by $Ru(NH_3)^{2+}$ always exhibited biphasic kinetics with the fast phase taking place on the millisecond time scale. Due to the large rate constant for this fast phase, the range of $Ru(NH_3)_6^{2+}$ concentration achievable was limited. Concentration dependences were performed over the range 0.04 - 0.20 m*M*. Fast phase rates at concentrations higher than 0.2 m*M* were too fast for accurate measurement and it was found to be very difficult to keep $Ru(NH_3)_6^{2+}$ solutions of concentrations less than .04 m*M* completely reduced. The enzyme concentration was usually ~2.8 μ*M* (5.6 μ*M* heme) but in some cases was varied from 1.4 to 3.0 μ*M*. Thus, $Ru(NH_3)_6^{2+}$ was always present in pseudo-first order excess over cytochrome aa_3.

All kinetics were performed in cacodylate buffer at pH 6.0 with a total ionic strength of 0.1 *M*. The cacodylate buffer (adjusted with NaOH) contributed .05 *M* to the ionic strength with the rest

being made up by $Ru(NH_3)_6^{2+}$ and an inert salt (Na_2SO_4). The Tween-20 concentration (for solubilization of the enzyme and added to reagent solutions to avoid Schlieren effects in the observation chamber) was varied from 0.05 - 0.50% (w/v) without any observable effect on the kinetics. Depending on the extent of detergent exchange and on the final Tween-20 concentration, some turbidity was observed in the enzyme solution during kinetics runs. Except for a higher background absorbance (due to scattering), this turbidity did not seem to affect the kinetics observed, indicating that it probably did not involve enzyme denaturation. However, none of the kinetics results obtained with turbid enzyme solution were used in the final analysis.

Temperature equilibration was obtained by use of a circulating constant temperature bath (Forma) and the temperature was measured next to the syringe barrels in the Durrum bath to assure accuracy. In general, the temperatures quoted for the temperature dependence data are good to within ±0.1° C (and ±.05° C at 25° C). The enzyme reservoir flask was kept jacketed with a flexible plastic bag filled with ice throughout the experiment and both enzyme and reagent solutions were allowed to equilibrate for 15-20 minutes in the syringes before using for kinetics.

The Ar gas used for degassing and purging was passed through a MnO/vermiculite tower and then through a train of proflavine/methylviologen gas scrubbers before use. The MnO tower was ~24" long by ~3" diameter and the MnO/vermiculite was prepared by a published procedure.[260] Reduced methylviologen ($MV^{+\cdot}$) was generated by

illumination of the gas scrubbers while bubbling with Ar. Once generated, room light was sufficient to maintain a level of $MV^{+\cdot}$ sufficient for scavenging any O_2 left over from the MnO tower.

To scavenge any O_2 adsorbed to the flow system interior, a preflush was performed for approximately 10 hours before each kinetics run. This preflush consisted of pumping $MV^{+\cdot}$ (electrochemically generated as discussed in the Materials Section) through the flow system, recycling it to the electrochemical reservoir, followed by flushing with degassed buffer, then Ar gas. $MV^{+\cdot}$ was circulated by a peristaltic pump through plastic (PVC) tubing with luer end hubs as follows. The solution was withdrawn from the electrochemical reservoir through two 17 gauge needles into two PVC lines which ran through two channels of the peristaltic pump and into the modified Durrum reservoir adapters (see Fig. 1-3). One of the reagent flasks was already installed on the right reservoir adapter (by O-ring) and the preflush passed through a serum stopper (via a short 18 gauge needle) into the glass adapter (Fig. 1-7(b)) and through the three-way stopcock into the Durrum valve block. The other PVC line passed through a serum stopper on a glass adapter designed to fit directly onto the other Durrum reservoir adapter (by O-ring). With all the Durrum valves open, the preflush passed out the exhaust valve through another length of PVC tubing and back into the electrochemical reservoir. This preflush was continued overnight (with dry N_2 from liquid nitrogen boil-off purging the syringe plungers and valve stems) during which several fills and flushes of the syringes allowed all

the O_2 adsorbed to the Teflon plunger tips to be scavenged. Once the enzyme solution was prepared (by pumping and flushing on a vacuum line), the glass adapter on the left Durrum reservoir adapter was replaced by the O-ring joint of the enzyme reservoir and the $MV^{+\cdot}$ flush was rerouted through a serum stopper on the glass adapter (Fig. 1-6(c) of the enzyme reservoir, through the three-way stopcock into the valve block. Meanwhile an Ar flush of the Teflon valve adapter of the enzyme flask (Fig. 1-6(b)) through a serum stopper placed on the 14/20 ₹-joint was begun after which the Teflon valve was opened and the atmosphere above the enzyme solution was continuously purged with Ar. After another half hour of $MV^{+\cdot}$ flushing, the peristaltic pump was shut off and the 17 gauge needles in the electrochemical reservoir were switched to start a degassed buffer flush (~50 ml total) after which the 18 gauge needles into the glass adapters on the three-way stopcocks of the reservoirs are switched for needles directly from the Ar line. Ar was allowed to purge the system for a while before the Durrum valves were closed and the reactants drawn into the syringes for the kinetics run. Once each reagent reservoir was installed, flushed with Ar, and the reagent syringe filled, the glass adapter (Fig. 1-7 (b)) was detached and attached to the stopcock sidearm of the next reagent reservoir to flush the stopcock with Ar before installation on the Durrum. Since each change of reagent reservoir allowed a small amount of O_2 into the system, a 20 minute Ar purge was used each time to restore the anaerobicity.

Kinetics Analysis. Due to the complexity of the kinetics observed for the reduction of cytochrome aa_3 by $Ru(NH_3)_6^{2+}$, standard kinetics analytical techniques were inadequate. A computer program (KINPRO) was written to analyze complicated kinetics progress curves using an iterative nonlinear least squares method based on the Newton-Gauss approach. This program will fit kinetics data to a sum of up to four separate kinetics functions, this sum being any combination of first order, second order, approach to equilibrium, or two-reactant second order decays. The program optimizes all parameters, including the infinity absorbance and preexponential constants, and proved ideal for this study since biphasic kinetics of non-first order decays were always observed. The program is described in more detail elsewhere [261] and the theoretical aspects of the method are described in Chapter 2. Plots of absorbance versus time along with fits and residuals plots were all performed on a Tektronix 4010 Graphics terminal interfaced to the PDP-10 timesharing computer system.

RESULTS

The reduction of cytochrome aa_3 by electrochemically generated hexammineruthenium(II) ($Ru(NH_3)_6^{2+}$) was observed to be biphasic at 444 nm (reduced Soret maximum) and at 605 nm (reduced α maximum). At 444 nm, both phases contributed approximately equally to the total change in absorbance (ΔA), but preliminary results at 605 nm indicate that the fast phase contributes ~75-80% of the total ΔA. All of the rate constants reported herein were measured at 444 nm.

Initial attempts at fitting the slow phase (data collected over ~20 seconds) to a standard first order exponential decay resulted in rather poor fits (large chi squares) and analyses by the Guggenheim method[262] always predicted infinity absorbance values significantly different from those observed. For this reason, attempts were made to fit the slow phase data to other possible kinetics functions (*e.g.*, second order decay, approach to equilibrium). Figure 1-9 shows the fit of the slow phase data to both first order and second order decays. By examination of the residuals (data minus fit) for both functions it can be concluded that the data behaves as a second order decay (rather than a first order decay).

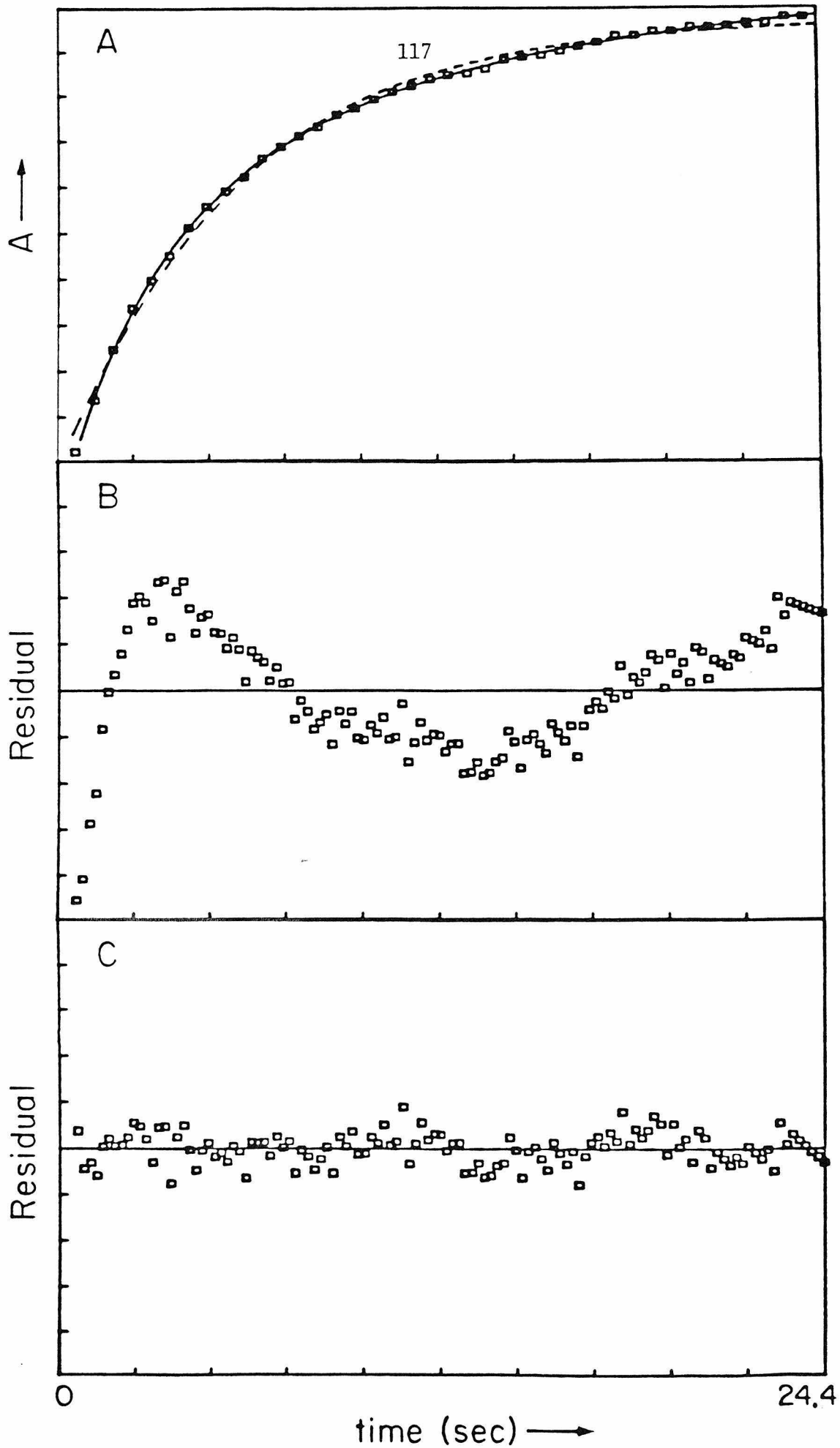
Although the slow phase was easily analyzed without interference from the fast phase (by simple deletion of a few initial data points), analysis of the fast phase required the ability to fit both phases simultaneously. A computer program (KINPRO - see Experimental Section) was written for this purpose and was general enough to allow fits to any combination of kinetics functions. With the aid of KINPRO, it was

Fig. 1-9. Typical absorbance-time fits to slow phase. Only the slow phase was fit (to either a first or second order decay).

(A) Original absorbance versus time data (□, 120 points acquired, every third point plotted) with best first order fit (---) and best second order fit (——).

(B) Residuals (data minus fit) for the first order fit in (A).

(C) Residuals (data minus fit) for the second order fit in (A). (Plots (B) and (C) are on the same scale).


A
117
A
B
Residual
C
Residual
0
24.4
time (sec)

found that fits of data sets covering both phases (with equal numbers of points in each phase) to functions consisting of a fast first order decay and slow second order decay (or fast first order decay and slow first order decay) could not adequately reproduce the data. The data for each phase was necessarily collected separately and then combined into one data set for analysis. The absorbances of each phase can be shifted slightly with respect to each other (to compensate for any time-dependent drift introduced by the separate collection processes) and this shift can be adjusted (by KINPRO) to optimize the fit (minimize chi square). Only for the case of a fast second order decay and a slow second order decay did this optimization result in accurate splicing of the two data sets (fast and slow phases). A comparison between this fit and one which assumed a fast first order decay is made in Fig. 1-10. Again the distribution of the residuals apparently shows that the fast phase also exhibits second order kinetics. All the data were thus analyzed as the sum of two second order decays and the observed rate constants (both k_{fast} and k_{slow}) have units of M^{-1}-s^{-1}.

In order to better characterize the nature of the observed biphasicity, the wavelength dependence (in the Soret region) of the amplitudes of the respective phases was studied by measuring the kinetics at several discrete wavelengths between ~390 and ~460 nm. These kinetic difference spectra are displayed in Fig. 1-11 for both the native enzyme and the oxidized-cyanide derivative (aa_3-CN). From Fig. 1-11, it can be seen that the fast phase appears insensitive to the effect of cyanide, whereas the slow phase difference spectrum changes considerably upon

Fig. 1-10. Typical absorbance-time fits to fast phase. The total fit consisted of a slow phase second order decay plus a fast phase first or second order decay.

(A) Original absorbance versus time data (□, 122 points acquired, every fourth point plotted) with best first order fit (---) and best second order fit (——).

(B) Residuals (data minus fit) for the first order fit in (A).

(C) Residuals (data minus fit) for the second order fit in (A). (Plots (B) and (C) are on the same scale.)

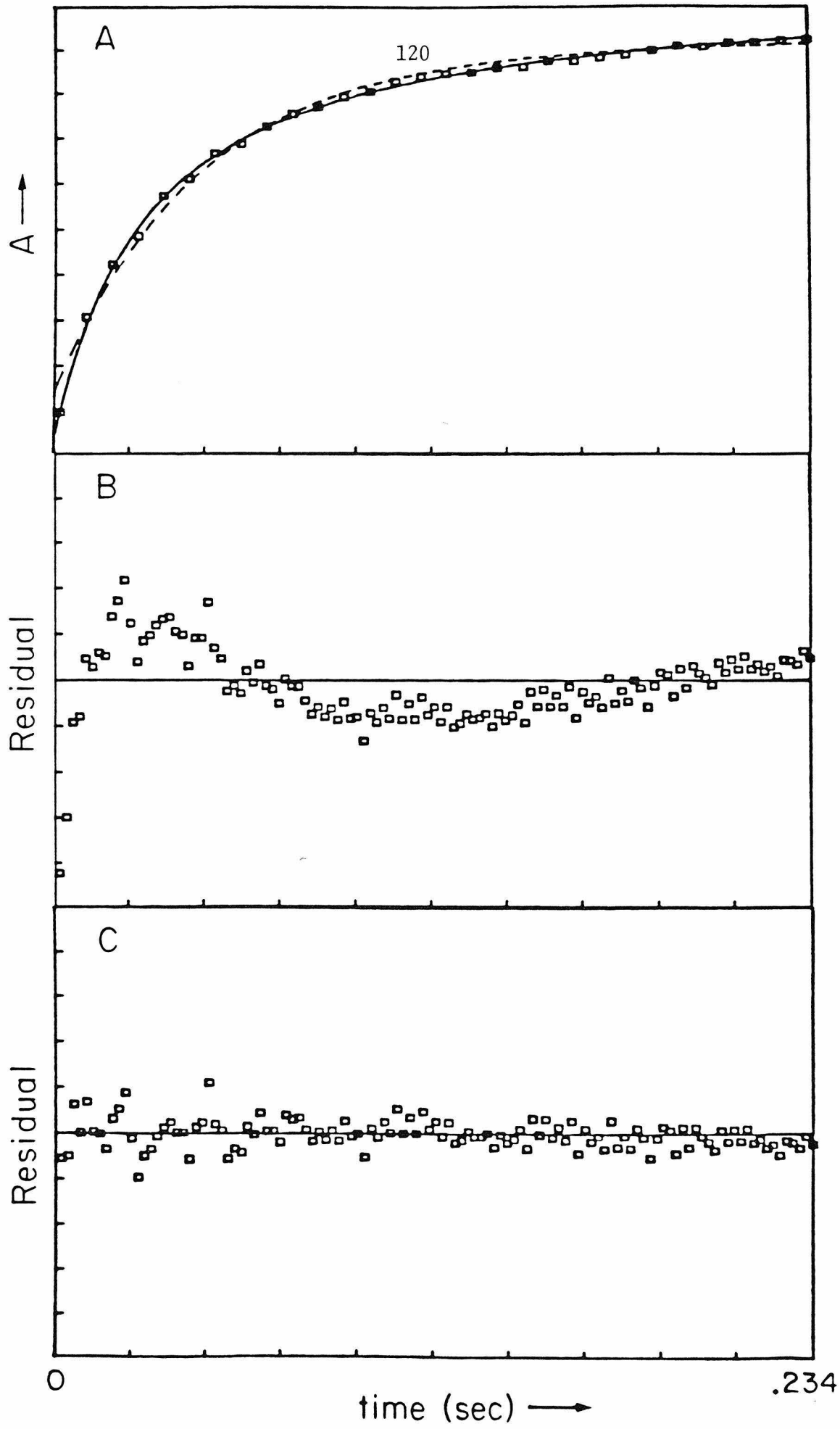
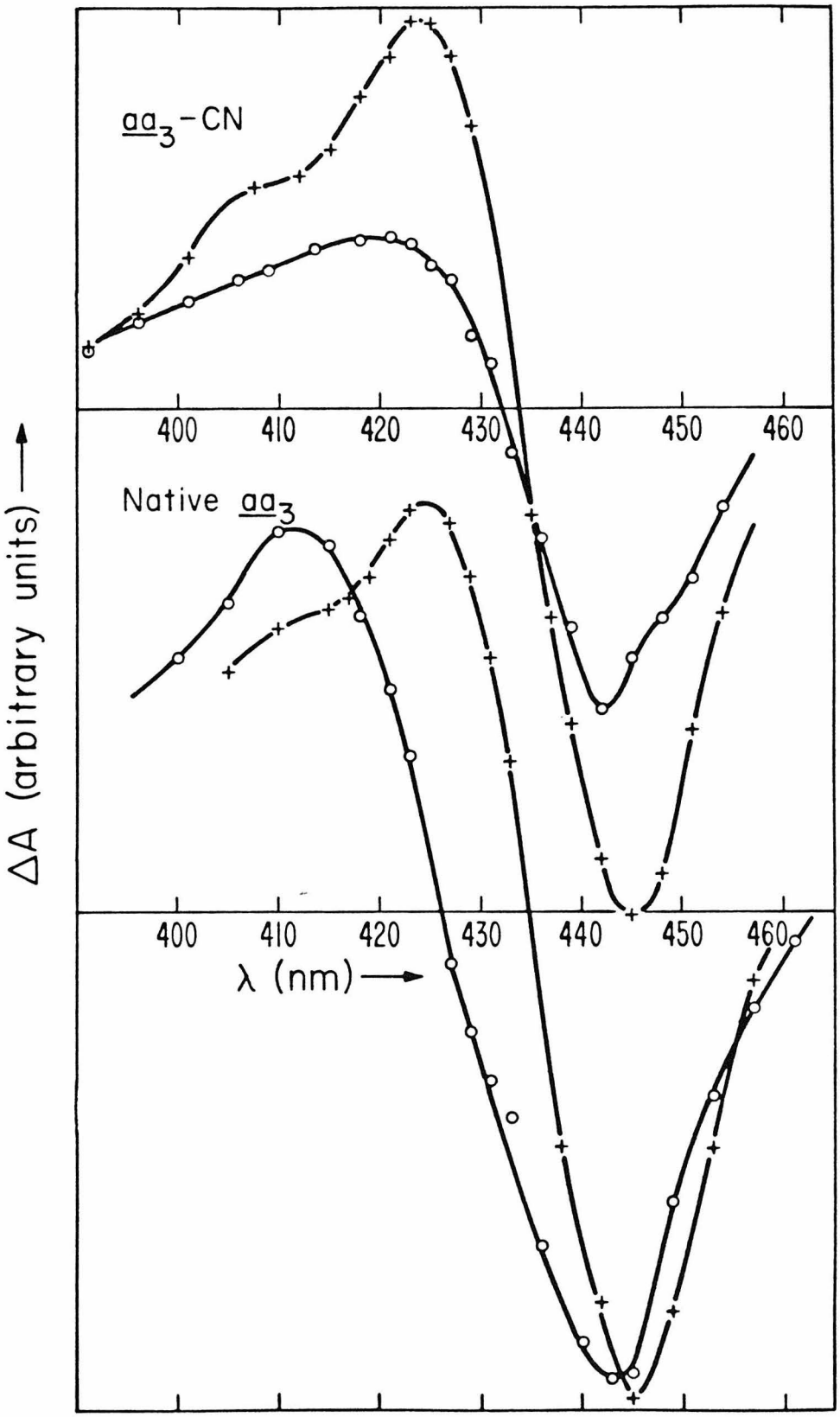

A
120
A
B
Residual
C
Residual
0
.234
time (sec)

Fig. 1-11. Kinetic difference spectra (Soret) for both phases of the reactions between $Ru(NH_3)_6^{2+}$ and native cytochrome aa_3 (lower) and $Ru(NH_3)_6^{2+}$ and the cyanide derivative of oxidized cytochrome aa_3 (upper). The plotted points represent the preexponential constants calculated for a particular phase at a particular wavelength: +-+, fast phase; o-o, slow phase. The absolute ΔA's are arbitrary but within each half of the figure, the ΔA's are relatively correct.


aa3 - CN
Native aa3
400
410
420
430
440
450
460
ΔA (arbitrary units) →
λ (nm) →

cyanide-binding. A closer examination of these kinetic difference spectra is postponed until the Discussion Section.

The dependence of the observed fast and slow rate constants on $[Ru(NH_3)_6^{2+}]$ is illustrated in Fig. 1-12 and the rate constants are tabulated in Table 1-4. Each pair of (fast and slow) rate constants in Table 1-4 is the weighted mean of $\gtrsim 3$ determinations. Each determination was the mean of at least four separate runs and each run consisted of at least two fast phase and one slow phase scans, the fast phase scans being signal averaged and spliced to the slow phase scan before being analyzed by KINPRO. (The aa_3-CN rate constants are less well-determined than those for the native enzyme.) From Fig. 1-12 it can be seen that the fast phase is not only second order in enzyme but first order in $Ru(NH_3)_6^{2+}$ as well. The slope of the best linear least squares fit gives a third order rate constant (for the fast phase) of (1.68±.02) x 10^{11} M^{-2}-s^{-1} (pH 6.0 (cacodylate), μ=0.1 M, 25° C) (the intercept is (2.4±2.0) x 10^5 M^{-1}-s^{-1}). Although, as mentioned above, the fast phase rate constants for $Ru(NH_3)_6^{2+}$ reduction of the oxidized cyanide derivative are less well determined, they are very similar to those for the reduction of native aa_3.

Figure 1-12 also shows the $[Ru(NH_3)_6^{2+}]$-dependence of the slow phase rate constants. Over the $[Ru(NH_3)_6^{2+}]$ range available, the slow phase appears to be independent of the reductant concentration with a second order rate constant of (1.04±.06) x 10^5 M^{-1}-s^{-1} for native aa_3 and (1.99±.06) x 10^4 M^{-1}-s^{-1} for aa_3-CN (pH 6.0 (cacodylate), μ=0.1 M, 25° C). Thus, the binding of cyanide to aa_3 results in a slowing of the slow phase by a factor of ~5 as well as altering the kinetic difference spectrum of the slow phase (see Fig. 1-11). The difficulties involved in working at

Fig. 1-12. $[Ru(NH_3)_6^{2+}]$-dependence of k_{fast} and k_{slow} for the reduction of cytochrome aa_3 by $Ru(NH_3)_6^{2+}$. The lines are the best first and zeroth order least squares fits to the fast (□) and slow (o) phases, respectively. See text for fit parameters.

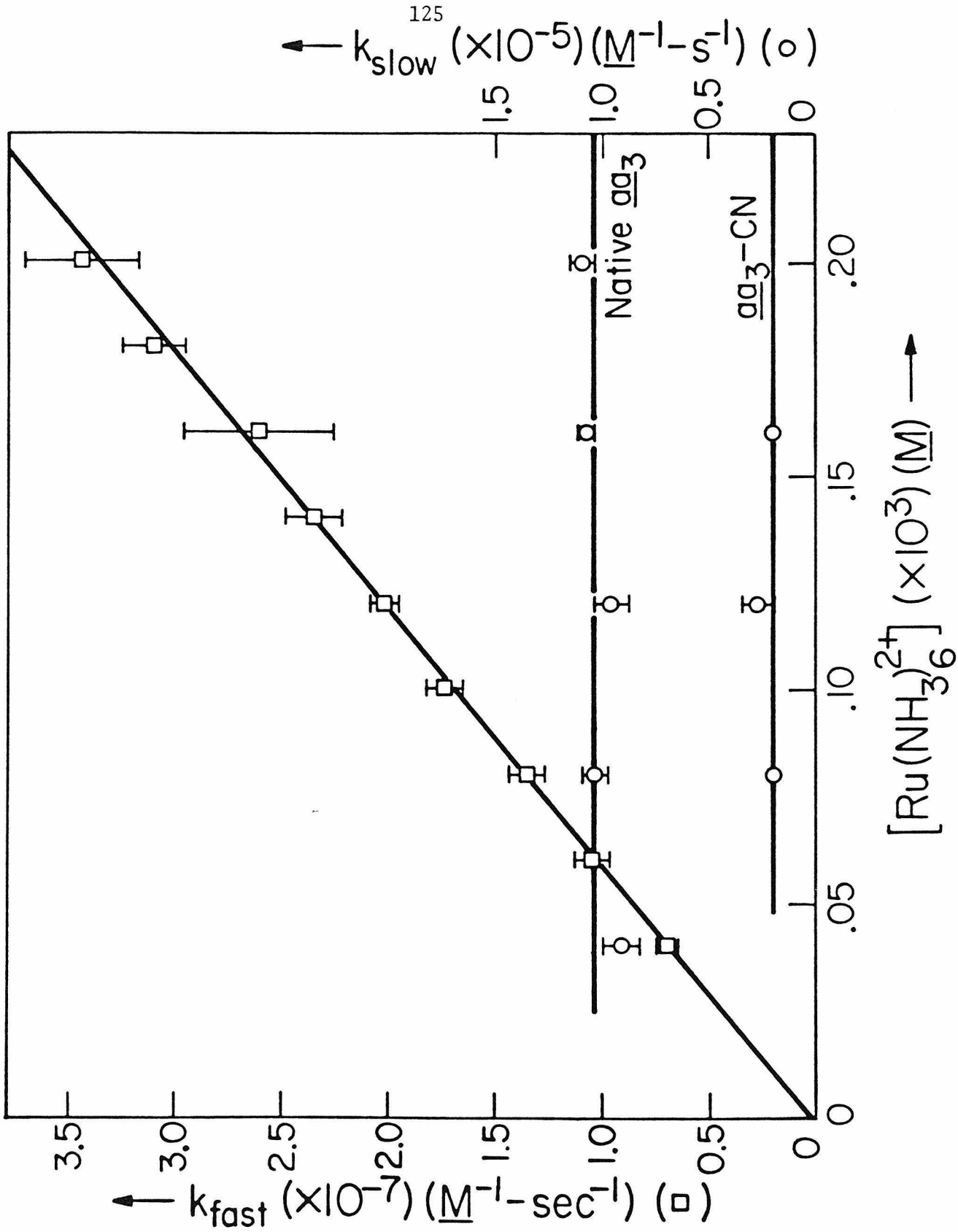

← k_{slow} (×10^{-5}) ($\underline{M}^{-1}$-s^{-1}) (○)
1.5
1.0
0.5
0
Native $\underline{aa}_3$
$\underline{aa}_3$-CN
.20
.15
.10
.05
0
[$Ru(NH_3)_6^{2+}$] (×10^3) ($\underline{M}$) →
3.5
3.0
2.5
2.0
1.5
1.0
0.5
0
← k_{fast} (×10^{-7}) ($\underline{M}^{-1}$-sec^{-1}) (□)

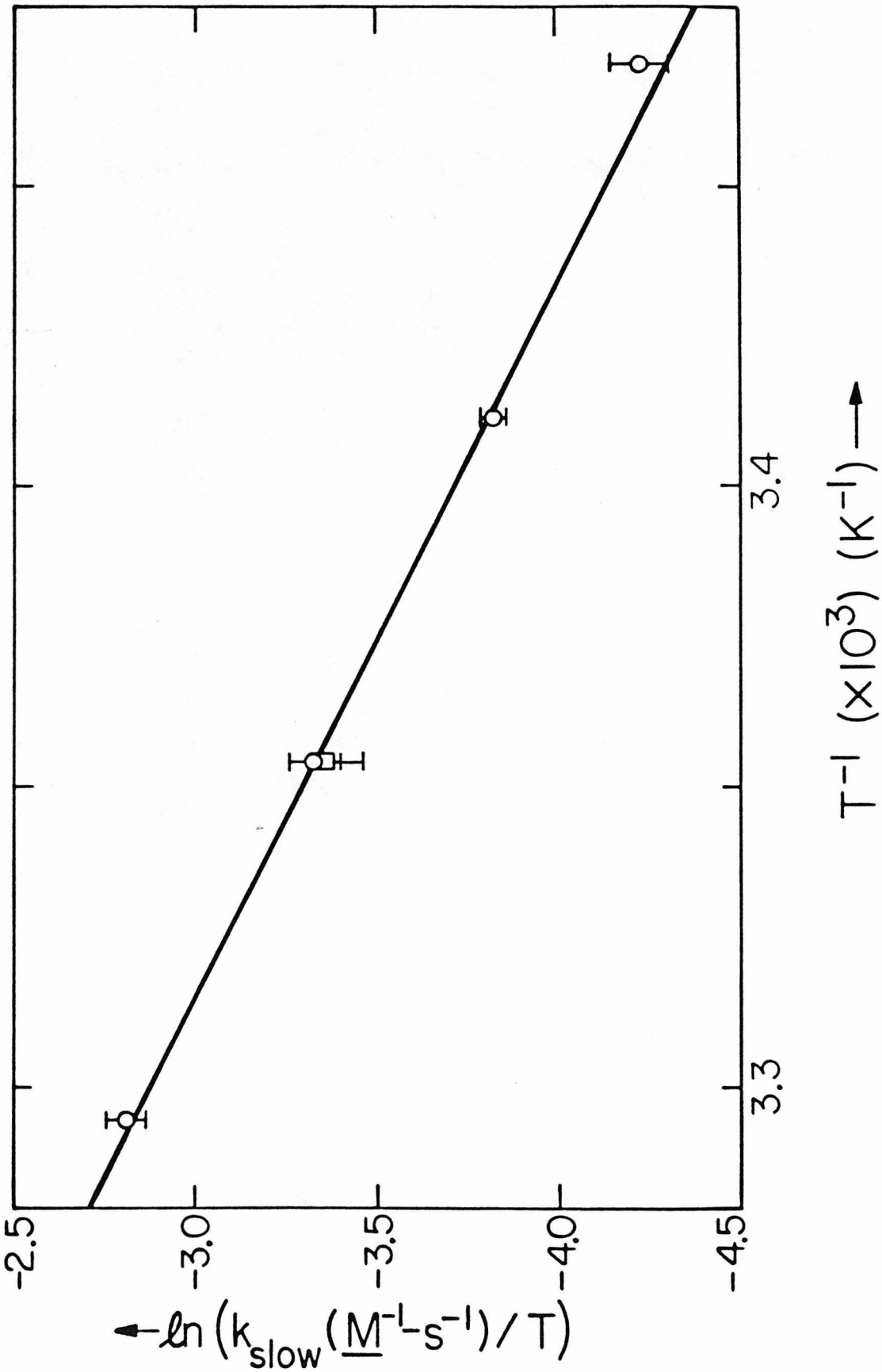
TABLE 1-4. Rate Constants for $Ru(NH_3)_6^{2+}$ Reduction of Cytochrome aa_3.

aa_3 Derivative	$[Ru(NH_3)_6^{2+}]$ (m*M*)	T (°C)	$k_{fast} \pm \sigma$ ($x10^{-6}$) (M^{-1}-s^{-1})	$k_{slow} \pm \sigma$ ($x10^{-4}$) (M^{-1}-s^{-1})
Native	0.04	25.0	7.01±.49	9.10±.82
"	0.06	"	10.5±0.8	-
"	0.08	"	13.5±0.8	10.4±0.5
"	0.10	"	17.4±0.8	-
"	0.12	"	20.2±0.7	9.60±.75
"	0.14	"	23.6±1.3	-
"	0.16	"	26.2±3.5	10.7±0.4
"	0.18	"	31.1±1.5	-
"	0.20	"	34.6±2.7	10.9±0.6
"	0.12	12.0	15.7±0.8	-
"	"	15.0	17.7±0.3	4.20±.34
"	"	20.0	19.0±0.8	6.39±.19
"	"	25.0	16.5±1.6	10.7±0.4
"	"	30.4	18.9±2.4	18.2±1.0
aa_3-CN	0.08	25.0	12.0±0.7	1.98±.08
"	0.12	"	14.2±1.0	2.71±.73
"	0.16	"	25.3±1.5	1.99±.11

$Ru(NH_3)_6^{2+}$ concentrations below ~.04 m*M* preclude the measurement of rate constants in the low [Ru(II)]-region so that the possibility of saturation behavior for the slow phase cannot be excluded.

The temperature-dependence of the rate constants for both the fast and slow phases (for $Ru(NH_3)_6^{2+}$ reduction of native aa_3) is tabulated in Table 1-4 and the Eyring plot for the slow phase is given in Fig. 1-13. Examination of the fast phase rate constants in Table 1-4 shows that the fast phase is temperature independent within experimental error ($\Delta H^{\ddagger}$ = 0.4±1.2 kcal-mole^{-1}). The activation parameters for the slow phase of $Ru(NH_3)_6^{2+}$ reduction of native aa_3 (calculated from Fig. 1-13) are $\Delta H^{\ddagger}$ = 16.6±0.6 kcal-mole^{-1}, $\Delta S^{\ddagger}$ = 20.2±2.0 e.u. (pH = 6.0 (cacodylate), μ=0.1 *M*, $[Ru(NH_3)_6^{2+}]$ = .12 m*M*). The averaged second order rate constant for the slow phase taken from the $[Ru(NH_3)_6^{2+}]$-dependence data is also indicated in Fig. 1-13.

Fig. 1-13. Eyring plot of slow phase rate constants for $Ru(NH_3)_6^{2+}$ reduction of native cytochrome aa_3. (O - $[Ru(NH_3)_6^{2+}]$ = .12 m*M*; □ - value calculated from $[Ru(NH_3)_6^{2+}]$-dependence.


-2.5
-3.0
-3.5
-4.0
-4.5
3.3
3.4
$\leftarrow \ln\left(k_{slow}(\underline{M}^{-1}s^{-1})/T\right)$
T^{-1} $(\times 10^3)$ $(K^{-1})\longrightarrow$

DISCUSSION

As mentioned in the Introduction, the work described herein was initiated as part of a search for a well-behaved inorganic reductant which rapidly and specifically reduced the cytochrome a^{3+} moiety of cytochrome aa_3. The initial phase observed for the reduction of cytochrome aa_3 by $Ru(NH_3)_6^{2+}$ is indeed fast (occurring over $\lesssim$100 msec even at submillimolar concentrations of reductant). This rate seems to be mainly determined by the charge of the reductant since preliminary results indicate that reduction of aa_3 by $Ru(NH_3)_5py^{2+}$ (py = pyridine) is also fast ($t_{1/2} \approx$ 140 msec at [Ru(II)] = 0.1 m*M*) whereas reduction by $Fe(EDTA)^{2-}$ (EDTA = ethylenediaminetetraacetate) ($t_{1/2} \approx$ 500 sec at [Fe(II)] = 0.1 m*M*), $Fe(dipic)_2^{2-}$ (dipic = 2,6-dipicolinate) ($t_{1/2} \approx$ 10 sec at [Fe(II)] = 0.1 m*M*), or $Fe(CDTA)^{2-}$ (CDTA = trans-1,2-cyclohexane-diaminetetraacetate) ($t_{1/2} \approx$ 15 sec at [Fe(II)] = 0.1 m*M*) is much slower.[263] It has been shown[216-218] that the interaction of the physiological reductant (ferrocytochrome *c*) with cytochrome aa_3 is mainly electrostatic. Since cytochrome *c* has an overall positive charge, this implies the presence of negatively charged groups in the vicinity of the cytochrome *c* interaction site (at cytochrome *a*). This would predict a preference of cytochrome *a* for positively-charged reductants and the prediction is borne out by the results reported herein.

Several independent lines of evidence support the assignment of the fast phase of $Ru(NH_3)_6^{2+}$ reduction to the reduction of cytochrome a^{3+}

(and the slow phase to reduction of cytochrome a_3^{3+}). First, the kinetic difference spectrum of the fast phase (see Fig. 1-11) is essentially unaltered upon binding of cyanide to the enzyme (it is well established that cyanide binds to a_3^{3+}) while the addition of cyanide causes drastic changes in the slow phase kinetic difference spectrum. In addition, the rate constants reflect the same type of response to the addition of cyanide, the slow phase rate constants diminishing by a factor of ~5 while the fast phase rate constants remain unchanged. Preliminary experiments at 605 nm also indicate that (for $Ru(NH_3)_6^{2+}$ reduction of the native enzyme) the fast phase contributes ~75-80% of the total ΔA. It is fairly well established (for discussion, see Current Knowledge Section) that cytochrome a contributes ~80-100% of the ΔA at 605 nm. Comparison of the kinetic difference spectra with published difference spectra which have been previously assigned separate cytochrome a and a_3 contributions[71,73] completely corroborates the assignment of the fast-phase to cytochrome a^{3+} reduction and the slow phase to cytochrome a_3^{3+} reduction.

As stated in the Results Section, the residuals plots (see Figs. 1-9 and 1-10) convincingly indicate that the slow (and perhaps the fast) phase of reduction obeys strict second order kinetics (instead of first order kinetics). This result may at first seem completely unreasonable considering the fact that such a complex reaction scheme has never before been reported for this enzyme. However, the rarity of such results may instead be an artifact of the analytical techniques currently in common use by most kineticists. The standard first order kinetics

analysis (and even the more complicated sum of first order exponentials analysis) have become so widely accepted that they tend to be used exclusively for cases in which a more thorough survey is desirable. Indeed, the two fits shown in Figs. 1-9 or 1-10 are close enough that, without a check of the residuals (which is often not performed), one might be satisfied with the simpler first order fits. However, it is clear (from the viewpoint of the residuals plot and the chi square statistics) that the data do obey second order kinetics. The interpretation of these observations is quite another matter.

Consider first the slow phase attributed to the reduction of cytochrome a_3^{3+}. Since all the cytochrome a^{3+} has been reduced in the fast phase, the initial conditions for the slow phase can be assumed to involve a pool of "half-reduced" enzyme ($a^{2+}a_3^{3+}$, note that the oxidation states of the coppers are not specified; the present data do not yield any information on these sites). The simplest interpretation of the second order behavior of the slow phase involves a mechanism wherein two molecules of "half-reduced" aa_3 exchange electrons (*i.e.*, cytochrome a_3^{3+} of one molecule accepts electrons from cytochrome a^{2+} of the other. The number of electrons involved is unknown since the copper sites may or may not be involved.):

$$a^{2+}a_3^{3+} + a^{2+}a_3^{3+} \xrightarrow{k_{slow}} a^{2+}a_3^{2+} + a^{3+}a_3^{3+} \qquad \text{Scheme I}$$

Any oxidized enzyme formed by this process would be immediately consumed by the excess $Ru(NH_3)_6^{2+}$ in a process identical to that involved in the

fast phase. Thus, the only detectable change would be the reduction of one a_3^{3+} (as is observed in the slow phase). Since the electron transfer is *inter*molecular, the rate law would be second order in enzyme (as observed).

The ramifications of this mechanism are worth noting. First, analysis of the present slow phase data as a first order decay yields a first order rate constant of ~0.2 - 0.4 s^{-1} which is independent of the $Ru(NH_3)_6^{2+}$ concentration. This rate constant is remarkably similar to the rate constant measured by Greenwood and coworkers for the slow phase of the biphasic reaction observed for the Cr^{2+} reduction of cytochrome aa_3.[71] These workers interpreted this [Cr^{2+}]-independent rate as the *intra*molecular electron transfer from a^{2+} to a_3^{3+}. The present work indicates that a more detailed reanalysis of the Cr^{2+}-reduction kinetics would be desirable. The possibility of misanalyzing a second order decay as first order is rather likely (as mentioned above) and the interpretation of the results is strongly dependent on the correct analysis. According to the above interpretation (Scheme I), the reported intramolecular electron transfer rate (of ~0.5 s^{-1}) is not that at all, but is actually a manifestation of a bimolecular electron transfer between aa_3 molecules (with a rate constant of ~10^5 M^{-1} s^{-1}).

Other interpretations of the second order dependence of the slow phase on aa_3 are possible. For instance, rate limiting formation of a dimer of "half-reduced" enzyme molecules followed by $Ru(NH_3)_6^{2+}$ reduction of the dimer would also give second order kinetics:

$$a^{2+}a_3^{3+} + a^{2+}a_3^{3+} \xrightarrow{k_{slow}} (a^{2+}a_3^{3+})_2$$

$$(a^{2+}a_3^{3+})_2 + Ru(NH_3)_6^{2+} \xrightarrow{k_2} a^{2+}a_3^{2+} + a^{2+}a_3^{3+} + Ru(NH_3)_6^{3+} \quad \text{Scheme II}$$

$$(k_2 >> k_{slow})$$

This mechanism is more complicated than Scheme I but cannot be ruled out kinetically. The main requirement in any proposed mechanism is an interaction between two enzyme molecules giving rise to the second order behavior. The simplest type of interaction is still the intermolecular electron transfer of Scheme I. It should be mentioned that the activation parameters for the slow phase also support some type of strong enzyme-enzyme interaction (probably involving conformational changes and displacement of ordered solvent structure).

As suggested by Figure 1-10, the residuals plots of the fast phase argue less convincingly that the fast phase is actually second order. Other alternatives (*e.g.*, the sum of two first order reactions with similar rate constants) do exist and would probably fit the observed data as well as, if not better than, second order (as would be expected with more parameters to optimize). Thus, the interpretation of the fast phase is less straightforward. One mechanism which would predict the third order (first order in $Ru(NH_3)_6^{2+}$, second order in aa_3) behavior of the fast phase involves $Ru(NH_3)_6^{2+}$ reduction of a transient enzyme dimer:

$$a^{3+}a_3^{3+} + a^{3+}a_3^{3+} \underset{k_{-0}}{\overset{k_0}{\rightleftharpoons}} (a^{3+}a_3^{3+})_2 \qquad K_0 = k_0/k_{-0}$$

Scheme III

$$(a^{3+}a_3^{3+})_2 + Ru(NH_3)_6^{2+} \xrightarrow{k_1} a^{2+}a_3^{3+} + a^{3+}a_3^{3+} + Ru(NH_3)_6^{3+}$$

Assuming that the dimer is present at a steady state concentration and $k_{-0} >> k_1[Ru(NH_3)_6^{2+}]$ results in the following rate law:

$$\text{Rate} = k_1K_0[a^{3+}a_3^{3+}]^2[Ru(NH_3)_6^{2+}]$$

This would yield $k_1K_0 \simeq 2 \times 10^{11}\ M^{-2}\ s^{-1}$. However, the magnitude of k_1 is limited (by the diffusion-limited rate of a small molecule and a large protein colliding) and the measured k_1K_0 requires $K_0 >> \sim 10^3$. If this were the case, this "kinetic" dimer would be the dominant species in solution and the reaction would then be observed as a simple first order reaction of dimer with $Ru(NH_3)_6^{2+}$. (Of course, as already mentioned, cytochrome aa_3 does exist predominantly as a dimer in Tween-20 solution so that the dimerization discussed above must involve tetramers or some other type of dimers.) Another argument against the validity of Scheme III lies in the temperature-independence of the fast phase. If K_0 is involved in the observed rate constant, a large temperature dependence would be expected as discussed above for the slow phase.

If it is assumed that the fast phase is not second order but some unresolvable combination of first order decays, other possible inter-

pretations present themselves. The occurrence of two similar (but not identical) reactions, both of which are first order in $Ru(NH_3)_6^{2+}$ and aa_3 suggests the existence of two forms of oxidized enzyme:

$$(a^{3+}a_3^{3+})_1 + Ru(NH_3)_6^{2+} \xrightarrow{k_1} a^{2+}a_3^{3+} + Ru(NH_3)_6^{3+}$$

$$(a^{3+}a_3^{3+})_2 + Ru(NH_3)_6^{2+} \xrightarrow{k_2} a^{2+}a_3^{3+} + Ru(NH_3)_6^{3+}$$

$$k_2 \simeq k_1$$

The two variants of the oxidized enzyme may just be the monomer and dimer forms. The first order dependence of both phases on $[Ru(NH_3)_6^{2+}]$ would then be reflected in the $[Ru(NH_3)_6^{2+}]$-dependence shown in Figure 1-12. (It should be noted that the good linearity of this plot using the second order rate constants may just be a result of the better fit to the fast phase data. This linearity does not necessarily require that the second order fit be the correct one.)

CONCLUSION

Although the fast phase of $Ru(NH_3)_6^{2+}$-reduction of cytochrome aa_3 has elicited much speculation above, the more clearly second order nature of the slow phase lends more credence to the conclusions to be drawn from the interpretation of this phase. It has been shown that the second order nature of the slow phase indicates that the major pathway for reduction of cytochrome a_3^{3+} in the "half-reduced" enzyme occurs by some type of *inter*molecular electron transfer rather than by an intramolecular a^{2+} to a_3^{3+} step. Although this result may or may not extend to other instances of biphasic kinetics (*e.g.*, the Cr^{2+} reduction experiments[71]), the necessity of examining all possible kinetic alternatives during the analysis of such data has been clearly shown.

REFERENCES AND NOTES

1. P. George, in "International Symposium on Oxidases and Related Redox Systems," vol. 1, T. E. King, H. S. Mason, M. Morrison, eds., John Wiley and Sons, Inc., N.Y., 1964, p. 3.
2. S. Wherland and H. B. Gray, in "Biological Aspects of Inorganic Chemistry," A. W. Addison, W. Cullen, B. R. James, and D. Dolphin, eds., Wiley, N.Y., 1977, p. 289.
3. D. L. Schneider, Y. Kagawa, and E. Racker, J. Biol. Chem., 247, 4074 (1972).
4. M. S. Rubin and A. Tzagoloff, J. Biol. Chem., 248, 4269 (1973).
5. G. D. Eytan, R. C. Carroll, G. Schatz, and E. Racker, J. Biol. Chem., 250, 8598 (1975).
6. S. H. Phan and H. R. Mahler, J. Biol. Chem., 251, 257 (1976).
7. S. H. Phan and H. R. Mahler, J. Biol. Chem., 251, 270 (1976).
8. R. C. Carroll and G. D. Eytan, Fed. Proc., 34, 579 (1975).
9. R. W. Yatscoff and K. B. Freeman, FEBS Lett., 81, 7 (1977).
10. N. W. Downer, N. C. Robinson, and R. A. Capaldi, Biochemistry, 15, 2930 (1976).
11. R. A. Capaldi, R. L. Bell, and T. Branchek, Biochem. Biophys. Res. Commun., 74, 425 (1977).
12. M. M. Briggs and R. A. Capaldi, Biochemistry, 16, 73 (1977).
13. S. Gutteridge, D. B. Winter, W. J. Bruyninckx, and H. S. Mason, Biochem. Biophys. Res. Commun., 78, 945 (1977).
14. C. -A. Yu and L. Yu, Biochim. Biophys. Acta, 495, 248 (1977).

15. M. M. Briggs and R. A. Capaldi, Biochem. Biophys. Res. Commun., 80, 553 (1978).

16. R. Bisson, A. Azzi, H. Gutweniger, R. Colonna, C. Montecucco, and A. Zanotti, J. Biol. Chem., 253, 1874 (1978).

17. T. G. Frey, S. H. P. Chan, and G. Schatz, J. Biol. Chem., 253, 4389 (1978).

18. S. H. P. Chan and R. P. Tracy, Eur. J. Biochem., 89, 595 (1978).

19. C. H. A. Seiter, R. Margalit, and R. A. Perreault, Biochem. Biophys. Res. Commun., 86, 473 (1979).

20. J. R. Bucher and R. Penniall, FEBS Lett., 60, 180 (1975).

21. G. Steffens and G. Buse, Hoppe-Seyler's Z. Physiol. Chem., 357, 1125 (1976).

22. S. J. Butler and M. Landon, Biochem. Soc. Trans., 7, 397 (1979).

23. R. O. Poyton, E. McKemmie, and C. George-Nascimento, J. Biol. Chem., 253, 6303 (1978).

24. A. McGeer, B. Lavers, and G. R. Williams, Can. J. Biochem., 55, 988 (1977).

25. R. J. Rascati and P. Parsons, J. Biol. Chem., 254, 1594 (1979).

26. M. Fry, H. Van de Zande, and D. E. Green, Proc. Natl. Acad. Sci. (USA), 75, 5908 (1978).

27. B. Ludwig, N. W. Downer, and R. A. Capaldi, Biochemistry, 18, 1401 (1979).

28. B. Love and H. E. Auer, Biochem. Biophys. Res. Commun., 41, 1437 (1970).

29. B. Love, S. H. P. Chan, and E. Stotz, J. Biol. Chem., 245, 6664 (1970).

30. S. H. P. Chan, B. Love, and E. Stotz, J. Biol. Chem., 245, 6669 (1970).

31. *e.g.*, the cytochrome *c* oxidase activity is dependent on the medium.

32. D. H. MacLennan and A. Tzagoloff, Biochim. Biophys. Acta, 96, 166 (1965).

33. M. Tanaka, M. Haniu, S. Zeitlin, K. T. Yasunobu, C. -A. Yu, L. Yu, and T. E. King, Biochem. Biophys. Res. Commun., 66, 357 (1975).

34. C. -A. Yu, L. Yu, and T. E. King, Biochem. Biophys. Res. Commun., 74, 670 (1977).

35. M. Tanaka, M. Haniu, K. T. Yasunobu, C. -A.Yu, L. Yu, Y. -H. Wei, and T. E. King, Biochem. Biophys. Res. Commun., 76, 1014 (1977).

36. M. Tanaka, M. Haniu, K. T. Yasunobu, C. -A. Yu, L. Yu, Y. -H. Wei, and T. E. King, J. Biol. Chem., 254, 3879 (1979).

37. M. Erecinska, Biochem. Biophys. Res. Commun., 76, 495 (1977).

38. E. Racker, A. Loyter, and R. O. Christiansen, in "Probes of Structure and Function of Macromolecules and Membranes," vol. 1, B. Chance, C. -P. Lee, J. K. Blasie, eds., Academic Press, N.Y., 1971, p. 407.

39. M. Swanson, L. C. Petersen, and L. Packer, in "International Symposium on Mechanisms of Oxidizing Enzymes," T. P. Singer, R. N. Ondarza, eds., Elsevier, North-Holland, Amsterdam, 1978, p. 251.

40. M. Sharrock and T. Yonetani, Biochim. Biophys. Acta, 434, 333 (1976).

41. M. Sharrock and T. Yonetani, Biochim. Biophys. Acta, 462, 718 (1977).

42. M. Denis and G. M. Clore, Biochim. Biophys. Acta, 545, 483 (1979).

43. B. Chance, J. S. Leigh, Jr., and A. Waring, in "Structure and Function of Energy-Transducing Membranes," K. van Dam and B. F. van Gelder, eds., Elsevier, North-Holland, Amsterdam, 1977, p. 1.

44. B. Chance, A. Waring, and C. Saronio, in "Energy Conservation in Biological Membranes," G. Schafer and M. Klingenberg, eds., Springer-Verlag, Berlin, 1978, p. 56.

45. W. S. Caughey, R. A. Bayne, and S. McCoy, J. Chem. Soc., D, 950 (1970).

46. S. Yoshikawa, M. G. Choc, M. C. O'Toole, and W. S. Caughey, J. Biol. Chem., 252, 5498 (1977).

47. B. Chance, C. Saronio, J. S. Leigh, Jr., W. J. Ingledew, and T. E. King, Biochem. J., 171, 787 (1978).

48. W. R. Heineman, T. Kuwana, and C. R. Hartzell, Biochem. Biophys. Res. Commun., 49, 1 (1972).

49. Q. H. Gibson and C. Greenwood, J. Biol. Chem., 240, 2694 (1965).

50. L. -E. Andréasson, B. G. Malmström, C. Strömberg, and T. Vänngård, FEBS Lett., 28, 297 (1972).

51. C. R. Hartzell, R. E. Hansen, and H. Beinert, Proc. Natl. Acad. Sci. (USA), 70, 2477 (1973).

52. H. Beinert, R. W. Shaw, and R. E. Hansen, in "International Symposium on Mechanisms of Oxidizing Enzymes," T. P. Singer, R. N. Ondarza, eds., Elsevier, North-Holland, Amsterdam, 1978, p. 239.

53. M. K. F. Wikström, H. J. Harmon, W. J. Ingledew, and B. Chance, FEBS Lett., 65, 259 (1976).

54. M. Denis, FEBS Lett., 84, 296 (1977).

55. M. Erecinska and D. F. Wilson, Arch. Biochem. Biophys., 188, 1 (1978).

56. D. Keilin and E. F. Hartree, Proc. Roy. Soc., London, Ser. B, 127, 167 (1939).

57. M. R. Lemberg, Physiol. Rev., 49, 48 (1969).

58. D. F. Wilson, J. G. Lindsay, and E. S. Brocklehurst, Biochim. Biophys. Acta, 256, 277 (1972).

59. D. F. Wilson and J. S. Leigh, Jr., Arch. Biochem. Biophys., 150, 154 (1972).

60. J. S. Leigh, Jr., D. F. Wilson, C. S. Owen, and T. E. King, Arch. Biochem. Biophys., 160, 476 (1974).

61. D. F. Wilson, M. Erecinska, and C. S. Owen, Arch. Biochem. Biophys., 175, 160 (1976).

62. P. Nicholls and L. C. Petersen, Biochim. Biophys. Acta, 357, 462 (1974).

63. G. Palmer, T. Antalis, G. T. Babcock, L. Garcia-Iniguez, M. Tweedle, L. J. Wilson, and L. E. Vickery, in "International Symposium on Mechanisms of Oxidizing Enzymes," T. P. Singer, R. N. Ondarza, eds., Elsevier, North-Holland, Amsterdam, 1978, p. 221.

64. R. H. Tiesjema, G. P. M. A. Hardy, and B. F. van Gelder, Biochim. Biophys. Acta, 357, 24 (1974).

65. R. H. Tiesjema, A. O. Muijsers, and B. F. van Gelder, Biochim. Biophys. Acta, 305, 19 (1973).

66. A. O. Muijsers, R. H. Tiesjema, R. W. Henderson, and B. F. van Gelder, Biochim. Biophys. Acta, 267, 216 (1972).

67. W. H. Vanneste, Biochemistry, 5, 838 (1966).

68. P. Nicholls, Biochem. Soc. Trans., 3, 316 (1975).

69. T. Brittain, C. Greenwood, and A. Johnson, Biochem. J., 167, 531 (1977).

70. P. Nicholls, Biochim. Biophys. Acta, 430, 13 (1976).

71. C. Greenwood, T. Brittain, M. Brunori, and M. T. Wilson, Biochem. J., 165, 413 (1977).

72. C. -A. Yu and L. Yu, Biochem. Biophys. Res. Commun., 70, 1115 (1976).

73. M. V. Gilmour, D. F. Wilson, and R. Lemberg, Biochim. Biophys. Acta, 143, 487 (1967).

74. P. Nicholls, Biochim. Biophys. Acta, 396, 24 (1975).

75. P. Nicholls, Biochem. Biophys. Res. Commun., 67, 610 (1975).

76. P. Nicholls, M. Erecinska, and D. F. Wilson, in "Mechanisms in Bioenergetics," G. F. Azzone, L. Ernster, S. Papa, E. Quagliariello, and N. Siliprandi, eds., Academic Press, N.Y., 1973, p. 561.

77. M. K. F. Wikström, in "Electron Transfer Chains and Oxidative Phosphorylation," E. Quagliariello, S. Papa, F. Palmieri, E. C. Slater, and N. Siliprandi, eds., American Elsevier, Inc., N.Y., 1975, p. 97.

78. M. K. F. Wikström, Biochim. Biophys. Acta, 283, 385 (1972).

79. M. K. F. Wikström and H. T. Saari, Molec. Cell. Biochem., 11, 17 (1976).

80. M. G. Choc, S. Yoshikawa, and W. S. Caughey, Fed. Proc., 36, 900 (1977).

81. J. A. Volpe, M. C. O'Toole, and W. S. Caughey, Biochem. Biophys. Res. Commun., 62, 48 (1975).

82. H. Wohlrab and G. B. Ogunmola, Biochemistry, 10, 1103 (1971).

83. Q. H. Gibson, G. Palmer, and D. C. Wharton, J. Biol. Chem., 240, 915 (1965).

84. D. C. Wharton and Q. H. Gibson, J. Biol. Chem., 251, 2861 (1976).

85. N. A. Schroedl and C. R. Hartzell, Biochemistry, 16, 4961 (1977).

86. C. R. Hartzell and H. Beinert, Biochim. Biophys. Acta, 423, 323 (1976).

87. G. T. Babcock, L. E. Vickery, and G. Palmer, J. Biol. Chem., 253, 2400 (1978).

88. J. G. Lindsay and D. F. Wilson, FEBS Lett., 48, 45 (1974).

89. D. F. Wilson and Y. Miyata, Biochim. Biophys. Acta, 461, 218 (1977).

90. N. A. Schroedl and C. R. Hartzell, Biochemistry, 16, 4966 (1977).

91. D. F. Wilson, M. Erecinska, and J. G. Lindsay, in "Electron Transfer Chains and Oxidative Phosphorylation," E. Quagliariello, S. Papa, F. Palmieri, E. C. Slater, and N. Siliprandi, eds., American Elsevier, Inc., N.Y., 1975, p. 69.

92. R. Wever, J. H. van Drooge, A. O. Muijsers, E. P. Bakker, and B. F. van Gelder, Eur. J. Biochem., 73, 149 (1977).

93. D. C. Wharton, Biochim. Biophys. Acta, 92, 607 (1964).

94. L. C. Petersen, Eur. J. Biochem., 85, 339 (1978).

95. W. S. Caughey, W. J. Wallace, J. A. Volpe, and S. Yoshikawa, in "The Enzymes," vol. 13, P. D. Boyer, ed., Academic Press, N.Y., 1976 p. 299.

96. C. Greenwood, M. T. Wilson, and M. Brunori, Biochem. J., 137, 205 (1974).

97. P. Nicholls, Biochem. J., 175, 1147 (1978).

98. R. Wever and B. F. van Gelder, Biochim. Biophys. Acta, 368, 311 (1974).

99. Q. H. Gibson, C. Greenwood, D. C. Wharton, and G. Palmer, in "International Symposium on Oxidases and Related Redox Systems," T. E. King, H. S. Mason, and M. Morrison, eds., John Wiley and Sons, Inc., New York, 1964, p. 591.

.00. D. F. Wilson and M. Erecinska, Meth. in Enzymol., 53, 191 (1978).

.01. L. C. Petersen, Biochim. Biophys. Acta, 460, 299 (1977).

.02. K. De Fonseka and B. Chance, Biochem. J., 175, 1137 (1978).

.03. H. J. Harmon and M. Sharrock, Biochim. Biophys. Acta, 503, 56 (1978).

04. B. Chance, J. Harmon, and M. Wikström, in "Electron Transfer Chains and Oxidative Phosphorylation," E. Quagliariello, S. Papa, F. Palmieri, E. C. Slater, and N. Siliprandi, eds., American Elsevier, Inc., New York, 1975, p. 81.

05. A. J. Thomson, T. Brittain, C. Greenwood, and J. Springall, FEBS Lett., 67, 94 (1976).

06. T. Brittain, J. Springall, C. Greenwood, and A. J. Thomson, Biochem. J., 159, 811 (1976).

07. R. W. Shaw, R. E. Hansen, and H. Beinert, Biochim. Biophys. Acta, 504, 187 (1978).

08. R. Wever, J. H. van Drooge, G. Van Ark, and B. F. van Gelder, Biochim. Biophys. Acta, 347, 215 (1974).

109. C. Hartzell and H. Beinert, Biochim. Biophys. Acta, 368, 318 (1974).

110. J. S. Leigh, Jr. and D. F. Wilson, Biochem. Biophys. Res. Commun., 48, 1266 (1972).

111. G. M. Clore and E. M. Chance, Biochem. J., 175, 709 (1978).

112. B. Chance, J. Biol. Chem., 202, 383, ff.(1953).

113. B. Chance and M. Erecinska, Arch. Biochem. Biophys., 143, 675 (1971).

114. B. Chance and J. S. Leigh, Jr., Proc. Natl. Acad. Sci. (USA), 74, 4777 (1977).

115. B. Chance, C. Saronio, and J. S. Leigh, Jr., Biochem. J., 177, 931 (1979).

116. S. Yoshida and Y. Orii, FEBS Lett., 79, 129 (1977).

117. K. J. H. van Buuren, P. F. Zuurendonk, B. F. van Gelder, and A. O. Muijsers, Biochim. Biophys. Acta, 256, 243 (1972).

118. K. J. H. van Buuren, P. Nicholls, and B. F. van Gelder, Biochim. Biophys. Acta, 256, 258 (1972).

119. S. Yoshikawa and Y. Orii, J. Biochem., 76, 271 (1974).

120. S. Yoshikawa and Y. Orii, J. Biochem., 71, 859 (1972).

121. S. Yoshikawa and Y. Orii, J. Biochem., 73, 637 (1973).

122. E. Antonini, M. Brunori, C. Greenwood, B. G. Malmström, and G. C. Rotilio, Eur. J. Biochem., 23, 396 (1971).

123. V. W. Hu, S. I. Chan, and G. S. Brown, FEBS Lett., 84, 287 (1977).

124. P. Nicholls and V. Hildebrandt, Biochim. Biophys. Acta, 504, 457 (1978).

125. P. Nicholls and V. Hildebrandt, Biochem. J., 173, 65 (1978).

126. Q. H. Gibson and C. Greenwood, Biochem. J., 86, 541 (1963).

127. D. V. Devartanian, I. Y. Lee, E. C. Slater, and B. F. van Gelder, Biochim. Biophys. Acta, 347, 321 (1974).

128. R. W. Shaw, R. E. Hansen, and H. Beinert, J. Biol. Chem., 253, 6637 (1978).

129. K. -E. Falk, T. Vänngård, and J. Ångström, FEBS Lett., 75, 23 (1977).

130. M. F. Tweedle, L. J. Wilson, L. García-Iñiguez, G. T. Babcock, and G. Palmer, J. Biol. Chem., 253, 8065 (1978).

131. T. H. Moss, E. Shapiro, T. E. King, H. Beinert, and C. Hartzell, J. Biol. Chem., 253, 8072 (1978).

132. R. Wever, B. F. van Gelder, and D. V. Devartanian, Biochim. Biophys. Acta, 387, 189 (1975).

133. S. Yoshikawa and Y. Orii, J. Biochem., 71, 873 (1972).

134. P. Nicholls, K. J. H. van Buuren, and B. F. van Gelder, Biochim. Biophys. Acta, 275, 279 (1972).

135. T. Brittain and C. Greenwood, Biochem. J., 155, 453 (1976).

136. S. Yoshikawa, T. Ueno, and T. Sai, J. Biochem., 82, 1361 (1977).

137. E. Antonini, M. Brunori, C. Greenwood, and M. T. Wilson, Biochem. Soc. Trans., 1, 34 (1973).

138. R. H. Tiesjema and B. F. van Gelder, Biochim. Biophys. Acta, 347, 202 (1974).

139. D. F. Wilson and B. Chance, Biochim. Biophys. Acta, 131, 431 (1967).

140. R. Wever, A. O. Muijsers, B. F. van Gelder, E. P. Bakker, and K. J. H. van Buuren, Biochim. Biophys. Acta, 325, 1 (1973).

141. B. F. van Gelder, R. Wever, and A. O. Muijsers, in "Mechanisms in Bioenergetics," G. F. Azzone, L. Ernster, S. Papa, E. Quagliariello, and N. Siliprandi, eds., Academic Press, New York, 1973, p. 571.

142. D. F. Wilson and B. Chance, Biochim. Biophys. Acta, 131, 421 (1967).

143. B. F. van Gelder and H. Beinert, Biochim. Biophys. Acta, 189, 1 (1969).

144. P. Nicholls, L. C. Petersen, M. Miller, and F. B. Hansen, Biochim. Biophys. Acta, 449, 188 (1976).

145. B. F. van Gelder, W. H. Orme-Johnson, R. E. Hansen, and H. Beinert, Proc. Natl. Acad. Sci. (USA), 58, 1073 (1967).

146. R. Wever, A. O. Muijsers, and B. F. van Gelder, Biochim. Biophys. Acta, 325, 8 (1973).

147. C. H. A. Seiter, S. G. Angelos, and R. A. Perreault, Biochem. Biophys. Res. Commun., 78, 761 (1977).

148. A. O. Muijsers, K. J. H. van Buuren, and B. F. van Gelder, Biochim. Biophys. Acta, 333, 430 (1974).

149. S. Yoshikawa and Y. Orii, J. Biochem., 68, 145 (1970).

150. M. F. J. Blokzijl-Homan and B. F. van Gelder, Biochim. Biophys. Acta, 234, 493 (1971).

151. D. J. Meyer, Nature (London), New Biology, 245, 276 (1973).

152. T. H. Stevens, D. F. Bocian, and S. I. Chan, FEBS Lett., 97, 314 (1979).

153. H. Kon and N. Kataoka, Biochemistry, 8, 4757 (1969).

154. C. Barlow and M. Erecinska, FEBS Lett., 98, 9 (1979).

155. M. K. F. Wikström and H. Saari, Biochim. Biophys. Acta, 408, 170 (1975).

156. L. -E. Andréasson, Eur. J. Biochem., 53, 591 (1975).

157. E. Antonini, M. Brunori, A. Colosimo, C. Greenwood, and M. T. Wilson, Proc. Natl. Acad. Sci. (USA), 74, 3128 (1977).

158. I. Sekuzu, S. Takemori, T. Yonetani, and K. Okunuki, J. Biochem., 46, 43 (1959).

159. J. A. Kornblatt, D. I. C. Kells, and G. R. Williams, Can. J. Biochem., 53, 461 (1975).

160. B. Lanne and T. Vänngård, Biochim. Biophys. Acta, 501, 449 (1978).

161. L. N. Mackey, T. Kuwana, and C. R. Hartzell, FEBS Lett., 36, 326 (1973).

162. W. R. Heineman, T. Kuwana, and C. R. Hartzell, Biochem. Biophys. Res. Commun., 50, 892 (1973).

163. D. F. Wilson and P. L. Dutton, Arch. Biochem. Biophys., 136, 583 (1970).

164. P. L. Dutton, D. F. Wilson, and C. -P. Lee, Biochemistry, 9, 5077 (1970).

165. D. F. Wilson, P. L. Dutton, M. Erecinska, and J. G. Lindsay, in "Mechanisms in Bioenergetics," G. F. Azzone, L. Ernster, S. Papa, E. Quaglieriello, and N. Siliprandi, eds., Academic Press, New York, 1973, p. 527.

166. M. K. F. Wikström, Ann. N.Y. Acad. Sci., 227, 146 (1974).

167. D. C. Wharton and M. A. Cusanovich, Biochem. Biophys. Res. Commun., 37, 111 (1969).

168. T. Tsudzuki and D. F. Wilson, Arch. Biochem. Biophys., 145, 149 (1971).

169. Y. Fujihara, T. Kuwana, and C. R. Hartzell, Biochem. Biophys. Res. Commun., 61, 538 (1974).

170. D. F. Wilson and J. S. Leigh, Jr., Ann. N.Y. Acad. Sci., 227, 630 (1974).

171. D. F. Wilson and E. S. Brocklehurst, Arch. Biochem. Biophys., 158, 200 (1973).

172. J. G. Lindsay, C. S. Owen, and D. F. Wilson, Arch. Biochem. Biophys., 169, 492 (1975).

173. D. F. Wilson, P. L. Dutton, and M. Wagner, Curr. Topics in Bioenerg., 5, 233 (1973).

174. R. Szentirmay and T. Kuwana, Anal. Chem., 50, 1879 (1978).

175. M. C. Sorgato and S. J. Ferguson, FEBS Lett., 90, 178 (1978).

176. M. Wikström and K. Krab, FEBS Lett., 91, 8 (1978).

177. E. Sigel and E. Carafoli, Eur. J. Biochem., 89, 119 (1978).

178. K. Krab and M. K. F. Wikström, Biochim. Biophys. Acta, 504, 200 (1978).

179. B. F. van Gelder, J. L. M. L. van Rijn, G. J. A. Schilder, and J. Wilms, in "Structure and Function of Energy-Transducing Membranes," K. van Dam and B. F. van Gelder, eds., Elsevier, North-Holland, Amsterdam, 1977, p. 61.

180. B. Lanne, B. G. Malmström, and T. Vänngård, Biochim. Biophys. Acta, 545, 205 (1979).

181. J. G. Lindsay and D. F. Wilson, Biochemistry, 11, 4613 (1972).

182. J. L. Anderson, T. Kuwana, and C. R. Hartzell, Biochemistry, 15, 3847 (1976).

183. A. H. Caswell, Arch. Biochem. Biophys., 144, 445 (1971).

184. S. Ferguson-Miller, D. L. Brautigan, and E. Margoliash, J. Biol. Chem., 251, 1104 (1976).

185. B. F. van Gelder, K. J. H. van Buuren, J. Wilms, and C. N. Verboom, in "Electron Transfer Chains and Oxidative Phosphorylation," E. Quagliariello, S. Papa, F. Palmieri, E. C. Slater, and N. Siliprandi, eds., American Elsevier, Inc., New York, 1975, p. 63.

186. N. A. Schroedl and C. R. Hartzell, Biochemistry, 16, 1327 (1977).

187. R. H. Sands and H. Beinert, Biochem. Biophys. Res. Commun., 1, 175 (1959).

188. H. Beinert, D. E. Griffiths, D. C. Wharton, and R. H. Sands, J. Biol. Chem., 237, 2337 (1962).

189. H. Beinert and G. Palmer, J. Biol. Chem., 239, 1221 (1964).

190. F. T. Greenaway, S. H. P. Chan, and G. Vincow, Biochim. Biophys. Acta, 490, 62 (1977).

191. V. W. Hu, S. I. Chan, and G. S. Brown, Proc. Natl. Acad. Sci. (USA), 74, 3821 (1977).

192. J. Peisach and W. E. Blumberg, Arch. Biochem. Biophys., 165, 691 (1974).

193. W. R. Hagen and S. P. J. Albracht, in "Structure and Function of Energy-Transducing Membranes," K. van Dam and B. F. van Gelder, eds., Elsevier, North-Holland, Amsterdam, 1977, p. 23.

194. H. L. van Camp, Y. -H. Wei, C. P. Scholes, and T. E. King, Biochim. Biophys. Acta, 537, 238 (1978).

195. H. Beinert, in "The Biochemistry of Copper," J. Peisach, P. Aisen, and W. E. Blumberg, eds., Academic Press, New York, 1966, p. 253.

196. R. Wever, G. van Ark, and B. F. van Gelder, FEBS Lett., 84, 388 (1977).

197. H. Beinert, R. E. Hansen, and C. R. Hartzell, Biochim. Biophys. Acta, 423, 339 (1976).

198. G. T. Babcock, L. E. Vickery, and G. Palmer, J. Biol. Chem., 251, 7907 (1976).

199. A. J. Thomson, T. Brittain, C. Greenwood, and J. P. Springall, Biochem. J., 165, 327 (1977).

200. A. Ehrenberg and T. Yonetani, Acta Chem. Scand., 15, 1071 (1961).

201. T. Tsudzuki and K. Okunuki, J. Biochem., 69, 909 (1971).

202. G. Palmer, G. T. Babcock, and L. E. Vickery, Proc. Natl. Acad. Sci. (USA), 73, 2206 (1976).

203. T. H. Moss and J. A. Fee, Biochem. Biophys. Res. Commun., 66, 799 (1975).

204. D. F. Wilson, M. Erecinska, J. G. Lindsay, J. S. Leigh, Jr., and C. S. Owen, in "Enzymes. Electron Transport Systems," Proceedings of the 10th FEBS Meeting, Paris, P. Desnuelle and A. M. Michelson, eds., North-Holland, American Elsevier, New York, 1975, p. 195.

205. W. E. Blumberg and J. Peisach, Biophys. J., 25, 37a (1979).

206. B. Chance, A. Waring, and E. Yang, Biophys. J., 25, 44a (1979).

207. B. G. Malmström, in "Membrane Proteins," FEBS 11th Meeting, Copenhagen, vol. 45, Symp. A4, P. Nicholls, J. V. Møller, P. L. Jørgensen, A. J. Moody, eds., Pergamon Press, Oxford, 1978, p. 61.

208. H. Beinert and R. W. Shaw, Biochim. Biophys. Acta, 462, 121 (1977).

209. M. Erecinska, D. F. Wilson, and J. K. Blasie, in "Membrane Proteins," FEBS 11th Meeting, Copenhagen, vol. 45, Symp. A4, P. Nicholls, J. V. Møller, P. L. Jørgensen, A. J. Moody, eds., Pergamon Press, Oxford, 1978, p. 69.

210. T. Stevens, G. Brudvig, D. Bocian, and S. Chan, Biophys. J., 25, 274a (1979).

211. Y. Orii and T. E. King, J. Biol. Chem., 251, 7487 (1976).

212. B. G. Malmström, Adv. Chem. Ser., vol. 162, p. 173 (1977).

213. P. Nicholls, Arch. Biochem. Biophys., 106, 25 (1964).

214. E. Mochan and P. Nicholls, Biochim. Biophys. Acta, 267, 309 (1972).

215. S. Ferguson-Miller, D. L. Brautigan, and E. Margoliash, J. Biol. Chem., 251, 1104 (1976).

216. H. C. Davies, L. Smith, and A. R. Wasserman, Biochim. Biophys. Acta, 85, 238 (1964).

217. P. Maurel, P. Douzou, J. Waldmann, and T. Yonetani, Biochim. Biophys. Acta, 525, 314 (1978).

218. P. Nicholls and B. Chance, in "Molecular Mechanisms of Oxygen Activation," O. Hayaishi, ed., Academic Press, New York, 1974, p. 479.

219. S. Takemori, K. Wada, K. Ando, M. Hosokawa, I. Sekuzu, and K. Okunuki, J. Biochem., 52, 28 (1962).

220. K. J. H. van Buuren, B. F. van Gelder, J. Wilting, and R. Braams, Biochim. Biophys. Acta, 333, 421 (1974).

221. R. Timkovich, Fed. Proc. 36, 891 (1977).

222. L. C. Dickinson and J. C. W. Chien, Biochemistry, 14, 3526 (1975).

223. N. Staudenmayer, M. B. Smith, H. T. Smith, F. K. Spies, Jr., and F. Millett, Biochemistry, 15, 3198 (1976).

224. N. Staudenmayer, S. Ng, M. B. Smith, and F. Millett, Biochemistry, 16, 600 (1977).

225. S. Ferguson-Miller, D. L. Brautigan, B. Chance, A. Waring, and E. Margoliash, Biochemistry, 17, 2246 (1978).

226. N. Osheroff, R. Jemmerson, and S. Ferguson-Miller, Fed. Proc., 37, 1326 (1978).

227. S. H. Speck, S. Ferguson-Miller, N. Osheroff, and E. Margoliash, Proc. Natl. Acad. Sci. (USA), 76, 155 (1979).

228. B. Errede, G. P. Haight, Jr., and M. D. Kamen, Proc. Natl. Acad. Sci. (USA), 73, 113 (1976).

229. L. C. Petersen and L. -E. Andréasson, FEBS Lett., 66, 52 (1976).

230. L. C. Petersen, Biochem. Soc. Trans., 6, 1274 (1979).

231. Q. H. Gibson, C. Greenwood, D. C. Wharton, and G. Palmer, J. Biol. Chem., 240, 888 (1965).

232. M. T. Wilson, C. Greenwood, M. Brunori, and E. Antonini, Biochem. J., 147, 145 (1975).

233. C. Greenwood, T. Brittain, M. Wilson, and M. Brunori, Biochem. J., 157, 591 (1976).

234. R. Lemberg and M. E. Cutler, Biochim. Biophys. Acta, 197, 1 (1970).

235. E. Antonini, M. Brunori, C. Greenwood, and B. G. Malmström, Nature, 228, 936 (1970).

236. C. Greenwood and Q. H. Gibson, J. Biol. Chem., 242, 1782 (1967).

237. L. Smith, H. C. Davies, and M. E. Nava, Fed. Proc., 37, 1326 (1978).

238. K. Minnaert, Biochim. Biophys. Acta, 50, 23 (1961).

239. L. C. Petersen, P. Nicholls, and H. Degn, Biochim. Biophys. Acta, 452, 59 (1976).

240. S. Rosén, R. Brändén, T. Vänngård, and B. G. Malmström, FEBS Lett., 74, 25 (1977).

241. B. Chance, C. Saronio, and J. S. Leigh, Jr., Proc. Natl. Acad. Sci. (USA), 72, 1635 (1975).

242. B. Chance, N. Graham, and V. Legallais, Anal. Biochem., 67, 552 (1975).

243. B. Chance, C. Saronio, and J. S. Leigh, Jr., J. Biol. Chem., 250, 9226 (1975).

244. B. Chance, C. Saronio, A. Waring, and J. S. Leigh, Jr., Biochim. Biophys. Acta, 503, 37 (1978).

245. H. J. Harmon and M. K. F. Wikström, Biochim. Biophys. Acta, 503, 67 (1978).

246. B. Chance, J. Harmon, and C. Saronio, in "Enzymes. Electron Transport Systems," Proc. 10th FEBS Meeting, P. Desnuelle and A. M. Michelson, eds., North-Holland, American Elsevier, New York, 1975, p. 187.

247. G. M. Clore and E. M. Chance, Biochem. J., 173, 799 (1978).

248. G. M. Clore and E. M. Chance, Biochem. J., 173, 811 (1978).

249. G. M. Clore and E. M. Chance, Biochem. J., 177, 613 (1979).

250. D. D. Perrin, W. L. F. Armarego, and D. R. Perrin, "Purification of Laboratory Chemicals," Pergamon Press, New York, 1966, p. 294.

251. R. W. Shaw, personal communication.

252. J. R. Pladziewicz, T. J. Meyer, J. A. Broomhead, and H. Taube, Inorg. Chem., 12, 639 (1973).

253. P. B. Sweetser, Anal. Chem., 39, 979 (1967).

254. R. A. Scott, unpublished (in "Methods in Bioinorganic Chemistry," available, A. G. Mauk, Department of Biochemistry, University of British Columbia, Vancouver, B.C.).

255. O. H. Lowry, N. J. Rosebrough, A. L. Farr, and R. J. Randall, J. Biol. Chem., 193, 265 (1951).

256. L. Smith, in "Methods of Biochemical Analysis," vol. II, D. Glick, ed., Interscience, New York, 1955, p. 427.

257. W. H. Vanneste, M. Ysebaert-Vanneste, and H. S. Mason, J. Biol. Chem., 249, 7390 (1974).

258. J. A. Peterson, R. E. White, Y. Yasukochi, M. L. Coomes, D. H. O'Keeffe, R. E. Ebel, B. S. Masters, D. P. Ballou, and M. J. Coon, J. Biol. Chem., 252, 4431 (1977).

259. D. P. Ballou, C. Veeger, T. A. van der Hoeven, and M. J. Coon, FEBS Lett., 38, 337 (1974).

260. D. F. Shriver, "The Manipulation of Air-Sensitive Compounds," McGraw-Hill, New York, 1969, p. 199.

261. Supplementary volume of this thesis.

262. E. A. Guggenheim, Phil. Mag., 2, 538 (1926).

263. The $t_{1/2}$ values reported were calculated *assuming* first order kinetics were obeyed in each case. This assumption may or may not be valid for these reactions. The numbers are quoted only to indicate the relative rates of the reactions.

264. R. P. Tracy and S. H. P. Chan, Biochim. Biophys. Acta, 576, 109 (1979).

265. M. Erecinska, Biochem. Biophys. Res. Commun., 76, 495 (1977).

CHAPTER II

Analytical Techniques

INTRODUCTION

Without a proper analytical approach, even the best data acquisition can be made virtually useless. Misapplication of the simplest data reduction techniques can lead not only to mistaken results but also to a false sense of security about the validity of these results when done blindly. The potential for misuse has resulted in the inclusion of this seemingly innocuous subject as a major section of this dissertation. What follows is a useful, but by no means complete, summary of the basic methodology necessary to perform a proper analysis on a data set assumed to be a sample of a population of discrete observations as well as the techniques for properly weighted fits of the data to a given functional form. Examples given will include the techniques used in all the analytical routines discussed herein.

PART I. BASIC TECHNIQUES

For the purposes of this discussion, several assumptions about the statistical characteristics of the experimental data will be made. Among the most important are: (1) The parent distribution of the population from which the data set is taken is assumed to be Gaussian (normal); (2) any errors associated with the actual experimental measurements are random (*i.e.*, either there are no systematic errors or all systematic errors have been corrected for); (3) for the cases in which the quantity of interest is dependent on several other parameters, the errors in the independent parameters are assumed uncorrelated (*i.e.*, all covariances are assumed equal to zero). The first assumption is usually valid, since the data are expected to obey either a Gaussian or Poisson distribution and these are indistinguishable for most cases. The second assumption is equivalent to assuming that the data is accurate but imprecise. In other words, if the data were perfectly precise, then the answer obtained would be the true (accurate) answer. This assumption is not necessarily valid, but the resolution of inaccuracies (systematic errors) is outside the realm of statistical methods. The third assumption is just a simplifying assumption which is not necessarily strictly valid in all cases, but may be at least a good approximation to reality. Some of the less well-behaved cases will be discussed below.

One of the important goals of this discussion will be to point out the universality and generality of the techniques described. It will be seen that a few basic concepts will serve

to allow extensions of the simpler techniques to more complicated analyses. Also, many of the expressions developed for complicated cases will be applicable to simpler cases. Thus, development of a unified analytical approach is possible. Many treatments of the basic techniques described below have been given but the delightful treatise by Bevington[1] is one of the best and will be referred to often.

Notation

In general, the following discussion will be concerned with a set of N data points, the i-th data point consisting of values for a dependent variable (y_i) and perhaps for one or more independent variables (in the case of one independent variable, it will be notated as x_i). The i-th dependent variable value (y_i) will be assumed to be taken from a Gaussian distribution with mean μ and standard deviation σ_i (for expression, see below). The parent distribution of the data set (which is a function of the independent variable if there is one) will be assumed to have mean μ and standard deviation σ. Thus, the data set is collected from a Gaussian distribution with the same mean as the parent distribution (*i.e.*, systematic errors are assumed absent). In much of the following, the notation:

$$\sum_{i=1}^{N} a_i(\lambda)$$

will be abbreviated:

$$\Sigma_i a_i(\lambda)$$

In either case, the sum runs over all i from 1 to N.

Mean and Standard Deviation

In the simplest case, an experiment is performed to determine the value of a particular quantity. Several measurements are made and the goal is to calculate the best estimate of the actual physical quantity from the experimental measurements.

The physical quantity has a certain inherent error associated with it and there are other random errors inherent in the measurement process which contribute to the actual uncertainty in the value. Thus, the parent Gaussian distribution representing the actual physical quantity has a mean μ and an associated standard deviation σ. The Gaussian characteristic of the distribution can be described by the probability P_i of of making any particular observation y_i:

$$P_i = (2\pi\sigma^2)^{-1/2} \exp\left[- \frac{1}{2}\left(\frac{y_i - \mu}{\sigma}\right)^2 \right] \qquad (2\text{-}1)$$

In general, the value of μ (the actual physical quantity) is unknown and the goal (which is applicable for all the more complicated cases as well) is to find a way of calculating the best estimate of μ from the y_i. Hypothesizing that the measured y_i belong to a Gaussian distribution with mean μ' and standard deviation $\sigma'(= \sigma)$ (and that the probability of measuring a particular y_i is given by P_i') allows one to use the method of maximum likelihood[2] which results in the conclusion that the probability is highest that the y_i were taken from a Gaussian distribution with mean μ (*i.e.*, the parent distribution).

The best estimate of μ' is then found by maximizing the total probability that the data is from a distribution of mean

μ' and then finding the value of μ' which gives this maximum probability. This total probability is the product of the probabilities that any particular y_i will be measured and is given by:

$$P' = \prod_{i=1}^{N} P_i' = (2\pi\sigma^2)^{-N/2} \exp\left[-\frac{1}{2}\Sigma_i \left(\frac{y_i - \mu'}{\sigma}\right)^2 \right] \qquad (2\text{-}2)$$

Maximizing P' can be accomplished by minimizing the argument of the exponential:

$$\frac{\partial}{\partial \mu'} \left[-\frac{1}{2}\Sigma_i \left(\frac{y_i - \mu'}{\sigma}\right)^2 \right] = 0 \qquad (2\text{-}3)$$

Performing the differentiation and solving for μ' gives the best estimate of the mean μ of the parent distribution:

$$\mu' = \bar{y} \equiv \frac{1}{N}\Sigma_i y_i \qquad (2\text{-}4)$$

$\bar{y}$ is the (unweighted) average of the set of N measurements (y_i) and is thus the best estimate of the physical quantity (μ) desired.

To find the best estimate of the error in the calculated estimate (μ') of the mean, the variance (square of the standard deviation) for the mean (σ_μ^2) must be calculated and is equal to the sum of the variances σ_i^2 for the individual data points y_i weighted by the squares of the effects ($\partial\mu'/\partial y_i$) which the individual data points have on the result[3]:

$$\sigma_\mu^2 = \Sigma_i \left[\sigma_i^2 \left(\frac{\partial \mu'}{\partial y_i}\right)^2 \right] \qquad (2\text{-}5)$$

(It should be noted that this simplified expression makes use of the assumption that the covariances between the y_i are negligible. In this case, since the value measured for any individual y_i is usually independent of the values measured for the

other y_i, the assumption is valid.) So far, it has been assumed that all of the measurements (y_i) are taken from a distribution with the same standard deviation $\sigma'=\sigma$. With this assumption (*i.e.*, $\sigma_i=\sigma$, for all i), the result of applying equation (2-5) to the expression for μ' in equation (2-4) yields:

$$\sigma_\mu^2 = \sigma^2/N \qquad (2\text{-}6)$$

Thus, the best estimates of the mean of the parent distribution and the standard error of this mean are given by μ' and σ_μ, respectively.

Equation (2-6) is easily employed assuming knowledge of σ (*i.e.*, the error associated with each measurement y_i). However, in many cases, σ is not known and an estimate of its value must be made. It can be shown that a good estimate of σ can be made by using the sample standard deviation s:

$$\sigma^2 \simeq s^2 \equiv \frac{1}{(N-1)}\Sigma_i(y_i-\bar{y})^2 \qquad (2\text{-}7)$$

Using this estimate for σ^2 in equation (2-6) gives the following estimate of the uncertainty in the estimate of the mean (for y_i with all $\sigma_i=\sigma$):

$$\sigma_\mu \simeq \left(\frac{s^2}{N}\right)^{1/2} = \left(\frac{\Sigma_i(y_i-\bar{y})^2}{N(N-1)}\right)^{1/2} \qquad (2\text{-}8)$$

The distinction between σ_μ and σ should be clear. σ_μ is the estimated *standard error* (of the mean), whereas σ is the *standard deviation* of the parent distribution (and can be estimated as s).

Weighting

The above discussion assumed that all the measurements y_i were of the same precision (*i.e.*, $\sigma_i=\sigma$ for all i). However, in

many instances, measurements are often made with varying amounts of precision (*e.g.*, measurements at different scale factors, etc.). In these cases, each y_i has an error σ_i associated with it (the σ_i's being unequal). Intuition suggests that a relatively imprecise measurement should not contribute as much to the estimation of the mean as a more precise measurement. Thus, a weighting scheme is necessary for these cases. It is satisfying that merely the assumption that the parent distribution is Gaussian allows a derivation of the proper weighting scheme. The extreme importance of this minor sophistication (weighting) cannot be overemphasized. An example illustrating this point is described later.

Assuming different σ_i for the individual y_i leads to an expression for the total probability that the data is from a Gaussian distribution of mean μ' analogous to that of equation (2-2)[5]:

$$P' = \prod_{i=1}^{N} (2\pi\sigma_i^2)^{-1/2} \exp\left[-\frac{1}{2}\Sigma_i\left(\frac{y_i-\mu'}{\sigma_i}\right)^2\right] \qquad (2\text{-}9)$$

Finding the value of μ' which maximizes P' (as above) yields the result:

$$\mu' = \bar{y} \equiv \frac{\Sigma_i w_i y_i}{\Sigma_i w_i} \qquad (w_i = 1/\sigma_i^2) \qquad (2\text{-}10)$$

This gives μ' as the weighted average ($\bar{y}$) of the y_i data set (which is the best estimate of the parent distribution mean μ). Thus, the standard inverse variance (or "inverse sigma squared") weighting scheme is seen to be a direct result of the assumption of a Gaussian distribution. In the event that $\sigma_i=\sigma$ for all i, equation (2-10) simplifies to:

$$\mu' = \frac{(1/\sigma^2)\Sigma_i y_i}{N(1/\sigma^2)} = \frac{1}{N}\Sigma_i y_i$$

which is identical to equation (2-4) (the unweighted mean of the y_i data set). This also illustrates that the weighted estimate of μ' (equation (2-10)) is insensitive to the absolute magnitude of the σ_i. Thus, in the absence of knowledge of the absolute σ_i, relative errors in the y_i measurements (σ_i') can be used for weighting the estimate of the mean with identical results.

In the case of unequal uncertainties σ_i in the measurements y_i, equation (2-5) can again be used to calculate an estimate of σ_μ (the standard error of μ'). However, μ' is now given by equation (2-10) and the calculation results in:

$$\sigma_\mu^2 = [\Sigma_i w_i]^{-1} \tag{2-11}$$

Again, in the event that only relative values (σ_i') of the σ_i were used for weighting, the absolute magnitudes of the σ_i can be estimated from the dispersion of the data points about the estimated mean. The calculation of s^2 (see equation (2-7)) must now be weighted with the same weighting factors used in the $\bar{y}$ calculation (equation (2-10)) and the result is[6]:

$$\sigma^2 \simeq s^2 = \frac{N\Sigma_i[w_i'(y_i-\bar{y})^2]}{(N-1)\Sigma_i w_i'} \tag{2-12}$$

$$\sigma_\mu^2 = \sigma^2/N \simeq s^2/N \tag{2-13}$$

Propagation of Errors

Consideration of data analyses more complicated than simple estimations of the mean and standard deviation requires a means of determining how deviations in one parameter (or independent variable) affect another parameter (or dependent variable) the value of which depends upon the first. In general, consider the parameter y which can be described as a function of other para-

meters (*e.g.*, u,v, etc.):

$$y = f(u,v,\ldots) \tag{2-14}$$

Then the dependence of y on each of the other parameters will determine the effect a deviation in any of these other parameters will have on the value of y. That is, the larger the magnitudes of the partial derivatives $\frac{\partial y}{\partial u}$, $\frac{\partial y}{\partial v}$, etc., the larger the dependence of the variance (or square of the standard deviation) of y upon the variances (and covariances) of the other parameters[3]:

$$\sigma_y^2 \simeq \sigma_u^2\left(\frac{\partial y}{\partial u}\right)^2 + \sigma_v^2\left(\frac{\partial y}{\partial v}\right)^2 + 2\sigma_{uv}^2\left(\frac{\partial y}{\partial u}\right)\left(\frac{\partial y}{\partial v}\right) + \cdots \tag{2-15}$$

In this expression, σ_u^2 and σ_v^2 are the variances in the parameters u and v, respectively, while σ_{uv}^2 is the covariance between the parameters u and v. The theoretical definitions of these terms are as follows[7]:

$$\sigma_u^2 \equiv \lim_{N\to\infty} \frac{1}{N}\Sigma_i (u_i - \bar{u})^2 \tag{2-16}$$

$$\sigma_{uv}^2 \equiv \lim_{N\to\infty} \frac{1}{N}\Sigma_i [(u_i - \bar{u})(v_i - \bar{v})] \tag{2-17}$$

(The expression for σ_v^2 is completely analogous to the σ_u^2 expression.) In the event that the individual u_i and v_i measurements are uncorrelated, then it would be expected that as many negative as positive terms would occur in the summation of equation (2-17) and the covariance term would be negligible compared to the first two terms of equation (2-15). This is assumed to be the case from here on. It should be noted however, that it is difficult in any particular case to estimate the covariances and correlation of parameters may indeed exist. Of course, the correlation may be such that the third term in equation (2-15)

is negative and the σ_y^2 calculated will be overestimated by neglecting the covariance. Other approximations in equation (2-15) include the neglect of higher order cross terms in the expansion and the approximate nature of the experimental variances (*i.e.*, use of a relatively small value of N in equation (2-16)). Thus, it can be argued that equation (2-15) (neglecting the third term) gives the best possible estimate of σ_y^2 under the circumstances.

The utility of equation (2-15) becomes most apparent in determining the proper weighting factors for cases in which the quantity of interest is functionally dependent on (but not equivalent to) the measured parameter. A relevant example will serve to illustrate this point. Consider the case of a first order kinetics decay. The measured parameter y (usually absorbance or some other quantity linearly related to concentration) is a function of several other parameters:

$$y = (y_0 - y_\infty)\exp(-kt) + y_\infty$$

where, t = time
y_0 = value of y at $t = 0$
y_∞ = value of y at $t = \infty$
k = first order rate constant

This equation can be rearranged to give:

$$\ln|y - y_\infty| = \ln|y_0 - y_\infty| - kt$$

and thus, the standard first order kinetics analysis[8,9] consists of plotting $\ln|y_i - y_\infty|$ versus t_i and using the slope of a linear least squares fit (see next section) of the data as an estimate of k. (The intercept can be used to calculate y_0.) In this case, the quantity to be plotted (call it Y) is a function of the measured quantity y:

$$Y \equiv \ln|y-y_\infty|$$

The goal will be to develop a proper weighting scheme for the Y values. Since the y_i have been measured, an estimate of the error in this quantity is available (or can be calculated). Assuming that each y_i has some error σ_i associated with it, the goal becomes determining the error (σ_Y) associated with Y due to the error (σ) in y. For this particular case, equation (2-15) becomes:

$$\sigma_Y^2 \simeq \sigma^2\left(\frac{\partial Y}{\partial y}\right)^2 + \sigma_\infty^2\left(\frac{\partial Y}{\partial y_\infty}\right)^2$$

where, $\sigma \equiv$ error in y
$\sigma_\infty \equiv$ error in y_∞

(The cross term (covariance term) has been neglected as discussed above.) For the purposes of this example, σ_∞ will be assumed equal to σ (a reasonable assumption if y_∞ was measured in the same manner as the y_i). The partial derivatives are easily evaluated:

$$\frac{\partial Y}{\partial y} = \frac{1}{|y-y_\infty|}$$

$$\frac{\partial Y}{\partial y_\infty} = -\frac{1}{|y-y_\infty|}$$

and using these expressions to evaluate σ_Y^2:

$$\sigma_Y^2 = 2(\sigma/|y-y_\infty|)^2$$

$$\sigma_Y = (2)^{1/2}\sigma/|y-y_\infty|$$

These σ_Y should then be used to calculate the weighting factors for the linear least squares fit.

If the y_i data were measured out to $t = \infty$ ($y_i = y_\infty$), the Y values would approach $-\infty$ ($\ln(0)$). Thus, small deviations in y_i values near y_∞ can cause very large changes in the calculated Y values. This is clearly reflected in the σ_Y expression

which approaches $+\infty$ as $y \to y_\infty$. Thus, a constant amount of error (σ) in y_i values makes a much larger difference (σ_Y) in the Y values as $y_i \to y_\infty$. If the Y values were fit by unweighted least squares (see next section), these "noisier" points at the end of the data would contribute more to the fit than their precision warrants. Thus, a $1/\sigma_Y^2$ weighting scheme *must* be used for a proper fit to be performed and the proper parameters to be calculated.

Least Squares

In the preceding, the emphasis has been on finding the best estimates for the mean and standard deviation of a parent distribution from which a set of measurements y_i were taken. In this section, the measured quantity y will be assumed to be dependent on another measured quantity x:

$$y = f(x) \tag{2-18}$$

Each data point of the set of N data points will now consist of a measurement of both x and y and will be designated as (x_i, y_i). In the simplest case, y will be linearly dependent on x:

$$y = a + bx \tag{2-19}$$

and the goal is to find the values of a and b which "best" predict the observed dependence of y on x (as described by the (x_i, y_i) data). There are several possible definitions of "best" but the usual choice is the "least squares" criterion. For this case, the "best" values of a and b are those which minimize the sum of the squares of the deviations between the measured y_i and the calculated $y(x_i)$:

$$y(x_i) = a + bx_i \tag{2-20}$$

Descriptions of the least squares method abound (Bevington's[10] is as good as any) and thus a much abbreviated version is given here for the sake of completeness.

The parent Gaussian distribution is now modified to include the dependence on x. The probability (P_i) of observing a particular y_i is given by:

$$P_i = (2\pi\sigma_i^2)^{-1/2}\exp\left\{-\frac{1}{2}\left[\frac{y_i - y(x_i)}{\sigma_i}\right]^2\right\} \tag{2-21}$$

$$\text{where, } y(x) = a_0 + b_0 x$$

Here, a_0 and b_0 are the coefficients of the parent distribution. In analogy to the discussion above (and in Bevington) the method of maximum likelihood may be used to find the values of a and b which maximize the probability that the data (x_i,y_i) came from the parent distribution (*i.e.*, the values of a and b which are the best estimates of a_0 and b_0). The quantity which is to be minimized (to accomplish the above goal) is:

$$\chi^2 \equiv \Sigma_i\left(\frac{\Delta y_i}{\sigma_i}\right)^2 = \Sigma_i\left[\frac{1}{\sigma_i^2}(y_i - y(x_i))^2\right] \tag{2-22}$$

where $y(x_i)$ is given in equation (2-20). This quantity is defined as χ^2 and will be discussed in detail later. It should be noted that the weighting factors ($1/\sigma_i^2$) are identical to the weighting factors used in the mean estimation procedures of earlier sections and are again a direct result of the assumption of a Gaussian distribution. Minimization of χ^2 with respect to both parameters (a and b) results in two simultaneous linear equations to be solved for a and b which can be written in matrix form:

$$\begin{bmatrix} \Sigma_i w_i & \Sigma_i w_i x_i \\ \Sigma_i w_i x_i & \Sigma_i w_i x_i^2 \end{bmatrix} \begin{bmatrix} a \\ b \end{bmatrix} = \begin{bmatrix} \Sigma_i w_i y_i \\ \Sigma_i w_i x_i y_i \end{bmatrix} \qquad (2\text{-}23)$$

$$\text{where, } w_i = 1/\sigma_i^2$$

Estimation of the errors associated with the calculated parameters a and b can easily be accomplished by making use of an expression analogous to that of equation (2-15):

$$\sigma_a^2 \simeq \Sigma_i \left[\sigma_i^2 \left(\frac{\partial a}{\partial y_i} \right)^2 \right] \qquad (2\text{-}24)$$

A similar expression holds for σ_b^2. Solution of the matrix equation (2-23) results in expressions for a and b which can be used to calculate the partial derivatives in equation (2-24). In the event that absolute σ_i's are known and used for the weighting factors, the results are[11]:

$$\begin{aligned} \sigma_a^2 &\simeq \Delta^{-1} \Sigma_i w_i x_i^2 \\ \sigma_b^2 &\simeq \Delta^{-1} \Sigma_i w_i \\ \Delta &\equiv \Sigma_i w_i \Sigma_i w_i x_i^2 - (\Sigma_i w_i x_i)^2 \end{aligned} \qquad (2\text{-}25)$$

If only relative σ_i (σ_i') are known, s^2 can again be used to estimate the errors:

$$s^2 = [N \Sigma_i w_i' (y_i - y(x_i))^2] / [(N-2) \Sigma_i w_i'] \qquad (2\text{-}26)$$

$$\begin{aligned} \sigma_a^2 &\simeq \frac{N s^2}{\Delta} \frac{\Sigma_i w_i' x_i^2}{\Sigma_i w_i'} \\ \sigma_b^2 &\simeq \frac{N s^2}{\Delta} \end{aligned} \qquad (2\text{-}27)$$

Δ is defined as in equation (2-25) with w_i' replacing w_i. These expressions for s^2 and σ_a^2 differ slightly from those given in Bevington. The differences will be discussed later.

It is relatively simple to extend the linear least squares analysis to higher order polynomials.[12] Assuming that y is a polynomial function of x (of order m):

$$y(x) = \sum_{j=0}^{m} a_j x^j$$

and again minimizing χ^2 (as above) results in a matrix equation which is an extension of the one given in equation (2-23):

$$\begin{bmatrix} \Sigma_i w_i & \Sigma_i w_i x_i & \Sigma_i w_i x_i^2 & \cdots & \Sigma_i w_i x_i^m \\ \Sigma_i w_i x_i & \Sigma_i w_i x_i^2 & \Sigma_i w_i x_i^3 & \cdots & \Sigma_i w_i x_i^{(m+1)} \\ \Sigma_i w_i x_i^2 & \Sigma_i w_i x_i^3 & \Sigma_i w_i x_i^4 & \cdots & \Sigma_i w_i x_i^{(m+2)} \\ \vdots & \vdots & \vdots & & \vdots \\ \Sigma_i w_i x_i^m & \Sigma_i w_i x_i^{(m+1)} & \Sigma_i w_i x_i^{(m+2)} & \cdots & \Sigma_i w_i x_i^{2m} \end{bmatrix} \begin{bmatrix} a_0 \\ a_1 \\ a_2 \\ \vdots \\ a_m \end{bmatrix} =$$

$$\begin{bmatrix} \Sigma_i w_i y_i \\ \Sigma_i w_i x_i y_i \\ \Sigma_i w_i x_i^2 y_i \\ \vdots \\ \Sigma_i w_i x_i^m y_i \end{bmatrix} \qquad (2\text{-}28)$$

This results in (m+1) simultaneous linear equations which can be solved for the a_j coefficients. These coefficients are then the best estimates (in a least squares sense) of the coefficients which define the parent distribution (assuming that the parent distribution can be described as an m-th order polynomial in x). In principal, estimation of the errors in the coefficients can be accomplished in a manner completely analogous to that used for the linear case. In practice, however, this is tedious and the estimation procedure can be more readily performed by other means. It can be shown[12] that the inverse of the (m+1)x(m+1) matrix on the left hand side of equation

(2-28) is closely related to the error quantities of interest. In fact, in the event that the absolute σ_i's used in equation (2-28) are correct, the variance (square of the error) in the j-th coefficient is simply the j-th diagonal element of this inverse matrix:

$$\sigma^2(a_j) = [\alpha^{-1}]_{jj} \qquad (2\text{-}29)$$

Here, α is the (m+1)x(m+1) matrix in equation (2-28) and the error in a_j is given by $\sigma(a_j)$. Again, if the σ_i's are only relatively correct (= σ_i'), they can be used for weighting ($w_i = w_i' = 1/\sigma_i'^2$) and the absolute magnitude of the error can be estimated by use of s^2 (as for the linear case):

$$s^2 = [N\Sigma_i w_i'(y_i - y(x_i))^2]/[(N-m-1)\Sigma_i w_i] \qquad (2\text{-}30)$$

$$\sigma^2(a_j) \simeq Ns^2[\alpha^{-1}]_{jj}/\Sigma_i w_i' \qquad (2\text{-}31)$$

Bevington[13] gives a slightly different expression for $\sigma^2(a_j)$, based on the value of the diagonal term of the inverse matrix calculated assuming all $w_i = 1$ ($\equiv [\alpha^{-1}]_{jj}(w_i=1)$). The expression given above utilizes a $[\alpha^{-1}]_{jj}$ calculated with the w_i' weights and normalized to account for the fact that the calculation was not done with all $w_i = 1$. That is, the following approximation was used:

$$[\alpha^{-1}]_{jj}(w_i=1) \simeq N[\alpha^{-1}]_{jj}(w_i=w_i')/\Sigma_i w_i' \qquad (2\text{-}32)$$

This $N/\Sigma_i w_i'$ normalization factor can be used to correct for the use of $w_i' \neq 1$ as relative weighting factors in other cases and is employed in the weighted s^2 expressions of equations (2-12), (2-26), and (2-30). This normalization will be discussed in detail in the next section.

It is important to note the generality of the extension to higher order polynomial least squares. The matrix equation (2-28) holds as well for first order (linear, m=1) and zeroth order (mean, m=0) polynomials as for higher order polynomials. In the first order case, the matrix equation reduces to that of equation (2-23), while in the zeroth order case, (2-28) reduces to:

$$[\Sigma_i w_i][a_0] = [\Sigma_i w_i y_i] \tag{2-33}$$

where a_0 is then just the μ' of equation (2-10). The results are identical in all cases. The error analysis employed for the higher order polynomial least squares holds for the degenerate cases as well (with one minor exception). The relevant general expressions are reproduced below:

$$s^2 = [N\Sigma_i w_i (y_i - y(x_i))^2]/[(N-m-1)\Sigma_i w_i] \tag{2-30}$$

$$\sigma^2(a_j) \simeq [\alpha^{-1}]_{jj} \quad (w_i \text{ are correct absolute weighting factors}) \tag{2-29}$$

$$\sigma^2(a_j) \simeq s^2[\alpha^{-1}]_{jj}(w_i=1) \quad (w_i \text{ are relative weighting factors}) \tag{2-31}$$

$$[\alpha^{-1}]_{jj}(w_i=1) \simeq \left(\frac{N}{\Sigma_i w_i}\right)[\alpha^{-1}]_{jj}(w_i=w_i) \tag{2-34}$$

In the linear case, the errors are as follows:

$$[\alpha^{-1}]_{00} = \Delta^{-1}\Sigma_i w_i x_i^2$$

$$[\alpha^{-1}]_{11} = \Delta^{-1}\Sigma_i w_i$$

absolute w_i's:

$$\sigma_a^2 \equiv \sigma^2(a_0) \simeq \Delta^{-1}\Sigma_i w_i x_i^2$$

$$\sigma_b^2 \equiv \sigma^2(a_1) \simeq \Delta^{-1}\Sigma_i w_i$$

relative w_i's:

$$\sigma_a^2 \simeq \left(\frac{N}{\Sigma_i w_i}\right)\frac{s^2}{\Delta}\Sigma_i w_i x_i^2$$

$$\sigma_b^2 \simeq \left(\frac{N}{\Sigma_i w_i}\right)\frac{s^2}{\Delta}\Sigma_i w_i = \frac{Ns^2}{\Delta}$$

The last four expressions are identical to those of equations (2-25) and (2-27) and the s^2 expression of equation (2-30) reduces to the expression of equation (2-26) with m=1. In the case of m=0, σ_μ^2 ($\equiv \sigma^2(a_0)$) is predicted correctly if the w_i are assumed the correct weighting factors since $[\alpha^{-1}]_{00} = [\Sigma_i w_i]^{-1}$ for this case. However, for the case of only relatively correct w_i's, equation (2-34) turns out to be a bad approximation for $[\alpha^{-1}]_{00}(w_i=1)$. Fortunately, in this case, $[\alpha^{-1}]_{00}(w_i=1)$ is easily calculable exactly (and is equal to 1/N) and equation (2-31) then predicts the correct expression:

$$\sigma_\mu^2 \equiv \sigma^2(a_0) \simeq s^2/N \quad \text{(relative } w_i\text{'s)}$$

The general expressions of equations (2-30), (2-29), (2-31), (2-34) (and (2-28)) can also be used for unweighted polynomial least squares simply by setting all the w_i=1. With the proper normalization (as is incorporated into these expressions), the same effect can be obtained by merely setting all the w_i equal (to some positive value).

Chi Square

As discussed in the previous section, the quantity to be minimized is the sum of the squares of the errors (χ^2). In its simplest form, the χ^2 expression is as follows:

$$\chi^2 \equiv \Sigma_i (y_i - y(x_i))^2 \qquad (2\text{-}35)$$

However, as discussed by Bevington,[14] a more appropriate quantity to use as a measure of goodness-of-fit is the reduced chi square (χ_ν^2):

$$\chi_\nu^2 \equiv \chi^2/\nu = \Sigma_i (y_i - y(x_i))^2/(N-m-1) \qquad (2\text{-}36)$$

$$\nu = (N-m-1)$$

$$\equiv \text{degrees of freedom}$$

Here, N is the number of data points in the sum used to calculate χ^2 and m is the number of parameters calculated from the fit minus 1 (*e.g.*, the order of the polynomial fit in polynomial least squares). Of course, in the event of unequal uncertainties (σ_i) in the data points, the proper expression includes the weighting factors:

$$\chi_\nu^{2\prime} \equiv \Sigma_i w_i (y_i - y(x_i))^2/(N-m-1) \qquad (2\text{-}37)$$

Unfortunately, $\chi_\nu^{2\prime}$ is dependent on the actual values chosen for the w_i and thus is not very useful as a goodness-of-fit parameter for cases in which only the relative weighting factors are known. It is possible to normalize the $\chi_\nu^{2\prime}$ statistic to give the same value for different absolute magnitudes of w_i by multiplying by the normalization constant $N/\Sigma_i w_i$ mentioned in the last section. This normalization constant is termed $\overline{\sigma_i^2}$ (weighted average of the individual variances) by Bevington[15] and the resultant statistic is termed s^2 (variance of the fit).

For the purposes of this discussion, this statistic will be called the normalized weighted reduced chi square (and notated χ_N^2):

$$(s^2 =)\ \chi_N^2 \equiv [N\Sigma_i w_i(y_i - y(x_i))^2]/[(N-m-1)\Sigma_i w_i] \qquad (2\text{-}38)$$

(It should be noted that this expression is identical to that for s^2 given in equation (2-30).) χ_N^2 can be seen to simplify to the χ_ν^2 expression (2-36) if $w_i=w$ for all i. Since $\Sigma_i w_i = Nw$ in this case:

$$\chi_N^2 = [Nw\Sigma_i(y_i - y(x_i))^2]/[(N-m-1)Nw]$$
$$= \Sigma_i(y_i - y(x_i))^2/(N-m-1) \equiv \chi_\nu^2$$

χ_N^2 is probably the best statistic to use for tests of goodness-of-fit between *similar* data sets. However, χ_N^2 is dependent on the absolute magnitude of the observed y_i and thus, cannot be used to compare goodness-of-fit between data sets of varying magnitude (in y_i). It may prove potentially useful to normalize χ_N^2 by use of some average (or median) of the set of y_i values in an attempt to minimize this discrepancy. Perhaps the best means of accomplishing this is by using the weighted average ($\bar{y}$) of the y_i data (as calculated by equation (2-10)), and modifying χ_N^2 as follows:

$$\chi_N^{2\prime} \equiv \chi_N^2/\bar{y}^2 \qquad (2\text{-}39)$$

$\chi_\nu^{2\prime}$ or χ_N^2 are the usual chi square statistics used in goodness-of-fit tests. Their main utility comes in comparison of two (or more) fits to the same or similar data sets. However, the use of $\chi_N^{2\prime}$ could allow the χ^2 statistic to be used as a more absolute criterion of goodness-of-fit and give it a more general utility. It is already clear that the chi square statistic is,

in general, more sensitive to deviations from a "good fit" than, for example, the correlation coefficient (which is one of the few absolute statistical guides to goodness-of-fit available).

PART II. APPLICATIONS

In the first part of this chapter, a summary was given of the important basic analytical techniques useful for data reduction in all of the physical sciences. This part will present numerous applications of these techniques to the field of chemical kinetics (and at times, more specifically, electron transfer kinetics). The emphasis will be placed on the propagation of errors and proper weighting schemes useful in fitting kinetics data. Most of the specific applications that follow have been incorporated into Fortran computer routines which are individually mentioned in the context of their application.

In general, each case involves the development of the proper functional form describing the parent distribution (*i.e.*, the functional form to which the data are to be fit), followed by an analysis of the proper weighting factors to be used in the fit, and an error analysis of the parameters calculated by the fit. In some cases, the development of the appropriate model is omitted either because the derivations are discussed elsewhere or because the functional forms are obvious.

Propagation of Errors - Specific Formulae

The example of calculating weighting factors given in the first part of this chapter illustrated the importance of being able to determine how errors propagate from an independent parameter to the dependent parameter. The general method of partial differentiation (see equation (2-15)) is accurate but tedious and it will aid in the future discussion to list specific

examples of results of this analysis on several basic functional forms. The following examples are listed in Bevington[16] and are reproduced here only for convenience (note that all covariances are assumed equal to 0):

General function:

$$x = f(u,v) \qquad \sigma_x^2 = \sigma_u^2 \left(\frac{\partial x}{\partial u}\right)^2 + \sigma_v^2 \left(\frac{\partial x}{\partial v}\right)^2 \tag{2-40}$$

Addition/Subtraction:

$$x = au \pm bv \qquad \sigma_x^2 = a^2\sigma_u^2 + b^2\sigma_v^2 \tag{2-41}$$

Multiplication/Division:

$$x = \pm auv \quad \text{or} \quad x = \pm au/v \qquad \frac{\sigma_x^2}{x^2} = \frac{\sigma_u^2}{u^2} + \frac{\sigma_v^2}{v^2} \tag{2-42}$$

Powers:

$$x = au^{\pm b} \qquad \frac{\sigma_x}{x} = b\frac{\sigma_u}{u} \tag{2-43}$$

Exponentials:

$$x = ae^{\pm bu} \qquad \frac{\sigma_x}{x} = b\sigma_u \tag{2-44}$$

Logarithms:

$$x = a\,\ell n(\pm bu) \qquad \sigma_x = a\frac{\sigma_u}{u} \tag{2-45}$$

Double Reciprocal Plot (Routine DRFIT)

In the event that the observed rate constants for a particular reaction exhibit saturation dependence on excess reagent concentration, the following analysis allows a determination of the kinetic parameters of the system.

The mechanistic interpretation of saturation behavior is usually assumed to be a pre-equilibrium complex formation:

$$\begin{aligned} A + B &\overset{K}{\rightleftharpoons} AB \\ AB &\xrightarrow{k} \text{products} \end{aligned} \qquad (2\text{-}46)$$

Assuming reagent B is in pseudo-first order excess over A and the measured quantity is directly proportional to the concentration of A ($\equiv$ [A]), the integrated rate law can be derived as follows:

$$\text{Rate} = \frac{d[\text{products}]}{dt} = k[AB] = kK[A][B] \qquad (2\text{-}47)$$

But, if AB looks identical to A (*i.e.*, the measured quantity is actually directly proportional to the total concentration of all species involving A, $[A]_{tot}$), then:

$$\begin{aligned} [A]_{tot} &= [A] + [AB] \\ &= [A](1 + K[B]) \\ \text{or, } [A] &= [A]_{tot}/(1 + K[B]) \end{aligned} \qquad (2\text{-}48)$$

Substituting (2-48) into (2-47) yields:

$$\text{Rate} = kK[A]_{tot}[B]/(1 + K[B])$$

Since pseudo-first order conditions hold:

$$\begin{aligned} \text{Rate} &= k_{obs}[A]_{tot} \\ k_{obs} &= kK[B]/(1 + K[B]) \end{aligned} \qquad (2\text{-}49)$$

This describes the saturation dependence of k_{obs} on [B]. By changing variables, it is possible to linearize this function:

$$\frac{1}{k_{obs}} = \frac{1}{kK}\left(\frac{1}{[B]}\right) + \frac{1}{k} \qquad (2\text{-}50)$$

The measured data pairs will be $(k_{obs}(i), [B](i))$ and the independent (X) and dependent (Y) variables are:

$$X \equiv 1/[B] \qquad Y \equiv 1/k_{obs} \qquad (2\text{-}51)$$

Assuming no (or negligible) inherent error in the measurement of [B] and an error of σ_i in each $k_{obs}(i)$, $\sigma_Y(i)$ can be found by application of equation (2-42):

$$\sigma_Y(i) = \sigma_i/(k_{obs}(i))^2 \qquad (2\text{-}52)$$

The proper weighting factors to be used in the linear least squares analysis (of Y versus X) are given by:

$$w_i = 1/(\sigma_Y(i))^2 \qquad (2\text{-}53)$$

and the slope (a_1) and intercept (a_0) of the best linear least squares fit will have standard errors σ_1 and σ_0, respectively (for details of the fitting procedure, see the first part of this chapter). From equation (2-50), the values of k and K can be determined using these best fit parameters:

$$\begin{aligned} k &= 1/a_0 \\ K &= a_0/a_1 \end{aligned} \qquad (2\text{-}54)$$

and the propagation of errors formulae of the last section (specifically, equation (2-42)) can be used to determine the errors as follows:

$$\frac{\sigma_k}{k} = \frac{\sigma_0}{a_0}$$

$$\sigma_k = k\frac{\sigma_0}{a_0} = \left(\frac{1}{a_0}\right)\frac{\sigma_0}{a_0} = \sigma_0/{a_0}^2$$

$$\frac{\sigma_K^2}{K^2} = \frac{{\sigma_1}^2}{{a_1}^2} + \frac{{\sigma_0}^2}{{a_0}^2}$$

$$\sigma_K^2 = \frac{{a_0}^2}{{a_1}^2}\left(\frac{{\sigma_1}^2}{{a_1}^2} + \frac{{\sigma_0}^2}{{a_0}^2}\right)$$

$$= \frac{{a_0}^2}{{a_1}^4}{\sigma_1}^2 + \frac{{\sigma_0}^2}{{a_1}^2}$$

$$\sigma_K = \left[\left(\frac{a_0}{a_1}\right)^2 \sigma_1^2 + \sigma_0^2 \right]^{1/2} / a_1$$
$$\sigma_k = \sigma_0 / a_0^2 \qquad (2\text{-}55)$$

Eyring Plot (Routine EYRFIT)

The temperature dependence of the rate constant (k) is described (in transition state theory) by the Eyring expression:[17,18]

$$k = \frac{k_B T}{h} \exp\left(-\frac{\Delta H^{\ddagger}}{RT}\right) \exp\left(\frac{\Delta S^{\ddagger}}{R}\right) \qquad (2\text{-}56)$$

where, $k_B \equiv$ Boltzmann's constant

$h \equiv$ Planck's constant

$R \equiv$ gas constant

$T \equiv$ absolute temperature

Equation (2-56) can be rearranged to linearize the expression and aid in calculating the enthalpy ($\Delta H^{\ddagger}$) and entropy ($\Delta S^{\ddagger}$) of activation:

$$\ell n\left(\frac{kh}{k_B T}\right) = -\frac{\Delta H^{\ddagger}}{RT} + \frac{\Delta S^{\ddagger}}{R} \qquad (2\text{-}57)$$

Assuming that (k(i), T(i)) are measured with each k(i) having an error σ_i and each T(i) potentially having an error σ_T, the variables of interest are:

$$Y \equiv \ell n\left(\frac{kh}{k_B T}\right) \qquad X \equiv 1/T$$

Using equations (2-42) and (2-45), the correct $\sigma_Y(i)$ (for weighting) can be calculated:

$$A \equiv kh/k_B T$$
$$\frac{\sigma_A}{A} = \left(\frac{\sigma_i^2}{k(i)^2} + \frac{\sigma_T^2}{T(i)^2}\right)^{1/2}$$
$$\sigma_Y(i) = \sigma_A / A$$
$$\sigma_Y(i) = \left(\frac{\sigma_i^2}{k(i)^2} + \frac{\sigma_T^2}{T(i)^2}\right)^{1/2} \qquad (2\text{-}58)$$

It should be noted that, under normal circumstances, σ_T is small

enough to neglect the second term of equation (2-58). The fit of Y versus X (weighted with $w_i = 1/\sigma_Y(i)^2$) yields a slope (a_1) and intercept (a_0) with standard errors σ_1 and σ_0, respectively. $\Delta H^{\ddagger}$, $\Delta S^{\ddagger}$ and their errors (σ_H and σ_S, respectively) can be calculated by:

$$\begin{aligned} \Delta H^{\ddagger} &= - Ra_1 & \sigma_H &= R\sigma_1 \\ \Delta S^{\ddagger} &= Ra_0 & \sigma_S &= R\sigma_0 \end{aligned} \qquad (2\text{-}59)$$

Van't Hoff Plot (Routine VHFIT)

The temperature dependence of an equilibrium constant (K) may be described by the van't Hoff equation:[19]

$$K = \exp\left(- \frac{\Delta H^\circ}{RT}\right)\exp\left(\frac{\Delta S^\circ}{R}\right) \qquad (2\text{-}60)$$

Rearrangement of equation (2-60) gives:

$$\ell n\,(K) = - \frac{\Delta H^\circ}{RT} + \frac{\Delta S^\circ}{R} \qquad (2\text{-}61)$$

(K(i), T(i)) are the measured quantities and each K(i) has an error σ_i associated with it. The variables of interest are:

$$Y \equiv \ell n\,(K) \qquad X \equiv 1/T$$

The weighting factors are given by $w_i = 1/\sigma_Y(i)^2$ where:

$$\sigma_Y(i) = \sigma_i/K(i) \qquad (2\text{-}62)$$

The slope (a_1) and intercept (a_0), along with their standard errors (σ_1, σ_0) can be used to calculate ΔH°, ΔS°, and their standard errors (σ_H, σ_S):

$$\begin{aligned} \Delta H^\circ &= - Ra_1 & \sigma_H &= R\sigma_1 \\ \Delta S^\circ &= Ra_0 & \sigma_S &= R\sigma_0 \end{aligned} \qquad (2\text{-}63)$$

First Order Kinetics Analysis with Absorbance Data (Routine FORABS)

If species C decays (or forms) in a first order (or pseudo-first order) process, the integrated rate law is:[8,9,20]

$$[C] = [C]_0 \exp(-kt) \qquad (2\text{-}64)$$

where, $[C] \equiv$ concentration of species C

$[C]_0 \equiv$ concentration of species C at t=0

$t \equiv$ time

$k \equiv$ first order rate constant

In general, the measured dependent variable is linearly dependent on (but not necessarily directly proportional to) the concentration [C]. In many situations, this variable is absorbance, and the rest of this development assumes that absorbance is the measured variable and is related to [C] by:

$$\begin{aligned} [C] &= \varepsilon^{-1}(A - A_\infty) \\ [C]_0 &= \varepsilon^{-1}(A_0 - A_\infty) \end{aligned} \qquad (2\text{-}65)$$

where, $\varepsilon \equiv$ extinction coefficient

$A \equiv$ absorbance

$A_0 \equiv$ absorbance at t=0

$A_\infty \equiv$ absorbance at t=∞

Substituting these expressions into (2-64):

$$(A - A_\infty) = (A_0 - A_\infty)\exp(-kt) \qquad (2\text{-}66)$$

The usual rearrangement of (2-66) to the logarithmic form requires the use of the absolute value of the absorbance difference for extension to the cases in which the absorbance increases with time (*i.e.*, negative ε):

$$\ell n\,|A - A_\infty| = \ell n\,|A_0 - A_\infty| - kt \qquad (2\text{-}67)$$

The measured quantities are t_i (≡ X) and A_i (as well as A_∞).

Defining:

$$Y \equiv \ell n |A - A_\infty| \tag{2-68}$$

and assuming that each A_i has an error σ_i[21] and A_∞ has the same error (*i.e.*, A_∞ is determined with no better precision than A_i), the weighting factors ($w_i = 1/\sigma_Y(i)^2$) can be calculated:

$$\begin{aligned} B &\equiv |A_i - A_\infty| \\ \sigma_B &= (2)^{1/2}\,\sigma_i \\ \sigma_Y(i) &= \sigma_B/B \\ \sigma_Y(i) &= (2)^{1/2}\,\sigma_i/|A_i - A_\infty| \end{aligned} \tag{2-69}$$

The slope (a_1) and intercept (a_0) of a linear least squares fit of Y versus X (and their errors, σ_1 and σ_0) can be used to calculate k and A :

$$\begin{aligned} k &= -\,a_1 \\ \sigma_k &= \sigma_1 \\ A_0 &= \pm\exp(a_0) + A_\infty \\ \sigma_{A_0} &= [\sigma_0{}^2\exp(2a_0) + \sigma_i{}^2]^{1/2} \end{aligned} \tag{2-70}$$

The calculation of σ_{A_0} is as follows:

$$\begin{aligned} D &\equiv \exp(a_0) \\ \sigma_D &= D\sigma_0 \\ A_0 &= \pm D + A_\infty \\ \sigma_{A_0} &= (\sigma_D{}^2 + \sigma(A_\infty)^2)^{1/2} \\ &= (D^2\sigma_0{}^2 + \sigma_i{}^2)^{1/2} \\ &= [\sigma_0{}^2\exp(2a_0) + \sigma_i{}^2]^{1/2} \end{aligned}$$

Guggenheim Analysis with Absorbance Data (Routine GUGABS)

Analysis of absorbance data obeying first order kinetics by the technique described in the previous section is often hampered by the inaccessibility of an accurate measure of A_∞ (the absorbance at t=∞). Several techniques are available for the analysis of such data in the absence of a value for A_∞. The classical technique used was developed by Guggenheim[22] over 50 years ago and still bears his name. Nominally, this technique requires the collection of two sets of data (A_i,t_i) and (A_i',t_i') such that t_i and t_i' are related by:

$$t_i' = t_i + \tau \qquad (2\text{-}71)$$

In practice, this usually involves the collection of one set of N data points at equal time intervals (Δt) and using the last half of the data set as (A_i',t_i') with:

$$\tau = N\Delta t/2 \qquad (2\text{-}72)$$

(If N is odd, then the last point is unused - N = N-1.) Both data sets obey (pseudo-)first order kinetics with the same rate constant (k) and other parameters (A_0, A_∞):

$$(A_i - A_\infty) = (A_0 - A_\infty)\exp(-kt_i) \qquad (2\text{-}73)$$

$$(A_i' - A_\infty) = (A_0 - A_\infty)\exp(-kt_i') \qquad (2\text{-}74)$$

Subtracting (2-74) from (2-73) and taking logarithms:

$$\ell n\,|A_i - A_i'| = \ell n\{|A_0 - A_\infty|[1 - \exp(-k\tau)]\} - kt_i \qquad (2\text{-}75)$$

(As for the normal first order analysis, the absolute values prevent taking the logarithm of a negative number in the event that A increases with time.) Plotting $Y \equiv \ell n\,|A_i - A_i'|$ versus $X \equiv t_i$ should result in a straight line. The proper weighting factors ($w_i = 1/\sigma_Y(i)^2$) can be calculated from:

$$\sigma_Y(i) = (2)^{1/2}\,\sigma_i/|A_i - A_i'| \qquad (2\text{-}75)$$

The slope (a_1) and intercept (a_0) of the linear least squares fit (and their errors σ_1, σ_0) can be used to calculate k (and σ_k) and $\Delta A \equiv (A_0 - A_\infty)$ (and $\sigma_{\Delta A}$):

$$\begin{aligned} k &= -a_1 \\ \sigma_k &= \sigma_1 \\ \Delta A &= \pm \exp(a_0)/(1 - \exp(a_1\tau)) \\ &\quad (+, \text{ absorbance decreases with time;} \\ &\quad\ -, \text{ absorbance increases with time}) \\ \sigma_{\Delta A} &= |\Delta A|(\sigma_0^2 + \tau^2\sigma_1^2)^{1/2} \end{aligned} \qquad (2\text{-}76)$$

Since only two parameters (a_0 and a_1) are available from the fit, it is impossible without further analysis to calculate A_0 and A_∞ separately. It is possible to get a good estimate of A_∞ (and thus A_0 from ΔA) by doing a weighted mean calculation on a set of $A_\infty(i)$'s calculated by:

$$A_\infty(i) = A_i - \Delta A \exp(-kt_i) \qquad (2\text{-}77)$$

The calculation of the proper weighting factors ($w_i = 1/\sigma_A^2$, σ_A is the error in $A_\infty(i)$) depends on the deviations in the A_i and also in the fit parameters (k, ΔA) from the linear least squares procedure:

$$\begin{aligned} D &\equiv \exp(-kt_i) \\ \sigma_D &= Dt_i\sigma_k \\ \sigma^2(\Delta AD) &= (\Delta AD)^2\left(\frac{\sigma_{\Delta A}^2}{\Delta A^2} + \frac{\sigma_D^2}{D^2}\right) \\ \sigma_A^2 &= \sigma_i^2 + \sigma^2(\Delta AD) \\ \sigma_A &= \{\sigma_i^2 + (A_i - A_\infty(i))^2[\sigma_0^2 + \sigma_1^2(t_i^2 + \tau^2)]\}^{1/2} \end{aligned} \qquad (2\text{-}78)$$

The weighted mean calculation will give A_∞ and its standard error ($\sigma(A_\infty)$) and A_0 (and $\sigma(A_0)$) can be calculated by:

$$A_0 = \Delta A + A_\infty$$
$$\sigma(A_0) = [\sigma^2(\Delta A) + \sigma^2(A_\infty)]^{1/2} \qquad (2\text{-}79)$$

Swinbourne Analysis with Absorbance Data (Routine SWNABS)

Another technique for analysis of first order kinetics in the absence of an A_∞ value is described by Swinbourne.[23] This technique is similar to the Guggenheim technique in requiring two "data sets" obeying the relationships (2-73) and (2-74). Dividing (2-73) by (2-74) and rearranging gives:

$$A_i = A_\infty[1 - \exp(k\tau)] + A_i'\exp(k\tau) \qquad (2\text{-}80)$$

The variables to be plotted are $Y \equiv A_i$ and $X \equiv A_i'$, and assuming that the A_i and A_i' all have the same error, no weighting is necessary. A linear least squares fit to a Y versus X plot gives a slope (a_1) and intercept (a_0) and their standard errors (σ_1 and σ_0) which can be used to calculate k and A_∞ (and errors σ_k, $\sigma(A_\infty)$):

$$k = \tau^{-1}\ell n(a_1)$$
$$\sigma_k = \tau^{-1}\sigma_1/a_1$$
$$A_\infty = a_0/(1 - a_1) \qquad (2\text{-}81)$$
$$\sigma(A_\infty) = (\sigma_0^2 + A_\infty^2\sigma_1^2)^{1/2}/(a_1 - 1)$$

As in the case of the Guggenheim analysis, the third parameter (A_0) must be found (if desired) by a further fitting procedure. For each A_i and t_i, it is possible to calculate an $A_0(i)$, and from the deviations in k (σ_k), A_∞ ($\sigma(A_\infty)$), and A_i (σ_i), the weighting factors ($w_i = 1/\sigma^2(A_0(i))$) for a weighted mean calculation with the $A_0(i)$ is possible:

$$A_0(i) = (A(i) - A_\infty)\exp(kt(i)) + A_\infty \qquad (2\text{-}82)$$

$$\sigma(A_0(i)) = \{\exp(2kt_i)[\sigma_i^2 + \sigma^2(A_\infty) + (A_i - A_\infty)^2 t_i^2 \sigma_k^2] + \sigma^2(A_\infty)\}^{1/2} \quad (2\text{-}83)$$

(The derivation of equation (2-83) is left as an exercise for the reader.) The weighted mean calculation will then give values for A_0 and $\sigma(A_0)$.

Second Order Kinetics Analysis with Absorbance Data (Routine SORABS)

The second order decay of a species C gives the integrated rate law:[24]

$$\frac{1}{[C]} - \frac{1}{[C]_0} = k_2 t \quad (2\text{-}84)$$

where, $[C] \equiv$ concentration of species C

$[C]_0 \equiv$ concentration of species C at t=0

$k_2 \equiv$ second order rate constant

Assuming that [C] and absorbance (A) are related as in equation (2-65):

$$\begin{aligned} [C] &= \varepsilon^{-1}(A - A_\infty) \\ [C]_0 &= \varepsilon^{-1}(A_0 - A_\infty) \end{aligned} \quad (2\text{-}65)$$

the integrated rate law (2-84) can be rewritten in terms of absorbance:

$$\frac{1}{|A - A_\infty|} = \frac{1}{|A_0 - A_\infty|} + k_2' t \quad (2\text{-}85)$$

where, $k_2' \equiv k_2/|\varepsilon|$

Since $(A - A_\infty)$ can be positive or negative but [C] must be positive, the quantity $\varepsilon^{-1}(A - A_\infty)$ must be positive and thus:

$$(A_0 - A_\infty)/\varepsilon \equiv |A_0 - A_\infty|/|\varepsilon| \quad (2\text{-}86)$$

This is the reason for the absolute values in equation (2-85). Experimentally, the absorbances A_i are measured at t_i and have

errors σ_i associated with them. Picking $Y \equiv 1/|A_i - A_\infty|$ and $X \equiv t_i$ allows a weighted linear least squares fit of Y versus X. The weighting factors ($w_i = 1/\sigma_Y{}^2(i)$) are calculated from:

$$\sigma_Y(i) = (2)^{1/2}\,\sigma_i/(A_i - A_\infty)^2 \qquad (2\text{-}87)$$

(This calculation assumes that the error in the measured A_∞ value is the same as the error (σ_i) in the A_i values.) The slope (a_1) and intercept (a_0) of the linear least squares fit of Y versus X (and their errors, σ_1 and σ_0) can be used to calculate k_2' and A_0 (and errors $\sigma(k_2')$ and $\sigma(A_0)$):

$$\begin{aligned} k_2' &= a_1 \\ \sigma(k_2') &= \sigma_1 \\ A_0 &= \pm(a_0)^{-1} + A_\infty \\ \sigma(A_0) &= [(\sigma_0/a_0{}^2)^2 + \sigma_i{}^2]^{1/2} \end{aligned} \qquad (2\text{-}88)$$

PART III. NONLINEAR LEAST SQUARES

Analysis of data which are thought to obey more complex functions (*i.e.*, functions which are not easily linearized) requires extension of the concepts discussed in the first part of this chapter. New techniques (which can deal with nonlinear functions) are necessary to achieve optimization of the independent parameters involved. The criterion for optimization, however, remains the same: minimization of the sum of the squares of the deviations between the data and the calculated fit. This type of nonlinear least squares analysis can theoretically be applied to any arbitrary functional form and thus lends itself to a myriad of applications.

One specific application of nonlinear least squares is in the kinetics field. There have been several examples in the literature[25-36] of the utility of this technique for kinetics analysis. The technique has been incorporated by this author into a major computer program (KINPRO) for analysis of kinetics progress curves of varying complexity. This program has the advantage of requiring no specific user-written subroutines for the functions to be used in the fits, being able to signal average and splice data sets (acquired at the same or different time intervals, respectively), and allowing the user to fit data to a linear combination of up to four different kinetics decay functions (in any combination and order). The main nonlinear least squares subroutine is written in a completely general fashion for ease of adaptation to other functional applications. The techniques and theory involved

in the analytical methods used by KINPRO are discussed here and the documentation, description, and source listing for KINPRO are contained in the supplementary volume of this thesis.

General Theory

The Newton-Gauss method[37] of nonlinear least squares optimization is described here. The general technique is applicable to fitting data to any functional form with optimization of any number of nonlinear (or linear) parameters provided that the function is differentiable (either analytically or numerically). The particular technique described here is the one used in KINPRO and the application of this technique to the specific functions used in KINPRO is discussed in the next section.

Assuming the data set of interest consists of N data points (t_i, y_i) (i=1,N), the goal will be to fit these data to a function $f(t,\underset{\sim}{\lambda})$, which is not only dependent on t, but also dependent on a set of p independent parameters $\underset{\sim}{\lambda} = (\lambda_1, \lambda_2, \ldots, \lambda_p)$. (The independent variable has been chosen as t ≡ time in anticipation of the applications presented in the next section.) The quantity to be minimized is the χ^2 defined in a manner analogous to that of equation (2-22):

$$\chi^2 = \sum_{i=1}^{N} [y_i - f(t_i,\underset{\sim}{\lambda})]^2 \qquad (2\text{-}89)$$

(In the most general case, χ^2 would be weighted with the appropriate $\sigma(y_i)$ values as in equation (2-22). The following discussion assumes w_i=1 for convenience although the

techniques used would be completely analogous.) The minimization criterion is then:

$$\left[\frac{\partial \chi^2}{\partial \lambda_j}\right]_{\lambda_j=\lambda_j^*} = 0 \quad (j=1,2,\ldots,p) \tag{2-90}$$

where, $\underset{\sim}{\lambda}^*$ is the set of best fit parameters.

The Newton-Gauss approach refers to the particular manner in which these partial derivatives are estimated and minimized. First, $f(t,\underset{\sim}{\lambda})$ is expanded in a Taylor series about a particular choice of $\underset{\sim}{\lambda}$ (*e.g.*, $\underset{\sim}{\lambda}^{(k)}$) and the expansion is truncated after the first order terms:

$$f(t,\underset{\sim}{\lambda}) \simeq f(t,\underset{\sim}{\lambda}^{(k)}) + \sum_{j=1}^{p} f'_{jk}(t)\Delta\lambda_j^{(k)} \tag{2-91}$$

$$\text{where, } f'_{jk}(t) \equiv \left[\frac{\partial f(t,\underset{\sim}{\lambda})}{\partial \lambda_j}\right]_{\lambda_j=\lambda_j^{(k)}}$$

and $\Delta\lambda_j^{(k)}$ is a finite difference in the j-th parameter at the k-th step (*vide infra*). Substituting the expression for $f(t,\underset{\sim}{\lambda})$ in equation (2-91) into equations (2-89) and (2-90) and performing the partial differentiations results in p simultaneous linear equations in the p variables $\Delta\lambda_j^{(k)}$ (j=1,2,...,p):

$$\sum_{j=1}^{p}\left[\sum_{i=1}^{N} f'_{jk}(t_i)f'_{mk}(t_i)\right]\Delta\lambda_j^{(k)} = \sum_{i=1}^{N}\left[y_i - f(t_i,\underset{\sim}{\lambda}^{(k)})\right]f'_{mk}(t_i) \quad (m=1,2,\ldots,p) \tag{2-92}$$

Thus, for any choice of $\underset{\sim}{\lambda}^{(k)}$, a set of finite differences $\Delta\underset{\sim}{\lambda}^{(k)}$ can be found by solving these simultaneous linear equations. The process is then reiterated by calculation of a new set of parameters (for the (k+1)-th step):

$$\lambda_j^{(k+1)} = \lambda_j^{(k)} + \Delta\lambda_j^{(k)} \quad (j=1,2,\ldots,p) \tag{2-93}$$

which can be used in equation (2-92) to calculate a new set of finite differences $\Delta\underset{\sim}{\lambda}^{(k+1)}$. Given a "reasonable" set of initial parameter estimates $\underset{\sim}{\lambda}^{(0)}$, convergence is predicted to a

self-consistent set of $\underset{\sim}{\lambda}^{*}$ which are the best fit parameters in a least squares sense (*i.e.*, which obey equation (2-90)).

Solving the set of p simultaneous linear equations in (2-92) is equivalent to solving the matrix equation:

$$\underset{\approx}{A}^{(k)} \times \Delta\underset{\sim}{\lambda}^{(k)} = \underset{\sim}{b}^{(k)} \tag{2-94}$$

where $\underset{\approx}{A}$ is a symmetric p×p matrix with elements given by:

$$A_{sr}^{(k)} = A_{rs}^{(k)} = \sum_{i=1}^{N} f'_{rk}(t_i) f'_{sk}(t_i) \tag{2-95}$$

$\Delta\underset{\sim}{\lambda}^{(k)}$ is the p×1 column vector for which the equation is to be solved, and $\underset{\sim}{b}^{(k)}$ is the p×1 column vector with elements given by:

$$b_{s}^{(k)} = \sum_{i=1}^{N} [y_i - f(t_i, \underset{\sim}{\lambda}^{(k)})] f'_{sk}(t_i) \tag{2-96}$$

Equation (2-94) can be easily solved by a number of standard techniques, including Gaussian elimination[38] (the technique chosen for use in KINPRO).

Applications - KINPRO.

As described previously, KINPRO is a program which uses the nonlinear least squares techniques described above to fit data to a master function which consists of a linear combination of individual basis functions. The basis functions are picked as common kinetics functions which may be observed experimentally. (The particular basis functions used were chosen with bimolecular electron transfer kinetics in mind and thus may be slightly biased toward this particular branch of kinetics.) Since the basis functions can be concatenated together in any order and composition to make up the master function (see description of KINPRO in the supplementary vol-

ume of this thesis), the A_∞ value is considered as a separate basis function and is automatically incorporated as one of the basis functions in the master function by the program. Thus, the discussion to follow will utilize basis functions which differ from the actual integrated rate law expressions by this A_∞ value. The names of the basis functions used by KINPRO are as follows:

(a) Absorbance infinity

(b) First order

(c) Second order (one reactant)

(d) Pseudo-first order reversible (second order reverse)

(e) Second order (two reactants)

Each of these basis functions (excluding the absorbance infinity) is described below with respect to three computations. First, the derivation of the rate expression and the particular form of the integrated rate law used (usually in terms of absorbance values) is described. Next, the necessary partial derivatives (see equation (2-91)) are analytically evaluated. Finally, appropriate procedures for calculation of initial parameter estimates are discussed. In all cases, it is assumed that the data are in the form (t_i,A_i) where the A_i are absorbances which are linearly dependent on the concentrations of interest as described by equations (2-65).

First Order. The integrated rate law for a first order process has already been derived and (by rearrangement of equation (2-66)) is given by:

$$f(t,\underset{\sim}{\lambda}) = (A_0 - A_\infty)\exp(-k_1 t) + A_\infty \qquad (2\text{-}97)$$
$$= f^b(t,\underset{\sim}{\lambda}) + f^a(t,\underset{\sim}{\lambda})$$

Here, the superscript letters are indices referring to the list of basis functions given above (*i.e.*, $f^b(t,\underset{\sim}{\lambda})$ represents the functional form of the first order basis function):

$$f^a(t,\underset{\sim}{\lambda}) = A_\infty$$
$$f^b(t,\underset{\sim}{\lambda}) = A_1\exp(-k_1 t) \qquad (2\text{-}98)$$
$$\text{where, } A_1 \equiv (A_0 - A_\infty)$$

The p (=2) parameters ($\underset{\sim}{\lambda}$) to be optimized (in the first order case) are chosen as:

$$\lambda_1 \equiv A_1$$
$$\lambda_2 \equiv k_1 \qquad (2\text{-}99)$$

and the appropriate partial derivatives can easily be analytically evaluated as:

$$\frac{\partial f^b(t,\underset{\sim}{\lambda})}{\partial \lambda_1} = \exp(-\lambda_2 t)$$
$$\frac{\partial f^b(t,\underset{\sim}{\lambda})}{\partial \lambda_2} = -t\lambda_1\exp(-\lambda_2 t) \qquad (2\text{-}100)$$

Once a set of initial parameter estimates $\underset{\sim}{\lambda}^{(0)} = (\lambda_1^{(0)},\lambda_2^{(0)})$ are chosen (see below), they are used in evaluating the matrix elements necessary for the matrix equation (2-94) using the following:

$$f^{b'}_{10}(t_i) = \exp(-\lambda_2^{(0)} t_i)$$
$$f^{b'}_{20}(t_i) = -t_i\lambda_1^{(0)}\exp(-\lambda_2^{(0)} t_i) \qquad (2\text{-}101)$$
$$f^b(t_i,\underset{\sim}{\lambda}^{(0)}) = \lambda_1^{(0)}\exp(-\lambda_2^{(0)} t_i)$$

Solution of the matrix equation gives $\Delta\underset{\sim}{\lambda}^{(0)}$ from which $\underset{\sim}{\lambda}^{(1)}$ is formed according to equation (2-93). Then $\underset{\sim}{\lambda}^{(1)}$ is used in a new iteration. Convergence is achieved when (for all j):

$$|\lambda_j^{(k)} - \lambda_j^{(k-1)}|/|\lambda_j^{(k)}| < R_c \qquad (2\text{-}102)$$

where R_c (the convergence ratio) is chosen by the user. (Of course, in general, other basis functions would also be incorporated into the master function and the total parameter set accumulated from all the appropriate basis functions would be optimized simultaneously.)

The procedures for estimation of initial parameter values must, in general, depend on whether the specific basis function being considered is expected to fit the fast phase or slow phase of the data (assuming more than one phase is present). KINPRO uses the following strategy: first, if the infinity absorbance value is not selected by the user to be the measured value, an estimate is calculated. This is done by extrapolating a plot of $Y \equiv A_i$ versus $X \equiv \exp[-t_i/(t_{max} - t_{min})]$ to $X = 0$ ($A_\infty^{(0)} = Y(X=0)$). t_{max} and t_{min} are the maximum and minimum time values of the data set. The fit is done in a linear least squares fashion on the final 40% of the final phase of the data. Once an initial estimate of A_∞ is found, the initial parameter values for the slow (or only) phase basis function are estimated utilizing the known $A_\infty^{(0)}$ value. Then, if a fast phase basis function exists, its initial parameter estimates are calculated using $A_\infty^{(0)}$ and the slow phase basis function initial parameter estimates. (The techniques used for the estimation of initial parameter values depend on the functional form of the basis function and are described in the appropriate sections.) To aid in the estimation of initial parameter values, the actual (t_i, A_i) data set is used to calculate two fit parameters α and β, which are given by:

$$\alpha \simeq A(t=0)$$
$$\beta \simeq \left(\frac{\partial A}{\partial t}\right)_{t=0} \qquad (2\text{-}103)$$

These parameters are calculated from a fit of the initial 10-20% of the (t_i,A_i) data set to a third order polynomial. The first two best fit polynomial coefficients (a_0 and a_1) are used as α and β, respectively.

In the case of the first order basis function ($f^b(t,\underset{\sim}{\lambda})$), the procedure for calculation of $\underset{\sim}{\lambda}^{(0)}$ (for fitting to a slow (or only) phase) is as follows: a properly weighted linear least squares fit of $Y \equiv \ell n|A_i - A_\infty^{(0)}|$ versus $X \equiv t_i$ (performed on the final 80% of the final phase of the data) gives a slope (a_1) and an intercept (a_0) from which $\underset{\sim}{\lambda}^{(0)}$ can be calculated:

$$\lambda_1^{(0)} \equiv A_1^{(0)} = \pm\exp(a_0)$$
$$(+, \text{ absorbance decreasing;}$$
$$-, \text{ absorbance increasing}) \qquad (2\text{-}104)$$
$$\lambda_2^{(0)} \equiv k_1^{(0)} = a_1$$

If the *fast* phase of the data is to be fit to the first order basis function, then a knowledge of the behavior of the first order basis function near t=0 is helpful. From equation (2-98), the following relationships can be derived:

$$f^b(t=0) = A_1$$
$$\left(\frac{\partial f^b}{\partial t}\right)_{t=0} = -k_1A_1 \qquad (2\text{-}105)$$

Since some information about the form of the slow phase is necessary, the procedure depends on the nature of the slow phase basis function. (The initial parameter estimates for this slow phase basis function are available for use and are

denoted as $\underset{\sim}{\lambda}^{m(0)}$, where m=b,c,d, or e indicating the slow phase basis function index in the list near the beginning of this section.) The expressions for $\lambda_1^{(0)}$ and $\lambda_2^{(0)}$ are dependent on m and are given below:

$$\begin{aligned} m=b: \quad \lambda_1^{(0)} &\equiv A_1^{(0)} = \alpha - A_\infty^{(0)} - \lambda_1^{b(0)} \\ \lambda_2^{(0)} &\equiv k_1^{(0)} = -(\beta + \lambda_2^{b(0)}\lambda_1^{b(0)})/\lambda_1^{(0)} \end{aligned} \tag{2-106}$$

$$\begin{aligned} m=c: \quad \lambda_1^{(0)} &\equiv A_1^{(0)} = \alpha - A_\infty^{(0)} - \lambda_1^{c(0)} \\ \lambda_2^{(0)} &\equiv k_1^{(0)} = -(\beta + \lambda_2^{c(0)}\lambda_1^{c(0)}|\lambda_1^{c(0)}|)/\lambda_1^{(0)} \end{aligned} \tag{2-107}$$

$$\begin{aligned} m=d: \quad \lambda_1^{(0)} &\equiv A_1^{(0)} = \alpha - A_\infty^{(0)} - \lambda_1^{d(0)}(1 + 2/\lambda_2^{d(0)}) \\ \lambda_2^{(0)} &\equiv k_1^{(0)} = -[\beta + \lambda_3^{d(0)}\lambda_1^{d(0)}(1 + 1/\lambda_2^{d(0)})]/A_1^{(0)} \end{aligned} \tag{2-108}$$

$$\begin{aligned} m=e: \quad \lambda_1^{(0)} &\equiv A_1^{(0)} = \alpha - A_\infty^{(0)} - \lambda_1^{e(0)} \\ \lambda_2^{(0)} &\equiv k_1^{(0)} = -(\beta + \lambda_2^{e(0)}\lambda_1^{e(0)}|\lambda_1^{e(0)}|R)/\lambda_1^{(0)} \end{aligned} \tag{2-109}$$

($R=[B]_0/[A]_0$, the ratio of concentrations of reagent in excess to limiting reagent.)

Second Order. The integrated rate law for a second order process has already been derived and (by rearrangement of equation 2-85) is given by:

$$\begin{aligned} f(t,\underset{\sim}{\lambda}) &= (A_0 - A_\infty)/(1 + k_2'|A_0 - A_\infty|t) + A_\infty \\ &= f^c(t,\underset{\sim}{\lambda}) + f^a(t,\underset{\sim}{\lambda}) \end{aligned} \tag{2-110}$$

$$f^c(t,\underset{\sim}{\lambda}) = A_1/(1 + k_2'|A_1|t) \tag{2-111}$$

A_1 is defined as in equation (2-98) and the p (=2) parameters ($\underset{\sim}{\lambda}$) to be optimized are chosen as:

$$\begin{aligned} \lambda_1 &\equiv A_1 \\ \lambda_2 &\equiv k_2' \end{aligned} \tag{2-112}$$

The necessary partial derivatives can be analytically evaluated as:

$$\begin{aligned} \frac{\partial f^c(t,\underset{\sim}{\lambda})}{\partial \lambda_1} &= (1 + \lambda_2|\lambda_1|t)^{-2} \\ \frac{\partial f^c(t,\underset{\sim}{\lambda})}{\partial \lambda_2} &= -t\lambda_1|\lambda_1|/(1 + \lambda_2|\lambda_1|t)^2 \end{aligned} \tag{2-113}$$

The initial parameter estimation procedure again depends on which phase is under consideration. If the second order basis function is to be fit to the slow (or only) phase, a properly weighted linear least squares fit to a second order plot (*i.e.*, $Y \equiv |A_i - A_\infty^{(0)}|^{-1}$ versus $X \equiv t_i$) performed on the final 80% of the final phase gives a slope (a_1) and an intercept (a_0) from which $\underset{\sim}{\lambda}^{(0)}$ can be found:

$$\begin{aligned} \lambda_1^{(0)} &\equiv A_1^{(0)} = \pm 1/a_0 \\ &(+, \text{ absorbance decreasing;} \\ &\ -, \text{ absorbance increasing}) \\ \lambda_2^{(0)} &\equiv k_2'^{(0)} = a_1 \end{aligned} \tag{2-114}$$

If the *fast* phase of the data set is to be fit with the second order basis function, the following relationships are useful:

$$\begin{aligned} f^c(t=0) &= A_1 \\ \left(\frac{\partial f^c}{\partial t}\right)_{t=0} &= -k_2' A_1 |A_1| \end{aligned} \tag{2-115}$$

The procedure again depends on m and $\underset{\sim}{\lambda}^{m(0)}$ (where m=b,c,d, or e again denotes the basis function to which the slow phase was fit) and $\underset{\sim}{\lambda}^{(0)}$ is calculated as below:

$$\text{m=b:} \quad \begin{aligned} \lambda_1^{(0)} &\equiv A_1^{(0)} = \alpha - A_\infty^{(0)} - \lambda_1^{b(0)} \\ \lambda_2^{(0)} &\equiv k_2'^{(0)} = -(\beta + \lambda_2^{b(0)}\lambda_1^{b(0)})/\lambda_1^{(0)}|\lambda_1^{(0)}| \end{aligned} \tag{2-116}$$

$$\text{m=c:} \quad \begin{aligned} \lambda_1^{(0)} &\equiv A_1^{(0)} = \alpha - A_\infty^{(0)} - \lambda_1^{c(0)} \\ \lambda_2^{(0)} &\equiv k_2'^{(0)} = -(\beta + \lambda_2^{c(0)}\lambda_1^{c(0)}|\lambda_1^{c(0)}|)/\lambda_1^{(0)}|\lambda_1^{(0)}| \end{aligned} \tag{2-117}$$

$$\text{m=d:} \quad \begin{aligned} \lambda_1^{(0)} &\equiv A_1^{(0)} = \alpha - A_\infty^{(0)} - \lambda_1^{d(0)}(1 + 2/\lambda_2^{d(0)}) \\ \lambda_2^{(0)} &\equiv k_2'^{(0)} = -[\beta + \lambda_3^{d(0)}\lambda_1^{d(0)}(1 + 1/\lambda_2^{d(0)})]/ \\ &\qquad \lambda_1^{(0)}|\lambda_1^{(0)}| \end{aligned} \tag{2-118}$$

$$\text{m=e:} \quad \begin{aligned} \lambda_1^{(0)} &\equiv A_1^{(0)} = \alpha - A_\infty^{(0)} - \lambda_1^{e(0)} \\ \lambda_2^{(0)} &\equiv k_2'^{(0)} = -(\beta + \lambda_2^{e(0)}\lambda_1^{e(0)}|\lambda_1^{e(0)}|R)/\lambda_1^{(0)}|\lambda_1^{(0)}| \end{aligned} \tag{2-119}$$

(R is defined as in equation (2-109).) Once the $\underset{\sim}{\lambda}^{(0)}$ are calculated, the iterations proceed as described for the first order basis function.

Pseudo-First Order Reversible. A bimolecular reversible reaction (*i.e.*, a reaction which does not go to completion) can be described by:[39]

$$A + B \underset{k_{-2}}{\overset{k_2}{\rightleftharpoons}} C + D \tag{2-120}$$

(The presence of a bimolecular reverse reaction (k_{-2}) is particularly useful for electron transfer kinetics.) The rate law for (2-120) is given by:

$$-\frac{d[A]}{dt} = k_2[A][B] - k_{-2}[C][D] \tag{2-121}$$

Assuming only species A and B are present initially (at concentrations $[A]_0$ and $[B]_0$, respectively) allows [B], [C], and [D] to be written in terms of [A]:

$$-\frac{d[A]}{dt} = k_2[A]([B]_0 - [A]_0 + [A]) - k_{-2}([A]_0 - [A])^2 \tag{2-122}$$

In the pseudo-first order limit, $[B]_0 \gg [A]_0$ (or $[B] \simeq [B]_0$ for all t) and (2-122) can be rewritten:

$$-\frac{d[A]}{dt} = k_2[A][B]_0 - k_{-2}([A]_0 - [A])^2 \tag{2-123}$$

The boundary conditions at equilibrium ($t=\infty$) are given by:

$$\begin{aligned} [A] &\equiv [A]_{eq} \\ \left(\frac{d[A]}{dt}\right)_{t=\infty} &= 0 \end{aligned} \tag{2-124}$$

Applying these boundary conditions to (2-123) gives:

$$k_{-2} = k_2[B]_0 \frac{[A]_{eq}}{([A]_0 - [A]_{eq})^2} \tag{2-125}$$

Substituting (2-125) back into (2-123) gives:

$$-\frac{d[A]}{dt} = k_2[B]_0\left\{[A] - [A]_{eq}\frac{([A]_0 - [A])^2}{([A]_0 - [A]_{eq})^2}\right\} \qquad (2\text{-}126)$$

Frost and Pearson[39,40] derive a rate law for the first order, second order reversible case:

$$A \underset{k'}{\overset{k}{\rightleftharpoons}} C + D$$

which is identical to (2-126) except that $k_2[B]_0$ has replaced k. The integration yields:

$$\ell n\frac{[A]_0^2 - [A]_{eq}[A]}{([A] - [A]_{eq})[A]_0} = k_2[B]_0\left(\frac{[A]_0 + [A]_{eq}}{[A]_0 - [A]_{eq}}\right)t \qquad (2\text{-}127)$$

The pseudo-first order rate constant is $k_1' \equiv k_2[B]_0$ and defining:

$$Q \equiv \left(\frac{[A]_0 + [A]_{eq}}{[A]_0 - [A]_{eq}}\right) \qquad (2\text{-}128)$$

allows rearrangement of (2-127) to give:

$$[A] = [A]_0\left\{\frac{[A]_0 + [A]_{eq}\exp(k_1'Qt)}{[A]_{eq} + [A]_0\exp(k_1'Qt)}\right\} \qquad (2\text{-}129)$$

It is instructive to note that (2-129) simplifies to the pseudo-first order case if $[A]_{eq} \to 0$ (since, then $Q \to 1$).

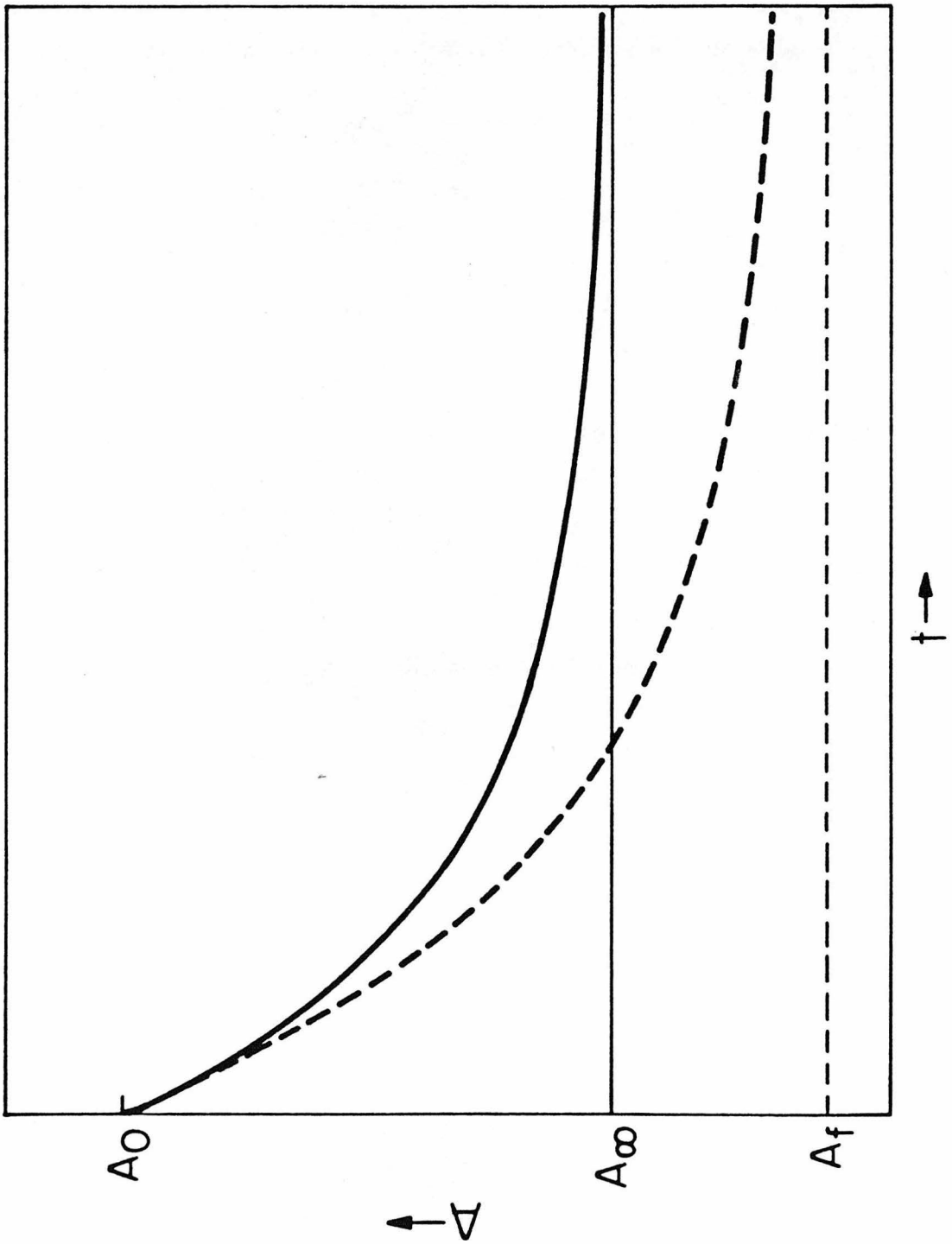
An examination of Figure 2-1 is helpful in converting equation (2-129) to absorbances. The parameters indicated in the figure are defined as follows:

$$\begin{aligned} A_0 &\equiv \text{absorbance at } t=0 \\ A_\infty &\equiv \text{absorbance at } t=\infty \\ A_f &\equiv \text{absorbance at } [A]=0 \\ &\quad (i.e., A_\infty \text{ if reaction went to completion}) \end{aligned} \qquad (2\text{-}130)$$

The following relationships hold:

$$\begin{aligned} \varepsilon[A]_0 &= (A_0 - A_f) \\ \varepsilon[A]_{eq} &= (A_\infty - A_f) \\ \varepsilon[A] &= (A - A_f) \end{aligned} \qquad (2\text{-}131)$$

Figure 2-1. Relationship between absorbance/time curves of a (pseudo-)first order reaction (---) and a (pseudo-)first order reversible reaction (——) with the same forward rate constant and the same A_0. See text for more detail.


A
t
A_0
A_∞
A_f

$$Q = \frac{(A_0 + A_\infty - 2A_f)}{(A_0 - A_\infty)}$$

Substituting the relationships (2-131) into equation (2-129) yields:

$$A = (A_0 - A_f)\left[\frac{(A_0 - A_f) + (A_\infty - A_f)\exp(k_1' Qt)}{(A_\infty - A_f) + (A_0 - A_f)\exp(k_1' Qt)}\right] + A_f \quad (2\text{-}132)$$

Definition of the parameters (*cf.*, Figure 2-1):

$$\begin{aligned} \Delta &\equiv (A_0 - A_\infty) \\ K &\equiv (A_0 - A_\infty)/(A_\infty - A_f) \end{aligned} \quad (2\text{-}133)$$

allows rearrangement of (2-132) to give the expression for $f(t,\underset{\sim}{\lambda})$:

$$f(t,\underset{\sim}{\lambda}) = A = \frac{\Delta}{K}\left\{(K+1)\left[\frac{(K+1) + \exp(k_1' Qt)}{1 + (K+1)\exp(k_1' Qt)}\right] - 1\right\} + A_\infty \quad (2\text{-}134)$$

$$= f^d(t,\underset{\sim}{\lambda}) + f^a(t,\underset{\sim}{\lambda})$$

$$f^d(t,\underset{\sim}{\lambda}) = \frac{\Delta}{K}\left\{(K+1)\left[\frac{(K+1) + \exp(k_1' Qt)}{1 + (K+1)\exp(k_1' Qt)}\right] - 1\right\} \quad (2\text{-}135)$$

where, $Q = (1 + 2/K)$

The p (=3) parameters to be optimized are chosen as:

$$\begin{aligned} \lambda_1 &\equiv \Delta \\ \lambda_2 &\equiv K \\ \lambda_3 &\equiv k_1' \end{aligned} \quad (2\text{-}136)$$

and the required partial derivatives can be anlytically evaluated as:

$$\begin{aligned} \frac{\partial f^d(t,\underset{\sim}{\lambda})}{\partial \lambda_1} &= \eta/\lambda_2 \\ \frac{\partial f^d(t,\underset{\sim}{\lambda})}{\partial \lambda_2} &= \frac{\lambda_1}{\lambda_2}\left\{-\frac{\eta}{\lambda_2} + \frac{1}{\xi}\left[\delta + (\lambda_2 - 1)\left(1 - \frac{\gamma\delta}{\xi} + 2\lambda_3 t\gamma\eta\lambda_2^{-2}\right)\right]\right\} \\ \frac{\partial f^d(t,\underset{\sim}{\lambda})}{\partial \lambda_3} &= -\frac{\lambda_1 Qt\gamma\eta(\lambda_2 + 1)}{\lambda_2\xi} \end{aligned} \quad (2\text{-}137)$$

where, $\gamma \equiv \exp(\lambda_3 Qt)$

$$\delta \equiv (\lambda_2 + 1) + \gamma$$

$$\xi \equiv 1 + (\lambda_2 + 1)\gamma$$

$$\eta \equiv (\lambda_2 + 1)(\delta/\xi) - 1$$

Again, the initial parameter estimation procedure depends on the phase to which this basis function is being fit. Since this particular basis function requires estimation of three parameters, the procedures are more complicated (and more susceptible to error). The following relationships hold for this basis function:

$$f^d(t=0) = \Delta$$
$$\left(\frac{\partial f^d}{\partial t}\right)_{t=0} = -\Delta(1 + 1/K)k_1' \qquad (2\text{-}138)$$

The initial parameter estimations become more manageable if the basis function is temporarily reparameterized:

$$\Delta_0 \equiv \Delta(1 + 1/K)$$
$$\Delta_\infty \equiv \Delta/K \qquad (2\text{-}139)$$
$$k_1' \equiv k_1'$$

If the data has only one phase, then α and β (as defined in equations (2-103)) are used in a successive iteration cycle to calculate a self-consistent $\underset{\sim}{\lambda}^{(0)}$. The iterations are performed as follows:

(1) An initial estimate of $\Delta_\infty(0)$ is guessed as:

$$\Delta_\infty(0) \simeq \alpha - A_\infty^{(0)} \qquad (2\text{-}140)$$

(2) In the j-th iteration, $\Delta_0(j)$ and $k_1'(j)$ are given by:

$$\Delta_0(j) = (\alpha - A_\infty^{(0)}) + \Delta_\infty(j) \qquad (2\text{-}141)$$

$$k_1'(j) = -\beta/\Delta_0(j) \qquad (2\text{-}142)$$

(3) The (j+1)-th estimate of Δ_∞ is then calculated by:

$$\Delta_\infty(j+1) = \Delta_0(j)\left[\frac{\Delta_0(j) + \Delta_\infty(j)\exp(k'(j)Q(j)t^*)}{\Delta_\infty(j) + \Delta_0(j)\exp(k'(j)Q(j)t^*)}\right] - <A(t^*)> \quad (2\text{-}143)$$

where, Q(j) can be calculated from equation (2-135):

$$Q(j) = \left[\frac{\Delta_0(j) + \Delta_\infty(j)}{\Delta_0(j) - \Delta_\infty(j)}\right]$$

t^* is picked at a time approximately 20% from the start of this phase and $<A(t^*)>$ is a five-point triangle average[41] of $A(t^*)$ (the absorbance value associated with $t=t^*$).

(4) $\Delta_\infty(j+1)$ is compared to $\Delta_\infty(j)$ and, if they are nearly equal, the iterations are assumed to have converged (and the initial parameter estimates are calculated as in step (5)). Otherwise, another iteration is performed by recycling to step (2).

(5) The initial parameter estimates are calculated:

$$\lambda_1^{(0)} \equiv \Delta^{(0)} = \Delta_0(j) - \Delta_\infty(j)$$
$$\lambda_2^{(0)} \equiv K^{(0)} = \lambda_1^{(0)}/\Delta_\infty(j) \quad (2\text{-}144)$$
$$\lambda_3^{(0)} \equiv k_1'^{(0)} = k_1'(j)$$

In the event that this basis function is being fit to the *slow* phase of a data set with two phases, a slight modification of the above procedure in necessary. The fit parameters α and β that were used above no longer describe the behavior of the phase under consideration near t=0 (they describe the *fast* phase), so that new parameters must be found to take their place. Thus α and β are recalculated by extrapolation of the slow phase back to t=0. The extrapolation is carried out by use of a second order polynomial least squares fit to a portion of the data starting at $t=t^*$ and extending for a time range

equal to approximately 30% of the slow phase. t* is chosen as a time which is 500 times the size of the fast phase time interval. This assures that the fast phase will make a minimum contribution to the extrapolated fit. Once the new α and β are calculated, they are used in the successive iteration cycle described above to calculate $\underset{\sim}{\lambda}^{(0)}$.

If this basis function is being fit to the *fast* phase, the procedure is again dependent on m (representing the form of the basis function fit to the slow phase). In general, the same successive iteration cycle is used, with slight modification of some of the expressions (as follows):

$$\Delta_\infty(0) \simeq \mu \qquad (2\text{-}140')$$

$$\Delta_0(j) = \mu + \Delta_\infty(j) \qquad (2\text{-}141')$$

$$k_1'(j) = -\nu/\Delta_0(j) \qquad (2\text{-}142')$$

The t* (and thus $\langle A(t^*)\rangle$) used in (2-143) is now chosen as a point in time approximately 20% of the way through the fast phase. The μ and ν values used in (2-140') through (2-142') are dependent on m (m=b,c,d, or e) as follows:

m=b:
$$\mu = \alpha - A_\infty^{(0)} - \lambda_1^{b(0)}$$
$$\nu = -(\beta + \lambda_2^{b(0)}\lambda_1^{b(0)}) \qquad (2\text{-}145)$$

m=c:
$$\mu = \alpha - A_\infty^{(0)} - \lambda_1^{c(0)}$$
$$\nu = -(\beta + \lambda_2^{c(0)}\lambda_1^{c(0)}|\lambda_1^{c(0)}|) \qquad (2\text{-}146)$$

m=d:
$$\mu = \alpha - A_\infty^{(0)} - \lambda_1^{d(0)}(1 + 2/\lambda_2^{d(0)})$$
$$\nu = -[\beta + \lambda_3^{d(0)}\lambda_1^{d(0)}(1 + 1/\lambda_2^{d(0)})] \qquad (2\text{-}147)$$

m=e:
$$\mu = \alpha - A_\infty^{(0)} - \lambda_1^{e(0)}$$
$$\nu = -(\beta + \lambda_2^{e(0)}\lambda_1^{e(0)}|\lambda_1^{e(0)}|R) \qquad (2\text{-}148)$$

Here, α and β are the original fit parameters defined by equa-

tions (2-103) and R is defined as in equation (2-109). Once the $\underset{\sim}{\lambda}^{(0)}$ are calculated, the nonlinear least squares iterations proceed as described previously.

Second Order (Two Reactants). The bimolecular reaction between two reactants (in the absence of pseudo-first order conditions) can be described by the following derivation:[42]

$$A + B \xrightarrow{k_2} C \tag{2-149}$$

$$-\frac{d[A]}{dt} = k_2[A][B] \tag{2-150}$$

Frost and Pearson[42] derive the integrated form of the rate law (2-150) as:

$$([B]_0 - [A]_0)^{-1} \ell n \frac{[A]_0([B]_0 - [A]_0 + [A])}{[B]_0[A]} = k_2 t \tag{2-151}$$

Solving (2-151) for [A] gives:

$$[A] = ([B]_0 - [A]_0) / \left(\frac{[B]_0}{[A]_0} \exp(k_2([B]_0 - [A]_0)t) - 1 \right) \tag{2-152}$$

It becomes obvious that knowledge of both $[B]_0$ and $[A]_0$ is required to make this function amenable in practice to the nonlinear optimization techniques discussed. (Theoretically, of course, one could add $[B]_0$ and $[A]_0$ to the $\underset{\sim}{\lambda}$ below as parameters to be optimized. However, this would result in a four-parameter function which would almost assuredly be badly behaved or divergent or which would result in fits relatively insensitive to the parameter values. It is assumed that making $[B]_0$ and $[A]_0$ user-input constants is the more practical approach.)

Conversion of (2-152) to absorbances requires the use of the relationships similar to those of equations (2-65):

$$[A] = \varepsilon^{-1}(A - A_\infty)$$
$$[A]_0 = \varepsilon^{-1}(A_0 - A_\infty) \tag{2-153}$$

Substituting these expressions into (2-152) and defining:

$$R \equiv [B]_0/[A]_0$$
$$k_2' \equiv k_2/|\varepsilon| \tag{2-154}$$
$$A_1 \equiv (A_0 - A_\infty)$$

results in:

$$f(t,\underset{\sim}{\lambda}) = A = \frac{A_1(R - 1)}{R\exp(k_2'|A_1|(R - 1)t) - 1} + A_\infty \tag{2-155}$$
$$= f^e(t,\underset{\sim}{\lambda}) + f^a(t,\underset{\sim}{\lambda})$$
$$f^e(t,\underset{\sim}{\lambda}) = \frac{A_1(R - 1)}{R\exp(k_2'|A_1|(R - 1)t) - 1} \tag{2-156}$$

The p (=2) parameters to be optimized are chosen as:

$$\lambda_1 \equiv A_1$$
$$\lambda_2 \equiv k_2' \tag{2-157}$$

and the required partial derivatives can be analytically evaluated as:

$$\frac{\partial f^e(t,\underset{\sim}{\lambda})}{\partial \lambda_1} = \frac{(R - 1)}{\kappa}(1 - R|f^e(t,\underset{\sim}{\lambda})|\theta\lambda_2 t)$$
$$\frac{\partial f^e(t,\underset{\sim}{\lambda})}{\partial \lambda_2} = -f^e(t,\underset{\sim}{\lambda})|\lambda_1|R(R - 1)\theta t/\kappa \tag{2-158}$$
$$\text{where,} \quad \theta \equiv \exp(\lambda_2|\lambda_1|(R - 1)t)$$
$$\kappa \equiv R\theta - 1$$

The initial parameter estimation procedure is again dependent on the phase to which the basis function is being fit. The following relationships hold for this basis function:

$$f^e(t=0) = A_1$$
$$\left(\frac{\partial f^e}{\partial t}\right)_{t=0} = -A_1|A_1|k_2'R \tag{2-159}$$

If the data set has only one phase, then α and β (see equations

(2-103)) can be used to calculate $\underset{\sim}{\lambda}^{(0)}$:

$$\begin{aligned} \lambda_1^{(0)} &\equiv A_1^{(0)} = \alpha - A_\infty^{(0)} \\ \lambda_2^{(0)} &\equiv k_2'^{(0)} = -\beta/(\lambda_1^{(0)}|\lambda_1^{(0)}|R) \end{aligned} \tag{2-160}$$

If this basis function is being fit to the slow phase, α and β have to be recalculated by extrapolating a second order polynomial fit to the initial 30% of the slow phase (after picking a portion of the slow phase lying past the end of the fast phase) back to t=0 as done for the previous basis function. These new values of α and β can then be used in equations (2-160) to get $\underset{\sim}{\lambda}^{(0)}$.

If the *fast* phase is to be fit by this basis function, the procedure depends on m (indicating the basis function to which the slow phase was fit) as always:

m=b:
$$\begin{aligned} \lambda_1^{(0)} &\equiv A_1^{(0)} = \alpha - A_\infty^{(0)} - \lambda_1^{b(0)} \\ \lambda_2^{(0)} &\equiv k_2'^{(0)} = -(\beta + \lambda_2^{b(0)}\lambda_1^{b(0)})/(\lambda_1^{(0)}|\lambda_1^{(0)}|R) \end{aligned} \tag{2-161}$$

m=c:
$$\begin{aligned} \lambda_1^{(0)} &\equiv A_1^{(0)} = \alpha - A_\infty^{(0)} - \lambda_1^{c(0)} \\ \lambda_2^{(0)} &\equiv k_2'^{(0)} = -(\beta + \lambda_2^{c(0)}\lambda_1^{c(0)}|\lambda_1^{c(0)}|)/(\lambda_1^{(0)}|\lambda_1^{(0)}|R) \end{aligned} \tag{2-162}$$

m=d:
$$\begin{aligned} \lambda_1^{(0)} &\equiv A_1^{(0)} = \alpha - A_\infty^{(0)} - \lambda_1^{d(0)}(1 + 2/\lambda_2^{d(0)}) \\ \lambda_2^{(0)} &\equiv k_2'^{(0)} = -[\beta + \lambda_3^{d(0)}\lambda_1^{d(0)}(1 + 1/\lambda_2^{d(0)})]/(\lambda_1^{(0)}|\lambda_1^{(0)}|R) \end{aligned} \tag{2-163}$$

m=e:
$$\begin{aligned} \lambda_1^{(0)} &\equiv A_1^{(0)} = \alpha - A_\infty^{(0)} - \lambda_1^{e(0)} \\ \lambda_2^{(0)} &\equiv k_2'^{(0)} = -(\beta + \lambda_2^{e(0)}\lambda_1^{e(0)}|\lambda_1^{e(0)}|R)/(\lambda_1^{(0)}|\lambda_1^{(0)}|R) \end{aligned} \tag{2-164}$$

Here, α and β are the original fit parameters defined by equations (2-103). The $\underset{\sim}{\lambda}^{(0)}$ can then be used in the nonlinear least squares iterations as before.

Summary. Although the $\underset{\sim}{\lambda}^{(0)}$ calculation procedures described above seem complicated, the code in KINPRO is rather simple and the computer time required is minimal. Thus, the disadvantage of requiring several different fits and many calculations to estimate initial parameter values is far outweighed by the advantage of circumvention of the requirement for the user to input initial guesses of all the parameters. Of course, the more complicated the master function, the more susceptible the results of the estimation procedures to data scatter. Thus, KINPRO always gives the user the option of changing the initial parameter estimates once they have been calculated. This approach seems to strike a happy medium between independence of the computer program on one hand and the versatility required on the other.

REFERENCES AND NOTES

1. P. R. Bevington, "Data Reduction and Error Analysis for the Physical Sciences," McGraw-Hill, New York, 1969.
2. see ref. 1, p. 67.
3. see ref. 1, chapter 4.
4. see ref. 1, chapter 2.
5. see ref. 1, p. 69.
6. see ref. 1, p. 73.
7. see ref. 1, p. 59.
8. A. A. Frost and R. G. Pearson, "Kinetics and Mechanism," 2nd edition, John Wiley and Sons, Inc., New York, 1961, p. 13.
9. C. Capellos and B. H. J. Bielski, "Kinetic Systems. Mathematical Description of Chemical Kinetics in Solution," Wiley-Interscience, New York, 1972, chapter 4.
10. see ref. 1, chapter 6.
11. see ref. 1, p. 116.
12. see ref. 1, chapter 8.
13. see ref. 1, p. 162.
14. see ref. 1, p. 84.
15. see ref. 1, p. 188.
16. see ref. 1, p. 64.
17. see ref. 8, p. 98.
18. R. G. Wilkins, "The Study of Kinetics and Mechanism of Reactions of Transition Metal Complexes," Allyn and Bacon, Inc., Boston, 1974, p. 79.

19. *e.g.*, W. J. Moore, "Physical Chemistry," 4th edition, Prentice-Hall, Englewood Cliffs, New Jersey, 1972, p. 294.

20. see ref. 18, p. 11.

21. If absorbance is the actual measured quantity, it is usually safe to assume that the error in absorbance values is constant throughout the range of interest (*i.e.*, $\sigma_i = \sigma_A$ for all i). This is probably the case at low absorbances (*e.g.*, 0.0 to 1.0) and since most experiments only cover a range of 0.1 to 0.2 absorbance units, the assumption is probably nearly exact over these ranges. Problems arise if one is measuring absorbances over a larger range at high absorbances (*e.g.*, $\gtrsim$ 2.0). In this case, σ_i increases as A(i) increases and the weighting factors should then be based on constant errors in intensity (directly related to % transmittance) rather than absorbance. If the normalized intensity is given by I and the error in I given by σ_I (assumed constant), the individual errors in absorbance (σ_i) are then dependent on the A(i)'s:

$$A(i) = -\frac{1}{2.303} \ell n\, I(i)$$

$$\sigma_i = -\frac{1}{2.303}[\sigma_I / \exp(-2.303A(i))]$$

In all the discussions of application of error propagation to analyses dealing with absorbance data, σ_i will be used to indicate the error in A(i), assuming that these values will be constant for normal experiments, but may depend on the A(i) under the special circumstances outlined above.

22. E. A. Guggenheim, Phil. Mag., 2, 538 (1926).

23. (a) E. S. Swinbourne, J. Chem. Soc., 2371 (1960).

(b) F. J. Kezdy, J. Jaz, and A. Bruylants, Bull. Soc. Chim. Belg., 67, 687 (1958).

(c) L. M. Schwartz and R. I. Gelb, Anal. Chem., 50, 1592 (1978).

24. *e.g.*, ref. 8, p. 13; ref. 9, chapter 5; or ref. 18, p. 10.

25. A. D. Zuberbühler and T. A. Kaden, Chimia, 31, 442 (1977).

26. D. I. Rubin, Chemical Engineering Progress Symposium Series, 59, 90 (1961).

27. L. Nondek and J. Málek, Collect. Czech. Chem. Commun., 43, 1907 (1978).

28. K. B. Wiberg, in "Techniques of Chemistry," vol. 6, A. Weissberger, ed., "Investigation of Rates and Mechanisms of Reactions," Part II, 3rd edition, G. G. Hammes, ed., Wiley-Interscience, New York, 1974, p. 741.

29. R. M. Alcock, F. R. Hartley, and D. E. Rogers, J. Chem. Soc., Dalton Trans., 123 (1978).

30. R. G. Duggleby and J. F. Morrison, Biochim. Biophys. Acta, 481, 297 (1977).

31. R. H. Matthews and J. O. Alben, J. Theor. Biol., 72, 219 (1978).

32. (a) P. A. D. deMaine, Computers and Chemistry, 2, 1 (1978).

(b) P. A. D. deMaine, G. K. Springer, and R. A. Mikelskas, Computers and Chemistry, 2, 7 (1978).

33. W. E. Wentworth, J. Chem. Ed., 42, 96 (1965).

34. J. L. Dye and V. A. Nicely, J. Chem. Ed., 48, 443 (1971).

35. H. O. Hartley, Technometrics, 3, 269 (1961).

36. R. H. Moore and R. K. Zeigler, Los Alamos Report LA 2367, 1959 and Addenda.

37. *e.g.*, J. L. Kuester and J. H. Mize, "Optimization Techniques with Fortran," McGraw-Hill, New York, 1973, p. 218.

38. P. A. Stark, "Introduction to Numerical Methods," Macmillan, London, 1970, p. 176.

39. see ref. 8, p. 187; or ref. 9, p. 38.

40. see ref. 9, p. 41.

41. A triangle average is performed to minimize errors due to noisy A_i data, In general, a (2n - 1)-point triangle average of the i-th data point (Y_i) of a set of data (Y) can be calculated as follows:

$$\langle Y_i \rangle^{(2n-1)} = [nY_i + \sum_{j=1}^{n-1} (n - j)(Y_{i-j} + Y_{i+j})]/n^2$$

42. see ref. 8, p. 15; ref. 9, p. 14; or ref. 18, p. 15.

CHAPTER III

The Importance of Distance in Electron Transfer

INTRODUCTION

The field of biochemistry is replete with examples of outer sphere electron transfer processes. This type of electron transfer (which will be taken here as involving no bond-breaking or -making) is found in the respiratory chains of animals and the photosynthetic reaction centers of plants and is probably crucial to many important bioenergetic processes. Since, in most of these systems, the process involves only the transfer of an electron from a donor molecule to an acceptor molecule, the apparent simplicity of the reactions has allowed several theoretical models to be developed. Some of these models will be explored here.

Theoretical interest in biological electron transfer processes was sparked by the observation of rates of transfer that exhibited a normal temperature dependence around and somewhat below room temperature, but exhibited a measurable (temperature independent) rate at very low temperatures (even down to 4 K).[1-4] The inability of classical theories to fit such a temperature dependence suggested quantum mechanical tunneling[5-7] as an explanation. Initially[1,2] it was assumed that tunneling was operative only at low temperatures with the usual activation mechanism predominating at high temperatures. However, theoretical work since then has shown that one theory (incorporating vibronic interactions with tunneling) can accomodate the entire temperature dependence. The theoretical rate expressions also exhibit a dependence on the distance between the donor and acceptor sites involved in the electron transfer and it is this distance dependence which will be of interest here.

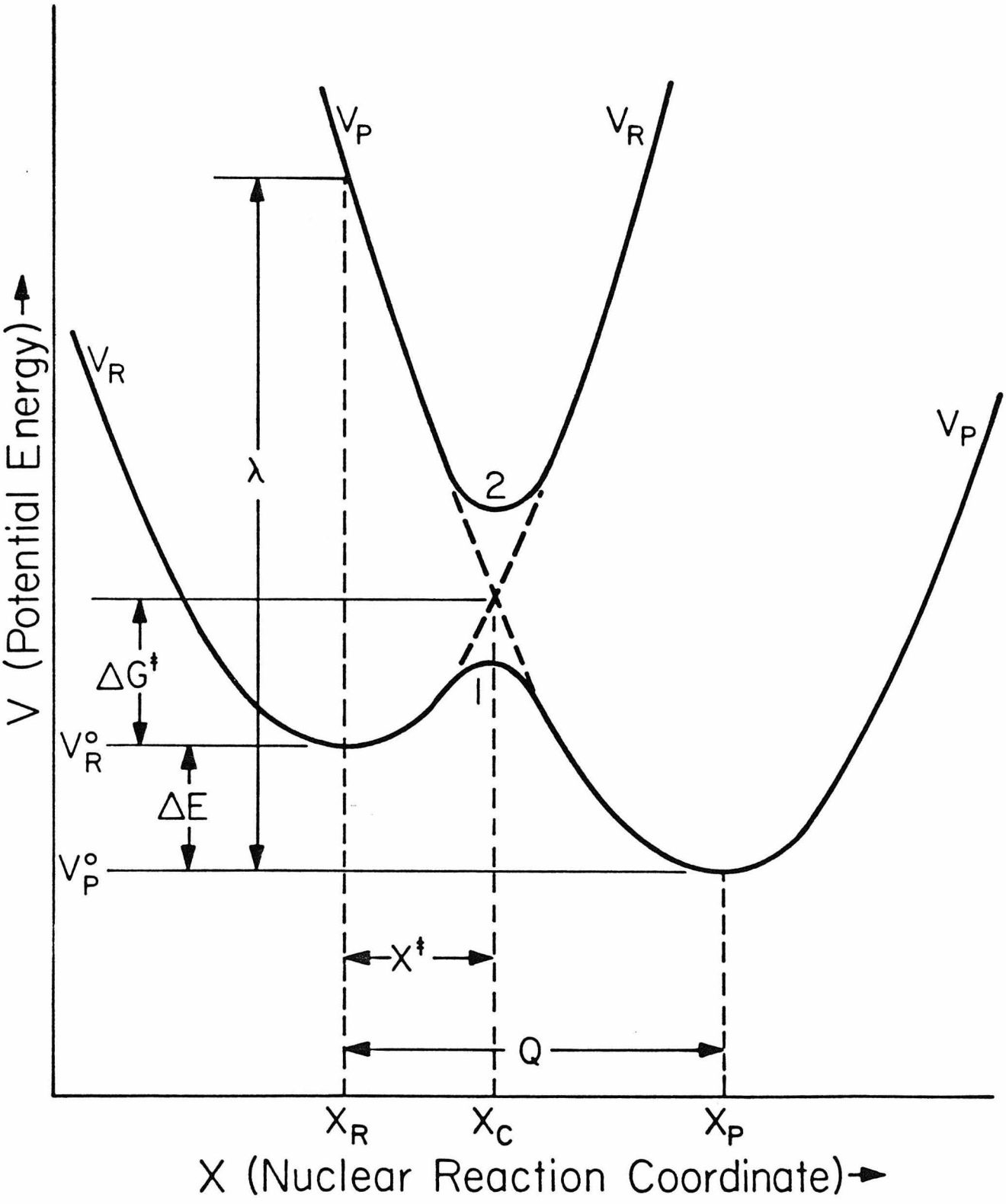
In recent years, our laboratory has been concerned with outer sphere electron transfer reactions between metalloproteins and inorganic (small molecule) redox agents. A method has been developed for analysis of such electron transfer rate data in terms of outer sphere adiabatic Marcus theory[8] which allows correction of the rate constants for differences in reactivity of the small molecule reagents, for differences in the driving force for electron transfer, and for nonspecific electrostatic interactions.[9-12] Although the mechanistic interpretations resulting from this type of analysis have shown that metalloprotein electron transfer rates reflect the relative "accessibility" of the protein metal centers to the various small molecule redox agents, a direct measure of this accessibility was not available. The desire to establish a more solid basis for discussion of this type of accessibility and its relationship to the physical distance between the protein metal center and the protein surface has prompted the development of new analytical techniques based on the use of a theoretical model involving the dependence of the electron transfer on the distance between the donor and acceptor sites. The present work interprets metalloprotein electron transfer rate measurements in terms of the distances of transfer involved and examines the mechanistic implications of these distances.

THEORY

To understand the theoretical implications of the observed temperature-independent rate observed at low temperatures in some biological systems, it is first necessary to examine the effect of nuclear motion on the electron transfer process.

The general case to be considered will be that of two sites, one (the donor) initially occupied by the electron to be transferred and the other (the acceptor) initially in the absence of an electron. This state of the system (reactants) has a nuclear potential energy described by the V_R curve in Fig. 3-1. The product state of the system (electron at the acceptor site) has a nuclear potential energy described by the V_P curve. As depicted, the shape of the nuclear potential energy well will depend on the location of the electron (whether at the donor or acceptor site), with certain molecular vibrations (for example) changing after the actual transfer. This is represented by the non-equivalence of the reactant and product potential energy curves in the reference frame of the nuclear reaction coordinate (which actually represents the combination of all such nuclear coordinates which are involved in the change from state R to state P). The shape of the potential wells is also affected by electronic interactions, which play a major role in determining the behavior of the potential energy surfaces near the crossing point (at X_C). In the absence of any electronic interaction, the V_R and V_P curves are the eigenstates of the system, whereas nonzero electronic interaction causes quantum

Fig. 3-1. Potential energy curves for the reactant and product states of the system. See text for description.


V (Potential Energy)→
X (Nuclear Reaction Coordinate)→
V_P
V_R
V_R
V_P
λ
2
1
$\Delta G^{\ddagger}$
V_R^o
ΔE
V_P^o
$X^{\ddagger}$
Q
X_R
X_C
X_P

mechanical resonance to occur in the region of the crossing point making potential surfaces similar to 1 and 2 (see Fig. 3-1) the eigenstates of the system.

The electron transfer act is subject to two very important restrictions:[13] (1) No energy may enter or leave the system during the electron transfer (energy conservation); and (2) during the time required for electron transfer ($\sim 10^{-15}$ sec), nuclear motion ($\sim 10^{-13}$ sec) does not occur (the Franck-Condon principle[14-16]). In terms of Fig. 3-1, this means that during the actual electron transfer, "motion" of the point representing the nuclear configuration can be only horizontal (restriction (1)) and only vertical (restriction (2)). The only place where these restrictions can both be satisfied is at the crossing point. Thus, the only time the electron can transfer is when the nuclear reaction coordinate has the value X_C.

The rate of electron transfer is influenced by two separate probabilities: (1) the probability that the nuclear configuration will be right for electron transfer (*i.e.*, the nuclear reaction coordinate will be X_C); and (2) the probability that, once the nuclei are in the right configuration, the electron will move to the acceptor site. The former is dependent on the shape of the nuclear potential energy surfaces (and, as will be discussed later, the population of the various vibrational levels within each well). The latter is dependent on the electronic interaction. If this interaction is large, the potential energy separation between the eigenstates 1 and 2 at the crossing point will also be large. In the classical description,

assuming the system has enough (kinetic) energy to surmount the activation barrier, then, once the nuclei are in the configuration represented by X_C, the probability that the electron will transfer from the donor to the acceptor (probably by tunneling[13]) approaches unity. If the probability of electron transfer is sufficiently close to unity (once the nuclear configuration is at X_C), the electron transfer is termed "adiabatic" (in the Ehrenfest sense[17]). In the case of small electronic interaction, the energy separation of states 1 and 2 near the crossing point is less and the chance becomes greater that, at the nuclear configuration X_C, no electron transfer will occur (*i.e.*, that the system will remain on the V_R potential surface). This lowering of the transfer probability (once at X_C) significantly below unity is described as "non-adiabaticity". Thus, the electron transfer event is described as non-adiabatic if it is slow enough (*i.e.*, has a low enough probability) to appreciably affect the rate.

For non-adiabatic reactions (at low values of the electron transfer probability, Landau[19] and Zener[20] developed the following expression for the probability of electron transfer (within the "activated complex" at X_C) from site d (donor) to site a (acceptor) upon single passage through the crossover region[13] (X_C in Fig. 3-1):

$$P_{da} \approx \frac{2\pi}{\hbar}|T_{RP}|^2/v_{\Delta F} \qquad (3\text{-}1)$$

where v is the velocity of passage through the crossover region, ΔF is the difference in slopes of the V_R and V_P potential energy curves at X_C, and T_{RP} is the Hamiltonian matrix element between state R and state P. (This term is the electronic interaction energy referred to above and is the sole determinant of the resonance energy separation between states 1 and 2 at the crossover region in Fig. 3-1.[19] T_{RP} is also the parameter described as the tunneling matrix element, T_{da} or T_{ab}, in the development by Hopfield.[20]) P_{da} is also directly related to the transmission coefficient (or adiabaticity factor) κ discussed by Marcus. He derives an expression for the transmission coefficient which is also dependent on $|T_{RP}|^2$ (for the non-adiabatic case):

$$\kappa = \frac{2\pi}{\hbar} |T_{RP}|^2 \left(\frac{2\pi}{m\omega^4 Q^2 k_B T}\right) \qquad (3\text{-}2)$$

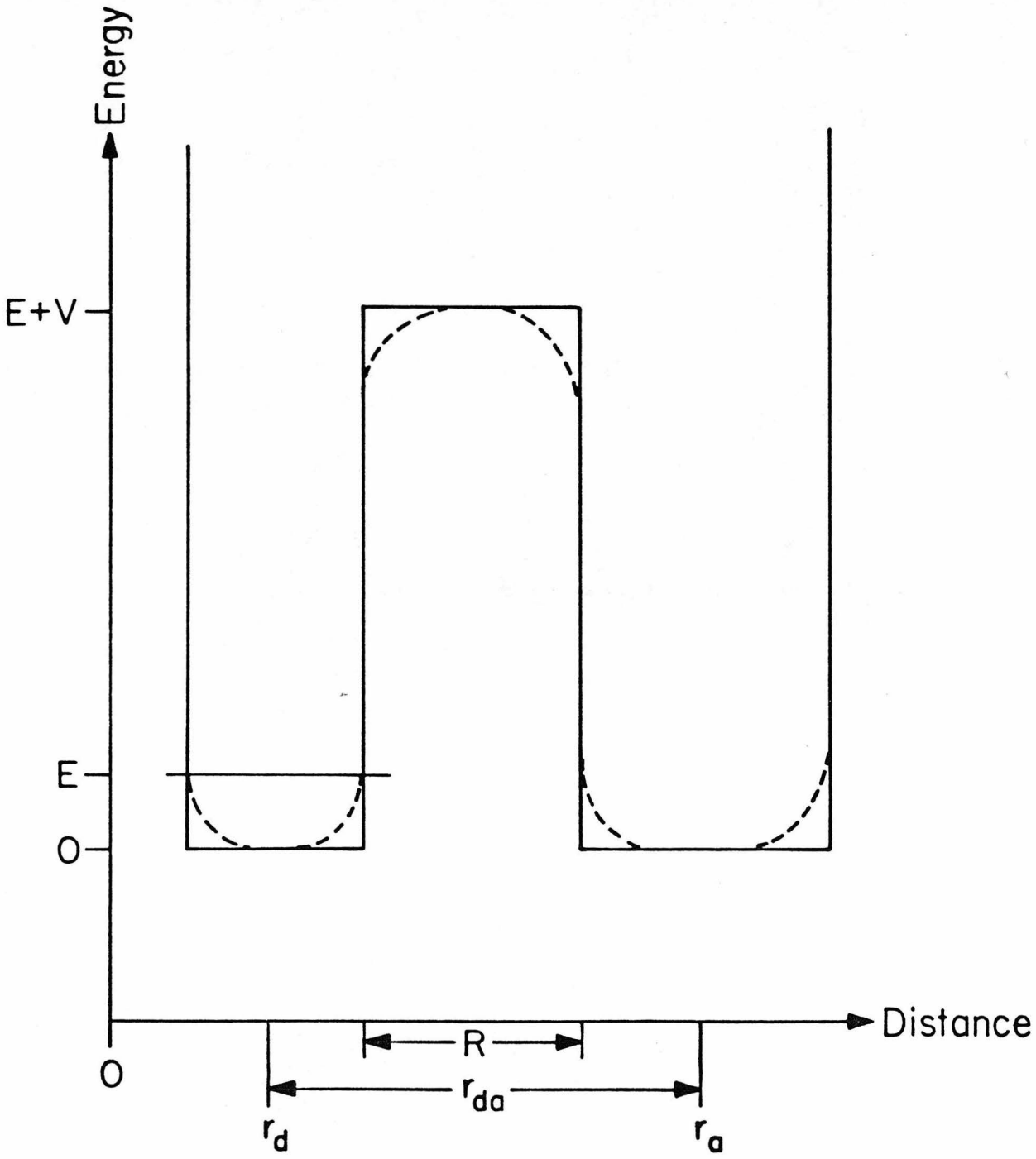
where m is the oscillator mass, ω is the oscillator frequency, k_B is Boltzmann's constant, T is the absolute temperature, and $Q = X_P - X_R$ (see Fig. 3-1). Thus, classical theories predict that, for very non-adiabatic cases, the electron transfer probability is directly proportional to the square of the electronic interaction Hamiltonian matrix element, T_{RP}. Since one might expect this interaction to be less for a and d sites separated by lower distances, the probability of transfer (and thus the rate of transfer) is expected to be dependent on distance through the T_{RP} term. That this is indeed the case will become apparent later on in the development.

If the classical "activated transfer" case discussed above were the whole story, one would not predict a temperature independent rate of electron transfer at low temperatures. In the quantum mechanical description, Fig. 3-1 should be modified to include molecular vibrational levels within each potential well. Then the vibrational eigenfunctions of the system in state R or state P will exhibit a probability distribution (square of the wavefunction amplitude) which extends outside the potential well. In other words, vibrational levels of state R with vibrational energies lower than the activation energy, $\Delta G^{\ddagger}$, will be associated with eigenfunctions that display a nonzero probability in the classically-forbidden region below the crossover point. The same is true for vibrational levels of the P state and there is then a finite (although small) probability that the system can exist in the X_C nuclear configuration without enough energy to surmount the activation barrier. The Franck-Condon restriction is satisfied and if a vibrational level of the P state exists with the same (or about the same[21]) total energy, the energy conservation restriction is satisfied. Once at this point, there is another probability (P_{da}) that the electron will (instantaneously, as viewed from the nuclear reference frame) transfer to the acceptor site, after which the system finds itself in the P state (at X_C) in a vibrational level of the same total energy (but not necessarily the same vibrational energy) as the vibrational level of the R state in which it initially resided. The system thus relaxes into the P state and the electron transfer is complete. This activationless

process is termed molecular or nuclear tunneling. It should be obvious that it only occurs because of the *quantum mechanical* description of the system giving a nonzero probability of the system existing at the crossover point below the activation barrier. The quantum mechanical treatment also predicts the low temperature behavior of the biological systems, since there is still a nonzero probability of the nuclear configuration being X_C in the lowest vibrational level of the R state. Thus, at low temperatures, this is the only vibrational level populated and the probability of transfer becomes temperature independent.

The situation, as viewed by the electron, is displayed in Fig. 3-2. This is an idealized plot of the electronic potential energy (*i.e.*, total energy minus electronic kinetic energy) which exists for one value of the nuclear reaction coordinate. The two potential energy minima (wells) are for the electron at the donor site (left well) and at the acceptor site (right well). The abscissa is simplified to represent only the physical distance between the sites although a general electronic reaction coordinate would be more appropriate. The particular situation depicted in Fig. 3-2 is for the system at X_C (in Fig. 3-1). At this point, the electronic potential energy minima are of equal value indicating that the two states (involving different locations of the electron) are isoenergetic. For other values of the nuclear coordinate, one site would be more favorable than the other.[13] The electron is initially assumed to be at the donor site with a kinetic energy E and with a barrier (made

Fig. 3-2. Energy diagram for electron tunneling from donor to acceptor potential wells. See text for details.


Energy
E+V
E
O
O
R
Distance
r_{da}
r_d
r_a

up of intervening dielectric material) of height V. Transfer of the electron from donor to acceptor is thus viewed as electron tunneling through this barrier of height V and width R. This model has been treated by Gamow[6] and the expression he developed for the probability of a free particle penetrating a rectangular barrier (solid line in Fig. 3-2) is:

$$P = \frac{16EV}{(V+E)^2} e^{-2R(2mV)^{1/2}/\hbar} \qquad (3\text{-}3)$$

where, m is the mass of the particle (here, an electron) and the other symbols have been defined previously. This early result already indicated that the tunneling probability (and thus, the electron transfer rate) was dependent exponentially on the distance transferred, R.[22] Many recent theories derive an exponential dependence on R very similar to the exponential factor (called the Gamow factor[13]) in equation (3-3).

Although not specifically stated above, the electron transfer process is stongly dependent on vibronic coupling. Physically, this coupling can be viewed as changes in the characteristics (*e.g.*, equilibrium displacements) of certain molecular vibrations dependent on the location of the electron (due to charge redistribution). This, of course, is the basis for the horizontal separation of the minima in the R and P curves in Fig. 3-1. Theoretically, energy matching (energy conservation) requirements are met through vibrational excitations and efficient thermal relaxation in the P state vibrational manifold is required to prevent back-electron transfer. In the

classical treatment, vibrational excitations supply the activation energy required for electron transfer. Treatment of this vibronic coupling to electron transfer is therefore required in a complete description of the processes involved. There are three basic treatments of this subject (classical, semiclassical, and quantum mechanical) and the similarities and differences involved in these treatments are discussed by DeVault in a refreshingly lucid and nontechnical account[13] which will serve as the basis for the brief discussion to follow.

DeVault uses a simple model consisting of one harmonic oscillator with the same frequency in both the R and P states (see Fig. 3-1). Although more sophisticated mutiple oscillator treatments have been given (notably that of Jortner[23]), DeVault points out[13] that the simpler single oscillator treatment seems to fit the data available as well as the more complicated ones. The various treatments will be examined with attention to their prediction of the temperature dependence of the electron transfer rate.

The classical treatment is mainly due to Marcus[18] who used a statistical mechanical treatment involving oscillators of different frequencies. Simplification to one oscillator which does not change frequency is equivalent to requiring $\Delta S^{\ddagger} = 0$.[13] Under these assumptions and making use of the expression for the transmission coefficient given in equation (3-2), the electron transfer rate constant is given by:[13]

$$k = \frac{2\pi}{\hbar}|T_{RP}|^2(4\pi k_B T)^{-1/2}\exp\left[-\frac{(\lambda-\Delta E)^2}{4\lambda k_B T}\right] \qquad (3\text{-}4)$$

where λ and ΔE are defined as in Fig. 3-1. This expression is seen to follow the Arrhenius law (except for the $T^{-1/2}$ preexponential dependence) and does not predict temperature independent behavior. The problem with equation (3-4) at low temperatures is that it assumes a classical description of the average energy (and distribution) of a set of oscillators in thermal equilibrium. In this treatment, the average energy is given by k_BT and the probability of having a displacement $(x-x_o)$ away from equilibrium is given by:

$$P(x) = (2\pi\sigma_x^2)^{-1/2}\exp[-\frac{(x-x_o)^2}{2\sigma_x^2}] \qquad (3\text{-}5)$$

where, $\sigma_x^2 = k_BT/k_H$ and k_H is the Hooke's law constant for the harmonic oscillators (described by the curvature of the parabolas of Fig. 3-1) which is related to the oscillator frequency ω by $\omega = (k_H/M)^{1/2}$ (M is the effective mass of the oscillator).

The semiclassical treatment can be derived similarly with consideration of the (harmonic) oscillator energy levels as quantized with the lowest level at $\hbar\omega/2$ and spacing of $\hbar\omega$. This treatment gives as the average energy of a set of oscillators:

$$\bar{E} = \frac{\hbar\omega}{2}\coth(\hbar\omega/2k_BT) \qquad (3\text{-}6)$$

and the probability of displacement $(x-x_o)$ given by equation (3-5) but with:

$$\sigma_x^2 = \frac{\hbar\omega}{2k_H} \coth(\hbar\omega/2k_BT) \tag{3-7}$$

At high temperatures, this σ_x^2 looks like k_BT (as the quantum mechanical description approaches the classical description), but at low temperatures, σ_x^2 approaches $\hbar\omega/2$, which is temperature independent. With the appropriate substitution ($\frac{\hbar\omega}{2}\coth(\hbar\omega/2k_BT)$ for k_BT) in equation (3-4), the semiclassical electron transfer rate constant is:

$$k = \frac{2\pi}{\hbar}|T_{RP}|^2(2\pi\sigma^2)^{-1/2}\exp[-\frac{(\lambda-\Delta E)^2}{2\sigma^2}] \tag{3-8}$$

This is exactly equivalent to the expression derived by Hopfield,[20] although he arrived at it by a completely different route. His derivation[20,29] emphasizes the similarities between the electron transfer process and the Förster[30] energy transfer process. Thus, the Franck-Condon contribution to the electron transfer probability is derived as the overlap between an electron removal spectral distribution (for removal of the electron from the donor site to a fictional electron state at zero energy) and an electron insertion spectral distribution (for insertion of an electron from the fictional state into the acceptor site). The vibronic coupling is then exhibited as the linewidths in these spectral distributions.

The full quantum mechanical treatment has been derived in slightly different ways (and with different applications in mind) by Huang and Rhys,[24] Levich[25,26] and Dogonadze,[27,28] Jortner,[23] and a simplified

(single-oscillator) description is provided by DeVault.[13] (An earlier treatment by Grigorov and Chernavskii[21] has all the essential elements.) Only a brief description of the important aspects of this treatment are given here. To understand the treatment, it is necessary to visualize a reactant and a product potential energy curve (as in Fig. 3-1), each of which has a manifold of vibrational levels which are populated according to Boltzmann statistics. For simplicity, each vibrational level of the R state is assumed to be isoenergetic with a vibrational level of the P state (of higher quantum number, of course) and the overlaps of the vibrational wavefunctions determine the "willingness" of the oscillators to undergo the changes required upon electron transfer. The contribution from each vibrational state to the probability of electron transfer is dependent not only on the Franck-Condon overlap factors (defined as the square of the overlap integral) but also on the electron tunneling probability. To get the total rate of electron transfer, one need only weight each Franck-Condon factor with the fraction of systems expected to be in that particular vibrational state (this is the temperature-dependent part), sum the contributions from all the vibrational levels and multiply by the electron tunneling probability. Assuming a specific form for the vibrational wave functions, it is not difficult to calculate these total probabilities numerically for a specific case (as done for the *Chromatium* data by DeVault[13]), and examine numerically the temperature dependence of the rate. In general, it is seen that, at very low temperatures, only the lowest vibrational level of the R state is populated and the electron transfer rate is completely

determined by the Franck-Condon factor of this level and the electron tunneling probability. As the temperature is raised, no temperature dependence is seen until there is enough energy to significantly populate the next highest vibrational level of the R state. The Franck-Condon factor for this level will be slightly larger and as this level becomes more populated, the electron transfer rate will increase. Of course, nuclear tunneling will predominate until vibrational levels above the activation barrier become populated. For vibrational levels near this energy, the Franck-Condon factors will be very large indeed and once these levels become significantly populated, they will tend to dominate the electron transfer. This would be termed by the classicists "activated electron transfer".

All the quantum mechanical attempts at fitting the biological electron transfer data, have derived functional forms in which the temperature dependence is due to the population of vibrational levels (combined with the changing Franck-Condon factors) and the distance dependence is due to the electron tunneling probability prefactor. This prefactor is always directly proportional to $|T_{RP}|^2$ as in the Landau-Zener formula (equation (2-1)) and the Marcus expression for the transmission coefficient (equation (3-2)). The distance dependence is due only to the occurrence of the barrier width in $|T_{RP}|^2$ (the electronic interaction energy) which can be calculated exactly for the hydrogen molecule ion (H_2^+) (as done by DeVault[13]) and, in the long distance asymptotic limit, is given by:

$$|T_{ab}|^2 \propto \exp(-0.983 \cdot 2R(2mV)^{1/2}/\hbar) \qquad (3\text{-}8)$$

(*cf.*, equation (3-3)). Since, at constant temperature, the Franck-Condon terms are not strongly dependent on the width of the barrier, the electron transfer rate is seen to be exponentially dependent on this barrier width. (As pointed out by Hopfield,[29] there is a difference between the barrier width, R, and the intersite separation r_{da} or r_{ab} (see Fig. 3-2).)

As discussed more fully in the next section, at constant temperature it is possible to consider the electron transfer rate as directly proportional to $|T_{RP}|^2$ (with a proportionality constant, C) and making use of equation (3-8), the electron transfer rate constant can be written:

$$k = C[\exp(-aR)]^2 \tag{3-9}$$

where,

$$a = 0.983(2mV)^{1/2}/\hbar \tag{3-10}$$

Hopfield has argued[20,29] that the upper limit of the barrier height (V) is about half of the $\sigma \rightarrow \sigma^*$ band gap of the surrounding material (*i.e.*, protein), giving $V \leq 3$ eV. Hopfield chooses 2 eV as a reasonable estimate of V and with m as the rest mass of the electron, he calculates $a \approx 0.72$ Å^{-1}. For a given range of rate constants, the absolute range of distances calculated from equation (3-9) will, of course, depend on the value of a chosen (determined by V). In general, a higher barrier (larger V) will result in the calculation of a shorter distance for

the same rate constant. The original theoretical fits of the *Chromatium* data (giving distances of ~30 Å[1,2]) assumed that the rate was completely determined by the electron tunneling probability. The use of Hopfield's expression to fit the same data[13] gives a distance of $\leq$10 Å with much of the rate limitation coming from the Franck-Condon factors. The analysis described below lumps the Franck-Condon factors into the pre-exponential constant C and the choice of a reference reaction determines their contribution to the rate.

S & M APPROACH

The ubiquity of metalloprotein electron transfer reactions in metabolic processes has made the mechanistic characterization of these reactions a subject of considerable importance and interest. Since the initial work of DeVault and Chance,[1,2] particular attention has been directed toward evaluating the magnitude and role of the distance over which electron transfer occurs in these reactions. The basis for this attention is seated in the implications of the distance of transfer for our understanding of metalloprotein redox mechanisms and their specificity. Although several theoretical descriptions of the relationship between distance of transfer and rate of reaction have been described,[20,21,23,28,31-33] none of these has been presented in a manner that makes it readily or unambiguously applicable to conventional rate data. For this reason, a simple, semi-empirical method has been developed (by the author, in collaboration with G. Mauk) for estimating the distance of metalloprotein electron

transfer and it has been used to analyze rate data on three types of metalloproteins. The results indicate that this approach (entitled the Scott-Mauk, or S and M approach) should be of considerable value in mechanistic appraisal of reactions of this type.

Methods. In recent years, several derivations of the functional dependence of rate on the distance of electron transfer have been proposed. Expressions for the electron transfer rate constant, k, have been derived by several authors[20,21,23,28] and all have the general form illustrated in equation (3-11).

$$k = C|T_{ab}|^2 \tag{3-11}$$

In equation (3-11), T_{ab} is the tunneling matrix element (or the electronic exchange interaction Hamiltonian matrix element[13]), the magnitude of which is dependent on the extent of donor and acceptor electronic wave function overlap. C is a complex function whose value is dependent on a number of properties of the donor and acceptor sites.[34] In general, the matrix element T_{ab} can be expressed as an exponential function of the intersite distance, R (as originally derived by Gamow[6]), and equation (3-11) may be rewritten as shown in equation (3-12).

$$k = C(e^{-aR})^2 \tag{3-12}$$

Assuming that the dependence of $|T_{ab}|$ on R is adequately represented by the function described by Hopfield (*i.e.*, a = 0.72 Å^{-1}),[20] equation (3-12) may be rewritten to yield equation (3-13).

$$R = -0.694 \ln(k/C) \qquad (3\text{-}13)$$

A major obstacle to use of the complete Hopfield expressions or those of other authors[21,23,28] is the lack of adequate information to permit objective estimation of the values for the adjustable parameters that comprise C. Previous calculations have attempted to guess tolerable estimates for these parameters and have enjoyed reasonable success.[35-37] However, the underlying operational premise in these reports assumes that much more information is available than can be reasonably substantiated. We prefer to reduce our assumptions by attempting to experimentally determine an acceptable value for C without defining the nature of its components. Such an estimate may be obtained by considering a reaction for which we know the rate and have an estimate for the distance of electron transfer. By calibrating and standardizing the calculations in this manner, the resulting distances are comparable at least in a relative sense. Nevertheless, the calculated distances reported here also appear to represent reasonable values on an absolute scale as well.

Analytical Procedure and Rationale. The reactions of interest in this analysis are those between a metalloprotein and a substitutionally inert transition metal complex. This selection is advantageous

because of the large volume of data available for consideration[9,10] and because of the mechanistic insight provided by previous detailed examination of these reactions. Three experimental measurements are required for the calculations:[11] (1) the cross-reaction rate constant for the reaction between the protein and the complex (k_{12}); (2) the self-exchange rate constant for the complex (k_{22}); and (3) the potential difference between the two reactants ($\Delta E°$). (In the present notation, the subscripts 1 and 2 refer to the protein and the small molecule reagent, respectively.)

In addition to the distance of transfer, several factors contribute to the observed rate of electron exchange. For this reason it is desirable to correct the observed rate constants for as many of these factors as possible before considering the contribution of distance. Our previous work provides a means for correcting the rate constant for three important factors. First, non-specific electrostatic contributions to k_{12} and k_{22} are removed by using Debye-Hückel theory to adjust the rate constants to infinite ionic strength:[11]

$$k_{12}^{\infty} = \exp\left[\ln(k) + 3.576 \left(\frac{\exp(-\kappa R_1)}{1 + \kappa R_2} + \frac{\exp(-\kappa R_2)}{1 + \kappa R_1}\right)\left(\frac{Z_1 Z_2}{R_1 + R_2}\right)\right] \qquad (3\text{-}14)$$

At 25° C,

$$\kappa = 0.329\ \mu^{1/2}\ \text{Å}^{-1}$$

In equation (3-14), Z and R refer to reactant charge and radius, respectively.

Next, correction for both the thermodynamic driving force of the reaction and for small molecule reactivity properties is accomplished through the use of the Marcus relationships:[8,38]

$$k_{12} = (k_{11}k_{22}Kf)^{1/2} \tag{3-15}$$

$$\log(f) = [\log(k_{12})]^2/[4\ \log(k_{11}k_{22}/Z^2)] \tag{3-16}$$

where Z is the collision frequency (taken to be $10^{11}\ M^{-1}\ s^{-1}$). In making this correction, k_{12}^{∞} and k_{22}^{∞} calculated from equation (3-14) are substituted and the value of k_{11}^{∞} determined.[39] The calculated value of k_{11}^{∞} is the self-exchange rate that the protein exhibits in its reaction with the reagent concerned and is a reflection of the mechanism employed by the protein in that particular cross-reaction. If a protein obeys Marcus theory, then the values of k_{11}^{∞} calculated from its reactions with a variety of complexes will be the same (within an order of magnitude, the limit of experimental and theoretical error). If a protein does not obey Marcus theory, then k_{11}^{∞} may vary over several orders of magnitude, indicating that the mechanism of electron transfer employed by the protein is highly dependent upon the nature of the complex with which it is reacted. Having obtained a rate constant that is independent of nonspecific electrostatic effects, reagent reactivity, and driving force of reaction,

we can use this rate in equation (3-13) to estimate the distance of electron transfer. However, if the intersite distance, R, for the reaction between a protein and an inorganic complex is regarded as the sum of a contribution from the protein (R_p) and from the reagent (R_r), then the distance calculated from the protein self-exchange rate using equation (3-13) will be $2R_p$.[40] Clearly, this distance will reflect mechanistic characteristics of the reaction concerned as does the k_{11}^{∞} from which it is derived.

As outlined above, use of equation (3-13) requires selection of a reference reaction to serve as a calibration point for estimation of the value of C. The reference protein reactions that we have selected are those of the blue copper protein stellacyanin. This protein has been chosen because several observations lead us to believe that the distance of electron transfer to or from this protein should approach double the van der Waals' contact radius for carbon, 3.35 Å.[41] The principal reason leading to this conclusion is that stellacyanin is the only protein that appears to obey Marcus theory.[9] For this to be true, the metal site in the protein must be relatively accessible to solvent so that the protein does not impose any protein-reagent interactions that are unanticipated by theory. Moreover, the k_{11}^{∞} values calculated for stellacyanin are generally at the upper limit of those calculated for any protein-small molecule reactions, indicating that the distance of transfer must be quite small. Finally, stellacyanin is one of the few proteins that is able to exchange electrons with electrodes reasonably well without the

aid of mediators, further suggesting an accessible redox site.[42] In the treatment that follows, we assume that any increase in the redox partner contact distance from the reference limit will lead to non-adiabatic electron transfer, and that equation (3-13) may be applied to estimate that distance. The reasonableness of this assumption is the main issue to be addressed in this Chapter.

To avoid dependence on a single experimental value, the present calculations employ the average of the k_{11}^{∞} calculated for stellacyanin in its reactions with $Fe(EDTA)^{2-}$ ($k_{11}^{\infty} = 2.3(10^5)\ M^{-1}\ s^{-1}$), $Co(phen)_3^{3+}$ ($k_{11}^{\infty} = 3.3(10^5)\ M^{-1}\ s^{-1}$), and $Ru(NH_3)_5py^{3+}$ ($k_{11}^{\infty} = 1.6(10^5)\ M^{-1}\ s^{-1}$).[9] Substituting this average, $2.4(10^5)\ M^{-1}\ s^{-1}$, into equation (3-13) along with an R_p value of 1.7 Å yields:[43]

$$R_p = 5.976 - 0.347\ \ln(k_{11}^{\infty}) \qquad (3\text{-}17)$$

The discussion leading to equation (3-17) has tacitly assumed that the reactions of interest do not demonstrate kinetically detectable precursor complexes. As this assumption does not pertain to certain reactions that are of particular interest, it is useful to also consider the analysis of such cases. Reactions of this type are usually discussed in terms of the following mechanism:[44]

$$A^{ox} + B^{red} \overset{K}{\rightleftharpoons} [A^{ox}|B^{red}]$$

$$[A^{ox}|B^{red}] \xrightarrow{k_{et}} [A^{red}|B^{ox}]$$

$$[A^{red}|B^{ox}] \longrightarrow A^{red} + B^{ox}$$

In this scheme, precursor complex formation is assumed to be rapid and the electron transfer step represented by k_{et} is taken to be rate limiting. As k_{et} is a unimolecular rate constant, it is necessary to accomodate this feature in the strategy outlined above. Such consideration is necessary because C depends on collision probability and because the Marcus calculations require second order rate constants. The simplest approach to handling this situation is to convert the first order rate constant into a "synthetic" second order rate constant (k_{12}^{est}) by multiplying k_{et} by the quotient of the usual value for collision frequency (10^{11} M^{-1} s^{-1}) divided by a reasonable value for molecular vibrational frequency (10^{13} s^{-1}). The resulting product will have the units of a second order rate constant and may be processed as already described. As there is no reaction employing this type of mechanism for which the distance of electron transfer can be reasonably surmised, the present analysis will use the relationship described in equation (3-17) for these calculations. For consistency, it would, of course, be preferable to base these distances on reference reactions of the same mechanistic type.

Reliability of Calculated Distances. Before rational conclusions may be drawn from the present calculations, it is necessary to consider the uncertainty in R_p values reported. The *accuracy* of R_p for a given reaction depends on the validity of two factors: the value of the exponential factor, a, in equation (3-12) and the

reliability/identity of the reference reaction used to estimate C. The reference reaction is expected to be most accurate in defining distances employed by proteins having the same type of metal centers as the protein in the reference reaction. Thus, in the present case, distances estimated for proteins with blue copper centers should correspond more accurately to absolute physical distances than those estimated for heme proteins or iron-sulfur proteins. This difference in uncertainty arises from differences in site characteristics that contribute to the value of C. For greatest accuracy, then, it is necessary to use a different reference reaction (*i.e.*, different form of equation (3-17)) for each type of protein involved. Although the size of this error in the present calculations on proteins is likely to be relatively small, use of equation (3-17) to calculate distances involved in reactions between two inorganic complexes is expected to produce unreasonable values. Clearly, considerations of this type only pertain to comparison of R_p values between types of proteins and not to comparisons made between proteins with similar redox centers.[43]

The *precision* of these calculations is determined by the uncertainty of the Marcus calculations. Rate constants calculated from Marcus theory are generally regarded as being reliable within an order of magnitude. From equation (3-17) it can be seen that an error of this size translates into an uncertainty of ± 0.8 Å. This is the minimum error, therefore, that must be considered when comparing R_p values obtained from reactions of a given protein with a series of

complexes or when comparing R_p values from reactions of a given complex with several proteins of a given structural type.

Caveats. The assumptions made in the present analysis merit enumeration: (1) Correction of rate constants to infinite ionic strength presumes the adequacy of Debye-Hückel theory and its inherent limitations. The justification for its use is the belief that an approximate correction is preferable to no correction. (2) Derivation of equation (3-17) assumes that the Hopfield exponential form of the wave function is correct. Hopfield's choice of the exponential factor a is in turn dependent on knowledge of the characteristics of the potential barrier separating the sites.[20] (3) Conversion of a first order rate constant to a second order rate constant provides a number that reflects mechanistic characteristics of intramolecular electron transfer.

The danger in presentation of a simple and useful function such as that in equation (3-17) is the ease with which it may be misused. The importance of restricting its use to reactions of the type specified and of acknowledging its limitations cannot be over-emphasized.

RESULTS AND DISCUSSION

The data considered in the present analysis include results on heme proteins, blue copper proteins, and iron-sulfur proteins. The properties of the inorganic complexes considered are listed in Table 3-1 along with the calculated k_{22}^{∞} values. The metalloprotein/transition metal complex reactions of interest are collected in Table 3-2. The protein properties and the calculated k_{11}^{∞} and ΔR_p values for these reactions are included in this table. (ΔR_p for a particular reaction is the difference between the R_p for that reaction and the R_p calculated for the stellacyanin reactions, 1.675 Å.)

From examination of the R_p values calculated for a given protein in its reactions with a variety of complexes, it is apparent that complexes having hydrophilic ligand surfaces (*e.g.*, $Fe(EDTA)^{2-}$) are associated with R_p values that are larger than those calculated from reactions with complexes having hydrophobic, π-conducting ligand surfaces (*e.g.*, $Co(phen)_3^{3+}$, $Ru(NH_3)_5py^{3+}$). This result is consistent with the conclusion that complexes of the latter type are able to effectively interact with hydrophobic regions of proteins to shorten the intersite distance of electron transfer while complexes with hydrophilic ligand surfaces are not capable of such penetration and are effectively forced to exchange electrons from the surface of the protein. It is further apparent that of all the proteins examined, the range in distances of transfer is relatively large for the proteins azurin and HiPIP. As these proteins are thought to have relatively inaccessible metal sites, the influence of reagent structure

Table 3-1. Small molecule reagent properties

Reagent couple	Radius (Å)	k_{22} ($M^{-1}s^{-1}$) / μ (M)	k_{22}^{∞} ($M^{-1}s^{-1}$)	E° (V)
$Fe(EDTA)^{2-/-}$	4	3 (10^4) / 0.10	6.9(10^4)	0.120
$Fe(CDTA)^{2-/-}$	4.6	3 (10^4) / 0.10	5.8(10^4)	0.090
$Ru(NH_3)_6^{2+/3+}$	3	4.7(10^3) / 0.10	2.5(10^5)	0.052
$Ru(NH_3)_5py^{2+/3+}$	3.5	7.4(10^2) / 0.10	1.7(10^4)	0.253
$Co(EDTA)^{2-/-}$	4	3.4(10^{-7}) / 0.10	7.8(10^{-7})	0.380
$Co(phen)_3^{3+}$	7	4.2(10^1) / 0.10	9.8(10^1)	0.370
$Fe(CN)_6^{4-/3-}$	4.5	2.0(10^4) / 0.20	4.6(10^5)	0.420

Table 3-2. Protein-small molecule kinetic data for calculation of k_{11}^{∞} and ΔR_p.

Protein	Reagent	k_{12} ($M^{-1}s^{-1}$)	μ (M)	R_1/R_2 (Å)/(Å)	Z_1/Z_1'	Z_2/Z_2'	k_{12}^{∞} ($M^{-1}s^{-1}$)	k_{22}^{∞} ($M^{-1}s^{-1}$)	$\Delta E°$ (V)	k_{11}^{∞} ($M^{-1}s^{-1}$)	ΔR_p (Å)
cytochrome *c* (horse heart)	$Fe(EDTA)^{2-}$	$2.57(10^4)$	0.10	16.6/4	7.5/6.5	-2/-1	$9.87(10^3)$	$6.9(10^4)$	0.140	$1.2(10^1)$	3.4
	$Ru(NH_3)_6^{2+}$	$3.8\ (10^4)$	0.10	16.6/3	7.5/6.5	2/3	$1.15(10^5)$	$2.5(10^5)$	0.209	$3.0(10^1)$	3.1
	$Ru(NH_3)_5py^{3+}$	$9.26(10^3)$	0.10	16.6/3.5	6.5/7.5	3/2	$3.52(10^4)$	$1.7(10^4)$	-0.007	$7.2(10^4)$	0.4
	$Co(phen)_3^{3+}$	$1.5\ (10^3)$	0.10	16.6/7	6.5/7.5	3/2	$3.43(10^3)$	$9.8(10^1)$	0.110	$1.5(10^3)$	1.8
cytochrome c_{551} (*Pseudomonas aeruginosa*)	$Fe(EDTA)^{2-}$	$4.2\ (10^3)$	0.10	14.4/4	-2/-3	-2/-1	$5.83(10^3)$	$6.9(10^4)$	0.140	$2.3(10^0)$	4.0
	$Co(phen)_3^{3+}$	$3.26(10^4)$	0.10	14.4/7	-3/-2	3/2	$3.26(10^4)$	$9.8(10^1)$	0.110	$2.2(10^5)$	0
myoglobin (sperm whale)	$Fe(EDTA)^{2-}$	$3.1\ (10^1)$	0.18	18.4/4	4.5/3.5	-2/-1	$2.3\ (10^1)$	$6.9(10^4)$	-0.070	$1.5(10^{-1})$	5.0
	$Fe(CDTA)^{2-}$	$2.8\ (10^1)$	0.18	18.4/4.6	4.5/3.5	-2/-1	$2.1\ (10^1)$	$5.8(10^4)$	-0.040	$4.5(10^{-2})$	5.4
	$Fe(CDTA)^{-}$	$1.48(10^2)$	0.18	18.4/4.6	3.5/4.5	-1/-2	$1.3\ (10^2)$	$5.8(10^4)$	0.040	$5.6(10^{-2})$	5.3
hemoglobin (human)	$Fe(EDTA)^{2-}$	$2.9\ (10^1)$	0.20	28.2/4	9/5	-2/-1	$2.3\ (10^1)$	$6.9(10^4)$	0.030	$2.8(10^{-3})$	6.3
	$Fe(CDTA)^{2-}$	$1.25(10^1)$	0.18	28.2/4.6	9/5	-2/-1	$9.91(10^0)$	$5.8(10^4)$	0.060	$2.0(10^{-4})$	7.3
	$Fe(CDTA)^{-}$	$1.48(10^2)$	0.18	28.2/4.6	5/9	-1/-2	$2.53(10^0)$	$5.8(10^4)$	-0.060	$1.0(10^{-3})$	6.7
stellacyanin (*Rhus vernicifera*)	$Fe(EDTA)^{2-}$	$4.3\ (10^5)$	0.50	19.5/4	0/0	-2/-1	$4.3\ (10^5)$	$6.9(10^4)$	0.064	$2.3(10^5)$	0
	$Ru(NH_3)_5py^{3+}$	$1.94(10^5)$	0.10	19.5/3.5	0/0	3/2	$1.94(10^5)$	$1.7(10^4)$	0.069	$1.6(10^5)$	0.1
	$Co(phen)_3^{3+}$	$1.8\ (10^5)$	0.10	19.5/7	0/0	3/2	$1.8\ (10^5)$	$9.8(10^1)$	0.186	$3.3(10^5)$	-0.1
plastocyanin (*Phaseolus vulgaris*)	$Fe(EDTA)^{2-}$	$8.2\ (10^4)$	0.10	15.8/4	-9/-10	-2/-1	$2.88(10^5)$	$6.9(10^4)$	0.230	$1.5(10^2)$	2.6
	$Ru(NH_3)_5py^{3+}$	$7.1\ (10^3)$	0.50	15.8/3.5	-10/-9	3/2	$3.88(10^3)$	$1.7(10^4)$	-0.097	$4.3(10^4)$	0.6
	$Co(phen)_3^{3+}$	$4.9\ (10^3)$	0.10	15.8/7	-10/-9	3/2	$4.9\ (10^3)$	$9.8(10^1)$	0.020	$1.2(10^4)$	1.0
azurin (*Pseudomonas aeruginosa*)	$Fe(EDTA)^{2-}$	$1.3\ (10^3)$	0.20	17.2/4	-1/-2	-2/-1	$1.39(10^3)$	$6.9(10^4)$	0.184	$2.8(10^{-2})$	5.5
	$Ru(NH_3)_5py^{3+}$	$2.0\ (10^3)$	0.10	17.2/3.5	-2/-1	3/2	$1.36(10^3)$	$1.7(10^4)$	-0.051	$1.1(10^3)$	1.9
	$Co(phen)_3^{3+}$	$3.2\ (10^3)$	0.20	17.2/7	-2/-1	3/2	$2.82(10^3)$	$9.8(10^1)$	0.066	$7.0(10^3)$	1.2
HiPIP (*Chromatium vinosum*)	$Fe(EDTA)^{2-}$	$1.7\ (10^3)$	0.10	15.5/4	-2.5/-3.5	-2/-1	$2.44(10^3)$	$6.9(10^4)$	0.230	$1.5(10^{-2})$	5.8
	$Ru(NH_3)_6^{2+}$	$3.1\ (10^5)$	0.10	15.5/3	-2.5/-3.5	2/3	$2.04(10^5)$	$2.5(10^5)$	0.299	$2.0(10^0)$	4.0
	$Ru(NH_3)_5py^{3+}$	$1.1\ (10^3)$	0.50	15.5/3.5	-3.5/-2.5	3/2	$8.83(10^2)$	$1.7(10^4)$	-0.072	$2.5(10^3)$	1.6
	$Co(phen)_3^{3+}$	$2.8\ (10^3)$	0.10	15.5/7	-3.5/-2.5	3/2	$1.70(10^3)$	$9.8(10^1)$	0.020	$1.8(10^4)$	0.9
ferredoxin (spinach)	$Fe(EDTA)^{2-}$	$2.9\ (10^5)$	0.10	15.7/4	-17.5/-16.5	-1/-2	$9.96(10^5)$	$6.9(10^4)$	0.548	$1.8(10^{-1})$	4.9

is expected to be more apparent in their reactions with these proteins. A similar range of distances might be expected for Mb and Hb, but data on their reactions with hydrophobic reagents are not available.

If complexes with hydrophilic ligand structures do transfer electrons from the surface of the proteins with which they are reacted, then it might be expected that the calculated ΔR_p values from their reaction with a given protein may approximate the distance from the active site to the surface of the protein. Comparison of the calculated ΔR_p values with metal site-protein surface distances from protein crystallographic data would, therefore, provide some indication of how well our calculations correspond to physical measurements. Unfortunately, the apparent simplicity of such comparisons is deceptive. The primary problem is that in most cases, the two points between which the distance is to be determined are relatively ill-defined. In many cases, electron transfer may not occur at the metal atom but at some point along the perimeter of an extended, π-conducting ligand. The extreme example of this would be heme proteins wherein electron transfer may proceed by a heme edge mechanism. The definition of the protein surface, however, is even more uncertain. In principle, it would be desirable to consider an imaginary average surface described by the protein atoms that are most exposed to the solvent. As crystallographic data are not presented in this form, it is necessary to rely on careful examination of the molecular models to estimate these features of protein structure. Our attempts at such an analysis are of varying quality. The following

suggested values represent the approximate distance from the "surface" of the indicated proteins to the nearest atom that is contiguous with the metal center: cytochrome *c*, 2 Å; HiPIP, 5 Å; Mb and Hb, 4-5 Å. although the three-dimensional structure of plastocyanin has recently been determined, we are unable to make a reasonable guess of the distance of interest from the published information. Considering the uncertainty in the value of R_p discussed above, the kinetically determined values appear to agree (within experimental error) with the crystallographic data.

The discussion to this point has only considered reactions that do not demonstrate kinetically detectable precursor complex formation. Although precursor complex formation is regarded as a general feature of these reactions,[44] kinetically detectable precursor complex formation is relatively unusual (*i.e.*, the stability constant of the complex is usually too small to detect given the limited ranges of measurable rate constants and accessible reagent concentrations). Unequivocal demonstration of precursor complex formation requires more evidence than is usually presented. The most frequently cited basis for suggesting precursor complex formation is rate saturation at high concentrations of reagent; however, other mechanisms may also account for such behavior,[45] and these are frequently difficult to rule out.

The most carefully documented example of precursor complex formation is the ferricytochrome *c*-$Fe(CN)_6^{4-}$ reaction. Miller and Cusanovich first detected rate saturation for this reaction that is

consistent with a stability constant of ca. $3.0(10^2)$ M^{-1} (μ = 0.1 M, pH = 7.0).[46] Independent demonstration of $Fe(CN)_6^{4-}$ binding to cytochrome c was provided by the equilibrium dialysis study of Stellwagen and Cass that indicated an association constant comparable to that determined from the kinetics analysis.[47]

Using the stellacyanin-based relationship of equation (3-17) and the following parameter values: $k_{et} \simeq 1.3\ (10^2)\ s^{-1}$ [48] (k_{12}^{est} = 1.3 $M^{-1}\ s^{-1}$); $k_{22}^{\infty} = 4.6(10^5)\ M^{-1}s^{-1}$; $\Delta E° = -0.16$ V, gives a calculated ΔR_p of 6.4 Å ($k_{11}^{\infty} = 2.3(10^{-3})\ M^{-1}\ s^{-1}$). Ideally, a similarly well-defined case involving intramolecular electron transfer over a known distance should be used to obtain a relationship similar to equation (3-17) for use with reactions of this type. At present, however, no reaction involving a kinetically detectable precursor complex has been characterized in such detail. Without this type of information, it is difficult to evaluate how reasonable the calculated value of R_p is. However, Potasek and Hopfield have used excitation modulation spectroscopy to detect a charge-transfer band in the iron hexacyanide/cytochrome c complex from which they estimate that the total intersite distance is 7-10 Å.[20] The present calculation is remarkably consistent with their estimate.

REFERENCES AND NOTES

1. D. DeVault and B. Chance, Biophys. J., 6, 825 (1966).
2. D. DeVault, J. H. Parkes, and B. Chance, Nature, 215, 642 (1967).
3. B. Chance and M. Nishimura, Proc. Natl. Acad. Sci (USA), 46, 19 (1960).
4. W. Arnold and R. K. Clayton, Proc. Natl. Acad. Sci (USA), 46, 769 (1960).
5. F. Hund, Z. Physik., 43, 805 (1927).
6. G. Gamow, Z. Physik., 51, 204 (1928).
7. J. R. Oppenheimer, Phys. Rev., 13, 66 (1928).
8. R. A. Marcus and N. Sutin, Inorg. Chem., 14, 213 (1975).
9. S. Wherland and H. B. Gray, in "Biological Aspects of Inorganic Chemistry," A. W. Addison, W. Cullen, B. R. James, and D. Dolphin, eds., Wiley, New York, 1977, p. 289.
10. R. A. Holwerda, S. Wherland, and H. B. Gray, Ann. Rev. Biophys. Bioeng., 5, 363 (1976).
11. S. Wherland and H. B. Gray, Proc. Natl. Acad. Sci. (USA), 73, 2950 (1976).
12. S. Wherland, Ph.D. Thesis, California Institute of Technology, Pasadena, California, 1977.
13. D. DeVault, 6th International Biophysics Congress, Kyoto, Vanity, 1978, in press.
14. J. Franck, Trans. Far. Soc., 21, 536 (1926).
15. E. U. Condon, Phys. Rev., 28, 1182 (1926).

16. E. U. Condon, Phys. Rev., 32, 858 (1928).

17. W. L. Reynolds and R. W. Lumry, "Mechanisms of Electron Transfer," Ronald Press, New York, 1966, p. 11.

18. R. A. Marcus, J. Chem. Phys., 43, 679 (1965).

19. Ref. 17, p. 76.

20. J. J. Hopfield, Proc. Natl. Acad. Sci. (USA), 71, 3640 (1974).

21. L. N. Grigorov and D. S. Chernavskii, Biophysics (USSR), 17, 202 (1972).

22. R is the width of the barrier in Fig. 3-2 and differs from r_{da}.

23. J. Jortner, J. Chem. Phys., 64, 4860 (1976).

24. K. Huang and A. Rhys, Proc. Roy. Soc., A204, 406 (1950).

25. V. G. Levich, Adv. Electrochem. Electrochem. Eng., 4, 249 (1966).

26. V. G. Levich, "Physical Chemistry, An Advanced Treatise," Vol. 93, H. Eyring, D. Henderson, and W. Jost, eds., Academic, New York, 1970, p. 985.

27. V. G. Levich and R. R. Dogonadze, Dokl. Akad. Nauk. SSSR, 124, 123 (1959).

28. V. G. Levich and R. R. Dogonadze, Collect. Czech. Chem. Commun., 26, 193 (1961).

29. J. J. Hopfield, in "Electrical Phenomena at the Biological Membrane Level," E. Roux, ed., Elsevier, Amsterdam, 1977, p. 471.

30. T. Förster, Naturwissenschaften, 33, 166 (1946).

31. J. R. Miller, J. Chem. Phys., 56, 5173 (1972).

32. B. Brocklehurst, Chem. Phys., 2, 6 (1973).

33. S. A. Rice and M. J. Pilling, Prog. Reaction Kinet., 9, 93 (1978).

34. These properties have been discussed by several authors[20,21,23,28] but have been presented most recently by Hopfield as follows:

$$C = P\left(\frac{2\pi}{\hbar}\right)\left(2\pi\sigma^2\right)^{-1/2} \exp\left|\frac{-(E_a - E_b - \Delta)^2}{2\sigma^2}\right|$$

$$\text{where, } \sigma^2 = \Delta k_B T_a \coth(T_a/2T)$$

In this notation, the following definitions pertain: (1) Δ is the vibronic coupling parameter and reflects the shape of the potential energy surface for a reaction center. One major contribution to Δ is the Franck-Condon activation barrier for the site. (2) T_a is the characteristic temperature. $T_a/2$ is the temperature at which electron transfer becomes thermally activated. (3) $E_a - E_b$ is the potential difference between the sites. (4) T is the temperature at which the rate is to be determined. (5) P is a collision frequency factor and contributes to C only in the case of bimolecular reactions. (k_B is Boltzmann's and $\hbar$ Planck's constants.)

35. J. C. W. Chien and L. C. Dickinson, J. Biol. Chem., 253, 6965 (1978).

36. J. C. W. Chien, H. L. Gibson, and L. C. Dickinson, Biochemistry, 17, 2579 (1978).

37. J. C. W. Chien, J. Phys. Chem., 82, 2158 (1978).

38. R. A. Marcus, J. Phys. Chem., 67, 853 (1963).

39. In terms of the Hopfield formalism, use of the protein self-exchange rate constant fulfills the assumption of equivalent sites. Furthermore, because this stratagem removes dependence of the rate on the kinetic properties of the inorganic complex it eliminates the uncertainty in the values of the parameters (see note 35) that describe the small molecule site characteristics.

40. It must be remembered in all comparisons made here that R_p is only part of the total distance of electron transfer. Because R_r is presumably smaller than R_p, it is generally expected that $R_p < R < 2R_p$.

41. Estimated from the non-bonded C-C distance in graphite of 3.35 Å. (F. A. Cotton and G. Wilkinson,"Advanced Inorganic Chemistry," ed. 2, 1966, p. 297.

42. N. Sailasuta, F. C. Anson, and H. B. Gray, J. Am. Chem. Soc., 101, 455 (1979).

43. Even though the apoprotein does not impose any protein-reagent interactions on the kinetics of the blue copper center in stellacyanin, it does limit the surface area of the copper center that is available for reaction. This statistical factor is a major determinant of the absolute magnitude of k_{11}^{∞}. Sutin has treated this effect in detail for cytochrome *c* by showing that the self-exchange rate of this cytochrome ($\sim 10^3\ M^{-1}\ s^{-1}$) compared to that of $Fe(phen)_3^{3+}$ ($\sim 10^7\ M^{-1}\ s^{-1}$) is consistent with crystallographic data showing that about 3% of the porphyrin surface is available for electron transfer (N. Sutin, in "Bioinorganic Chemistry-II,"

Amer. Chem. Soc. Advances in Chemistry Series #162, K. N. ed., 1977, p. 156). A similar comparison of the self-exchange rate of stellacyanin (~10^5 M^{-1} s^{-1}) with that of $Fe(phen)_3^{3+}$ (~10^7 M^{-1} s^{-1}) would suggest that roughly 10% of the copper center "surface" is available for electron transfer in this protein. The use of a single value of C for all calculations based on equation (3-13) implies that the same statistical factor holds for all the proteins considered. This assumption should be nearly valid for cases involving hydrophilic (non-penetrating) reagents. However, the potential ability for penetrating (hydrophobic) reagents to sample a larger relative "surface area" of a "buried" site may contribute to a larger uncertainty in the R values calculated for proteins reacting with these reagents. The penetration of such reagents may also contribute to changes in the Franck-Condon factors (which are implicitly included in the constant C) and this would also affect the validity of the R values calculated.

44. N. Sutin, in"Inorganic Biochemistry," G. I. Eichhorn, ed., Elsevier, Amsterdam, 1973, p. 611.

45. The possible mechanisms which give rise to saturation behavior have been enumerated by Holwerda, *et. al.* (G. S. Yoneda and R. Holwerda, Bioinorg. Chem., 8, 139 (1978)) as: (a) precursor complex formation, (b) rate-limiting formation of an activated form of the protein, and (c) dead-end complex formation.

46. This value of the formation constant was calculated by extrapolation (linear in $\mu^{1/2}$) of the ionic strength dependent values given by

Miller and Cusanovich (see ref. 48).

47. E. Stellwagen and R. D. Cass, J. Biol. Chem., 250, 2095 (1975).

48. W. G. Miller and M. A. Cusanovich, Biophys. Struct. Mechanism , 1, 97 (1975).

PROPOSITIONS

PROPOSITION I

Copper EXAFS of Non-Blue Copper Proteins - Amine Oxidases

INTRODUCTION

The diversity of coordination chemistry displayed by copper in biological systems makes the copper metalloproteins particularly important in the examination of structure-function relationships. The study of the "blue" (or Type I) copper center has received the most attention lately and the insight gained into the structure of this type of site has been substantial.[1-3] However, many copper-containing enzymes exhibit a more "normal" copper environment (as exhibited by larger $A_{||}$ values and weaker visible absorption bands compared to Type I) and can be collectively termed non-blue copper proteins. The Type II copper found in the multicopper oxidases (*e.g.*, laccase, ceruloplasmin, ascorbate oxidase) can be considered as a non-blue copper, but as pointed out by Fee,[1] this general class of protein-bound copper is chemically quite diverse. It is just this diversity that makes it important to examine the structural characteristics of the copper sites in these non-blue copper proteins.

To date, very little structural information has been obtained on any non-blue copper centers mainly due to a lack of applicable spectroscopic techniques. Recent progress in application of the Extended X-ray Absorption Fine Structure (EXAFS) has allowed this technique to become a powerful tool for the examination of the molecular framework of the metal centers in metalloproteins. The ability of this technique to provide de-

tailed structural information about the local environment of protein metal sites makes it ideal for the proposed work. The goal of this work is to initiate a study of non-blue copper protein centers with examination of a series of copper-containing amine oxidases.

The amine oxidases in general catalyze the oxidation of an amine to the corresponding aldehyde using O_2 as the oxidant:

$$RCH_2NH_2 + O_2 + H_2O \longrightarrow RCHO + NH_3 + H_2O_2$$

The substrate (amine) specificities of the various enzymes in this class are the basis for the nomenclature used. Classically, the diamine oxidases were specific for diamines and the monoamine oxidases for monoamines, although a nomenclature system has been suggested which is based on inhibitor reactivities.[4] Most of the copper-containing proteins belong to the class of amine oxidases which are sensitive to carbonyl reagents and thus are believed to have some type of carbonyl-containing prosthetic group. Five different copper-containing amine oxidases are of interest. They include two kinds of diamine oxidases (EC 1.4.3.6, diamine:O_2 oxidoreductase (deaminating)), one from pig kidney, the other from plant sources (the most commonly studied is the DAO from pea seedling); two kinds of monoamine oxidases (EC 1.4.3.4, monoamine:O_2 oxidoreductase (deaminating)), one from the plasma of non-ruminant mammals (*e.g.*, pig), the other from microorganisms (*e.g.*, *Aspergillus niger*); and a spermine oxidase (EC 1.5.3.3, spermine:O_2 oxidoreductase (donor cleaving)) from the plasma of ruminant mammals (*e.g.*, beef). The monoamine oxidase from

pig plasma is more commonly referred to as benzylamine oxidase.[4]

These five amine oxidases have much in common but also exhibit minor spectral and structural differences in addition to the variation in substrate specificities inherent in their subclassification. It appears that each enzyme is made up of two (or three in the *A. niger* AO) identical or closely similar subunits (of ~90,000 molecular weight) held together rigidly[5] by disulfide bonds.[6,7] Each subunit probably contains one copper. In the pig plasma benzylamine oxidase, the two coppers appear inequivalent by electron paramagnetic resonance (epr) spectroscopy.[8] The stoichiometry and identity of the organic prosthetic group is less well determined. Titrations with substrates and inhibitors have led to separate findings of one[9-14] or more[15-18] active carbonyl groups. Pyridoxal phosphate has most often been suggested as the organic prosthetic group but it is apparently difficult to extract from these enzymes and evidence both in support of[16,19-22] and against[11,23-27] the presence of pyridoxal phosphate has been presented.

Anaerobic addition of substrate leads to reduction of the enzyme accompanied by immediate release of the product aldehyde suggesting a mechanism involving initial Schiff base formation followed by immediate hydrolysis of the substrate-enzyme complex.[28] However, the reduced enzyme shows no reduction of the Cu(II) epr signal[14,22,23,29-31] although changes in the signal shape of at least one of the coppers are evident.[12,14,32,33] Thus, the amine substrate probably does not bind directly to the copper[29] but there is some evidence (in the pig kidney DAO)

that a low-affinity substrate binding site exists very near the copper[34] and is responsible for substrate inhibition at high substrate concentrations.[34,35]

Though the copper centers are not significantly reduced during the catalytic cycle, they can be reduced (and reoxidized by O_2) in the presence of exogenous reductants such as dithionite.[22,29] The copper is generally believed to play a role in the O_2 reoxidation of the substrate-reduced enzyme (*e.g.*, ref. 28) perhaps acting as the O_2-binding site and an electron-shuttle. The O_2-reoxidation step is probably the rate-limiting step for enzymatic turnover[12,28] and there is evidence (in the pig kidney DAO) for involvement of the superoxide anion.[36,37]

Evidence has been presented for the involvement of solvent-accessible water as a possible copper ligand.[8,34] Nitrogen ligands may also be involved since N superhyperfine has been observed in the epr spectrum of the pig kidney enzyme.[38] In studies with the beef plasma amine oxidase, one histidine per subunit was determined to be essential for substrate binding[6] but the involvement of this histidine as a copper ligand was not explored. The copper does bind external ligands (inhibitors) such as cyanide and azide as indicated by effects on the epr[28,39] and the circular dichroism[40] spectra. The binding of these ligands appears to make the coppers in the pig plasma enzyme epr-equivalent.[8]

Although little is known about the structure of the prosthetic group(s) of these enzymes, the catalytic role of the copper makes it reasonable to expect that it would be bound

somewhere near the substrate-binding site (*e.g.*, pyridoxal phosphate). There have been suggestions that pyridoxal phosphate may be part of the coordination sphere of copper. This would explain the observation of fluorescence only after removal of the copper from the pig kidney enzyme.[41] The analogy between binding of copper to the pyridine nitrogen of pyridoxal and metal-binding to N(5) of flavins has been mentioned.[35] Other workers prefer a structure with copper chelated by the phenolic oxygen and the imine nitrogen of the Schiff base form of the carbonyl group.[19,36] The two most likely possibilities are illustrated in the figure.

PROPOSED EXPERIMENTS

For each enzyme, a general outline of appropriate derivatives to be examined is given below. Initially, work will be performed on a crystalline preparation of pig plasma benzylamine oxidase, followed by a study of the pig kidney diamine oxidase (also obtainable in crystalline form). Future work on the other enzymes will be obvious extensions of the presently proposed study. Since the argument as to whether any of the copper-containing enzymes also contain pyridoxal phosphate is still unsettled (the beef plasma and pea seedling enzymes are the only ones which have apparently been shown to be devoid of this prosthetic group), comparisons between different types of copper-containing amine oxidases will be of particular interest. If the pyridoxal phosphate content among these enzymes

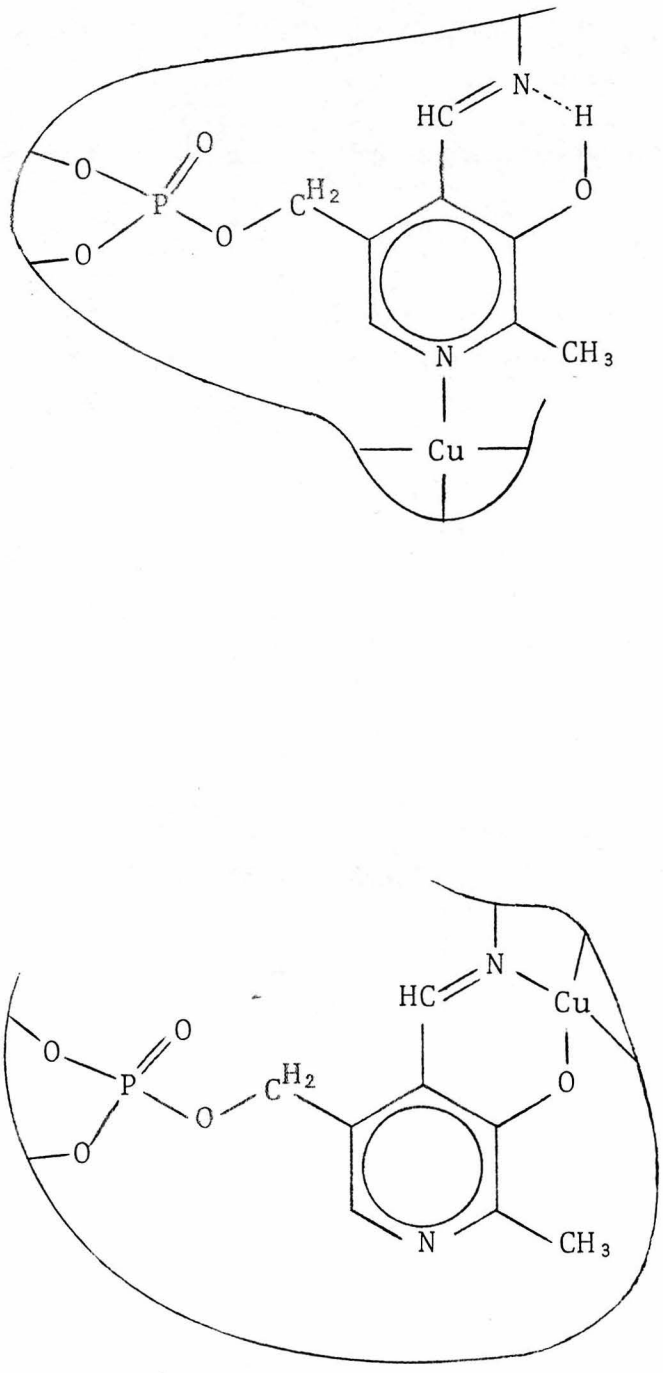


Figure. Two possible structures for a Cu(II)-pyridoxal phosphate prosthetic group

is variable, the copper ligand environment may reflect these differences. Appropriate model compounds will also be examined as detailed below. In all cases, parallel epr and optical absorption studies will be carried out to completely characterize the species involved.

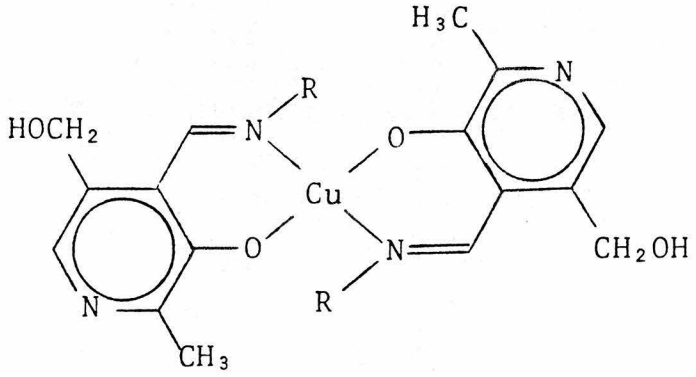
Enzymes. Examination of the copper edge and EXAFS of several derivatives of each enzyme is proposed: (1) the native (Cu(II)) oxidized enzyme will be studied for comparison with the other derivatives; (2) since the anaerobic addition of substrate results in reduction of the organic prosthetic group and changes the copper epr signal,[14,32,33] examination of this substrate-reduced enzyme derivative should help settle the question of involvement of the copper in substrate-binding. The choice of substrate will depend on the particular enzyme involved, the most active substrate being used (*e.g.*, benzylamine for the pig plasma enzyme, putrescine or cadaverine for the pig kidney enzyme, etc.); (3) substrate-inhibition at high substrate concentrations may involve the copper site.[34] Thus, examination of the anaerobically substrate-reduced enzyme in the presence of a high concentration of substrate will be performed; (4) the report that azide or cyanide binding renders the coppers equivalent in the pig plasma enzyme[8] makes it imperative to examine these derivatives (in the oxidized state); (5) finally, the dithionite-reduced (Cu(I)) enzyme will be examined to determine any oxidation state dependent changes in the copper coordination sphere.

Model Compounds. Several model compounds will also be

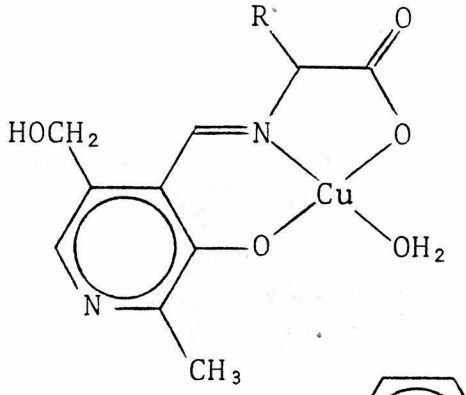
synthesized and their Cu EXAFS studied for comparison with the enzymes. Efforts will be concentrated on known Cu(II) complexes with various pyridoxal Schiff base ligands and analogs with mainly nitrogen and oxygen donor atoms. The syntheses of a series of $Cu(II)L_2$ complexes where L is a Schiff base of pyridoxal and various primary amines have been reported.[42] The Cu(II) complex of the Schiff base with aminomethane (I, $R=CH_3$) will be synthesized and examined by both epr and EXAFS.

Cu(II) complexes (II) of Schiff bases of pyridoxal with various amino acids have also been synthesized and found to have 1:1 stoichiometry with coordination by the carboxylate oxygen as well as one water molecule.[43] These authors concentrated on the Schiff base with valine, but claim that the synthesis works as well for other amino acids. The glycine adduct (II, R=H) will be synthesized and examined.

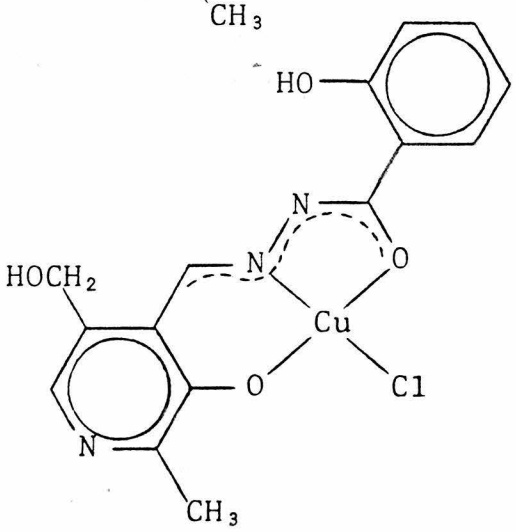
Pyridoxal can also form hydrazones and the 1:1 Cu(II) complex (III) with pyridoxal salicyloylhydrazone has recently been reported.[44] This complex may also be of interest as a possible model for the amine oxidase active site. Other Cu(II) complexes with N donor atoms have already been studied by EXAFS in the laboratory of Prof. K. O. Hodgson and these data will be available for comparison as well.



I



II



III

REFERENCES

1. J. A. Fee, Struct. Bonding (Berlin), 23, 1 (1975).
2. H. B. Gray, C. L. Coyle, D. M. Dooley, P. J. Grunthaner, J. W. Hare, R. A. Holwerda, J. V. McArdle, D. R. McMillin, J. Rawlings, R. C. Rosenberg, N. Sailasuta, E. I. Solomon, P. J. Stephens, S. Wherland, and J. A. Wurzbach, in "Bioinorganic Chemistry-II," Adv. Chem. Ser., vol. 162, K. N. Raymond, ed., Am. Chem. Soc., 1977, p. 145.
3. T. D. Tullius, P. Frank, and K. O. Hodgson, Proc. Natl. Acad. Sci. (USA), 75, 4069 (1978).
4. R. Kapeller-Adler, "Amine Oxidases and Methods for Their Study," Wiley-Interscience, London, 1970, p. 28.
5. J. B. Massey and J. E. Churchich, Biophys. Chem., 9, 157 (1979).
6. S. Tsurushiin, A. Hiramatsu, M. Inamasu, and K. T. Yasunobu, Biochim. Biophys. Acta, 400, 451 (1975).
7. H. Suzuki, Y. Ogura, H. Yamada, and K. Arima, Biochim. Biophys. Acta, 403, 23 (1975).
8. R. Barker, N. Boden, G. Cayley, S. C. Charlton, R. Henson, M. C. Holmes, I. D. Kelly, and P. F. Knowles, Biochem. J., 177, 289 (1979).
9. A. Lindström and G. Pettersson, Eur. J. Biochem., 34, 564 (1973).
10. A. Lindström and G. Pettersson, Eur. J. Biochem., 83, 131 (1978).
11. J. B. Massey and J. E. Churchich, J. Biol. Chem., 252, 8081 (1977).

12. J. Grant, I. Kelly, P. Knowles, J. Olsson, and G. Pettersson, Biochem. Biophys. Res. Commun., 83, 1216 (1978).

13. S. Oi, M. Inamasu, and K. T. Yasunobu, Biochemistry, 9, 3378 (1970).

14. U. Nylén and P. Szybeck, Acta Chem. Scand., B28, 1153 (1974).

15. F. Buffoni and G. Ignesti, Biochem. J., 145, 369 (1975).

16. H. Blaschko and F. Buffoni, Proc. Roy. Soc., London, Ser. B, 163, 45 (1965).

17. F. Buffoni, in "Pyridoxal Catalysis: Enzymes and Model Systems," E. E. Snell, A. E. Braunstein, E. S. Severin, and Y. M. Torchinsky, eds., Interscience, New York, 1968, p. 363.

18. H. Suzuki, Y. Ogura, and H. Yamada, J. Bicohem., 69, 1065 (1971).

19. F. Buffoni and L. Della Corte, Adv. Biochem. Psychoparmacol., 5, 133 (1972).

20. B. Olsson, J. Olsson, and G. Pettersson, Eur. J. Biochem., 71, 375 (1976).

21. E. V. Goryachenkova, L. I. Shcherbatiuk, and C. I. Zamaraev, in "Pyridoxal Catalysis: Enzymes and Model Systems," E. E. Snell, A. E. Braunstein, E. S. Severin, and Y. M. Torchinsky, eds., Interscience, New York, 1968, p. 391.

22. H. Yamada, O. Adachi, and K. Ogata, *ibid.*, p. 347.

23. R. H. Suva and R. H. Abeles, Biochemistry, 17, 3538 (1978).

24. R. Neumann, R. Hevey, and R. H. Abeles, J. Biol. Chem., 250, 6362 (1975).

25. M. Inamasu, K. T. Yasunobu, and W. A. Konig, J. Biol. Chem., 249, 5265 (1974).

26. K. Watanabe, R. A. Smith, M. Inamasu, and K. T. Yasunobu, Adv. Biochem. Psychopharmacol., 5, 107 (1972).

27. J. M. Hill, Biochem. J., 104, 1048 (1967).

28. B. Olsson, J. Olsson, and G. Pettersson, Eur. J. Biochem., 87, 1 (1978).

29. F. Buffoni, L. Della Corte, and P. F. Knowles, Biochem. J., 106, 575 (1968).

30. A. Lindström, B. Olsson, and G. Pettersson, Eur. J. Biochem., 35, 70 (1973).

31. B. Mondovì, M. T. Costa, A. Finazzi Agrò, and G. Rotilio, in "Pyridoxal Catalysis: Enzymes and Model Systems," E. E. Snell, A. E. Braunstein, E. S. Severin, and Y. M. Torchinsky, eds., Interscience, New York, 1968, p. 403.

32. A. Lindström, B. Olsson, and G. Pettersson, Eur. J. Biochem., 42, 177 (1974).

33. B. Mondovì, Adv. Biochem. Psychopharmacol., 5, 181 (1972).

34. M. D. Kluetz and P. G. Schmidt, Biochemistry, 16, 5191 (1977).

35. E. A. Zeller, Adv. Biochem. Psychopharmacol., 5, 167 (1972).

36. M. Younes and U. Weser, Biochim. Biophys. Acta, 526, 644 (1978).

37. G. Rotilio, L. Calabrese, A. Finazzi Agrò, and B. Mondovì, Biochim. Biophys. Acta, 198, 618 (1970).

38. B. Mondovì, G. Rotilio, M. T. Costa, A. Finazzi Agrò, E. Chiancone, R. E. Hansen, and H. Beinert, J. Biol. Chem., 242, 1160 (1967).

39. A. Lindström, B. Olsson, and G. Pettersson, Eur. J. Biochem., 48, 237 (1974).

40. H. Ishizaki and K. T. Yasunobu, Adv. Exp. Med. Biol., 74, 575 (1976).

41. A. Finazzi Agrò, P. Guerrieri, M. T. Costa, and B. Mondovì, Eur. J. Biochem., 74, 435 (1977).

42. S. Yamada, Y. Kuge, and T. Yamayoshi, Inorg. Chim. Acta, 8, 29 (1974).

43. H. N. Christensen, J. Am. Chem. Soc., 79, 4073 (1957).

44. M. Nardelli, C. Pelizzi, and G. Predieri, Transition Met. Chem., 3, 233 (1978).

PROPOSITION II

Selenium Protein EXAFS

INTRODUCTION

Selenium is now known to be an essential micronutrient not only in microorganisms, but also in higher forms of life. It was not until 1973 that the specific requirement for selenium in mammals was found to be localized in the glutathione peroxidase of erythrocytes.[1] Only three other examples of selenium-containing proteins are known: formate dehydrogenase of *Escherichia coli* and several *Clostridium* species,[2-4] protein A of glycine reductase (from *Clostridium*),[5-7] and a poorly characterized low molecular weight muscle selenoprotein isolated from ovine sources.[8,9] Very little information is available on the nature or function of the muscle selenoprotein and for this reason, it is not considered in this proposal. (For a recent review, see ref. 10).

Although the exact nature of the selenium moiety incorporated into these proteins is still unknown, the selenium does appear to undergo oxidation-reduction during the catalytic cycle (at least, in the case of glutathione peroxidase and glycine reductase[6,11-13]) and thus is implicated as having an important role in the activity of the enzymes. In order to elucidate the role of selenium in the catalytic cycles of these enzymes, it will be necessary to gain further information about the structure of the selenium moiety in both the oxidized and reduced states. The goal of the work proposed herein is to use the

technique of Extended X-ray Absorption Fine Structure (EXAFS) to yield structural information on these selenium proteins.

Glutathione Peroxidase. Glutathione peroxidase (glutathione:H_2O_2 oxidoreductase, EC 1.11.1.9) has been isolated from the erythrocytes of several mammals (including humans) and is also found in the liver.[14] In all cases, the enzyme is found to consist of four identical (or nearly identical) subunits, each of ~19,000-23,000 molecular weight[11,14-16] and each containing one selenium.[11,14,15] Neutron activation analysis can detect no metals associated with the enzyme other than selenium[15] and the absorption spectrum shows no indication of the presence of heme or flavin.[14]

Glutathione peroxidase catalyzes the following oxidation-reduction reaction:

$$\underset{\text{(glutathione)}}{2\ GSH} + ROOH \longrightarrow GSSG + H_2O + ROH$$

(R may be H) and the enzyme can be prepared in oxidized (in the presence of H_2O_2) and reduced (in the presence of GSH) states. This redox change was shown to be localized in the selenium moiety by X-ray photoelectron spectroscopic (XPS) studies[12] and by studies showing that the selenium was protected from extraction by cyanide only in the reduced state.[17] The reduced enzyme can be alkylated by iodoacetate and analysis of the hydrolytic fragments of the alkylated enzyme provides support for the existence of selenocysteine in the reduced enzyme.[13] The presence of two free sulfhydryl (presumably cysteinyl) groups per subunit in the isolated (reduced) enzyme[14] makes the formation of a seleno-sulfide bridge (upon

oxidation) an attractive possibility. However, the XPS results were interpreted in terms of the existence of a Se-O bond in the oxidized form.[12] The actual structure of the oxidized selenium species in glutathione peroxidase should be considered still open for debate and it is hoped that the work proposed below will provide an answer to this question.

Glycine Reductase. Selenite is required for development of glycine reductase activity in many clostridial bacteria (*e.g.*, *C. sticklandii*, *C. lentoputrescens*).[5] The glycine reductase activity:

$$H_2NCH_2COOH + R(SH)_2 + P_i + ADP \longrightarrow CH_3COOH + NH_3 + R\begin{matrix}S\\|\\S\end{matrix} + ATP$$

is dependent on the incorporation of one selenium into a 12,000 molecular weight protein (Protein A) which is as essential component of the glycine reductase system.[5,6,10] When *Clostridium sticklandii* is grown on selenite, Protein A represents 0.14 % of the total soluble protein[10] and can be easily isolated from the other components of the glycine reductase complex.[5-7]

The selenium moiety of Protein A has been shown (by iodoacetamide alkylation) to be a selenocysteine[7] and Protein A shows remarkable similarity to the subunits of glutathione peroxidase in having two sulfur-cysteine groups in addition to the selenocysteine.[18] In the presence of air, Protein A exists in the oxidized state in which the cysteines and selenocysteine are not titratable, but anaerobic reduction by natural or artificial dithiol substrates (*e.g.*, dithiothreitol) or by KBH_4 results in reduction to the -SH and ionized $-Se^-$ forms.[7,10,18,19] The oxidation state of selenium can be monitored by the ultra-

violet absorption (at 238 nm) of this -Se^- group.[7,18] As in the case of glutathione peroxidase, the possibility of formation of a seleno-sulfide bridge upon air oxidation is intriguing.

Formate Dehydrogenase. Both selenium and molybdenum were shown to be required nutrients for formation of bacterial formate dehydrogenase (EC 1.2.2.1) activity in *E. coli* in 1954.[10] The requirement for selenium has since been shown to be specific for selenite or selenocysteine (not selenate or selenomethionine)[2,20-22] and is specifically involved in anaerobic formate-nitrate metabolism in *E. coli* as well as several *Clostridium* species.[10,21] Use of $^{75}SeO_3^{2-}$ in the growth medium results in specific uptake of ^{75}Se into formate dehydrogenase[3,20] which is isolated as a very large (~600,000 daltons) membrane-bound enzyme.[4] The enzyme contains four hemes per mole and probably exists as a tetramer of ~154,000 dalton units, each unit being separable into α(110,000), β(32,000), and perhaps γ(20,000) subunits.[4] The enzyme also contains (on a per heme basis) one molybdenum, one selenium, 14 non-heme irons, and 13 acid-labile sulfides with the selenium being localized in the largest (α) subunit.[4,10] The inability of selenomethionine to induce formate dehydrogenase activity suggests that the selenium is again present as selenocysteine and preliminary studies on formate dehydrogenase from *C. sticklandii* have provided supporting evidence.[10] The complexity of this enzyme has so far precluded a detailed elucidation of the catalytic mechanism or the redox role of the selenium. It had been speculated[5]

that the similarities between the selenium in formate dehydrogenase and that in glycine reductase may suggest a common protein unit (cofactor) but the localization of selenium in the 110,000 dalton subunit of formate dehydrogenase makes this assessment unrealistic. There is some debate as to whether the selenium is acid labile or not[3,4] which may have some bearing on the possible participation of the selenium in an Fe- or Mo- cluster. Whether or not the selenium interacts closely with Mo or Fe should be easily decided by the type of study proposed below.

PROPOSED EXPERIMENTS

Enzymes. The involvement of oxidation-reduction of selenium in the catalytic mechanisms of at least two of the enzymes discussed above makes it imperative to study both the oxidized and reduced forms of each enzyme (or protein). In addition, a study of some inhibited derivatives will be helpful in probing the role of the selenium. Thus, examination of the selenium edge and EXAFS of the following protein derivatives is proposed:

(1) Reduced glutathione peroxidase - as isolated (in crystalline form[15]) from bovine erythrocytes, glutathione peroxidase is most stable in its reduced form.[23] A slight excess of glutathione or other mercaptan will serve to maintain the enzyme reduced in the presence of air (and absence of H_2O_2).

(2) Oxidized glutathione peroxidase - addition of excess H_2O_2 results in oxidation of the enzyme (and apparently the selenium).[12]

(3) Cu^{2+}-inhibited glutathione peroxidase - the addition of Cu^{2+} (and some other metal ions) to glutathione peroxidase has been shown to completely inactivate the enzyme.[16] If this inhibition is due to interaction of Cu^{2+} with the selenium, the Cu^{2+} backscattering should be easily observable in the Se EXAFS region.

(4) Oxidized Protein A - aerobic isolation of Protein A (of glycine reductase) from *C. sticklandii* results in a homogeneous oxidized preparation.[10] This native protein will be used for examination of the oxidized selenium moiety.

(5) Reduced Protein A - anaerobic reduction of Protein A by KBH_4 or by dithiothreitol results in reduction of the selenium moiety.[10] Both of these treatments will be used to examine the structure of the reduced selenoprotein.

(6) Inhibited Protein A - arsenite has been suggested to interact with a disulfide group during its inhibition of glycine reductase activity in crude extracts from *C. sticklandii*.[24] An examination of the Se EXAFS of the arsenite-treated Protein A should help determine whether the arsenite interaction site is near the selenium.

The size of the formate dehydrogenase enzyme makes the examination of the selenium EXAFS of this protein more difficult. Also, the protein (from *E. coli*) is not as easily isolated in the quantities necessary for the proposed studies.[10] However, the presence of Mo and Fe in the enzyme (and the concomitant possibility of selenium involvement in one of these metal sites) make it the most interesting of the three enzymes

considered. Thus, it is considered worth the effort to attempt an examination of the selenium EXAFS of the native formate dehydrogenase since any close interaction with Mo or Fe should be easily detectable in the EXAFS.

Model Compounds. For purposes of comparison with the proteins, several model compounds containing selenium in various environments will be examined by EXAFS. These models were chosen to be representative of Se-bonding to carbon, oxygen, and/or sulfur. In addition, all the compounds are easily prepared or purchased and were used by Wendel, *et al.*, in their XPS studies.[12] The model compounds include: selenomethionine, selenocysteine, sodium selenite ($Na_2Se_2O_3$), selenium dioxide (SeO_2), and the seleno-sulfide analog of cysteine disulfide (Cys-Se-S-Cys). Some of these models as well as others not mentioned have already been characterized by EXAFS in the laboratory of Prof. K. O. Hodgson and these data will be available for comparison.

REFERENCES

1. J. T. Rotruck, A. L. Pope, H. E. Ganther, A. B. Swanson, D. G. Hafeman, and W. G. Hoekstra, Science, 179, 588 (1973).
2. R. L. Lester and J. A. deMoss, J. Bacteriol., 105, 1006 (1971).
3. J. R. Andreesen and L. G. Ljungdahl, J. Bacteriol., 116, 867 (1973).
4. H. G. Enoch and R. L. Lester, J. Biol. Chem., 250, 6693 (1975).
5. D. C. Turner and T. C. Stadtman, Arch. Biochem. Biophys., 154, 366 (1973).
6. T. C. Stadtman, Fed. Proc., 33, 1291 (1974).
7. J. E. Cone, R. Martín del Río, J. N. Davis, and T. C. Stadtman, Proc. Natl. Acad. Sci. (USA), 73, 2659 (1976).
8. N. D. Pedersen, P. D. Whanger, P. H. Weswig, and O. H. Muth, Bioinorg. Chem., 2, 33 (1972).
9. P. D. Whanger, N. D. Pedersen, and P. H. Weswig, Biochem. Biophys. Res. Commun., 53, 1031 (1973).
10. T. C. Stadtman, Adv. Enzymol., 48, 1 (1979).
11. S.-H. Oh, H. E. Ganther, and W. G. Hoekstra, Biochemistry, 13, 1825 (1974).
12. A. Wendel, W. Pilz, R. Landenstein, G. Sawatzki, and U. Weser, Biochim. Biophys. Acta, 377, 211 (1975).
13. A. L. Tappel, J. W. Forstrom, J. J. Zakowski, D. E. Lyons, and W. C. Hawkes, Fed. Proc., 37, 706 (1978).
14. W. Nakamura, S. Hosoda, and K. Hayashi, Biochim. Biophys. Acta, 358, 251 (1974).

15. L. Flohé, W. A. Günzler, and H. H. Schock, FEBS Lett., 32, 132 (1973).

16. Y. C. Awasthi, E. Beutler, and S. K. Srivastava, J. Biol. Chem., 250, 5144 (1975).

17. J. R. Prohaska, S.-H. Oh, W. G. Hoekstra, and H. E. Ganther, Biochem. Biophys. Res. Commun., 74, 64 (1977).

18. J. E. Cone, R. Martín del Río, and T. C. Stadtman, J. Biol. Chem., 252, 5337 (1977).

19. H. Tanaka and T. C. Stadtman, J. Biol. Chem., 254, 447 (1979).

20. A. C. Shum and J. C. Murphy, J. Bacteriol., 110, 447 (1972).

21. H. G. Enoch and R. L. Lester, J. Bacteriol., 110, 1032 (1972).

22. J. Ruiz-Herrera and A. Alvarez, Antonie van Leeuwenhoek J. Microbiol. Serol., 38, 479 (1972).

23. L. Flohé, G. Loschen, W. A. Günzler, and E. Eichele, Hoppe-Seyler's Z. Physiol. Chem., 353, 987 (1972).

24. T. C. Stadtman, Arch. Biochem. Biophys., 113, 9 (1966).

PROPOSITION III

Difference EXAFS.

Studies on Copper Dimers as Models for Copper Proteins

INTRODUCTION

The structural characterization of the active sites of several copper proteins and enzymes has been the subject of much research recently (for a review, see reference 1). The single-site copper proteins (*e.g.*, plastocyanin, azurin, and stellacyanin) have received the most attention due to their simplicity. However, some of the larger copper-containing enzymes (*e.g.*, laccase, ceruloplasmin, ascorbate oxidase, hemocyanin, tyrosinase, dopamine β-monooxygenase, etc.) are of more substantial interest because of their enzymatic capabilities (*e.g.*, O_2 reduction or transport). Due to the complexity of this latter group of multi-copper enzymes, detailed structural information about the copper sites is virtually unknown. Although, in the last few years, the technique of Extended X-ray Absorption Fine Structure (EXAFS) has begun to yield useful structural information on simple metalloproteins (*e.g.*, see ref. 2), the existence of different structural types of copper in the multi-copper enzymes makes the application of the EXAFS technique to these enzymes more difficult. It is the purpose of this proposal to begin the development of new EXAFS analytical techniques designed to aid in the interpretation of EXAFS obtained from samples with two (or more) different structural types of copper (or other metal). The goal

is to eventually utilize these techniques (developed with model compounds) to help deconvolute the EXAFS of the multi-copper enzymes so that structural characteristics of individual copper sites can be ascertained.

THEORY AND STRATEGY

The EXAFS ($\equiv \chi$) of a sample containing one absorbing atom ($\equiv$ M, a metal in this particular instance) can be described as a linear combination of contributions from each group of equivalent scattering atoms ($\equiv S_i$):[3]

$$\chi_M = \sum_i N_i \chi_{MS_i}$$

where the coefficient (N_i) denotes the number of equivalent scatterers in the i-th group. χ_{MS_i} is dependent on the backscattering amplitude and phase shift of the scatterer as well as on the distance between the absorber and scatterer. In the event that the sample contains a second absorber (both absorbers being the same element) in an altered environment ($\equiv$ M'), the observed EXAFS is again an additive combination of the two components:

$$\chi_{obs} = \chi_M + \chi_{M'}$$

In the most general case, both χ_M and $\chi_{M'}$ will consist of contributions from the scatterers making up its local ligand environment ($\equiv \chi_{ML}$ and $\chi_{M'L'}$, where L denotes the ligand environment of M and L' denotes the different ligand environment of M') as well as a contribution from the other absorber acting as a scatterer ($\equiv \chi_{MM'}$ and $\chi_{M'M}$):

$$\chi_M = \chi_{ML} + \chi_{MM'}$$

$$\chi_{M'} = \chi_{M'L'} + \chi_{M'M}$$

Assuming transferrable phase shift and amplitude factors between scatterers of the same atomic number, $\chi_{MM'} = \chi_{M'M}$, and:

$$\chi_{obs} = \chi_{ML} + \chi_{M'L'} + 2\chi_{MM'}$$

The ultimate goal of the techniques to be examined is to permit separate determination of the ligand environment EXAFS of an individual absorber (*e.g.*, M) in this two-absorber sample. The strategy involves a perturbation of the M absorber site combined with appropriate spectral difference techniques. A most useful perturbation involves the substitution of the M absorber with a different metal (≡ N) such that it no longer retains its "absorber" properties (in the spectral range of interest). In this case, the new observed EXAFS ($\equiv \chi'_{obs}$) can be described as:

$$\chi'_{obs} = \chi'_{M'} = \chi_{M'L'} + \chi_{M'N}$$

Then, assuming the χ's can be properly normalized (to reflect the fact that χ'_{obs} exhibits effects from only one absorber while χ_{obs} exhibits effects from two), a "difference EXAFS" ($\equiv \Delta\chi_{obs}$) can be obtained:

$$\Delta\chi_{obs} \equiv \chi_{obs} - \chi'_{obs} = \chi_{ML} + 2\chi_{MM'} - \chi_{M'N} \qquad (1)$$

Several points concerning equation (1) should be noted. First, it may not be a trivial matter to properly normalize χ_{obs} and χ'_{obs} as mentioned above resulting in some residual (diminished) contribution of $\chi_{M'L'}$ to $\Delta\chi_{obs}$. It seems probable that an empirical normalization could be developed by initially guessing the fraction (α) of χ'_{obs} to be subtracted from χ_{obs}:

$$\Delta\chi_{obs}^{corr} \equiv \chi_{obs} - \alpha\chi'_{obs}$$

and examining the relative contributions of all the components to $\Delta\chi_{obs}^{corr}$ (perhaps in the Fourier transform). By varying α, the particular components which make up $\chi_{M'L'}$ could be identified and then α picked to minimize their contribution to $\Delta\chi_{obs}^{corr}$. Also, in the most general case (described by equation (1)), $\Delta\chi_{obs}^{corr}$ still contains residual contributions from $\chi_{MM'}$ and $\chi_{M'N}$. Since these components are due to backscattering from high-Z atoms (the metals M and N), the distinction between their contribution to $\Delta\chi_{obs}^{corr}$ and the contribution from χ_{ML} should be obvious. (In this regard, it should be noted that the $\chi_{M'N}$ contribution will occur 180° out of phase (or with a negative N_i) as an artifact of the subtraction technique.) Of course, in the special case of the M and M' sites being physically separated such that they are not observed as scatterers, the last two terms in equation (1) become zero and the analysis simplifies considerably. The effectiveness of equation (1) also depends upon the ability of N to substitute for M without appreciably affecting the ligand environment of M' (*i.e.*, $\chi_{M'L'}$ does not change and subtracts out exactly).

Another possible perturbation consists of altering the ligand environment of the M absorber (to L") by some technique (*e.g.*, a change in oxidation state). This perturbation results in the following contributions to χ'_{obs}:

$$\chi'_{obs} = \chi'_{M} + \chi_{M'} = \chi_{ML''} + \chi_{M'L'} + 2\chi_{MM'}$$

(This expression assumes that the oxidation state change does not affect the $\chi_{MM'}$ interaction.) In this case, the difference

EXAFS can be written:

$$\Delta\chi_{obs} \equiv \chi_{obs} - \chi'_{obs} = \chi_{ML} - \chi_{ML''} \qquad (2)$$

Again, an empirical normalization may be required to minimize the contribution of $\chi_{M'L'}$ to $\Delta\chi_{obs}$. Also, any change in $\chi_{MM'}$ will result in another contribution from inexact cancellation of that term. (If M and M' are well separated, this is not a problem since $\chi_{MM'}$ is negligible.) In the best possible case (*i.e.*, if the M-M' interaction is negligible or unchanged upon oxidation state change and if the ML→ML'' structural change is large enough), this difference technique has the potential of yielding structural information on both oxidation states of the M site as two out-of-phase components in $\Delta\chi_{obs}$.

Although the theoretical background behind "difference EXAFS" techniques is simple, the inherent inaccuracies involved in subtracting linear combinations of noisy damped sine waves from each other will contribute to the practical difficulties encountered. For this reason, it is imperative that such difference techniques be tried on model compounds before being employed in copper protein EXAFS analysis.

PROPOSED EXPERIMENTS

As a prelude to a study of the application of difference EXAFS techniques to model copper compounds, several symmetric Cu(II) dimers of known structure will be examined in an effort to expand the knowledge of Cu-Cu backscattering phase shifts and amplitudes in compounds which also contain Cu-N interactions. The current extent of information on Cu-Cu backscat-

tering characteristics involves EXAFS on several carboxylate-bridged Cu(II) dimers[4] with Cu-Cu distances of ~2.5-3.0 Å. Preliminary EXAFS data[5] on deoxyhemocyanin seem to indicate a Cu-Cu distance of $\gtrsim$3.0 Å and several Cu-N interactions. Since the Cu-Cu phase shift is fortuitously ~2π different from the Cu-N phase shift, further examination of known systems containing both Cu-Cu and Cu-N interactions should prove helpful in interpreting the hemocyanin data. Copper dimers containing other "biological" type ligand atoms (*e.g.*, S and O) will also be studied.

The symmetric copper dimers of interest are the following (see Table and Appendix for structural information and references): (a) the binuclear complex with Schiff base ligands derived from 3-aminopropanol and 5-chlorosalicylaldehyde ($\underset{\sim}{\underset{\sim}{\text{IX}}}$) with the coordination geometry $(NO)Cu(O_2)Cu(NO)$ and a Cu-Cu distance of 3.03 Å; (b) the binuclear complex with the 2:1 Schiff base ligand derived from 1-imido-3-aminopropane and 5-methyl-2-hydroxyisophthalaldehyde ($\underset{\sim}{\text{X}}$) with the coordination geometry $(N_2)Cu(O_2)Cu(N_2)$ and a Cu-Cu distance of 3.05 Å; (c) the binuclear complex with the macrocyclic Schiff base ligand derived from *o*-phenylenediamine and 2,6-diacetylpyridine ($\underset{\sim}{\underset{\sim}{\text{XI}}}$) with the coordination geometry $(N_3)CuCu(N_3)$ and a weakly interacting Cu-Cu pair separated by ~2.64 Å; (d) the Cu_2Co_2 complex, $[Co(en)_2(SCH_2CH_2NH_2)Cu(CH_3CN)_2]_2^{6+}$ (en=ethylenediamine) ($\underset{\sim}{\underset{\sim}{\underset{\sim}{\text{XII}}}}$) with the coordination geometry $(N_2)Cu(S_2)Cu(N_2)$ and a Cu-Cu distance of 3.15 Å (the Cu-Co distances are $\gtrsim$4 Å); and (e) the dimer formed by pairs of dichloro(1H$^+$-thiosemicarbono-

Table. Structural Characteristics of Model Compounds

Compound	M	M'	$R_{MM'}$ (Å)	Ligand environment[a] M	M'	References
IA	Cu	Cu	2.96	N_2O_2	O_4	7
B	Cu	Co	b	"	"	7
IIA	Cu	Cu	b	N_2O_2	O_4	8,9,11
B	Cu	Co	3.02	"	"	10
IIIA	Cu	Cu	b	N_2O_2	O_4	11,12,13
B	Cu	Ni	b	"	"	11,13
IVA	Cu	Cu	3.01	N_2O_2	O_2Cl_2	14,15,16
B	Cu	Co	b	"	"	16
C	Ni	Cu	b	"	"	16
VA	Cu	Cu	3.03	N_2O_2	O_6	17
B	Cu	Co	b	"	"	17
C	Ni	Cu	b	"	"	17
VI	2 Cu[c]	Cu	b	N_2O_2	O_4	16,18,19
VII	2 Cu[c]	Cu	b	N_3O	N_2O_2	20
VIII	Cu	Cu	3.54	N_4	N_2O_3	21
IX	Cu	Cu	3.03	NO_3	d	22
X	Cu	Cu	3.05	N_2O_2	d	23
XI	Cu	Cu	~2.64[b,e]	N_3(Cu)	d	11,24
XII	Cu	Cu	3.15	N_2S_2	d	25
XIII	Cu	Cu	3.96	NS_2Cl_3	d	26,27

[a]The major ligand atoms coordinated to the metals. In some cases, solvent molecules may also be involved.

[b]Structure not available.

[c]Two equivalent M sites of trimer.

[d]The M and M' sites are identical (by symmetry).

[e]Cu-Cu distance estimated in ref. 8.

hydrazidium-NS)copper(II) chloride (XIII) with the coordination geometry $(Cl_3N)Cu(S_2)Cu(Cl_3N)$ and a Cu-Cu distance of 3.96 Å.

Several unsymmetrical copper dimers of known structure are available in the literature and the EXAFS of some of these models (for copper proteins with two inequivalent sites) will be examined so that the difference techniques discussed above can be tested. The strategy to be followed will begin with examination of Cu-Cu' compounds of known structure (IA, IVA, VA, and VIII, see Table and Appendix). The structural information available will be used to fit the EXAFS with the curve-fitting techniques developed by Hodgson and coworkers.[6] Then the EXAFS describing only the ligand environment of *one* of the coppers will be simulated and the subtraction technique (equation (1)) attempted with fitting of the residual $\Delta\chi_{obs}$ to the remaining structural parameters. Variation of the amount of the simulated EXAFS subtracted will serve to indicate whether empirical normalization procedures (*e.g.*, by examination of the residual Fourier transform) will be viable.

Successful demonstration of the applicability of simple difference schemes (as described above) will then lead to examination of the EXAFS of Cu-M' heterobinuclears (IB, IVB, IVC, VB, and VC) with M' = Co or Ni. The difference techniques will then be tested using actual data for both χ_{obs} and χ'_{obs} and the ability to empirically determine the correct amount of χ'_{obs} to subtract will be checked.

Once the techniques have been thoroughly tested on compounds of known structure, similar homobinuclears (Cu-Cu)

(II̲A, III̲A) and heterobinuclears (Cu-M') (II̲B, III̲B) of unknown structure will be used to further test the procedures. In addition, two CuCuCu' trimers exist (V̲I̲, V̲II̲), at least one of which (V̲I̲) can be substituted with M' at the Cu' site. The EXAFS of these trimers will also be examined with the intent of checking difference techniques and normalization procedures to be used eventually on copper proteins with more than two coppers.

The second difference technique suggested above (*i.e.*, oxidation state change as a minor perturbation of the structural environment of M) requires an unsymmetric binuclear model compound which can exist in both the fully oxidized (Cu(II), Cu'(II)) and a localized mixed valence (Cu(II), Cu'-(I)) state. Although some electrochemistry has been done on symmetric binuclear copper complexes, very little information is available on the possible existence of (Cu(II), Cu'(I)) mixed valence states of unsymmetric binuclears. The ideal situation would be a model compound with copper sites which are well-separated (both structurally and electronically so that reduction of one site caused little structural change at the other site and so that no intramolecular electron transfer could occur) with one of the sites having an easily accessible Cu(I) state. Of course, in the unsymmetrical dimers, thermodynamics may dictate a *localized* mixed valence state if the copper redox potentials are different enough. V̲I̲I̲I̲ may be a reasonable choice for such a study although it does exhibit a small amount of Cu-Cu magnetic interaction (a triplet epr).

SUMMARY

Although it may be more difficult to find model systems to use in testing the oxidized minus mixed-valence difference technique, the basic principles and practicalities of difference EXAFS techniques in general should become apparent through the experiments outlined above. The importance of developing such techniques for future use in examination of multi-site copper enzymes cannot be overemphasized. The studies proposed above will help make EXAFS a more viable technique for use with these complex enzyme systems.

REFERENCES

1. J. A. Fee, Struct. Bonding (Berlin), 23, 1 (1975).
2. T. D. Tullius, P. Frank, and K. O. Hodgson, Proc. Natl. Acad. Sci. (USA), 75, 4069 (1978).
3. S. P. Cramer and K. O. Hodgson, Prog. Inorg. Chem., 25, 1 (1979).
4. T. K. Eccles, Ph.D. Thesis, Stanford University, 1978.
5. K. O. Hodgson, personal communication.
6. S. P. Cramer, K. O. Hodgson, E. I. Stiefel, and W. E. Newton, J. Am. Chem. Soc., 100, 2748 (1978).
7. M. Vidali, G. Rizzardi, P. A. Vigato, U. Casellato, S. Kida, and H. Okawa, Inorg. Chim. Acta, 34, 19 (1979).
8. M. Vidali, P. A. Vigato, and U. Casellato, Inorg. Chim. Acta, 17, L5 (1976).
9. M. Tanaka, M. Kitaoka, H. Okawa, and S. Kida, Bull. Chem. Soc. Japan, 49, 2469 (1976).
10. M. Mikuriya, H.Okawa, S. Kida, and I. Ueda, Bull. Chem. Soc. Japan, 51, 2920 (1978).
11. S. E. Groh, Israel J. Chem., 15, 277 (1976/1977).
12. M. Vidali, U. Casellato, P. A. Vigato, and R. Graziani, J. Inorg. Nucl. Chem., 38, 1455 (1976).
13. D. E. Fenton, S. E. Gayda, and R. S. Z. Kowalski, Trans. Met. Chem., 1, 95 (1976).
14. E. Sinn and W. T. Robinson, J. Chem. Soc., Chem. Commun., 359 (1972).
15. R. M. Countryman, W. T. Robinson, and E. Sinn, Inorg. Chem., 13, 2013 (1974).

16. E. Sinn and C. M. Harris, Coord. Chem. Rev., 4, 391 (1969).

17. C. J. O'Connor, D. P. Freyberg, and E. Sinn, Inorg. Chem., 18, 1077 (1979).

18. C. M. Harris and E. Sinn, J. Inorg. Nucl. Chem., 30, 2723 (1968).

19. C. M. Harris, J. M. James, P. J. Milham, and E. Sinn, Inorg. Chim. Acta, 3, 81 (1969).

20. J. A. Bertrand, C. P. Marabella, and D. G. vanderVeer, Inorg. Chim. Acta, 25, L69 (1977).

21. H. J. Schugar, T. G. Fawcett, D. N. Hendrickson, and T. R. Felthouse, Inorg. Chem., 17, 2707 (1978).

22. E. Sinn, Inorg. Chem., 15, 358 (1976).

23. R. P. Kreh and R. R. Gagné, personal communication.

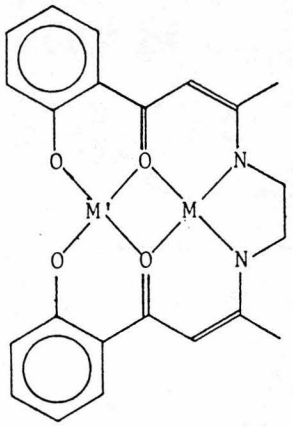
24. R. W. Stotz and R. C. Stoufer, J. Chem. Soc. Chem. Commun., 1682 (1970).

25. R. H. Lane, N. S. Pantaleo, J. K. Farr, W. M. Coney, and M. G. Newton, J. Am. Chem. Soc., 100, 1610 (1978).

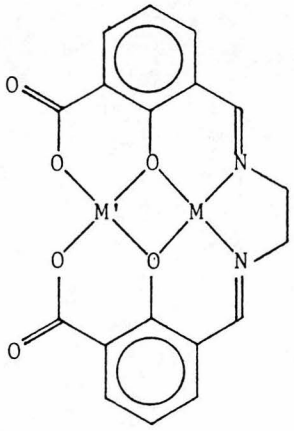
26. A. M. Lanfredi, A. Tiripicchio, and M. T. Camellini, J. Chem. Soc., Dalton Trans., 2168 (1975).

27. W. E. Hatfield, H. W. Richardson, and J. R. Wasson, Inorg. Nucl. Chem. Lett., 13, 137 (1977).

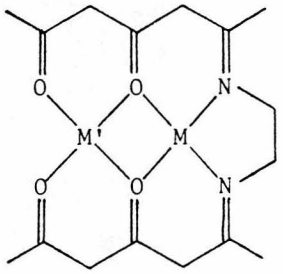
APPENDIX. Structures of Model Compounds



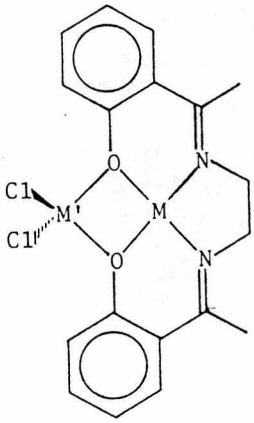
I



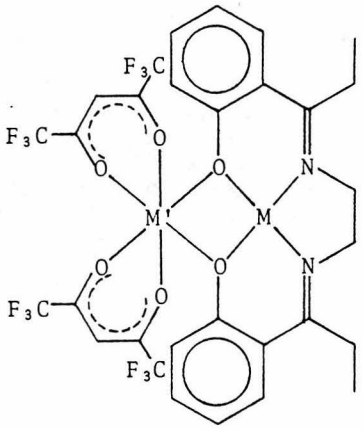
II



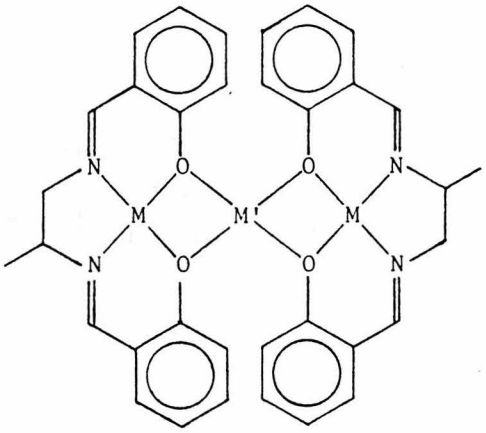
III



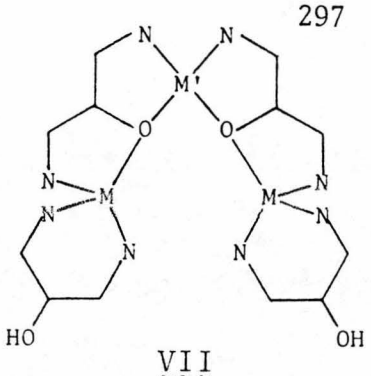
IV



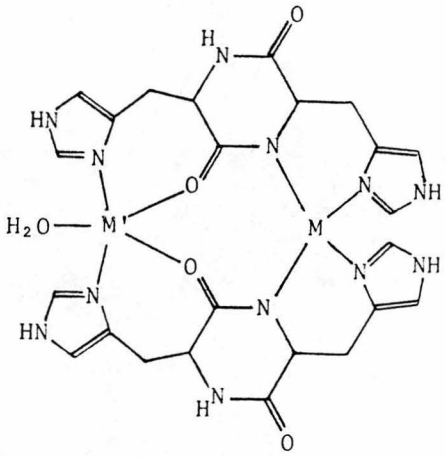
V



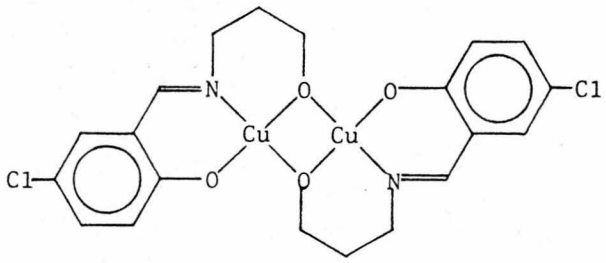
VI



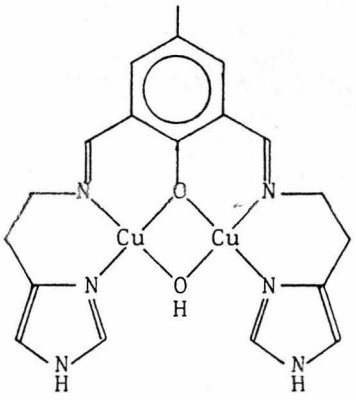
VII



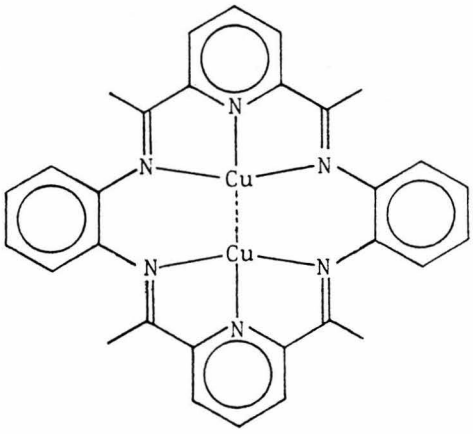
VIII



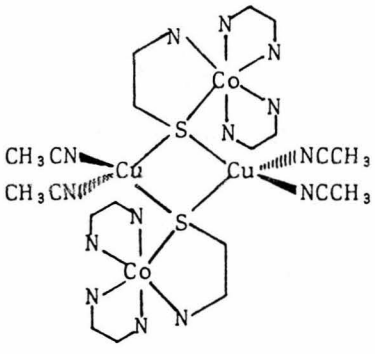
IX



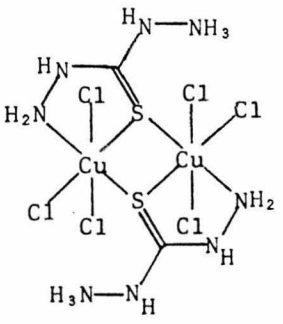
X



XI



XII



XIII

PROPOSITION IV

A Model for the (a_3-Cu_u) Site of Cytochrome aa_3

INTRODUCTION

The O_2 interaction site of cytochrome *c* oxidase (cytochrome aa_3) has recently been demonstrated to involve an antiferromagnetically coupled pair of Fe(III) and Cu(II) (with an S=2 ground state and a -2J value of $\gtrsim$200 cm^{-1}).[1,2] It is intriguing to suppose that this type of coupling enables this site to act as a two-electron donor in the reduction of O_2 to H_2O, thus circumventing the thermodynamically unfavorable one-electron reduction product, superoxide anion.[3]

An early proposal of a possible structure for this binuclear unit in cytochrome aa_3 suggested the presence of an imidazolate bridge between the Fe(III) of the heme (a_3) and the Cu(II) ion.[4] This type of structure has been observed in the bovine (Cu,Zn) superoxide dismutase.[5] All the attempts to date to model this unique coupled site have involved imidazolate (or similar nitrogen heterocycle) bridging.[6-9] So far, there has been no evidence of the existence of an imidazolate-bridged Cu(II)-Fe(III) dimer which exhibits coupling of the magnitude exhibited by the a_3-Cu_u site. Reed and coworkers showed that their imidazolate-bridged Fe(II)-Fe(II) dimers exhibited only weak antiferromagnetic coupling with -J $\simeq$ 8 cm^{-1}.[6] Wilson and coworkers came to the conclusion that their magnetic data did not support the existence of an antiferromagnetic coupling between Fe(II) and Cu(II) in their imidazolate-

bridged system.[7] The only model containing Fe(III) exhibits an epr spectrum characteristic of magnetically isolated (S=1/2) Cu(II).[9] There are also several examples of Cu(II)-Cu(II) systems bridged by imidazolates which exhibit -2J values usually $\lesssim 100$ cm^{-1} (*e.g.*, see ref. 10). The usual argument for the existence of an imidazolate bridge in cytochrome aa_3 comes from the observation of nitrogen as a fifth ligand in the a_3^{2+}-NO complex.[11,12] However, this argument appears fallacious. Since NO is an inhibitor of the enzymatic activity, one might expect it to occupy the O_2 binding site and since it is not unreasonable to suggest that O_2 binds in such a way as to interact with both metal ions, the observed nitrogenous fifth heme ligand could just as easily be facing away from the Cu(II).

The preceding discussion indicates that it is unreasonable to concentrate solely on models incorporating imidazolate bridges since other possibilities seem equally valid. The O_2 reductase activity of cytochrome aa_3 seems to suggest the most obvious bridging group may be a water molecule (or hydroxide ion or oxo group) as has been suggested by Wilson and coworkers.[13] This type of bridging group is often observed in Fe(III) and Cu(II) chemistry and would be easily incorporated into the catalytic function of the enzyme. The current proposal suggests a strategy whereby some interesting Cu(II)-Fe(III) dimers with μ-hydroxo- (or μ-oxo-) bridges may be synthesized and studied as possible models for the antiferromagnetically coupled site of cytochrome aa_3.

PROPOSED EXPERIMENTS

The synthetic strategy involves the use of specific ligands and conditions which have been shown to be involved in μ-hydroxo- or μ-oxo- dimer formation for both the high spin (S=5/2) Fe(III) and the (S=1/2) Cu(II) systems. At high pH, the high spin $Fe(III)(EDTA)^-$ (and Fe(III)(HEDTA)) complex has been shown to form μ-oxo (Fe-O-Fe) dimers.[14,15] Recently, Hendrickson and coworkers have prepared a μ-hydroxo-$[Cu(II)]_2$ dimer with a tren (2,2',2''-triaminotriethylamine) ligand on each copper which exhibits strong antiferromagnetic behavior ($2J \simeq -700\ cm^{-1}$).[16] This dimer was formed upon addition of aqueous NaOH to a Cu(II), tren solution followed by isolation with PF_6^- or ClO_4^- anions.

Attempts will be made to prepare the mixed metal μ-oxo-dimer [(EDTA)Fe(III)-O-Cu(II)(tren)] by addition of NaOH to an aqueous solution of stoichiometric amounts of $Fe(EDTA)^-$ and $Cu(tren)^{2+}$. Excess ligand will be minimized to avoid significant ligand exchange. It is expected that significant portions of Cu(II)-(OH)-Cu(II) and Fe(III)-O-Fe(III) homonuclear dimers will form. However, the three expected products will be significantly different in charge (Cu(OH)Cu, +3; Fe(O)Fe, -4; Fe(O)Cu, -1) and should be easily separable by ion exchange chromatography. It is also entirely possible that the μ-*hydroxo*-(Fe(III),Cu(II)) dimer will form. This species is neutral and may fall out of solution.

Once the (Fe,Cu) dimer is isolated (by addition of $NaClO_4$ if necessary), its magnetic properties will be closely

examined. All indications are that such a singly bridged species should exhibit strong antiferromagnetic coupling and this will be checked by epr (a strongly coupled system should exhibit no epr) and magnetic susceptibility studies.

The successful completion of the first part of the proposed experiments will lead to attempts to synthesize an analogous (Fe,Cu) dimer starting with some type of Fe(III)(porphyrin) since Fe(III) porphyrins are also known to form μ-oxo dimers.[17] Efforts will be concentrated on the Fe(III) complexes of water-soluble sulfonated porphyrins.[18] Again, successful preparation of a [(porphyrin)Fe(III)-O-Cu(II)(tren)] mixed-metal complex will lead to epr and magnetic susceptibility studies to determine the extent of any antiferromagnetic coupling. In the event that any of the isolated complexes show a significant similarity to the Cu(II)-Fe(III) system in cytochrome aa_3, X-ray crystallography will be performed (or in the absence of crystals, EXAFS will be performed) to check the nature of the actual bridging since μ-dihydroxo- bridges may also be involved.

REFERENCES

1. M. F. Tweedle, L. J. Wilson, L. García-Iñiguez, G. T. Babcock, and G. Palmer, J. Biol. Chem., 253, 8065 (1978).
2. T. H. Moss, E. Shapiro, T. E. King, H. Beinert, and C. Hartzell, J. Biol. Chem., 253, 8072 (1978).
3. P. George, in "International Symposium on Oxidases and Related Redox Systems," vol. 1, T. E. King, H. S. Mason, M. Morrison, eds., John Wiley and Sons, Inc., New York, 1964, p. 3.
4. G. Palmer, G. T. Babcock, and L. E. Vickery, Proc. Natl. Acad. Sci. (USA), 73, 2206 (1976).
5. J. S. Richardson, K. A. Thomas, B. H. Rubin, and D. C. Richardson, Proc. Natl. Acad. Sci. (USA), 72, 1349 (1975).
6. J. T. Landrum, C. A. Reed, K. Hatano, and W. R. Scheidt, J. Am. Chem. Soc., 100, 3232 (1978).
7. R. H. Petty and L. J. Wilson, J. Chem. Soc., Chem. Commun., 483 (1978).
8. D. Kovacs and R. E. Shepherd, J. Inorg. Biochem., 10, 67 (1979).
9. T. Prosperi and A. A. G. Tomlinson, J. Chem. Soc., Chem. Commun., 196 (1979).
10. G. Kolks, C. R. Frihart, H. N. Rabinowitz, and S. J. Lippard, J. Am. Chem. Soc., 98, 5720 (1976).
11. M. F. J. Blokzijl-Homan and B. F. van Gelder, Biochim. Biophys. Acta, 234, 493 (1971).
12. T. H. Stevens, D. F. Bocian, and S. I. Chan, FEBS Lett., 97, 314 (1979).

13. D. F. Wilson, M. Erecinska, J. G. Lindsay, J. S. Leigh, Jr., and C. S. Owen, in "Enzymes. Electron Transport Systems," Proc. 10th FEBS Meeting, P. Desnuelle and A. M. Michelson, eds., North-Holland, American Elsevier, New York, 1975, p. 195.

14. H. Schugar, C. Walling, R. B. Jones, and H. B. Gray, J. Am. Chem. Soc., 89, 3712 (1967).

15. H. J. Schugar, A. T. Hubbard, F. C. Anson, and H. B. Gray, J. Am. Chem. Soc., 91, 71 (1969).

16. M. S. Haddad and D. N. Hendrickson, Inorg. Chim. Acta Lett., 28, L121 (1978).

17. *e.g.*, D. H. O'Keeffe, C. H. Barlow, G. A. Smythe, W. H. Fuchsman, T. H. Moss, H. R. Lilienthal, and W. S. Caughey, Bioinorg. Chem., 5, 125 (1975).

18. *e.g.*, T. S. Srivastava and M. Tsutsui, J. Org. Chem., 38, 2103 (1973); P. K. Warme and L. P. Hager, Biochemistry, 9, 1599, 1606, 4244 (1970).

PROPOSITION V

Sepharose-Viologen, An Immobilized Reductant

INTRODUCTION

Anaerobic reoxidation kinetics of extremely O_2-sensitive electron transfer proteins and enzymes (*e.g.*, laccase, cytochrome *c* oxidase, etc.) is technically difficult because of the necessity to remove excess reductant after generation of the reduced state of the protein. Usually some sort of anaerobic dialysis or column techniques are required which are not only difficult and time-consuming, but almost always result in a small amount of reoxidation of the protein once the final reductant is removed. The current proposal involves the design and synthesis of a reductant attached to an insoluble support so that generation of the reductant and its separation from the anaerobically reduced enzyme solution can be accomplished *in situ* without the need for lengthy dialysis or chromatography and without unnecessary transfers and their concomitant dangers of aerobic exposure.

The reductant of choice for the immobilization procedure must have a potential low enough to be generally useful with many proteins and must be easily reducible itself and stable toward many cycles of reduction and reoxidation. It must also have a functional group available for ready attachment to a solid support. The viologens (1,1'-substituted-4,4'-bipyridinium) are well suited for these studies since they have potentials (for reduction of the dication to the cation radical

form) in the range of -350 to -450 mV versus NHE. In addition to being stable, they can be easily functionalized by substitution at the 1 and 1' positions.

One of the best known and most useful techniques used for immobilization of substrates on solid supports involves the use of cyanogen bromide to activate a polysaccharide matrix which is then reactive toward amine functional groups.[1-5] The technique has been developed into a safe, efficient means of achieving a controllable amount of activation of Sepharose[5] for attachment of amine-containing substrates (or proteins). Thus, substitution of a viologen with some type of aminoalkyl group should yield a material which could easily be attached to a CNBr-activated Sepharose resin. Such a viologen derivative (methylaminopropylviologen, MAV) has been prepared and bound to glassy carbon electrodes through a cyanuric chloride attachment procedure.[6] This viologen-modified electrode as well as polymeric viologens and viologen films coated on SnO_2[7] and gold minigrid[8,9] electrodes have demonstrated the feasibility of stable redox active viologens immobilized on surfaces and, in one case,[9] have indicated the applicability of electrode-bound viologens in the reduction of enzymes.

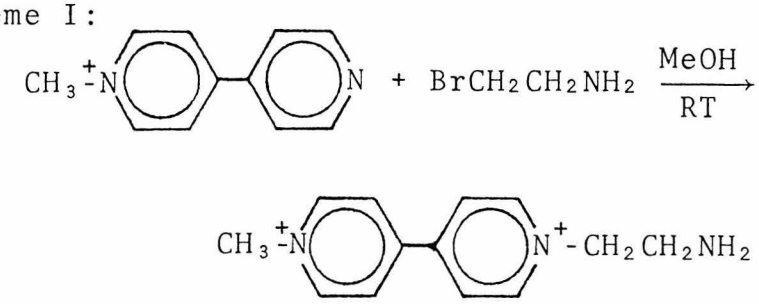
Although these viologen-modified electrodes appear to have promising applications, it is desirable to design an immobilized viologen "reagent" which does not depend on electrochemical techniques for its use. Such an immobilized reagent would be simpler and less expensive to use (especially in laboratories without electrochemical facilities) and may

have applications in which the use of an electrode would be unfeasible. MAV-modified Sepharose could be such an immobilized reagent.

PROPOSED EXPERIMENTS

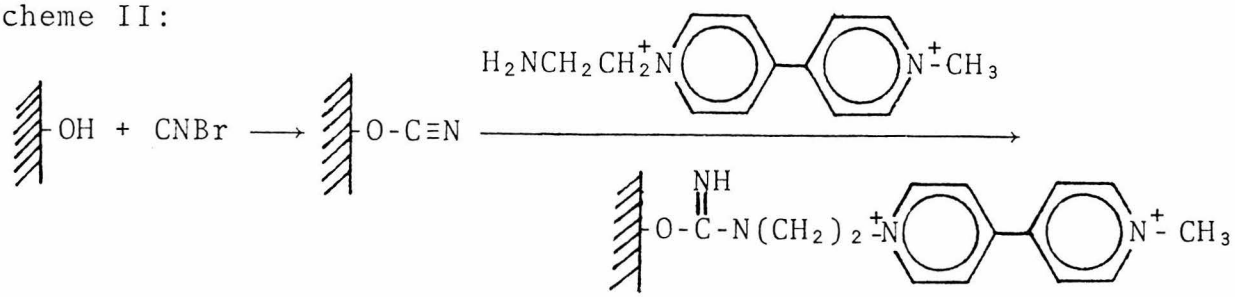
The methylaminopropylviologen will be prepared by the method used by Kuwana and coworkers[6] involving the reaction of bromopropylamine with monomethylbipyridyl (Scheme I).

Scheme I:



This will be attached to a Sepharose-4B support (beads) which has been activated by CNBr (using the method of Kümel, *et al.*[5]). This activation occurs through the formation of a cyanate ester and upon coupling with an amine yields an isourea linkage[10,11] (Scheme II). In addition to washing the resin after

Scheme II:



coupling, the resin will be reduced (with dithionite) to the viologen cation radical state in aqueous suspension and soaked in a high ionic strength buffer (at neutral pH) to remove any

unstably bound or adsorbed viologen. This treatment will assure that there is no leakage of the covalently-bound viologen from the resin during the enzyme reduction since the viologens are known to be least stable in the cation radical form.[6]

The immobilized reductant will be used in practice as follows (all steps will be carried out in a Schlenk-type flask with a frit for separation of aqueous solutions from the modified resin and serum caps for addition of solutions from gas-tight syringes): First, the resin will be aerobically equilibrated in the appropriate buffer (that which the protein is in) and a suspension of the resin in this buffer will be placed in the Schlenk flask. After pump-degassing the suspension, an anaerobic solution of reductant (*e.g.*, sodium dithionite) in the same buffer will be added (in large excess over the capacity of the modified resin) to reduce the immobilized viologen to the cation radical form. Once this reaction is complete, the reductant solution will be pulled through the frit and two or three volumes of degassed buffer will be anaerobically added to the resin to wash off any remaining unbound reductant (dithionite). After pulling the last volume of buffer through the frit, the degassed protein solution will be added (again anaerobically) to the resin. This suspension will be incubated with frequent mixing until the protein is completely reduced. The reduced protein solution will then be pulled through the frit and collected (in an attached reservoir) for future use.

Measurements will be made beforehand to determine the amount of viologen-resin necessary for a given protein concentration (*e.g.*, by reduction of a known concentration of $Fe(CN)_6^{3-}$) and initial studies with a particular protein will involve spectrophotometric monitoring of the protein solution as a determination of the effectiveness of the redox resin in reducing that protein.

Although the above procedure should yield an immobilized reductant capable of reducing many electron transfer proteins, fine tuning of the specificity of the attached viologen will be possible by simply varying the length of the aminoalkyl spacer arm. Thus, methylaminomethyl- and methylaminoethyl- as well as methylaminobutyl- and other variations of the MAV reductant can easily be synthesized by reactions completely analogous to that indicated in Scheme I. Use of these viologen derivatives in the immobilization procedure may yield redox resins with slightly altered characteristics and studies with a particular resin may give some insight as to how long (and/or flexible) the support arm needs to be to achieve rapid electron transfer. This type of fine tuning may, for example, allow the specific reduction of a particular protein in a mixture of proteins. The substituent on the free end of the viologen can also be changed and this may offer a means of fine tuning the potential of the viologen in order to build in even more specificity.

REFERENCES

1. R. Axén, J. Porath, and S. Ernback, Nature, 214, 1302 (1967).
2. P. Cuatrecasas, J. Biol. Chem., 245, 3059 (1970).
3. J. Porath, K. Aspberg, H. Drevin, and R. Axén, J. Chromatogr., 86, 53 (1973).
4. S. C. March, I. Parikh, and P. Cuatrecasas, Anal. Biochem., 60, 149 (1974).
5. G. Kümel, H. Daus, and H. Mauch, J. Chromatogr., 172, 221 (1979).
6. D. C. S. Tse, T. Kuwana, and G. P. Royer, J. Electroanal. Chem., 98, 345 (1979).
7. R. J. Jasinski, J. Electrochem. Soc., 125, 1619 (1978).
8. H. L. Landrum, R. T. Salmon, and F. M. Hawkridge, J. Am. Chem. Soc., 99, 3154 (1977).
9. J. F. Stargardt, F. M. Hawkridge, and H. L. Landrum, Anal. Chem., 50, 930 (1978).
10. J. Kohn and M. Wilchek, Biochem. Biophys. Res. Commun., 84, 7 (1978).
11. J. Turková,"Affinity Chromatography," Journal of Chromatography Library, vol. 12, Elsevier, Amsterdam, 1978, p. 151.